LBL-33205
UC-401

Lawrence Berkeley Laboratory
UNIVERSITY OF CALIFORNIA

CHEMICAL SCIENCES DIVISION

Femtosecond Dynamics of Fundamental Reaction Processes in Liquids: Proton Transfer, Geminate Recombination, Isomerization and Vibrational Relaxation

B.J. Schwartz
(Ph.D. Thesis)

November 1992

LOAN COPY
Circulates
for 4 weeks
Bldg. 50 Library.
LBL-33205
Copy 2

Prepared for the U.S. Department of Energy under Contract Number DE-AC03-76SF00098

DISCLAIMER

This document was prepared as an account of work sponsored by the United States Government. While this document is believed to contain correct information, neither the United States Government nor any agency thereof, nor the Regents of the University of California, nor any of their employees, makes any warranty, express or implied, or assumes any legal responsibility for the accuracy, completeness, or usefulness of any information, apparatus, product, or process disclosed, or represents that its use would not infringe privately owned rights. Reference herein to any specific commercial product, process, or service by its trade name, trademark, manufacturer, or otherwise, does not necessarily constitute or imply its endorsement, recommendation, or favoring by the United States Government or any agency thereof, or the Regents of the University of California. The views and opinions of authors expressed herein do not necessarily state or reflect those of the United States Government or any agency thereof or the Regents of the University of California.

LBL-33205

Femtosecond Dynamics of Fundamental Reaction Processes in Liquids:

Proton Transfer, Geminate Recombination, Isomerization and Vibrational Relaxation

by

Benjamin Joel Schwartz

Ph. D. Thesis

Department of Chemistry
University of California, Berkeley

and

Chemical Sciences Division
Lawrence Berkeley Laboratory
University of California
Berkeley, CA 94720

November, 1992

This work was supported by the Director, Office of Energy Research, Office of Basic Energy Sciences, Chemical Sciences Division of the United States Dept. of Energy, under contract number DE-AC03-76SF00098.

Abstract

Femtosecond Dynamics of Fundamental Reaction Processes in Liquids:

Proton Transfer, Geminate Recombination, Isomerization and Vibrational Relaxation

by

Benjamin Joel Schwartz

Doctor of Philosophy in Chemistry

University of California at Berkeley

Professor Charles B. Harris, Chair

Femtosecond and picosecond transient absorption spectroscopy are used to probe several fundamental aspects of chemical reactivity in the condensed phase including proton transfer, geminate recombination, isomerization and vibrational relaxation.

The fast excited state intramolecular proton transfer of 3-hydroxyflavone is measured for the first time, and the effects of external hydrogen-bonding interactions on the proton transfer are studied in detail. The proton transfer takes place in ~240 fsec in non-polar environments, but becomes faster than the instrumental resolution of 110 fsec in methanol solutions. A simple model is proposed to explain these results.

The dynamics following photodissociation of CH_2I_2 and other small molecules

provide the first direct observations of geminate recombination. The recombination of many different photodissociating species occurs on a ~350 fsec time scale. Results also show that recombination yields but not rates depend on the molecular details of the solvent environment and suggest that recombination kinetics are dominated by a single collision with the surrounding solvent cage.

Studies of sterically locked phenyl-substituted butadienes offer new insights into the electronic structure and isomerization behavior of conjugated polyenes. The data show no simple correlation between the hinderance of specific large amplitude motions and signatures of isomerizative behavior such as viscosity dependent excited state lifetimes. This strongly implies that the isomerization of these systems does not provide a suitable testing ground for simple condensed phase reaction rate theories.

The spectral dynamics of a photochromic spiropyran indicate that recombination, isomerization and vibrational relaxation all play important roles in the photoreactivity of complex molecules. The interplay of these microscopic phenomena and their effect on macroscopic properties such as photochromism are discussed. All the results indicate that the initial steps of the photochromic reaction process occur extremely rapidly.

A detailed discussion of the alignment of the femtosecond laser system used for all these experiments and a presentation of the code used for fitting and analyzing the data obtained are also included. In addition, advice for optimizing the laser alignment or modifying the data analysis software is presented.

To my parents,

who have loved and supported me all these years

and Sarah,

who will love and support me for many more.

Table of Contents:

Chapter 1: Introduction

1.1 Overview....1

1.2 Summary....4

1.3 References....7

Chapter 2: Experimental Apparatus

2.1 Overview....9

2.2 Background

A. Principles of Operation....13

B. History of the Harris Group CPM....17

2.3 Experimental Alignment

A. Aligning the CPM....21

B. Alignment of Pump-Probe Transient Absorption Experiments....25

2.4 References....30

Chapter 3: Direct Observation of Fast Proton Transfer -- Femtosecond Photophysics of 3-Hydroxyflavone

3.1 Overview....32

3.2 History of 3-Hydroxyflavone

A. Background....36

B. Early Time-Resolved Luminescence Studies of 3HF....41

C. Effect of Hydrogen-Bonding Impurities....44

D. Attempts to Measure the Intrinsic ESPT Rate....47

E. Isolation of 3HF-Solvent H-Bonded Complexes....49

3.3 Experimental

A. Femtosecond Laser Apparatus....51

B. Picosecond Laser Apparatus....53

C. Materials....54

3.4 Results

A. Picosecond Transient Absorption and Stimulated Emission....55

B. Femtosecond Transient Absorption....62

1. Investigation of Fast Rise Times....65
2. Effect of Hydrogen-Bonding Impurities in MCH....65
3. Effect of Deuteration....71
3.5 Discussion
A. Measurement of Intrinsic ESPT -- The Fast Rise in MCH....73
B. Fast ESPT in MeOH -- 3HF Monosolvate....77
C. Effect of Polarization....81
3.6 Summary....84
3.7 References....85
Chapter 4: Direct Femtosecond Measurements of Geminate Recombination Times of Small Molecules in Liquids
4.1 Overview....89
4.2 Background
A. History of Caging....93
B. The Photodissociation Dynamics of CH_2I_2....95
4.3 Experimental
A. Femtosecond Laser System....100
B. Materials....101
4.4 Results....101
4.5 Discussion....103
4.6 Summary....110
4.7 References....110
Chapter 5: Ultrafast Studies of 1,4-Diphenyl-1,3-Cyclopentadiene, a Locked s-*cis* Diphenylbutadiene Analog
5.1 Overview....113
5.2 Background
A. Electronic Structure of DPB....117
B. Comparison of the Electronic Properties of DPB and DPCP....120
1. Electronic Structure of DPCP....120
2. Evidence for s-*cis* Rotamers in the Electronic Structure of DPB....123

5.3 Experimental
A. Femtosecond Laser System....125
B. Picosecond Laser System....125
C. Materials....126
5.4 Results
A. DPCP Transient Absorption....127
B. Transient Absorption of TPCP and HHN....130
5.5 Discussion
A. Electronic Structure and State Ordering of Diphenylpolyenes....134
B. Isomerization of Diphenylpolyenes as Tests of Chemical Rate Theories..137
5.6 References....139

Chapter 6: Ultrafast Studies of Photochromic Spiropyrans in Solutions
6.1 Overview....143
6.2 Background
A. Photochromic Spiropyrans and Sprioxazines....144
B. HBPS....146
6.3 Results
A. Ground State Absorption Spectrum....148
B. Femtosecond Transient Absorption....150
C. Picosecond Transient Absorption....150
1. Red Transient Absorption Band....150
2. Blue Transient Absorption Band....157
D. Solvent Effects....157
6.4 Discussion
A. Molecular Structure and Electronic Absorption Spectrum....159
B. Dynamics on the Femtosecond Time Scale:
Direct Dissociation and Bond Reformation....161
C. Dynamics on the Picosecond Time Scale:
Vibrational Relaxation and Isomerization....163
D. Effect of Solvent Viscosity and Polarity....165

E. Model for Photochromic Reaction....166
6.5 Experimental
A. Picosecond and Femtosecond Laser Set-ups....166
B. Materials....168
6.6 Conclusions....168
6.7 References....169

Chapter 7: Fitting the Data
7.1 Overview....172
7.2 History....175
7.3 Using Convfit
A. Preparing Data for Convfit....178
B. Executing Convfit....180
C. Fitting with Convfit....182
D. Troubleshooting....183
7.4 Modifying Convfit....185
A. Compilation of Convfit....186
B. Compilation of Convplot....188
C. Adding New Functions to Convfit....189
1. Modifying Fitfunc.f....189
2. Modifying Convfit.f....192
3. Modifying Convplot.f....193
7.5 Maximizing Use of Convfit
A. Choosing the Correct Function....193
B. Fitting the Data....194

Appendix I: Program Logs.f....198
Appendix II: Program Convfit.f....201
Appendix III: Program Cvfitfunc.f....233
Appendix IV: Handling Routines for the HI Plotter Called from Convfit.f....242
Appendix V: Makefile and Compilation of Convfit....243
Appendix VI: Program Convplot.f....244

Acknowledgements

Looking back over the last 6.25 years, I realize that one of the most important aspects of graduate school has been the influence of the people around me. Some of these colleagues have contributed directly to the projects discussed in this thesis and to the publications on which I am an author; others have greatly influenced my scientific growth through conversations, arguments and inquiries. I would like to thank all the members of the Harris group, past and present, for providing such a unique and constructive environment for doing science. My coworkers have impressed me with their intelligence, experimental skills, perseverance and insight; I have greatly benefitted from many positive interactions with them during my graduate career. I am also pleased to count the members of the Harris group as friends as well as colleagues; the non-scientific things I have shared with the group have been an integral part of making my graduate experience enjoyable.

I would like to single out the people who have collaborated with me directly on the work that appears in this thesis or in the literature. Rebecca Hoff spent 2.5 long years building and rebuilding the femtosecond system with me, followed by another 2 years trying to understand the dynamics of "twisty molecules". The laser system described in Chapter 2 is as much hers as it is mine, and the groundwork for the material of Chapter 5 was also a joint effort. The extensive references to her thesis throughout these two chapters do not do justice to her contribution to this work.

Many of the ideas and thoughts (as well as the synthesis of some of the samples) discussed in Chapter 5 came from Professor Ashraf El-Bayoumi. In addition to being

an inexhaustible fount of ideas for experiments, Ashraf's cheery presence in the lab was a great enhancement to my graduate career. The discussion of Chapter 5 also has origins in many conversations with the Kliger group at U. C. Santa Cruz, especially Stacie Wallace-Williams. Stacie has directly contributed to this chapter by providing me with the samples of DPCP and HHN, sending me preprints of her work and the work of Kohler et al., taking the nsec absorption spectrum of TPCP and engaging in many interesting and insightful conversations.

Linda Peteanu, former Mathies group post-doc and Professor at Carnegie-Mellon got me started thinking about proton transfer and introduced me to 3HF. Without her inspiration, I don't know if I would have produced my first publication, and without her co-authorship, I doubt it would have turned out nearly as well.

Jason King and now U. C. Santa Cruz Professor Jin Zhang have been major contributors to the science I've done in the past 2 years. From innumerable conversations about everything from upconversion to geminate recombination, these two have helped me learn a great deal of science and a lot about how science is done. Discussions with Jason and Jin have heavily influenced the interpretation of results presented in Chapter 4, and have provided much of the organization behind the "theory" of data fitting outlined in Chapter 7.

I must extend a great deal of the credit for Chapter 6 to Jin: Jin initiated the HBPS project (despite my early pronouncements that it wouldn't work), took most of the data and provided nearly all of the references that allowed us to understand what was happening in this complex system. In this dissertation, this chapter is the work that I consider least to be my own because of the extraordinary contributions that Jin has

made.

Jason King has allowed me to collaborate with him on several other projects, including his relentless pursuit of understanding vibrational relaxation in metal carbonyls. Jason's good nature, fondness for learning by argument and perseverance in the lab have taught me a great deal. I feel no qualms about leaving the CPM in his capable hands.

Eric Peterson, in addition to filling my graduate career with innumerable cycling adventures, has collaborated with me on the xenon exciton project. I am grateful to him for initiating this project and sharing it with me. The progression of our interpretation of the data from electrons to ions to excitons to excimers has exemplified all the things that make science both frustrating and fun.

Vijaya Narasimhan has always been there to help with purchase orders and assist with cutting through university bureaucratic red tape.

Finally, I would like to thank Charles Harris for creating the research environment in his group. Charles is directly responsible for bringing all these people and me together, and for providing an atmosphere in which we were free to pursue our own ideas. The balance Charles has achieved in allowing his students to follow their own course while still providing subtle direction is one I hope to better understand if/when I have my own research group in the future. I appreciate the opportunities Charles has provided for me to present my work, including the trip to Ultrafast in France and his many behind the scenes phone calls which brought me post-doctoral interviews. I also acknowledge his candor in dealing with issues of my career and publications; I value his strong opinions on these subjects, and appreciate the fact that they have been offered

in a way which allows me to disregard them if I choose. The combination of Charles' direction style and the quality of my colleagues is what makes the Harris group outstandingly unique in the science community.

This work was supported by the National Science Foundation. I would also like to acknowledge the U. S. Dept. of Energy, Office of Basic Energy Sciences, Chemical Sciences Division under contract number DE-AC03-76SF00098 for some specialized equipment used in these experiments. I also acknowledge the National Science Foundation and the W. R. Grace and Company Foundation for their generous support with graduate fellowships.

Chapter 1: Introduction

1.1 Overview

One of the central themes of modern physical chemistry is to elucidate the elementary steps associated with a chemical reaction. While understanding of gas phase reactions has reached a high level of sophistication, there remain many open questions concerning reactivity in the liquid phase. In a typical room temperature liquid, reactant species can suffer 10^{13} collisions per second with the solvent. These collisions can cause energy exchange between the solvent and the reactant, perturb or mix the reactant potential energy surfaces and spatially localize or separate the reacting species, all on a picosecond or subpicosecond time scale. Thus, femtosecond laser technology is essential to the study of condensed phase reaction dynamics. These complex effects of the solvent on chemical reactivity have only become understood in the photodissociation and recombination of diatomic species in the past decade [1]; solvent effects on polyatomic reactants which can have multiple product branches and can distribute energy over many internal reactant degrees of freedom are extremely complex, and are only now beginning to be studied.

The effects of the condensed environment on chemical reactivity are manifest in a variety of phenomena, depending on the details of a particular reaction. For a photodissociation reaction, the surrounding solvent can keep the photofragments from flying apart, confining them to near proximity and enabling them to undergo a back reaction to reform the parent compound. Reactions which proceed by large amplitude motion, such as cis-trans isomerization reactions, can be both promoted by collisions

with solvent molecules and hindered by the viscous drag of the solvent; the two effects work in competition to control the rate of the reaction. The solvent can affect chemical transformations, such as proton transfer reactions, by forming hydrogen or chemical bonds at the reactive site, altering the reaction rate. In some cases, the solvent can actually participate in a chemical exchange reaction, serving as a catalyst to drive the reaction along a potential surface with a lower energy barrier. The liquid environment can also act as a thermal reservoir, allowing cooling of vibrationally hot molecules and providing for energy flow into and out of reactive degrees of freedom. Finally, the condensed environment can delocalize electronic excitations, blurring the distinction between individual atoms or molecules of the solvent by the formation of electronic bands or excitons.

The outcome of condensed phase chemical reactions can be determined by any or combinations of all of these various solvent effects. The microscopic details of how each of these mechanisms operates, however, is not yet well understood. During my graduate career, I have had the opportunity to use ultrafast transient absorption spectroscopy to study many of these mechanisms and their effects on chemical reactivity, both individually, and in combination. The individual projects which I have participated in are outwardly very different: proton transfer, geminate recombination, isomerization, vibrational cooling and exciton formation. The opportunity to work on such a diverse set of projects has piqued my interest and has provided a great deal of intellectual satisfaction, but more importantly, has taught me that phenomena which appear different upon first inspection can be subtly and deeply intertwined; all these projects are connected by the microscopic physics underlying the interactions of the

solvent and the reacting species.

This dissertation describes some of the projects I've worked on to help elucidate the microscopic basis for solvent effects on chemical reactivity. Much of the work I've done has been published in (or submitted to) the literature [2-8], and several of the joint projects have been (or will be) described in the theses of others [9-11]. The work which is not included in this dissertation consists of some studies of the isomerization of phenyl substituted butadienes [9], the formation, trapping and subsequent cooling of excitons in liquid xenon [7,10], the vibrational cooling and solvation of metal carbonyl complexes [4,8,11] and the cooling of other small polyatomics such as CH_2I_2 [11]. The next section contains a summary of the studies that are presented in this work: solvent effects on excited state proton transfer [2,3], observation of geminate recombination in small molecule photodissociation [4,5], the isomerization dynamics of synthetically locked and stiffened substituted butadienes and the reaction kinetics of a photochromic spiropyran molecule [6], which include a combination of vibrational relaxation, isomerization and recombination dynamics.

This thesis is organized in the following manner. Each chapter focusses on a single idea in the study of condensed phase reactivity: either a detailed description of one of the projects, or some aspect of the experimental apparatus or data analysis procedures necessary for obtaining and interpreting the data. Although the different projects are related to each other, each chapter is designed to stand alone; other chapters are referenced in the same manner as is any background material. Thus, each chapter begins with an overview section, providing perspective on the project to be presented and outlining the problem to be studied. This is followed by a background section,

which follows the historical development and presents specific details of the reaction to be investigated. The subsequent section recaps the experimental techniques used for the particular project under discussion. This is followed by a presentation of the experimental results, and a discussion of the results in terms of the overview and background information presented in the beginning of the chapter. The chapters close with a summary of the important conclusions, and a list of references in an independent reference section (each chapter's references are numbered independently, and reference numbers are consistent only within a given chapter).

1.2 Summary

A. Experimental Apparatus: Chapter 2 presents a description of the experimental apparatus used for all of the projects discussed in this thesis. Some of the design and construction considerations for the amplified, colliding-pulse modelocked ring laser (femtosecond laser system) are discussed, and routine operations and system characteristics are also presented. In addition, methods for data collection and signal improvement are addressed. This chapter, in combination with the thesis of Rebecca Hoff [9], should provide the working knowledge necessary to utilize the femtosecond laser system for transient absorption experiments.

B. Direct Observation of Proton Transfer -- Femtosecond Photophysics of 3-Hydroxyflavone: The first investigation of the fast excited state intramolecular proton transfer of 3-hydroxyflavone is reported in Chapter 3. Picosecond stimulated emission and transient absorption spectroscopy demonstrate that the tautomer formation can be monitored by 620 nm transient absorption. The excited state proton transfer was

studied at 620 nm with femtosecond time resolution, and determined to be 240±50 fsec in a non-polar solvent environment. The fast excited state proton transfer in methanol solution, however, was faster than the 125 fsec instrument response. A simple model describing the mechanism of the fast excited state proton transfer of 3–hydroxy flavone in different solvents is presented.

C. Direct Femtosecond Measurements of Geminate Recombination Times of Small Molecules in Liquids: Chapter 4 presents the femtosecond transient absorption spectra of the CH_2I photoproduct of the methylene iodide (CH_2I_2) photodissociation. The results indicate a disappearance of this photofragment on a ~350 fsec time scale in several different solvents. The implication is that in these simple liquids, methylene iodide is undergoing geminate recombination. Recombination yields, but not rates are shown to be solvent dependent. This suggests that the kinetics of geminate recombination are dominated by a single collision with the surrounding solvent cage.

D. Ultrafast Studies of 1,4-Diphenyl-1,3-Cyclopentadiene, a Locked s-*cis* Diphenylbutadiene Analog: In Chapter 5, the ultrafast studies on isomerization reactions of diphenylpolyenes presented in the thesis of Rebecca Hoff [9] are extended to additional molecular species. Picosecond and femtosecond transient absorption spectroscopy are used to monitor the excited state dynamics of 1,4-diphenyl-1,3-cyclopentadiene (DPCP) and similar rigid analogs of diphenylbutadiene (DPB). The results show that solvent assisted level inversion is not important in the excited state dynamics of these systems, and instead support a picture of different diene rotamers contributing to the observed transient absorption behavior. Comparisons between

DPB, DPCP and other species indicate that isomerative motion in these systems is not well understood, and that these molecules are poor choices to test theories of solution phase chemical reaction rates.

E. Ultrafast Studies of Photochromic Spiropyrans in Solution: Chapter 6 discusses the photochromic reaction dynamics of the spiropyran molecule 1',3',3'-trimethyl-6-hydroxyspiro[2H-1-benzopyran-2,2'-indoline] (HBPS) in solution, which have been studied with picosecond and femtosecond transient electronic absorption spectroscopy. Following excitation near 300 nm, the C-O bond of the molecule breaks in less than 100 fs to form a metastable species. A small fraction of this metastable species reforms the broken C-O bond on the time scale of 200 fs. The major fraction of the metastable photoproduct vibrationally relaxes in a few picoseconds, and then undergoes isomerization to form a merocyanine product with a decay time constant of about 100 ps, depending on solvent viscosity. This isomerization decay is faster at shorter probe wavelengths and slower at longer wavelengths, indicating that this isomerization gives rise to a red-shifted absorption spectrum. The final merocyanine isomers are stable on the nanosecond time scale. All the results indicate that the initial steps of the photochromic reaction process of HBPS are extremely fast.

F. Fitting the Data: The techniques used for analyzing and fitting the data presented in the previous chapters are summarized in Chapter 7. Use of the programs logs and convfit for interactive curve fitting is described. The structure and functional description of this software is presented, along with specific instructions for updating and modifying the code to fit to new functions or different types of data. The nature of the fitting errors generated by these programs, and their implications on the

interpretation of the data are discussed, along with advice for minimizing potential mistakes which could significantly affect the conclusions. The actual code for these programs, with comments, is presented in Appendices I - VI.

1.3 References

1. A. L. Harris, J. K. Brown and C. B. Harris, Ann. Rev. Phys. Chem., 39, 1988, p. 341 and references therein.
2. B. J. Schwartz, L. A. Peteanu and C. B. Harris, "Direct Observation of Fast Proton Transfer: Femtosecond Photophysics of 3-Hydroxyflavone", J. Phys. Chem., 96(9),1992, p. 3591.
3. B. J. Schwartz, L. A. Peteanu and C. B. Harris, "Solvent Effects on the Fast Proton Transfer of 3-Hydroxyflavone", Proc. Ultrafast Phenomena VIII, Springer Series in Chemical Physics, G. A. Mourou and A. H. Zewail, Editors, accepted for publication, June 1992.
4. C. B. Harris, J. C. King, K. E. Schultz, B. J. Schwartz and J. Z. Zhang, "Energy Redistribution in Large Molecules in Solution on Ultrafast Time Scales", Proc. Ultrafast Phenomena VIII, Springer Series in Chemical Physics, G. A. Mourou and A. H. Zewail, Editors, accepted for publication, June 1992.
5. B. J. Schwartz, J. C. King, J. Z. Zhang and C. B. Harris, "Direct Femtosecond Measurement of Geminate Recombination Times Following Photodissociation of Small Molcules in Solution", submitted to J. Chem. Phys., Sept. 1992.
6. J. Z. Zhang, B. J. Schwartz, J. C. King and C. B. Harris, "Ultrafast Studies of Photochromic Spiropyran in Solutions", J. Am. Chem. Soc., accepted for

publication, Sept. 1992.

7. E. S. Peterson, B. J. Schwartz and C. B. Harris, "Picosecond Dynamics of Exciton Tunneling and Trapping in Condensed Xenon", manuscript in preparation.
8. J. C. King, J. Z. Zhang, B. J. Schwartz and C. B. Harris, "Vibrational Relaxation of $M(CO)_6$ (M = Cr, Mo, W): Observations on the Effect of Metal Mass on Vibrational Cooling", submitted to *J. Chem. Phys.*, Oct. 1992.
9. R. L. Hoff, Ph.D. Dissertation, University of California, Berkeley, 1991.
10. E. S. Peterson, Ph.D. Dissertation, University of California, Berkeley, 1992.
11. J. C. King, Ph.D. Dissertation, University of California, Berkeley, to be published.

Chapter 2: Experimental Apparatus

2.1 Overview

Even well understood gas phase chemical reactions can behave in an unanticipated fashion in solution environments due to the complex interactions between the reacting species and the surrounding solvent molecules. In order to elucidate the microscopic physics underlying condensed phase reactivity, it is necessary to monitor the course of a chemical reaction on the same time scale as the solvent interactions which perturb it from its gas phase path. Since the average time between collisions in a typical room temperature liquid is $\sim 10^{-13}$ seconds, any spectroscopic methods used to investigate condensed phase reaction dynamics must have a time resolution on the order of 100 fsec. Unfortunately, the ability to make measurements on this rapid a time scale is completely beyond the scope of conventional electronics, where the fastest current transients that can be generated or measured take place in tens of picoseconds. Thus, ultrafast spectroscopy must be accomplished by insuring that the light itself interacts with the sample for only 100 fsec. The capability to produce light pulses with a duration this short and an intensity great enough for easy detection and characterization has been developed within the past decade [1,2], opening the possibility to study condensed phase chemical reactions on a time scale faster than the interactions with the surrounding medium.

There are two chief difficulties to studying solution phase reactivity with ultrashort laser pulses. The first lies in producing a high enough concentration of reacting species to probe. Many solution phase chemical reactions are rate controlled by diffusion of

the reacting species, that is, the amount of time it takes for the reactants to diffuse through the solvent and achieve a reactive configuration. This process occurs on the microsecond time scale for many reactions; if the actual reaction takes only a few picoseconds once diffusion is complete, then the molecules are exhibiting reactive behavior less than one one-millionth of the time. This means that the concentration of reacting species is more than a million times lower than the concentration of reactants, making spectroscopic probing of the species during the actual reaction difficult. To overcome this problem, a method of significantly increasing the concentration of reacting species must be used.

The second main complication to ultrafast study of liquid phase reactions lies in the lack of coherent synchronization of the reacting ensemble. Since the reaction of one set of reactants can start independently of that of a neighboring set of reactants, the solution contains an ensemble of reacting species, each at a slightly different point through the reaction process. This means that an ultrashort pulse interacting with the sample will probe species at many different points in time through the reaction, smearing out the dynamics of interest. To avoid this shortcoming, some means of initiating the reaction simultaneously (coherently) must be found.

The solution to both these problems lies in using two ultrafast pulses in the experiment: one pulse to coherently initiate a chemical reaction in a large number of reacting species, and a second pulse to probe the resulting dynamics a known time delay after the first. By sweeping the delay time between the pump and probe pulses, the entire course of the chemical reaction can be followed directly in the time domain. This technique, known as pump-probe spectroscopy, has the advantage that the time

delay between the pulses can be made essentially arbitrarily precise; this delay is easily controlled by varying the optical path length of the two pulses. For example, a path length variation of a few microns, which is easily accomplished with present technology, corresponds to a relative delay of only a few femtoseconds. Thus, the time resolution of the pump-probe technique is limited only by the temporal width of the actual light pulses, not by electronics or the ability to control the time delay between them.

The principal drawback of pump-probe spectroscopy lies is its limitation to study only photoinitiated reactions. This means that bi-molecular or other diffusion controlled reactions are not amenable to study with this technique; only reactions which can be initiated by absorption of a femtosecond light pulse can be examined in this fashion. For many classes of reactions, this limitation can be overcome through the study of chemically similar systems. For example, proton transfer reactions (many of which are bi-molecular in nature) can be probed directly in the time domain if a system which undergoes intramolecular proton transfer upon electronic excitation is studied, as described in the next chapter. Similar chemical tricks can be employed to make a wide range of chemical phenomena available for study with pump-probe spectroscopy. The largest obstacle to researching many chemical systems lies in the lack of ultrashort pulses at wavelengths necessary for photoexcitation of many chemical systems, in particular, the absence of a tunable source of femtosecond pulses in the near ultraviolet, where many small molecules of interest have their primary absorption. This precludes the study of many chemical phenomena exhibited by these simple systems. There is still a great deal of knowledge to be gained, however, from experiments with presently

available ultrafast lasers, and continually emerging femtosecond technologies assure that a wide range of new systems will be accessible for study in the near future.

In this chapter, the design, construction and use of an amplified, colliding-pulse-modelocked (CPM) femtosecond laser system for performing pump-probe experiments is described [1,2]. This apparatus, along with the amplified synchronously-pumped picosecond laser system, has been used for all the experiments reported in chapters 3-6 in this thesis. The picosecond laser system has been described previously in the literature and in the theses of others [3-6]. The operation of this picosecond apparatus is briefly summarized in those chapters which report experiments using this system; further detail will not be given here. The CPM femtosecond laser system was built jointly by Rebecca Hoff and myself. Many of the details of the laser construction, the use of the system for pump-probe experiments and some of the theory behind the operation of this laser are presented in the thesis of Rebecca Hoff [7]. The purpose of this chapter is to present additional information describing some of the more practical aspects of aligning, tweaking and using this apparatus for pump-probe spectroscopy as a supplement to the description presented in Rebecca's thesis. Hopefully, the combination of this chapter and Rebecca's thesis contain the information necessary for a new user to learn to utilize the laser system for femtosecond experiments.

In the next section, a brief history of the CPM laser system in the Harris group as well as a summary of the work contained in Rebecca Hoff's thesis is presented. This is followed by a section describing methods for adjusting the CPM oscillator cavity and advice for the alignment of femtosecond pump-probe experiments. Further details of the copper-vapor-laser (CVL) based bow-tie amplifier [8] and the synchronization

electronics between the cavity dumper and the CVL will not be presented; Rebecca's thesis [7] and reference 8 do an especially nice job describing the amplifier operation, and present Harris group plans are to retire the CVL amplifier in favor of a transversely pumped YAG based system.

2.2 Background

A. Principles of Operation: The colliding pulse modelocked (CPM) laser is a continuously pumped, passively modelocked ring dye laser [1,2]. Unlike conventionally modelocked lasers in which an electrooptic device actively modulates the cavity gain, or synchronously pumped lasers, where the extremely short duration of excitation results in a cavity gain modulation, the CPM has no active elements which change its gain characteristics. Pulse formation in the CPM, shown schematically in Figure 2.2.1, can be thought of as follows: CW light from the argon ion laser continuously pumps the gain jet, the fluorescence of which is gathered by the gain cavity subresonator mirrors (marked 'a' in Figure 2.2.1) and sent in both directions around the ring. Eventually, the light reaches the saturable absorber jet, the concentration of which is carefully adjusted to just completely absorb all the fluorescence coming from one or the other of the directions around the ring. When the fluorescence from both directions reaches the saturable absorber simultaneously however, there is just enough light intensity to excite all the saturable absorber dye molecules at the focus, leading to a temporary bleach of the absorption (i.e., the absorption is saturated). This effectively opens a window in the cavity, allowing a little pulse of fluorescence to pass through the saturable absorber jet. The fluorescence from

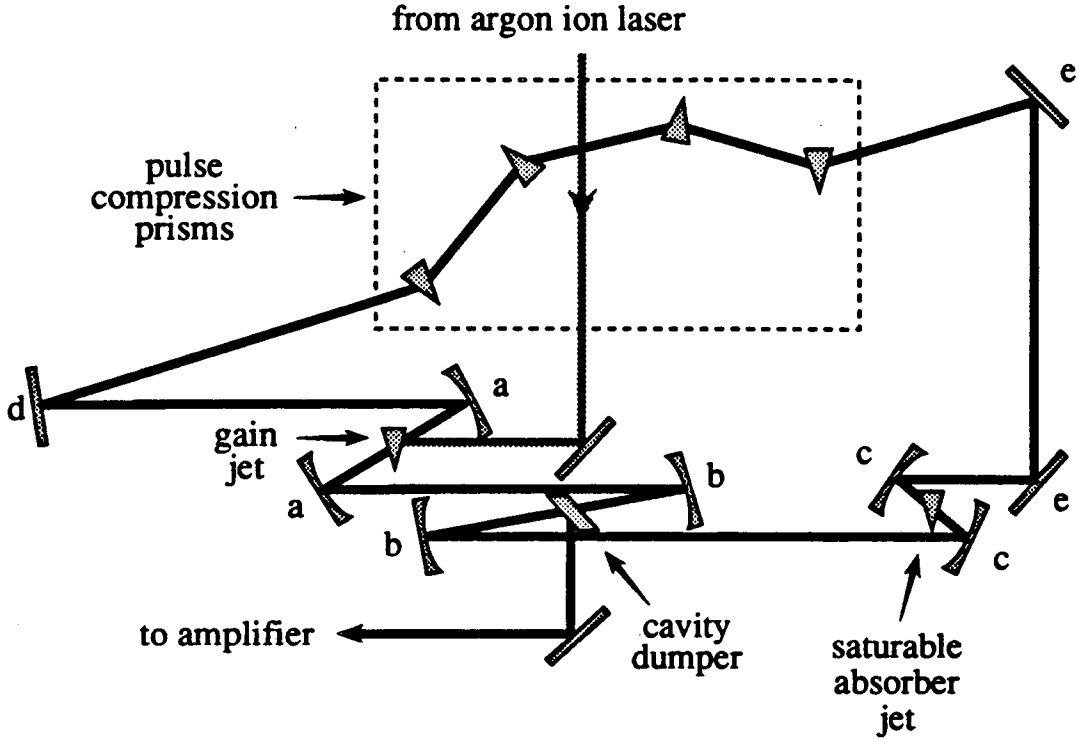

Figure 2.2.1: Schematic of CPM laser system. Fluorescence collection mirrors 'a' have a 10 cm radius of curvature and comprise the gain jet subresonator; the cavity dumper subresonator 'b' has 20 cm radius of curvature mirrors and contains the Bragg cell; the saturable absorber subresonator 'c' uses mirrors with 5 cm radius of curvature. Corner mirror 'd' is coated for 620 nm broad-band reflection at 0°; the mirrors labelled 'e' are 620 nm broad-band high reflectors for 45°.

either direction eventually reaches the gain jet, which has been continuously pumped during the entire process, and stimulates emission from the excited gain dye. Note that the distance between the gain jet and the saturable absorber jet is roughly 1/4 of the total cavity round trip distance; this maximizes the time between the intersections of the two counterpropagating fluorescence pulses with the gain jet, allowing sufficient time for the gain to recover between the pulses. Since both fluorescence pulses are travelling at the same speed around the same cavity, they will meet again exactly where they originated: back in the saturable absorber jet. As before, the beginnings of the two pulses will be absorbed in the jet until saturation, allowing the remainder of the two pulses to propagate through the bleached absorber and into the cavity. This process continues in a self-consistent fashion, allowing stable pulse formation in the cavity, hence the name colliding pulse modelocking.

The actual process of pulse formation in the CPM is a bit more complex than the simple description outlined above. A subtle interplay of self-phase modulation [9] and the formation of transient gratings due to pulse interference [10] in the saturable absorber jet are responsible for much of the CPM pulse characteristics and stability. The gain characteristics of the CPM can be described by the non-linear Schroedinger equation, leading to a soliton-like description of CPM pulse formation [11]. These details are discussed more completely in the thesis of Rebecca Hoff [7].

The largest problem facing stable pulse formation in the CPM is dispersion. The pulses formed in the CPM are so short (~100 fsec) that they have an enormous bandwidth (nearly 200 cm^{-1} or roughly 10 nm FWHM at 620 nm). For most of the materials in the cavity, e.g. the ethylene glycol in the jets, the coatings on the mirrors or

the quartz in the prisms, the index of refraction is lower at longer wavelengths and higher at shorter wavelengths. This means that the red portions of the pulse travel through these cavity elements more quickly than the blue portions, causing the pulse to spread temporally. Without some means of reversing this process, pulses could not remain stable in the cavity for very long; every time the pulses passed through one of the cavity elements, they would broaden in time, eventually smearing themselves out to the point where they no longer have enough intensity to bleach the saturable absorber.

Fortunately, simple prism optics can be used to provide negative dispersion, that is, put the blue components ahead of the red ones to compensate for the change in index of refraction of the different cavity elements [12]. The four prism pulse compressor in the cavity, shown in Figure 2.2.1, spreads the pulses out angularly. Since the blue wavelengths are refracted more sharply than the red ones, they travel a lower net distance through the prism sequence, providing for a dispersion in the opposite direction from the change in index of refraction with wavelength. Brewster cut prisms can be used to minimize reflection losses and to insure that the beam does not deviate from its original path after traversing the prism combination.

This type of prism sequence can correct completely for a linear chirp on the pulse, but does not compensate for higher order frequency sweeps. A grating pair, however, can be used in the same manner as the prism sequence to compensate for the linear chirp, but in addition, its next order correction term is opposite from that of the prisms. Thus, a combination of prisms and gratings can compress the pulses down to the third order term, providing the capability to make extremely short (sub-10 fsec) pulses [13]. Careful choice of optical elements can also minimize these higher order terms; special,

carefully chosen glass components have recently been used in Ti:Sapphire systems to produce 17 fsec pulses directly from the oscillator [14].

The largest advantage of an intracavity prism sequence is that it provides essentially one parameter tuning of the pulse-width. By introducing more or less glass into the intracavity beam by translation of a single prism, the amount of positive dispersion in the CPM cavity can be easily adjusted. This has the effect of tuning the pulse width with a simple prism translation; as zero net dispersion is approached, the pulse width goes to a minimum, when excess dispersion is introduced, the pulse broadens until the CPM enters an unstable operating regime. The CPM runs stably only with net excess negative dispersion; the stable operating regime of the CPM depends strongly on the net intracavity dispersion, position of the saturable absorber jet in the focus of its sub-resonator and other cavity parameters [2]. One additional advantage of operating the CPM with excess negative intracavity dispersion is partial pre-compensation of positive dispersion which occurs in the amplifier and experimental optics. For example, running the CPM to produce its minimum pulse width of roughly 75 fsec produces an amplified pulse of 180 fsec, whereas operating the CPM with 110 fsec pulses by introducing excess negative dispersion in the oscillator leads to amplified pulses of 120 fsec duration. Adjustment of the pulse compression prisms is an integral part of the CPM operating characteristics.

B. History of the Harris Group CPM: The CPM femtosecond laser system in the Harris labs has been built, re-built and modified a number of times. The original CPM was constructed as in Figure 2.2.1, but without the cavity dumper subresonator. The mounts for all the mirrors were made from aluminum, sapphire nozzles were used

for both the gain and saturable jets and the jet catcher tubes were made from soft tygon tubing. In this configuration, the CPM laser was not particularly stable; it was necessary to realign the laser on the average of every 20 minutes. Little by little, the sources of the instabilities were discovered, and steps taken to correct them. Many of these changes are described in Rebecca Hoff's thesis [7]; additional changes important to everyday CPM operation are described below.

Over the course of several months, it became clear that temperature instabilities were one of the primary contributors to the stability problem, the chief cause lying in the use of aluminum for the mirror mounts. On Christmas day 1988, a water main break flooded the entire lab and coated all the laser optics with water, necessitating rebuilding the entire laser cavity. New mounts were designed made out of hardened tool steel, which has a coefficient of thermal expansion 8 times smaller than that of aluminum. The tool steel comes stock in 1/2" thicknesses, with the top and bottom sides flat and parallel to better than 0.001". The new mounting system was designed to be as modular as possible: 1/2" thick translation stages can be inserted in place of any of the support plates, offering extra motional degrees of freedom for any of the cavity elements. The new mounts also placed the beam height at just over 3" from the breadboard, a considerable improvement from the 5" offered by the aluminum mounts (the higher off the table the optics are, the more small vibrations in the mount bases are amplified at the mirror positions). The flatness of the new mounts also improved the stability of the laser -- the mounting pieces fit together smoothly with no room for vibrations or rocking between them. The tool steel mounts have virtually eliminated the effect of temperature fluctuations on the laser stability.

A second major change in the CPM cavity was in the nozzles and catcher tubes used for the gain and saturable absorber jets. The very thin sapphire nozzles are prone to partial clogging; tiny particles block a small portion of the nozzle exit slit, leading to turbulence in the flow downstream where the beam intersects the jet. The turbulence patterns can change over time as the clog shifts, aggregates or escapes from the nozzle, leading to significant laser instability. The sapphire nozzles were replaced by more standard stainless steel nozzles: a 300 μm Coherent nozzle for the gain jet and a nozzle squeezed to ~ 100 μm for the saturable absorber jet. The effects of changing the thickness of the saturable absorber jet on CPM operating characteristics have been well discussed in the thesis of Rebecca Hoff [7]; use of the thicker squeezed steel nozzle instead of the thinner sapphire nozzle did not have a significant effect on pulse duration. An additional cause of jet instabilities was found in the positioning of the catcher tubes. Shock waves generated from the initial collision of the jet with the catcher tube can propagate back through the flow into the active beam region. Small changes in the position of the jet or relaxation of the soft plastic in the tube led to significant instabilities in the laser alignment. By using glass catcher tubes and ensuring that the tube catches the jet at a glancing angle, problems due to the jets were practically eliminated.

In addition to instabilities, the original laser system was not able to efficiently seed the CVL pumped bow-tie amplifier. The largest problem came from the repetition rate of the CPM and the pulse width of the CVL; the CPM pulses are separated by 11 nsec in time, and the CVL pulse width is on the order of 15 nsec. This means that a second pulse from the CPM could still see gain in the amplifier, resulting in a pulse train

consisting of one high energy pulse followed 11 nsec later by a lower energy pulse, significantly interfering with the ability to do pump-probe experiments. This motivated the installation of the cavity dumper, allowing a single pulse to be switched out of the cavity without the use of an output coupler. The effects of installing the cavity dumper on the laser performance are discussed in more detail in Rebecca's thesis [7]. The important result is that single pulses with higher energies were available to seed the amplifier, providing better gain saturation in the early amplifier stages and avoiding the problem of amplifying more than one pulse. The addition of the cavity dumper also serves to stabilize the entire laser; without the output coupler intracavity losses are significantly reduced so that small fluctuations are less likely to take the cavity below threshold and upset the laser stability.

The final series of improvements to laser stability came from redirecting the air flow in the laboratory containing the laser. The room design causes a strong airflow from the ceiling to the floor directly over the CPM. By placing cardboard baffles over the ceiling vents, using large curtains around the laser table and tightening the protective box around the CPM itself these airflow problems were reduced. Using flexible hosing to redirect the CVL heat exhaust away from the CPM and toward another part of the room provided addition protection against airflow problems, and also lead to improved temperature stability in the room near the CPM. Even with most of the airflow problems solved, the CPM laser is still sensitive to sudden breezes in the room: a noticeable decrease in stability can be observed if the main lab door is left open or if the door nearest the laser table is slammed open or shut. Imbalances in the building pressure also change the flow of air in the lab, and can adversely affect the laser

stability. The combination of all the changes listed above and in Rebecca's thesis [7], however, have made the CPM laser a reliable tool for use in femtosecond pump-probe experiments.

2.3 Experimental Alignment

A. Aligning the CPM: The basic method for aligning the CPM laser from scratch is outlined well in the thesis of Rebecca Hoff [7]. Briefly, the gain subresonator is optimized first by building a linear, CW laser cavity consisting only of four mirrors: the two fluorescence collection mirrors and two end mirrors. After optimizing the power and mode of this four mirror laser, one end mirror is removed and the cavity dumper subresonator added followed by a new end mirror. After optimizing the new configuration, the saturable absorber subresonator is added in the same fashion. Once all three subresonators are optimized, the ring can be completed, and the prism compressor inserted. After all the elements are in the cavity, DODCI should be slowly added to the saturable absorber jet until good modelocking is achieved. Important details such as keeping the Z-folds in the subresonators as tight as possible to minimize astigmatism in the beam are presented in Rebecca's thesis.

When aligning the CPM at any stage, whether in a linear form for subresonator optimization or in the ring configuration, it is important to study the shapes and sizes of the fluorescent spots. When all the subresonators are properly adjusted, the two principle fluorescence spots should be well-collimated or just slightly converging; the spots' size should not significantly change in the cavity and the fluorescence should never go through a focus. A large change in size of one of the spots implies that one of

the subresonators is not confocal, and needs to be readjusted. The shapes of the spots are also important. One spot should be nearly round, appearing as a circle with a small flat portion removed. The shape of this spot should be round, as determined by the fluorescence collection mirror that is a full circle, but partial clipping of the spot on the mount holding the other collection mirror as the fluorescence leaves the gain subresonator causes a non-circular shape. The other spot has a half-moon or hourglass appearance, the shape determined by the half-circular collection mirror and possible additional clipping against one of the mirror mounts or the ion laser turning mirror. Both spots have their tops and bottoms slightly truncated after passing through the prism sequence, but their centers should remain unaltered. If either of the spots varies significantly in its appearance, it is a good indication that either the beam is clipped in an unsuitable fashion, the Z-folds are too loose causing high astigmatism or that one of the subresonators is not confocal. Getting the spots to be the right size and shape is the first step to making the CPM lase after the cavity has been altered.

When overlapping the spots, it is usually best to watch in one of the end mirrors in the linear cavity, or one of the three corner mirrors when aligning the ring. Either of the two spots can be studied in isolation by blocking the other spot with a card in front of the appropriate collection mirror in the gain subresonator. Once the nearly round spot travels all the way through the cavity and is roughly centered on all the mirrors, the end or corner mirrors can be used to adjust the overlap and start lasing action. Using the end mirror or the two corner mirrors in which the spots are not being observed, adjust the position of the hourglass spot so that it is overlapped with the nearly round spot. The hourglass spot should be slightly smaller than the nearly circular spot, and

should be positioned between the center and the truncated edge of the round spot. Once this has been achieved, the mirror being used for observation can be tweaked until a third spot, due to the complete round trip of the fluorescence through the cavity, is observed and overlapped with the first two spots. This third spot should be roughly half the size of the hourglass spot; if it is too small or too diffuse the collimation of one of the subresonators needs to be adjusted slightly. Once the three spots are overlapped lasing should occur, or there should be a characteristic glow at the overlap point indicating the near presence of lasing action. In this case, the pump power can be increased and small adjustments made with the end or corner mirrors and one subresonator translation until lasing commences.

When aligning the CPM from scratch, the 3% output coupler can be used as one of the end mirrors to let some light leak out of the cavity for power measurements. When pumping with 4.5-5.0 W of argon ion laser power, the four mirror gain-subresonator-only cavity should produce over 200 mW of power. Addition of each of the other subresonators should decrease the power slightly, until the entire ring with all three subresonators and the prism sequence should lase CW with ~100 mW of power, and the lasing threshold should be around 2 W pump power. When aligned properly, the color of the CW laser in this configuration should change from yellow to orange when the angles of the mirrors or prisms are tweaked. Power levels significantly below 100 mW or the inability to tweak the system to lase orange indicate a general cavity misalignment or degradation of the R6G in the gain jet. Note that use of higher pumping powers than 5-6 W does not necessarily lead to increased output power of the dye laser due to thermal blooming in the gain jet. See Rebecca's thesis [7] for more

details.

Day to day adjustments to the CPM should consist of tweaking only the corner mirrors, the focus of one subresonator mirror, the position of the saturable absorber jet in its subresonator, the amount of prism glass in the beam, the vertical adjustment of the Bragg cell and the ion laser turning mirror; all the other optical elements' positions, once optimized, should be left alone. The pressures of the two jets should also be the same from day to day: 42 psi for the gain jet, 22 psi for the saturable absorber. Significant changes in pressure change the shape of the jet in the beam region, and would necessitate realigning the laser cavity for the new jet configuration. Additional advice concerning alignment of the Bragg cell and adjustment of the timing electronics for maximum pulse extraction can be found in Rebecca's thesis [7].

When everything seems to be aligned correctly and the CPM is still not modelocking stably, the most likely cause is degradation of the saturable absorber dye. The dye can degrade in as quickly as two weeks of continuous laser operation, although 4 to 6 weeks is more typical. Symptoms of dye degradation include: easy saturation of the absorber as indicated by the hopping of the laser color between red (modelocked) and yellow (quasi-CW), lower lasing threshold, double pulse formation (i.e., the cavity supports two pulses in each direction, so that the pulses occur at half the cavity round trip time) and excessive sensitivity of the laser to the intracavity dispersion. When the dye is changed, it is important to flush the reservoir and remove as much of the old dye as possible; DODCI undergoes a photoisomerization reaction, and the photoisomer which builds up interferes with the ability for the remaining DODCI to act as a saturable absorber.

B. Alignment of Pump-Probe Transient Absorption Experiments: Once the CPM is aligned correctly and seeding the amplifier, the amplified output can be used for pump-probe transient absorption experiments. The basic experimental schematic is shown in Figure 2.3.1, and is described in detail in the thesis of Rebecca Hoff [7]. The detection electronics and data collection set-up for transient absorption experiments have also been described in reference 7, and are similar to those used for experiments on the picosecond laser system [3,4]. The optical alignment of Figure 2.3.1 is fairly straightforward, although care must be taken to insure that the stage is aligned correctly and that the pump and probe beams are overlapped well.

Alignment of the translation stage is important for two reasons. First, the beam must enter and exit parallel to the stage's direction of travel for accurate knowledge of the change in optical delay. If the beam leaves the stage at some angle, then moving the stage a known amount changes the relative delay by the product of the cosine of that angle and the distance the stage has moved, leading to an error in the delay calibration. Second, the beam must not translate spatially for any movement of the stage. If the beam is not well aligned onto the stage, it will move in space when the stage is translated, changing the overlap with the probe beam at the sample and leading to artificial signal changes. Note also that the beam on the stage must be well collimated; if the beam converges or diverges on the stage, then stage motion will change the spot size of the beam at the sample, leading to spurious increases or decreases in signal size.

To align the beam going onto the stage, an aperture fixed on the table and an aperture attached to the stage can be used. With the stage all the way at one end of its travel, the beam should be adjusted with the two mirrors preceding the stage until it is

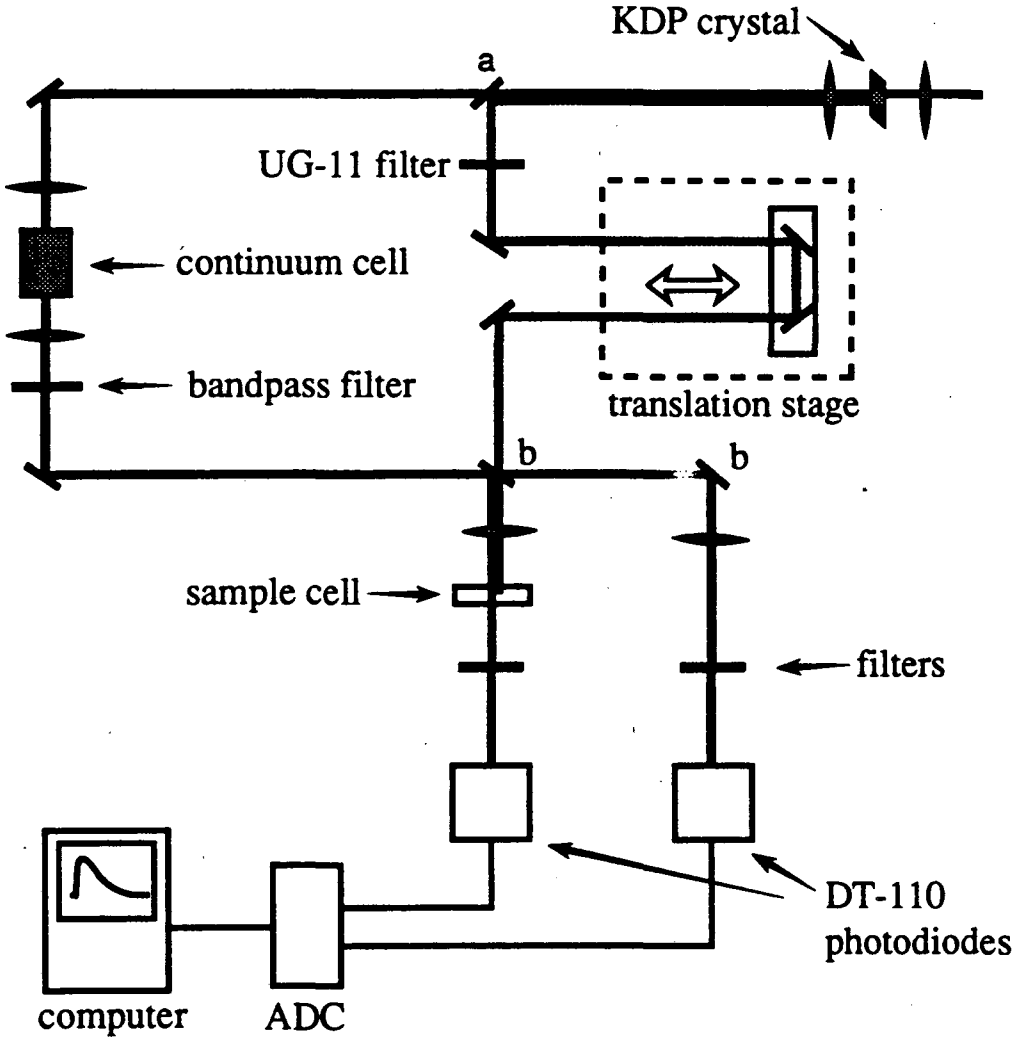

Figure 2.3.1: Experimental setup for pump-probe transient absorption. Beamsplitter 'a' separates the pump and probe beams; the pump beam travels on the translation stage, the probe beam goes through the continuum cell. The two beams are re-overlapped at recombination beamsplitter 'b', a quartz flat. Filters are used to prevent pump light or fluorescence from reaching the photodiodes.

centered on the two apertures. The stage should then be run to the other end of its travel and the position of the beam on the stage aperture checked and readjusted if necessary. This procedure should be iterated until the beam stays centered on both apertures for the entire travel of the stage, indicating correct alignment onto the stage. To align the beam leaving the stage, monitor the beam's position leaving the stage as far from the stage as possible (it is best to look several times further away then the beam travels from the end of the stage to the sample). If the beam moves detectably when the stage is run through its travel, use the mirror mounts on the stage to correct, iterating until the beam remains fixed in space for the entire travel of the stage. The spot size should also be checked to ensure that the beam is collimated on the stage; if the spot size changes when the stage is run, the recollimation optics after the doubling crystal should be readjusted until the beam is well collimated. Once the stage is aligned correctly, never change the position of the beam with the mirrors before (or on) the stage; only use optics after the beam leaves the stage or the alignment will be compromised.

To align the overlap of the pump and probe beams, a reference sample which provides large signals and has a known temporal response should be used. For visible pump, visible probe experiments, the bleach of malachite green (the same dye used as the saturable absorber in the CVL amplifier) laser dye, $\varepsilon_{620\,nm}$ = 185,000, in methanol solution can be used to provide signals of over 50% (changes in absorbance of ~ 0.3). The sample should be as concentrated as possible while still allowing enough probe light through for easy detection (usually around o.d. 1.5). This signal should have an instrumented limited rise followed by a 3.5 psec exponential bleach recovery, with a

small bleach offset. For UV pump, visible probe experiments, transient absorption of diphenylbutadiene (DPB) (discussed extensively in Rebecca's thesis as well as in chapter 5), $\varepsilon_{310nm} = 40{,}000$, $\varepsilon_{620\ nm} \approx 10{,}000$ provides signals of over 25%. For saturated DPB in hexane, this signal has an instrumented limited rise and a 465 psec single exponential decay. A quick scan of one of these test molecules should be run at the beginning and end of each day to insure that the instrument function, pulse characteristics and stage alignment have not changed during data collection.

The overlap of the pump and probe beams is the most critical factor in determining the size of the observed signals. For collinear geometries, the two beams should be overlapped on the recombination beamsplitter (quartz flat) with a mirror somewhere in the probe arm, and then the flat should be tweaked to overlap the two beams somewhere behind the sample position. This insures that the two beams are overlapped at two separate points, and hence, must lie everywhere on the same line. The focussing optics should be adjusted so that the two beams focus in as close to the same place as possible, or with the pump beam focussing just ahead of the probe beam (the pump focal spot should be just slightly smaller than the probe focal spot at the sample). For off-angle geometries, the beams should be overlapped as well as possible by eye, with the intersection as close as possible to the focal points. Once this level of overlap is achieved, the appropriate reference sample should be inserted at the intersection, and the stage set to a point a few picoseconds after tzero (for DPB, the stage position is not critical as long as the delay is after tzero since the absorption signal lasts for hundreds of picoseconds; for malachite green, it is important to be within 2-3 psec of tzero or most of the bleach dynamics will be over). If the overlap is set

correctly, there should be a spot in the probe beam due to induced absorption or induced bleaching by the pump beam which is visible to the eye. The overlap should be tweaked until this spot is centered in the probe beam, and an Airy diffraction pattern appears (this is actually the diffraction of the probe beam around the absorbing or bleaching species created in the pump beam focal spot). The central disk of the Airy pattern should nearly fill the probe beam; if it does not, the focal parameters of the pump and probe beams can be adjusted until a good pattern indicating maximum overlap is observed. From this point, the data collection program can be used to fine tune the signal size by watching the actual change in absorbance while tweaking the overlap. Once the signal size is maximized, the reference sample can be removed and the sample to be studied placed in the identical location, assuring the best possible overlap.

With the alignment complete, data collection should go smoothly. If there are any problems with the instrument function or the signal to noise, there are a few extra things that can be done to improve the signal quality. If the signal and reference beams are too tightly focussed onto the photodiodes, the photodiode will respond non-linearly, leading to a significant degradation in normalization. This can be checked by monitoring the signal directly out of the photodiodes; a long tail on the signal which extends past the A-D gate cut-off is a signature of operation in a non-linear regime. The other frequent cause of normalization problems is a ground loop between the photodiodes and the detection electronics. If the photodiodes and A-D converter are in electrical contact through both the signal cable and another route (e.g. through the optical table, etc.), the resulting loop acts as an antenna to pick up electrical noise in the

lab -- especially noise from high voltage switching in the amplifier pump laser which is synchronized to the experiment. By insuring that the photodiodes and their batteries are electrically isolated, many normalization problems can be readily cured.

Even with good normalization, there are situations in which the time resolution of the system can be significantly decreased. A noticeable smearing of the instrument function for UV pump, visible probe experiments can be a sign of a sample which is too dilute. Group velocity mismatch causes the t = 0 point to vary between the front and rear of the sample, as discussed in Rebecca's thesis [7]. This can be remedied by increasing the sample concentration so that all the pump light is absorbed in a smaller distance, or using a sample cell or jet with a smaller optical path length. An optical path length of 1 mm can cause a nearly 150 fsec sweep in tzero in quartz; the use of sample cells longer than 1 mm for two-color femtosecond experiments is not recommended.

The combination of the prescriptions presented in this chapter and the discussions in Rebecca's thesis [7] should provide a good working knowledge of the CPM laser system. Reference 2 also presents practical information about CPM alignment, especially the interplay of the saturable absorber jet and prism positions. With this chapter, I offer my best wishes to any new users of the CPM laser system.

2.4 References

1. R. L. Fork, B. I. Greene and C. V. Shank, Appl. Phys. Lett., 38, 1981, p. 671.
2. J. A. Valdmanis and R. L. Fork, IEEE JQE, QE-22, 1986, p. 112.
3. A. L. Harris, Ph.D. Dissertation, University of California, Berkeley, 1986.
4. M. Berg, Ph.D. Dissertation, University of California, Berkeley, 1986.

5. A. L. Harris, M. Berg and C. B. Harris, J. Chem. Phys., 84, 1986, p. 788.

6. M. Berg, A. L. Harris, J. K. Brown and C. B. Harris, Opt. Lett., 9, 1984, p. 50.

7. R. L. Hoff, Ph.D. Dissertation, University of California, Berkeley, 1991.

8. W. H. Knox, M. C. Downer, R. L. Fork and C. V. Shank, Opt. Lett., 9, 1984, p. 552.

9. see, e.g. R. H. Stolen and C. Lin, Phys. Rev. A, 17, 1978, p. 1448.

10. R. L. Fork, C. V. Shank, R. Yen and C. A. Hirlimann, IEEE J. Quant. Elec., QE-19, 1983, p. 500.

11. F. W. Wise, I. A. Walmsley and J. P. Gordon, Opt. Lett., 13, 1988, p. 129.

12. R. L. Fork, O. E. Martinez and J. P .Gordon, Opt. Lett., 9, 1984, p. 150.

13. R. L. Fork, C. H. Brito-Cruz, P. C. Becker and C. V. Shank, Opt. Lett., 12, 1987, p. 483.

14. C. P. Huang, M. T. Asaki, S. Backus, M. M. Murnane and H. C. Kapteyn, Opt. Lett., 17, 1992, p. 1289.

Chapter 3: Direct Observation of Fast Proton Transfer -- Femtosecond Photophysics of 3-Hydroxyflavone

3.1 Overview

Proton transfer reactions are one of the simplest chemical transformations. Ranging from simple acid-base reactions to complex isomerizations involving hydrogen atom motion, proton transfer reactions are widespread throughout chemistry. Despite their apparent chemical simplicity, subtleties in the shapes of the relevant potential energy surfaces, quantum mechanical tunneling effects and extremely high reaction rates ($>10^{11}$ s^{-1}) have made these reactions difficult to understand on a fundamental, microscopic level [1]. This suggests that femtosecond spectroscopic techniques, such as those described in Chapter 2, can be used to directly observe these proton transfer reactions, and thus can provide further insight into the microscopic details and mechanisms of this very general class of chemical reactions.

To study proton transfer with femtosecond time resolution, a reaction must be found that can be initiated by absorption of a femtosecond laser pulse. If the reaction is bi-molecular (e.g. a simple acid-base reaction such as HCl + NaOH --> H_20 + NaCl), then the rate becomes essentially controlled by diffusion; that is, how long it takes for the reacting species to find each other in solution. The pump-probe transient absorption technique described in Chapter 2 is unsuitable for studying such a reaction. The actual reaction takes place in $< 10^{-11}$ s, while the diffusional motion leading up to the reaction can take up to 10^{-6} s. This makes it impossible to probe the interesting part of the reaction; there is no way to get a sufficient concentration of species reacting all during

the same few picoseconds for study with the pump-probe technique. This problem can be avoided, however, if the proton transfer reaction can be controlled with the laser pulses. What is needed is a molecule ready to undergo proton transfer, but which does not do so until after photoexcitation with a femtosecond laser pulse. In this way, the entire ensemble of molecules will undergo proton transfer simultaneously, and the pump-probe transient absorption technique can be used to monitor the progress of the reaction on the femtosecond time scale.

Fortunately, there exists a large class of molecules with adjacent proton donor and proton acceptor sites which have the potential for undergoing proton transfer after photoexcitation [1]. Such a molecule is depicted schematically in Figure 3.1.1. In Figure 3.1.1, the proton donor and acceptor sites are identical (the oxygen atom in the carbonyl group becomes hydroxy-like upon accepting the proton, while the oxygen atom in the hydroxy group becomes more carbonyl-like after proton transfer), and R and R' represent generic organic portions of the molecule. If the groups R and R' are the same, then the molecule is symmetric, and there is no reason that the proton should prefer to reside on either of the two oxygen atoms. The proton transfer potential energy surface and reaction rate can be studied in this case by IR spectroscopy, where tunneling splittings can provide important information about the proton transfer process. If the groups R and R' are different, however, then the molecule can have vastly different electronic properties depending on the location of the proton, and transient absorption spectroscopy can be used to monitor the change in electronic structure of the molecule during the proton transfer process.

For many molecules of the class of Fig. 3.1.1 when the groups R and R' are

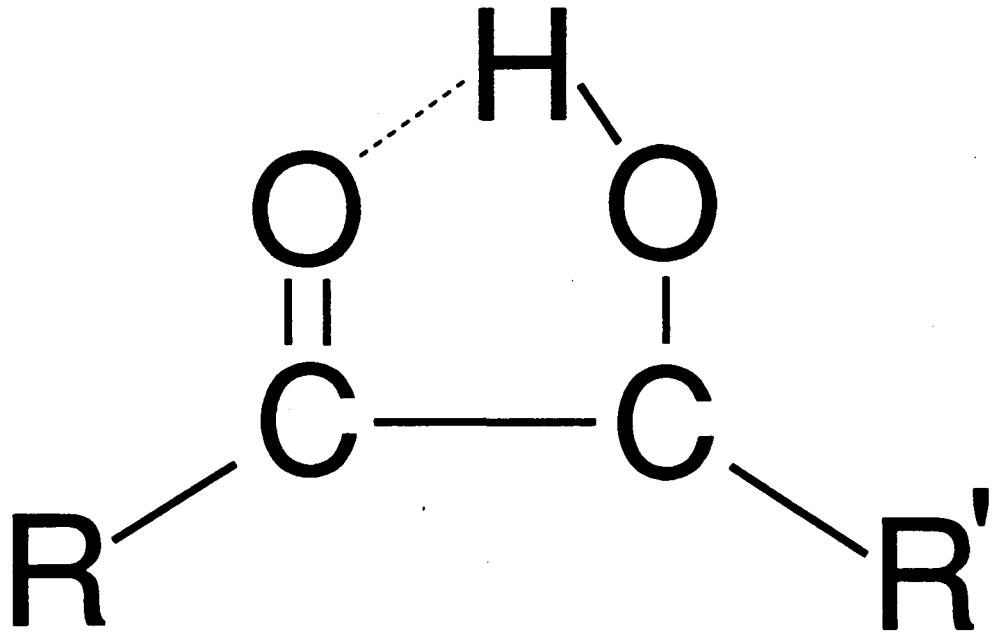

Figure 3.1.1: Schematic representation of a molecule with adjacent proton donor and proton acceptor sites. R and R' represent generic organic groups. Molecules with Nitrogen atoms instead of Oxygen atoms as proton donor and acceptor sites, such as HBT, also fall into this class.

different, the proton affinities of the two sites can change upon photoexcitation of the molecule, leading to excited state proton transfer (ESPT) [2,3]. ESPT has been observed for many molecules of the class of Figure 3.1.1 [1], one of the most widely studied of which is 3-hydroxyflavone [4-32]. Indeed, when combined with ultrafast spectroscopy, this class of molecules seems to offer the best chance for femtosecond observation of proton transfer reactions. Recently, the rate of intramolecular proton transfer in 2-(2'-hydroxyphenyl)benzothiazole (HBT) has been measured to be 170 ± 20 fsec by both transient stimulated emission and transient IR spectroscopy, demonstrating the need for femtosecond time resolution to measure ESPT processes [33,34].

Since the discovery of ESPT in this molecule in 1979 [4], numerous steady-state and kinetic experiments have been performed to determine the nature of the proton transfer in this molecular system [5-32]. These papers have often presented contradictory results and interpretations, leading to much confusion about the mechanism and rate of ESPT in 3HF as well as about the role of the solvent environment on the ESPT. Some of these studies, which will not be subsequently discussed, have focussed on the ground state reverse proton transfer which occurs after the ESPT is complete [8,18,21,27,28,30]. There have also been several studies of the triplet system of 3HF, in which there is an entirely separate set of energy levels and a different, triplet excited state proton transfer [26,28,29]. Since intersystem crossing to the triplet manifold does not play an important dynamical role during the first few picoseconds after photoexcitation, the role of triplet states in the proton transfer dynamics will not be considered further in this thesis. In the following section, a

historical account of the research on proton transfer in 3HF is given, with an emphasis on the evolution of the proposed mechanism of ESPT as more experimental information became available. This is followed by a brief recap of the experimental apparatus used to measure the ESPT in 3HF, a summary of the results obtained, and a discussion of the results which reconciles much of the conflict present in the literature.

3.2 History of 3-Hydroxyflavone

A. Background: 3-Hydroxyflavone (3HF) is a compound that occurs naturally in the petals of flowers, and is partially responsible for giving flower petals their bright fluorescent colors. The structure of 3HF in its ground and electronic excited states is shown in Figure 3.2.1. In the ground state (Figure 3.2.1 (a)), the proton of interest resides on the 3-hydroxy group. Upon photoexcitation, the proton affinities of the carbonyl and hydroxy groups switch, and the proton transfers to the carbonyl oxygen at the chromone 4-position. Several resonance configurations of the tautomeric structure, the excited state structure after the proton transfer, are shown in Figure 3.2.1 (b). The tautomer structure has no resonance configurations without charge separation; all the possible structures are zwitterionic in nature. This has lead to speculation that dielectric properties of the solvent or that addition of electron-withdrawing groups on the flavone backbone could significantly alter the rate of ESPT. Since the phenyl group is also involved in providing resonance stabilization for the charge separation in the excited state, there has been additional speculation that the ESPT may be modulated by large-amplitude phenyl twisting motion. Both of these points will be addressed further in sections 3.2.D and 3.5.A.

(a) Normal 3 - Hydroxyflavone (ground state)

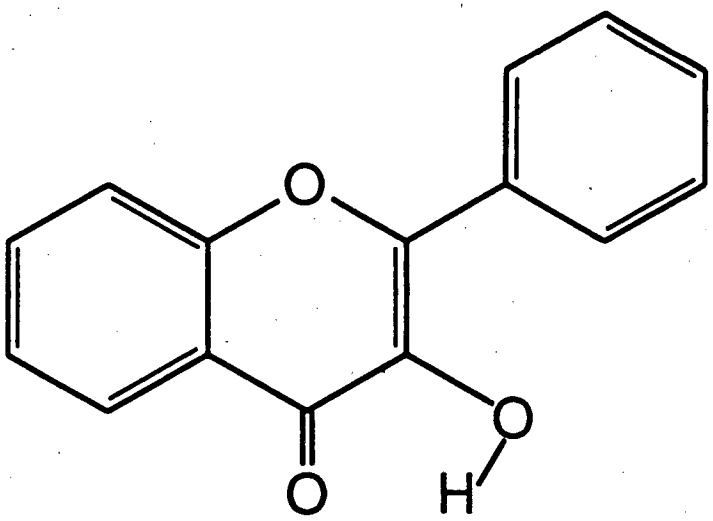

(b) 3HF Tautomer (excited state)

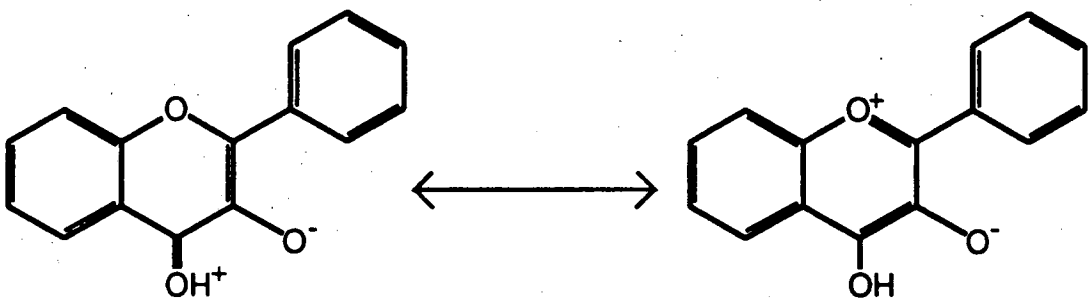

Figure 3.2.1: (a) Structure of 3-hydroxyflavone in the ground state (normal configuration). (b) 2 of the possible resonance structures of excited state 3-hydroxyflavone (tautomer configuration).

The UV-visible absorption spectrum of 3HF is shown in Figure 3.2.2 [4]. The spectrum consists of a single intense $\pi \rightarrow \pi^*$ absorption centered near 330 nm, with evidence for a high frequency vibrational progression which is probably a C=C stretching mode. Since tautomerization requires eventual breaking of the hydroxy bond, it is surprising that there is no evidence in the absorption spectrum for coupling of the electronic transition to the O-H stretch coordinate. This is further borne out by resonance Raman data, which shows no enhancement of any modes with O-H stretch character -- the resonance Raman spectrum does not change upon deuteration [48]. This implies that the reaction coordinate for the ESPT consists of some other motion than the O-H stretch; after excitation, the molecule moves on some complicated internal coordinate and tautomerization (breaking of the O-H bond) occurs only after this motion is complete. This idea is at odds with the usual picture of proton transfer, and will be discussed in more detail in section 3.5.

After absorption of a UV photon, 3HF has the unusual property of fluorescing in two distinct bands in the blue (410 nm) and green (540 nm) spectral regions [4,5]. A fluorescence spectrum of 3HF demonstrating this phenomenon is shown in Figure 3.2.3 [4]. To explain this dual fluorescence, Sengupta and Kasha proposed that 3HF undergoes ESPT [4]. They noticed that the blue fluorescence band is essentially the mirror image of the absorption spectrum and has only a small Stokes' shift; it is typical for the emission from a large organic molecule. The green fluorescence band, however, is broad and featureless, and is Stokes shifted by several thousand wavenumbers. This implies that the green emission is from a state which has undergone significant relaxation and has no memory of the initially prepared excited

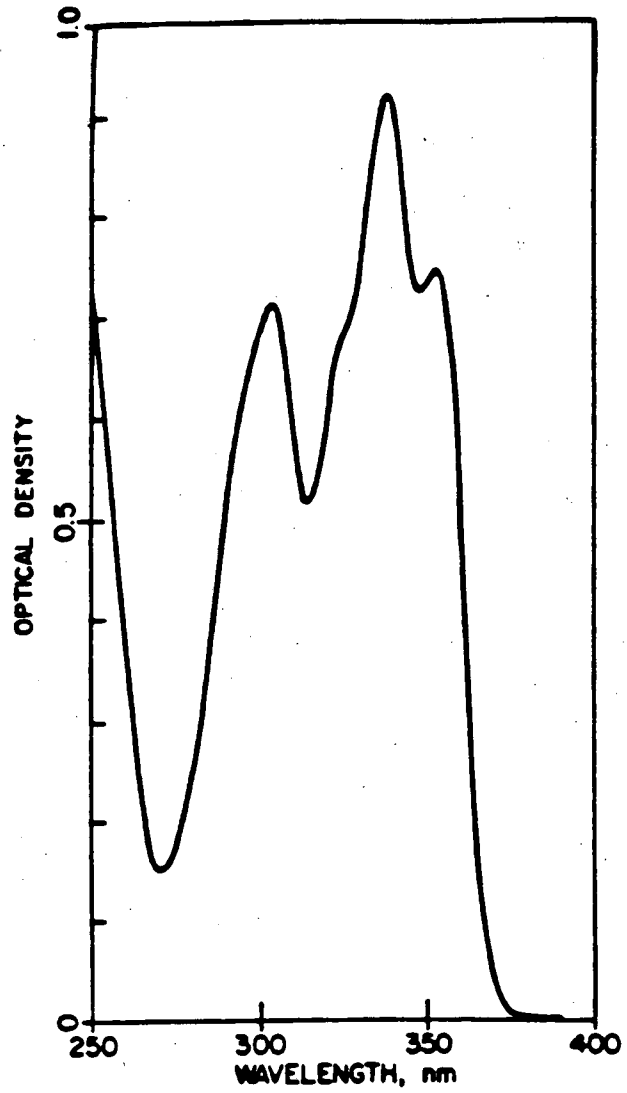

Figure 3.2.2: UV-visible absorption spectrum of 3-hydroxyflavone in solution. Excitation for transient absorption experiments was at either 295 nm or 310 nm.

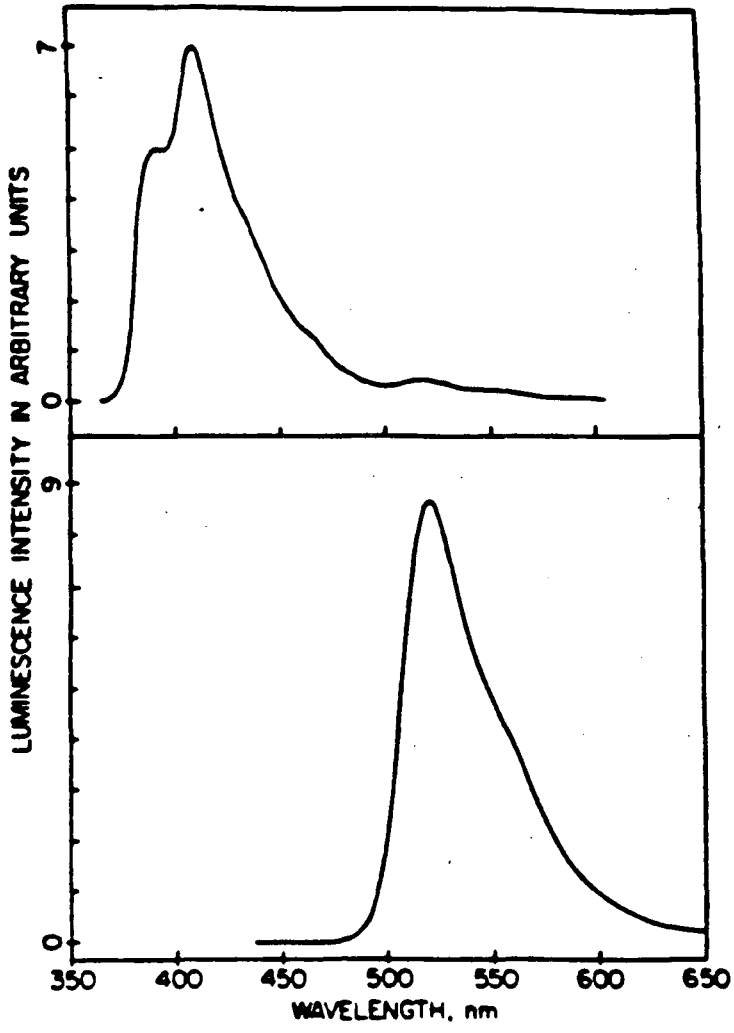

Figure 3.2.3: Emission spectra of 3HF showing blue (410 nm) "normal" emission (top) at 77 K, and green (540 nm) tautomer emission at room temperature.

state. So, Sengupta and Kasha assigned the blue emission to the excited, normal form of the molecule, whereas the green emission was assigned to the tautomeric species produced after ESPT [4]. This hypothesis is summarized by the energy level diagram depicted in Figure 3.2.4.

Sengupta and Kasha also noted that in a room temperature methylcyclohexane solution only the green tautomeric luminescence was present [4]. When frozen into a matrix at 77 K, however, excited 3HF only gives off the normal blue emission [4]. Sengupta and Kasha speculated that this was due to some type of viscosity effect; the large viscosity of the rigid matrix was shutting off some large amplitude motion of the molecule necessary for the proton transfer. Upon deuteration of 3HF, Sengupta and Kasha observed a mixture of the blue and green emission [4]. The amplitude ratio of the blue to the green emission changed when 3HF was in methanol (MeOH) versus methanol-*d* (MeOD) solvents. This suggests that hydrogen-bonding interactions with the solvent also play an important role in mediating the ESPT process.

Since the work of Sengupta and Kasha, several molecules of the class of Figure 3.1.1 have been shown to have this same dual fluorescence property [1]. It is now well-accepted that the presence of two distinct emission bands is a signature of ESPT. To learn more about the mechanism and rate of ESPT, the next logical course is to time-resolve the decay of the blue, normal emission or the rise of the green, tautomeric emission. 3HF was the first molecule on which this type of study was performed, leading the way to a better understanding of proton transfer.

B. Early Time-Resolved Luminescence Studies of 3HF: The first time-resolved luminescence experiments on 3HF were performed by Woolfe and Thistlethwaite [6].

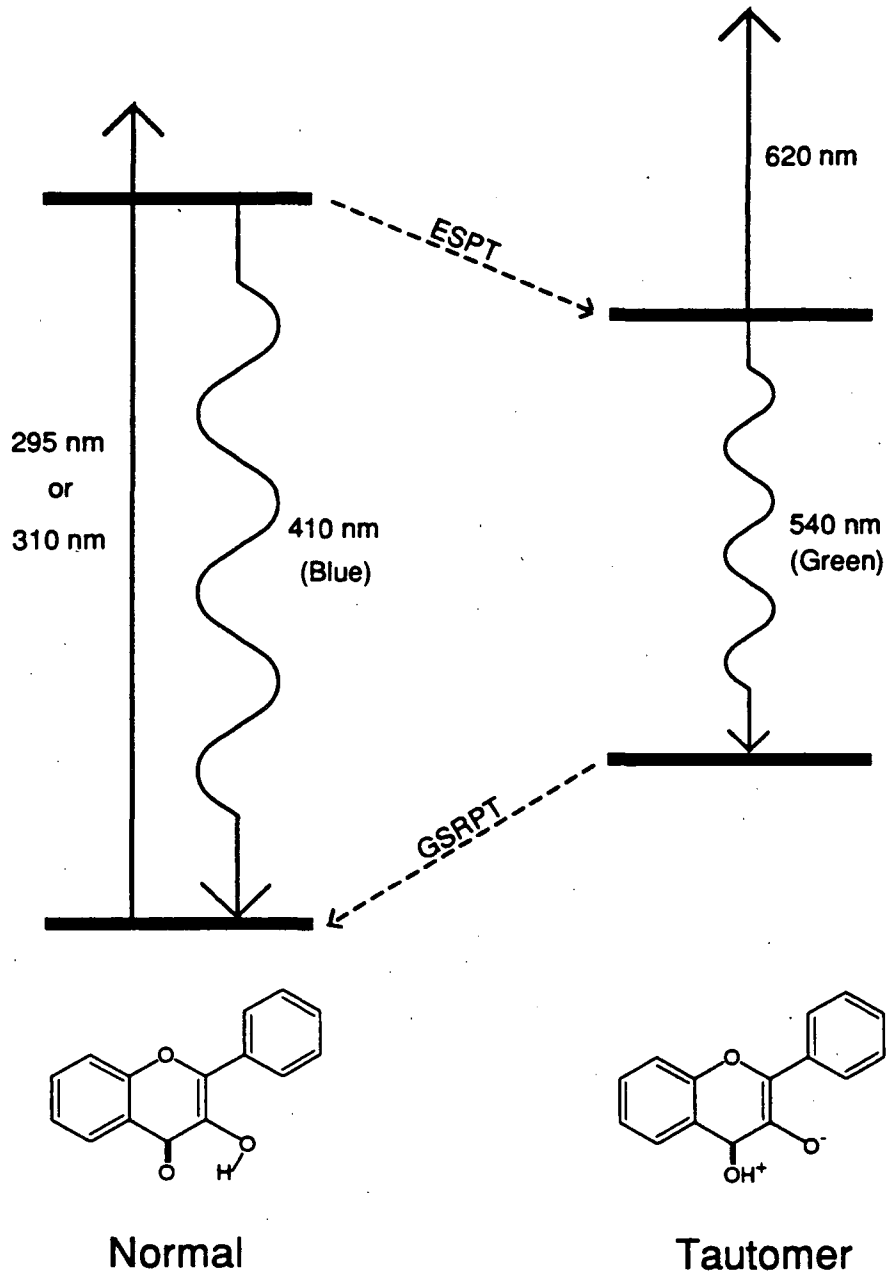

Figure 3.2.4: Energy level schematic for 3HF. UV excitation of normal 3HF leads to either blue fluorescence or excited state proton transfer (ESPT). After ESPT, excited tautomers can emit green fluorescence and undergo subsequent ground state reverse proton transfer (GSRPT). Excited tautomer formation can be monitored by 540 nm emission or 620 nm absorption.

With the use of a streak camera, they were able to measure the decay of the normal emission and the corresponding rise of the emission from the tautomer. By fitting their results to a simple kinetic model in which the excited normal state decays directly into the tautomeric form, they computed ESPT rate to be approximately 70 $psec^{-1}$ for 3DF in MeOD [6]. This result is surprisingly slow; it indicates that there is a significant barrier to proton transfer. The few other proton transfer reactions studied to that point indicated rates faster than available time resolution, i.e. $>10^{11}$ s^{-1}. Taking advantage of the slower observed rate for 3HF, Woolfe and Thistlethwaite also performed temperature and solvent dependent experiments [6]. By doing so, they were able to construct an Arrenhius plot and assign an activation energy to the proton transfer. They also determined that the activation barrier to ESPT was different in different solvents, suggesting that the hydrogen-bonding interactions and solvent viscosity play an important role in the ESPT.

Subsequent work with improved time resolution was performed by Barbara et al [9]. Barbara's group used fluorescence upconversion to time-resolve both the tautomer and normal luminescence. For 3HF at low temperatures (144 K), they found dual exponential kinetics for the growth of the tautomer emission, one component limited by their 25 psec instrument resolution, the other component taking tens of picoseconds in reasonable agreement with the results of Woolfe and Thistlethwaite. Temperature and solvent dependent experiments also lead to calculated activation energies, but the results differed greatly from those of Woolfe and Thistlethwaite, in some cases by an order of magnitude [9]. Barbara et al. fit their results to a complicated kinetic scheme involving two coupled routes to tautomerization. Noting a deuterium isotope effect on

the ratio of the two kinetic components [13], Barbara's group concluded that there is a large intrinsic barrier to ESPT in 3HF, and that solvent viscosity, polarity and hydrogen-bonding ability could further increase the barrier. The ratio of the proton to deuterium transfer rate, however, was essentially temperature independent [13], a result not expected from the standard picture of proton transfer.

Further experiments were carried out by Itoh et al. [7,8,21] and Salman and Drickamer [10,11]. These authors also studied the ESPT of 3HF in different environments, and found differing activation barriers from the above studies, and differing solvent dependent trends. The wide variety of published results and kinetic models describing ESPT in 3HF made it apparent that something more was needed to understand proton transfer in this system.

C. Effect of Hydrogen-Bonding Impurities: Reconciliation of these widely varying results came from an experiment performed by McMorrow and Kasha [12]. McMorrow and Kasha found that in highly purified and dried hydrocarbon solvents, no emission from the normal form of 3HF is observed, even in frozen matrices at low temperatures. In an unpurified spectrophotometric grade solution, however, only the normal luminescence was observed, indicating that some impurity in the solution was responsible for shutting off the proton transfer and trapping excited 3HF in its normal form. By titrating the carefully purified solution with hydrogen bonding impurities (water or MeOH), McMorrow and Kasha determined that interaction with hydrogen bonding species is responsible for stopping the proton transfer, leading to normal emission from excited 3HF [12]. The amount of impurity necessary to quench the proton transfer is stoichiometric; essentially only one hydrogen bonding impurity

molecule per 3HF molecule could stop the ESPT. The intrinsic proton transfer in non-polar solutions, however, must be exceedingly fast since even at low temperatures only the tautomeric emission is present, indicating that ESPT happens too quickly for emission to occur from the normal form of the molecule.

McMorrow and Kasha developed a simple picture of the excited state potential energy surface of 3HF to explain these results, presented in Figure 3.2.5 [12]. In the rear of the figure, the solvent-3HF hydrogen-bonded complex is locked into the normal form in the excited state, the barrier to tautomerization is very large. Only the blue, normal luminescence occurs from this complex. Motion along the solvation coordinate (out of the plane of the figure) breaks the solvent-3HF hydrogen bond(s), producing free 3HF. The free 3HF molecule then undergoes rapid tautomerization, producing only the green, tautomeric emission.

This picture can be used to successfully explain the contradictory results obtained in the time-resolved luminescence studies. Rather than measuring the barrier to the intrinsic, rapid proton transfer, the results of the above studies were altered by the presence of hydrogen bonding impurities which were artificially slowing the proton transfer rate. The activation energies computed were most likely the barrier for the rate limiting step in the ESPT process, the breaking of the 3HF-solvent hydrogen bond (motion along the solvation coordinate in Figure 3.2.5), not the intrinsic barrier to ESPT. The breaking of solvated complex is most certainly thermally activated, and the height of the solvation barrier in Figure 3.2.5 is probably solvent dependent as well. Since the different studies probably had differing amounts and types of hydrogen bonding impurities, the observed activation energies for this desolvation process were

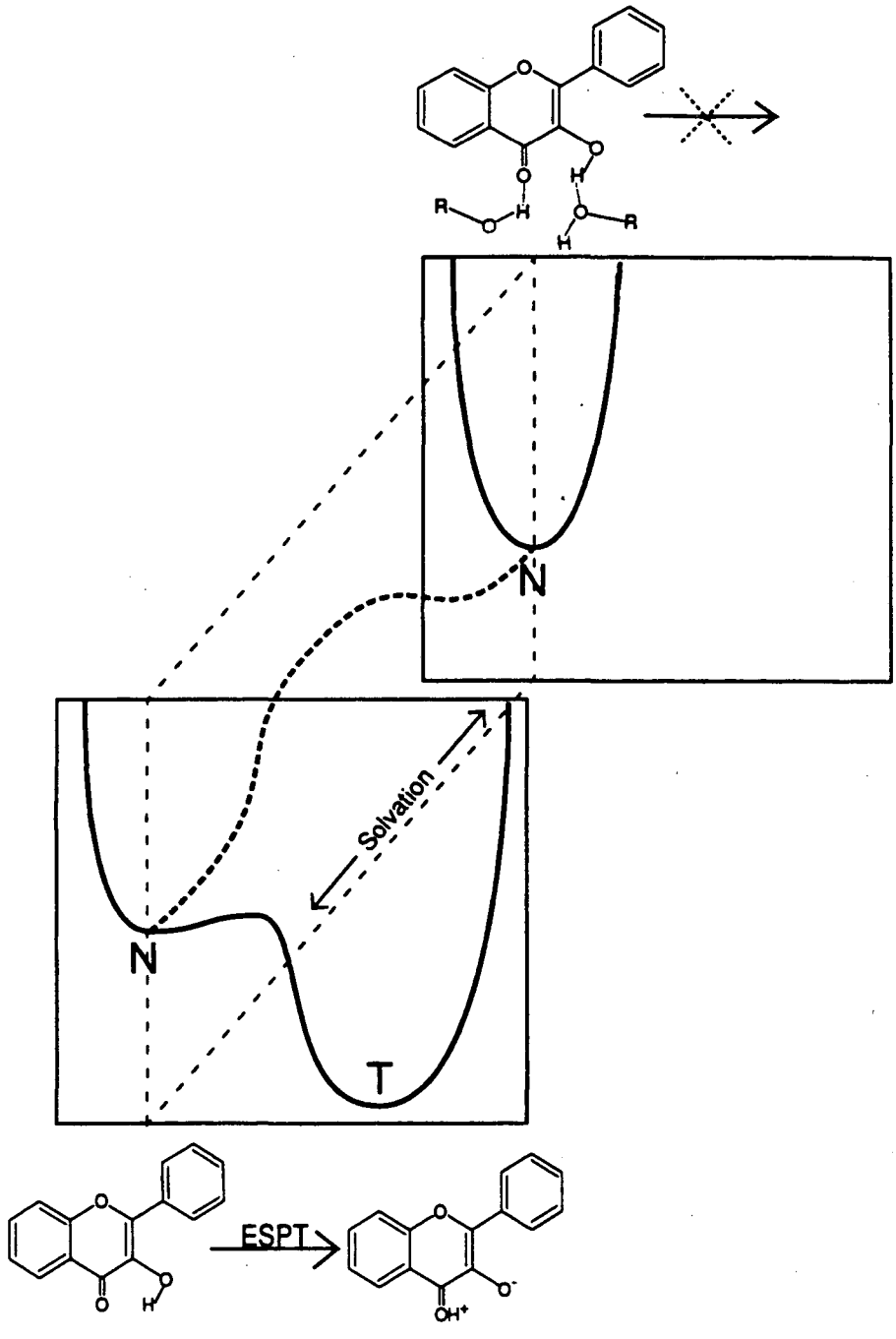

Figure 3.2.5: Effect of H-bonding impurities on the excited state surface of 3HF. 3HF-solvent H-bonded complexes cannot undergo ESPT (rear surface), but after desolvation (motion out of the plane of the page), ESPTcan occur on the free molecule's excited state surface (front surface). Thermal activation is required to overcome the barrier for desolvation. See reference 12.

measured differently, leading to the apparent contradictions in the literature.

D. Attempts to Measure the Intrinsic ESPT Rate: With the knowledge that the intrinsic proton transfer rate was rapid and that previous studies were measuring desolvation rates, not ESPT, several groups set out to investigate the intrinsic proton transfer rate of 3HF. To avoid problems with hydrogen-bonding impurities, Barbara's group performed a series of studies on 3HF in hydrogen-bonding solvents [14,15]. Barbara's group again found dual ESPT kinetics, with a fast, time-unresolved component and a slower kinetic component due to de-solvation. By studying this slower component as a function of temperature and solvent, they determined that the activation barrier for this slower ESPT was directly related to the hydrogen-bond donating ability of the solvent, but not to the solvent viscosity or dielectric constant [14]. This is in agreement with the picture of McMorrow and Kasha; in solvents with better H-bond donating ability, the 3HF-solvated complexes are more tightly bound and the activation energy to desolvate the 3HF for subsequent ESPT is higher. The lack of a rate dependence on solvent viscosity and dielectric constant implies that large amplitude motion of the 3HF is not important to this slower, ESPT process.

To further investigate this idea, Barbara's group also performed a series of experiments on substituted 3HF's [15]. Substitutions on the phenyl ring in all positions except the 2 position (ortho to the phenyl's attachment to the chromone backbone) made virtually no difference to the ESPT rate. Substitution at the 2 position, however, throws the phenyl group out of plane due to steric hinderance, and may also sterically interfere with how tightly the solvent can hydrogen-bond to the substituted 3HF. The slow ESPT rates of the 2-substituted 3HF were faster, indicating that

indeed, the substituted 3HF-solvated complex is more weakly bound than the unsubstituted, in agreement with the above results [15]. Barbara's group also speculated that the phenyl torsional angle is important to the energetics of the ESPT, but could not make any definitive statements about the importance of phenyl torsion to the dynamics of the proton transfer.

Several groups also set out to resolve the fast ESPT component which was not studied by Barbara's group. McMorrow, Dzugan and Aartsma used an optical Kerr shutter to time resolve the tautomer luminescence from excited 3HF in the absence of H-bonding impurities [20]. At room temperature, they determined the rise of the green emission to be < 8 psec, while at 77 K, they claimed to measure a tautomer emission rise of 37 psec. This would imply that there is barrier to the intrinsic proton transfer, and that the intrinsic ESPT can be thermally activated. The instrument function of McMorrow et al.'s apparatus, however, is essentially the convolution of two 35 psec Gaussians, giving a net time resolution of roughly 50 psec [20]. Thus, the low temperature tautomer rise times they obtained were by deconvolution of a signal faster than the instrument's capabilities, a risky procedure at best.

These results were called into question by the work of Dick and Ernsting [22]. Dick and Ernsting isolated 3HF in an Ar matrix at 15 K, and used 250 fsec pulses to excite the 3HF and a streak camera to time resolve the tautomeric emission. They were able to determine that the tautomer emission rise was faster than their 2.5 psec instrument resolution, even at 15 K [22]. This implies that there is essentially no barrier the intrinsic ESPT process and that thermal activation of the proton transfer is not necessary. To further test this idea, Ernsting and Dick isolated 3HF in a jet-cooled

molecular beam, and measured the fluorescence and fluorescence excitation spectra of the free molecule [23]. They found no normal emission from the free 3HF, in agreement with the idea of a barrierless ESPT. In addition, they observed several vibrational progressions in the fluorescence excitation spectrum. By fitting the observed lines to Lorentzian lineshapes, they calculated that the lines were lifetime broadened by a process taking roughly 1.3 psec, which they attributed to the intrinsic ESPT rate [23].

E. Isolation of 3HF-Solvent H-Bonded Complexes: To learn more about the nature of both the intrinsic proton transfer and the slower proton transfer in the 3HF solvated complexes, Brucker and Kelley performed a set of experiments to study ESPT in isolated free 3HF and in 3HF-solvent complexes of known stoichiometry [24,25]. By dissolving 3HF in an Ar matrix in 10 K, Brucker and Kelley were able to reproduce the results of Dick and Ernsting; they found that the tautomer emission rise time was less than their instrument response of a few picoseconds [24]. By then introducing tiny amounts of MeOH [24] (or NH_3 [25]) and annealing their matrix, Brucker and Kelley were able to prepare and characterize both monosolvated ($3HF(MeOH)_1$) and disolvated ($3HF(MeOH)_2$) 3HF hydrogen-bonded complexes. Proposed structures for these solvated complexes are shown in Figure 3.2.6. Brucker and Kelley found only tautomeric emission from the monosolvated 3HF, and determined that the rise of this emission was faster than a few psec, indicating that ESPT was essentially unaffected by the presence of one H-bonded MeOH molecule. For the disolvated species, however, only the normal emission was observed, indicating that the 3HF disolvated complex is unable to undergo ESPT [24]. This is

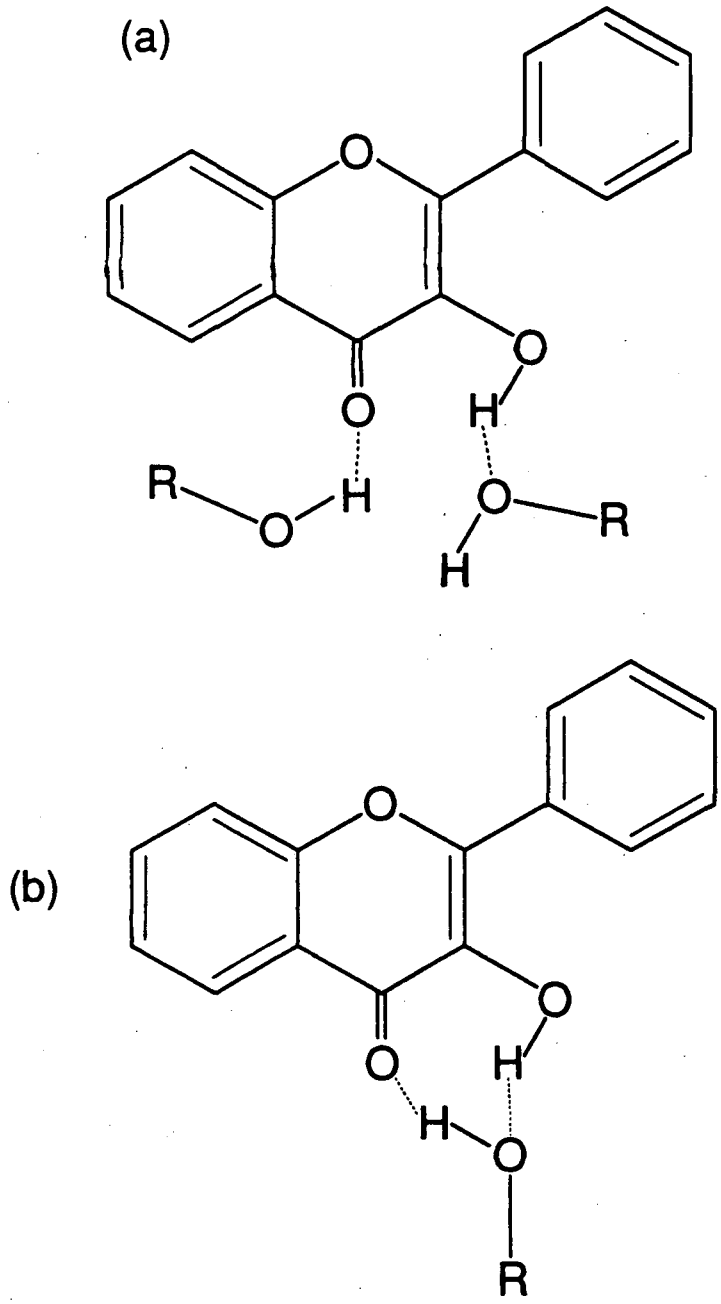

Figure 3.2.6: (a) Typical proposed structure for 3HF-MeOH disolvated complex. (b) Typcial proposed structure for cyclically H-bonded 3HF-MeOH monosolvated complex.

consistent with the picture proposed by McMorrow and Kasha (Figure 3.2.5). At 10 K, there is not enough thermal energy to surpass the barrier on the solvation coordinate, so the 3HF disolvate can not undergo proton transfer. Upon heating, one or both of the 3HF-MeOH hydrogen bonds can break, and the resulting free or monosolvated species can then undergo rapid tautomerization.

Kelley's group has also studied ESPT in 3HF in nitrile solvents which are hydrogen bond accepting but not hydrogen bond donating [16]. In these solvents, they find that the intrinsic ESPT is slowed enough to time-resolve with their instrument, and they explain the observed solvent dependence with a Marcus-like solvent polarization fluctuation model.

With the isolated study of the 3HF-solvent complexes, a clear picture of how ESPT works in this system was beginning to emerge. There still remained the question, however, of exactly what is the intrinsic ESPT rate, and which molecule coordinates are important to both the intrinsic and solvated ESPT. The experiments described below provide the first measurement of the intrinsic ESPT for both the free molecule and the monosolvated complex.

3.3 Experimental

A. Femtosecond Laser Apparatus: The apparatus for the femtosecond experiments has been previously described in Chapter 2, and in the thesis of Rebecca Hoff [35]. Briefly, the light source for the femtosecond experiments consists of a home built cavity-dumped, colliding pulse modelocked ring laser [36,37], amplified in a 6 pass bow-tie amplifier [38] pumped by a copper vapor laser (Metalaser). Partial

pre-compensation of the group velocity dispersion in the amplifier and experimental optics can be accomplished by careful adjustment of the prisms in the oscillator. With this excess negative dispersion, the oscillator produces 90 fsec pulses dumped at an 8 kHz repetition rate. Timing between the oscillator, cavity dumper and copper vapor laser is controlled by a digital delay generator (SRS DDG535) and standard NIM electronics. The final light output consists of 620 nm, 100 fsec, 3 μJ pulses at 8 kHz. This light is focussed into a thin (300 μm) KDP crystal to produce 400 nJ pump pulses at 310 nm. The residual fundamental light is attenuated by neutral density filters to provide probe pulses with energies of a few nJ.

The 310 nm pump light was passed through a variable delay stage with 1 μm resolution (Klinger MT150) before arriving at the sample. The probe light was split into signal and reference beams, collected on large area photodiodes (EG&G DT-110) and processed by a 386 computer-controlled gated integrator (LeCroy CAMAC 2323, 4300 and 4301). Probe light levels outside a preset range were rejected from data collection. Normalization of the data was achieved on every laser shot; the typical spread (± one standard deviation) in the normalized ratios for 100 shots was 0.2%.

Transient absorption data was collected in the following manner. 250 normalized laser shots were averaged for a single data point, the delay between the pump and probe pulses varied, and then another 250 shots were averaged at the new stage position until an entire scan was completed. 10-40 of these scans (2500-10000 averaged laser shots) were averaged together in the results presented below, with the stage moving in opposite directions every other scan to account for any forms of long term drift.

The pump and probe beams crossed through the sample at a 10° angle; this

prevented the formation of photoproducts where the pump beam intersected the cell wall from affecting the probe normalization. The beams were focussed into the sample with a 15 cm focal length lens, giving an estimated focal spot size of 50 μm. Typical signal sizes were changes in absorbance on the order of one percent. The observed signals were found to vary linearly in size with pump pulse intensity and were independent of the probe intensity, indicating that signals were not due to multiphoton processes. Blanks were run on the pure solvents and no signals were detected.

Polarization experiments were performed with a 1/2 wave plate used to rotate the probe polarization relative to that of the pump. These experiments, and the effect of the 1/2 wave plate on the time resolution of the instrument are discussed in section 3.5.C. The experiments reported below were performed without the 1/2 wave plate, leaving the relative polarizations of the pump and probe beams perpendicular, as produced by type II doubling in KDP.

B. Picosecond Laser Apparatus: The light source used for the picosecond transient absorption and stimulated emission experiments has also been described previously [39,40]. Briefly, a modelocked argon ion laser synchronously pumps a dye laser to produce 1-2 psec pulses at 590 nm. These pulses are amplified in a 3 stage dye cell amplifier pumped by a 10 Hz, Q-switched Nd:YAG laser. Final output consists of pulses ~1 psec in duration with ~1 mJ/pulse at 10 Hz. The light is doubled in a 1 mm thick KDP crystal, producing 0.1 mJ, 295 nm pump pulses. The residual fundamental light is focussed into a 5 cm cell containing water or acetone to generate a white-light picosecond continuum. Bandpass interference filters, 10 nm FWHM, are used to select a portion of the continuum to use as the probe light. Data collection is performed

in a manner similar to that described above.

The pump and probe beams passed through the sample collinearly. Care was taken to run blank measurements on the neat solvent samples; large pump intensities can produce multiphoton ionization in pure solvents, resulting in large transient absorption signals from solvent cations and/or solvated electrons. Pump power intensity was attenuated with neutral density filters until no transient signals were observed in the neat solvents. Typical pump pulse energies used in the experiments were 3-8 μJ. The addition of a strong UV absorbing species (like 3HF) should further prevent interfering signals from the solvents. Typical signal sizes obtained with this system were changes in absorbance or gain on the order of a few percent. There were usually 200-1000 laser shots averaged per point in the data presented below.

C. Materials: Methylcylcohexane (99+%) (MCH) was obtained from Aldrich, and purified by drying over $CaSO_4$ and molecular sieves. Dry nitrogen was bubbled through the MCH for at least 1 hour prior to use, and the MCH was stored under dry nitrogen between uses. This MCH was free of fluorescent impurities. As pointed out in reference [12], even trace amounts of hydrogen bonding impurities in non-polar solvents can have a dramatic effect on the ESPT dynamics of 3HF. Observation of bi-exponential ESPT kinetics in MCH indicates that these purification efforts were not completely successful in removing all traces of polar contaminants. All of the MCH experiments reported in this paper are thus affected by the trace amounts of hydrogen bonding substances present. The manner in which these impurities affect the results is discussed at great length in the next section.

3-Hydroxyflavone (CAS [577-85-5]) was obtained from Aldrich, and purified by

multiple recrystallizations from the purified MCH. Spectroscopic grade methanol (MeOH) and methanol-*d* (MeOD), free from fluorescent impurities, were obtained from Fisher and used without further purification.

Samples were 20 mL of $5x10^{-5}$-$5x10^{-4}$ M 3HF/MCH or 3HF/MeOH or 3DF/MeOD solution, flowed at ≥5 mL/min. through a 1 mm x 1 mm quartz cell (Hellma) with a peristaltic pump (Cole-Parmer) and Viton tubing. This ensured that a fresh sample volume was being probed every laser shot at 10 Hz, and every few laser shots at 8 kHz. The air-tight solution reservoir was continuously purged with dry nitrogen throughout the course of the experiment. All experiments were performed with the samples at room temperature. UV-visible absorption spectra of the samples did not show any significant changes before and after exposure to ultraviolet light.

3.4 Results

A. Picosecond Transient Absorption and Stimulated Emission: In order to probe the dynamics of ESPT, time resolved stimulated emission spectroscopy to observe the growth of the green tautomer fluorescence (Figure 3.2.4) was used. 3HF is excited with the picosecond laser second harmonic at 295 nm, and the tautomer fluorescence build-up is probed at a variable delay with a green picosecond pulse. To more directly compare the results to previous fluorescence [6-9,13-16] and stimulated emission [17-19] work done with poorer time resolution, a probe wavelength of 540 nm was chosen. The data are plotted as the change in absorbance of the sample, or $\Delta A = -\log[I/I_0]$ (I_0 = intensity of the probe pulse before the sample, I = intensity of the probe pulse after passing through the sample) as a function of delay time between the

pump and probe pulses. Since there are no ground state tautomer molecules initially present, formation of excited state tautomers by ESPT leads to a population inversion. The 540 nm probe pulses can undergo gain as they pass through the sample since they are amplified by stimulated emission, leading to negative changes in absorbance. All the data are fit to a dual exponential rise and single exponential decay, convoluted with a 1.1 psec Gaussian representing the instrument function. The fitting procedure used is summarize in Chapter 7. The results of all the fits are summarized in Table 3.1.

A typical picosecond transient stimulated emission scan of 3HF in MCH is shown in Figure 3.4.1. The emission shows a dual rise, with the slower rise component comprising 35% of the total gain signal. Comparison of the fast rise time to the instrument function (transient absorption of diphenylbutadiene (DPB) in hexane) shows that the fast rise component is not time resolved (Figure 3.4.1 inset). Assuming a δ-function response in DPB, our instrument function fits nicely to the convolution of two 0.8 psec gaussian pulses. Thus, the tautomer fluorescence rise time, and hence, the fast ESPT time must be significantly faster than 1 psec at room temperature. This extends previous upper limits obtained at low temperatures [20-22,24].

Picosecond stimulated emission spectroscopy also allows measurement of the fluorescence lifetime of the 3HF tautomer in MCH. Long time scans show the emission decays in 4.0±0.2 nsec (Table 3.1), in good agreement with previous room temperature, tautomer fluorescence lifetime measurements of 4.6 [6], 3.0 [8] and 4.0 [18] nsec.

The results of experiments studying the tautomer formation dynamics of 3HF in MeOH solutions are shown in Figure 3.4.2. The scans show a quickly rising transient

Table 3.1: Fit Parameters to Picosecond Absorption/Emission Scans[a]

Solvent	Wavelength (nm)[b]	Fast Rise Time (psec)	Slow Rise Time (psec)	Decay Time (nsec)	Fast/Slow Amp. Ratio
MCH	540	< 1.0	9.8±0.4	3.9±0.5	1.4±0.2
MCH	620	< 1.0	10.0±0.3	4.0±0.2	1.2±0.2
MeOH	540	< 1.0	10.4±0.3	0.28±0.04	-1.8±0.2[c]
MeOH	620	< 1.0	10.2±0.3	0.27±0.03	0.4±0.1

[a] Uncertainties based on quality of fit to double exp rise, single exp decay

[b] 540 nm scans are stimulated emission; 620nm scans are absorption

[c] Transient absorption decaying into slower stimulated emission

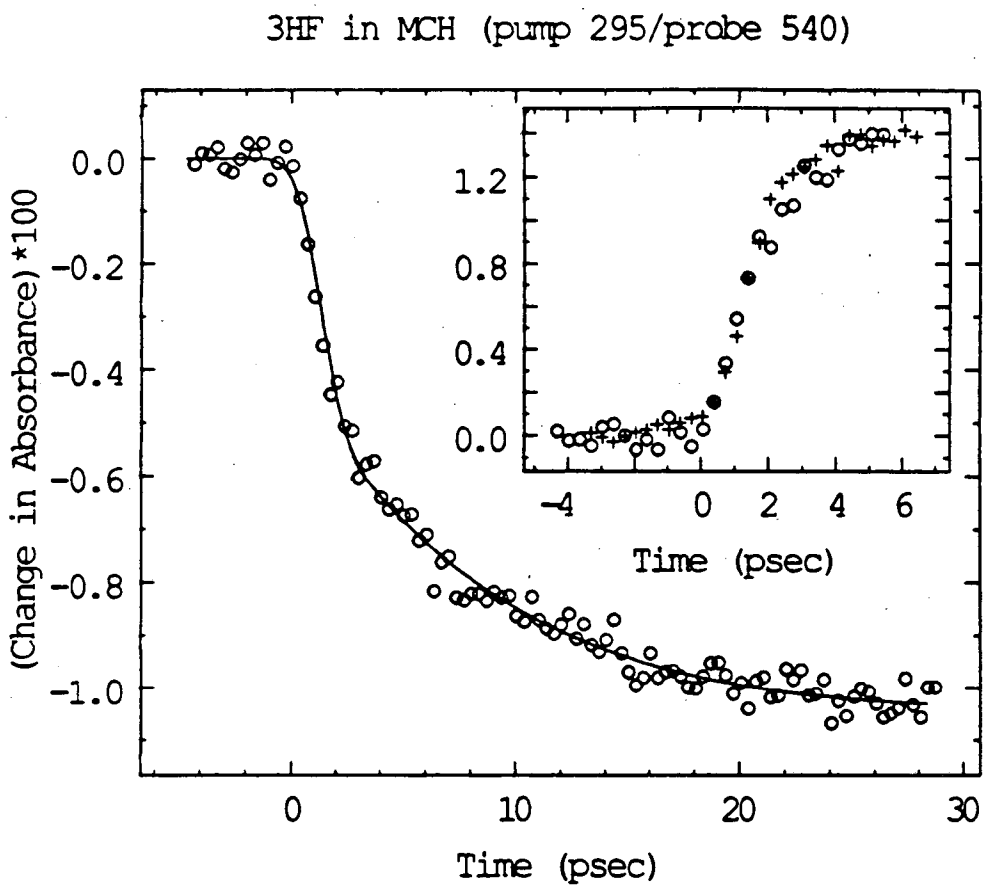

Figure 3.4.1: Transient 540 nm stimulated emission of 3HF in MCH. Line is fit given by parameters of Table 3.1, circles are data points. Inset: Scaled stimulated emission data (circles) overlaid on instrument function (crosses). The fast stimulated emission rise time is not resolved.

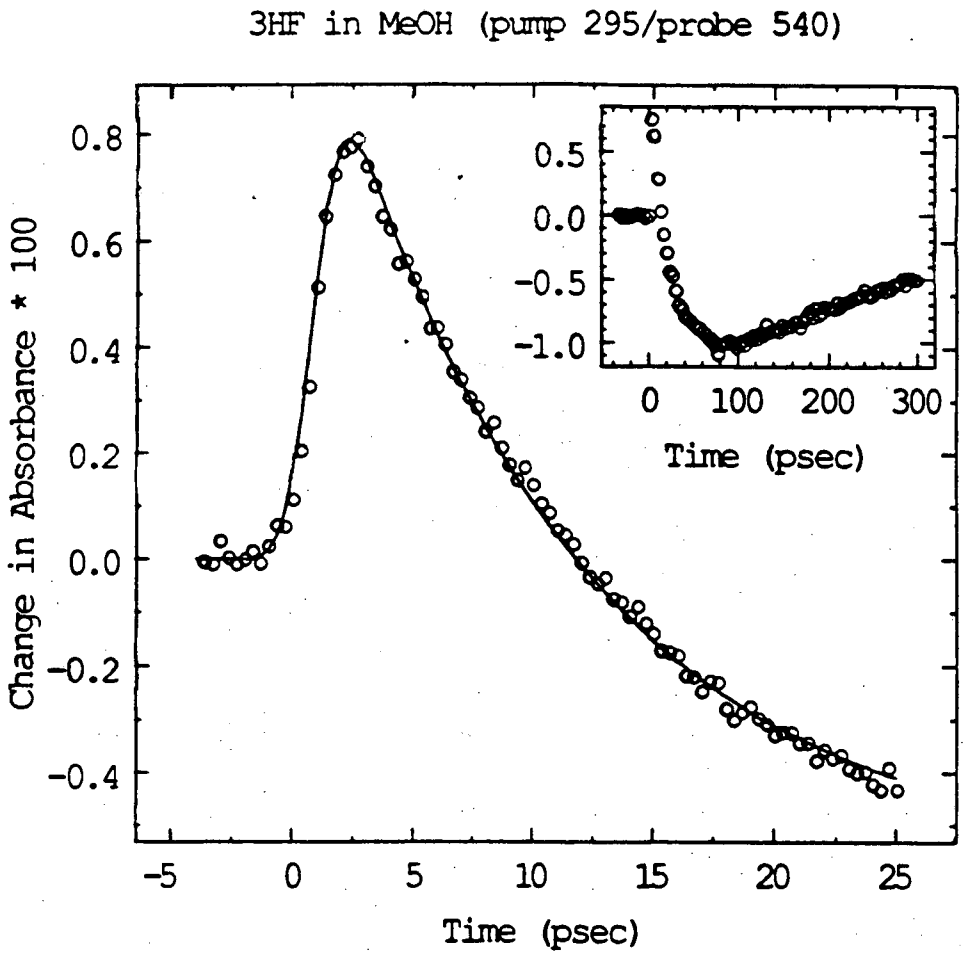

Figure 3.4.2: Transient 540 nm stimulated emission of 3HF in MeOH. Line is fit given by parameters of Table 3.1, circles are data points. Inset: Longer time scan of same sample, showing emission recovery.

absorption at 540 nm, decaying into a more slowly rising (10.4±0.4 psec) stimulated emission. The stimulated emission then exponentially decays in 280 psec (Fig. 3.4.2 inset, Fig. 3.4.3 (a)). Due to the large step size, the effective time resolution of the scans of Figure 3.4.3 is 35 psec; hence, the fast transient absorption at 540 nm does not appear. The traces of Figure 3.4.3 compare well with the fluorescence upconversion experiments of Barbara et al. taken with similar time resolution (Fig 3b of reference [14]).

All the results indicate that the fast ESPT occurs too quickly to be observed with picosecond time resolution at room temperature. This demonstrates the need to study the tautomer formation with femtosecond time resolution. The femtosecond laser system, however, is limited to probe wavelengths near 620 nm. If the 3HF tautomer excited state has good overlap with an even more highly excited (~16000 cm^{-1} higher) tautomer electronic state, then it should be possible to probe the tautomer formation by transient absorption spectroscopy at 620 nm in the same manner as stimulated emission (Figure 3.2.4). The transient absorption of 3HF in MCH at 620 nm shows identical dynamics to that observed in stimulated emission (Table 3.1). The long time transient absorption and emission scans of 3HF in MeOH also reflect identical dynamics (Figure 3.4.3). These identical kinetics at 540 nm and 620 nm indicate that the two wavelengths are probing the same electronic state of the 3HF tautomer.

The assignment of the 620 nm transient absorption to the tautomer excited state has been discussed by others [18,19,30,32]. Several groups have studied the transient absorption spectrum of 3HF with ~30 psec time resolution [17-19], and have presented conflicting results on the rise kinetics and assignments of some of the observed bands.

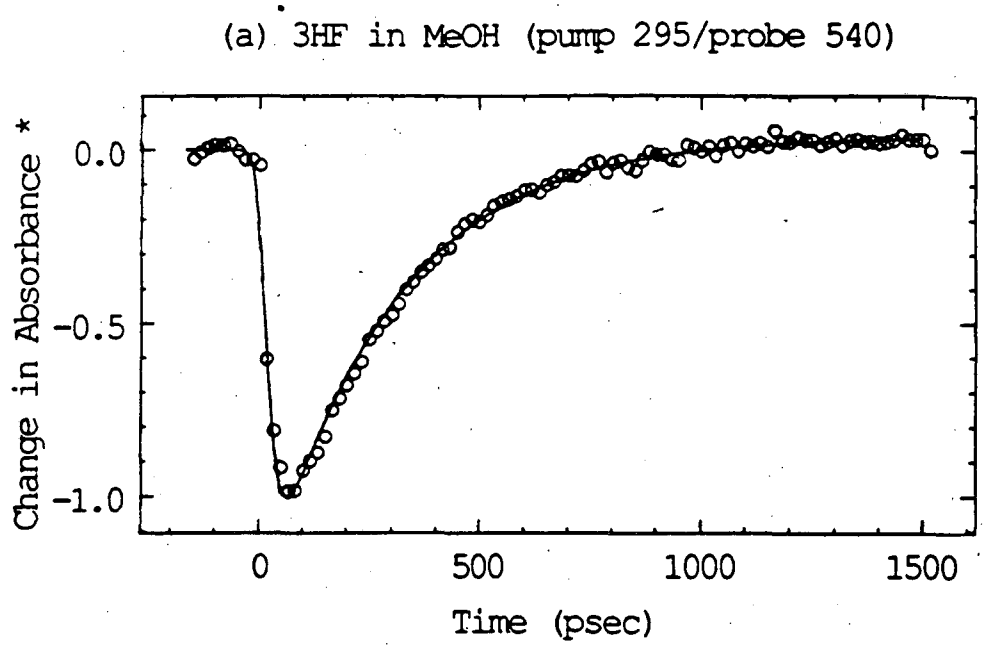

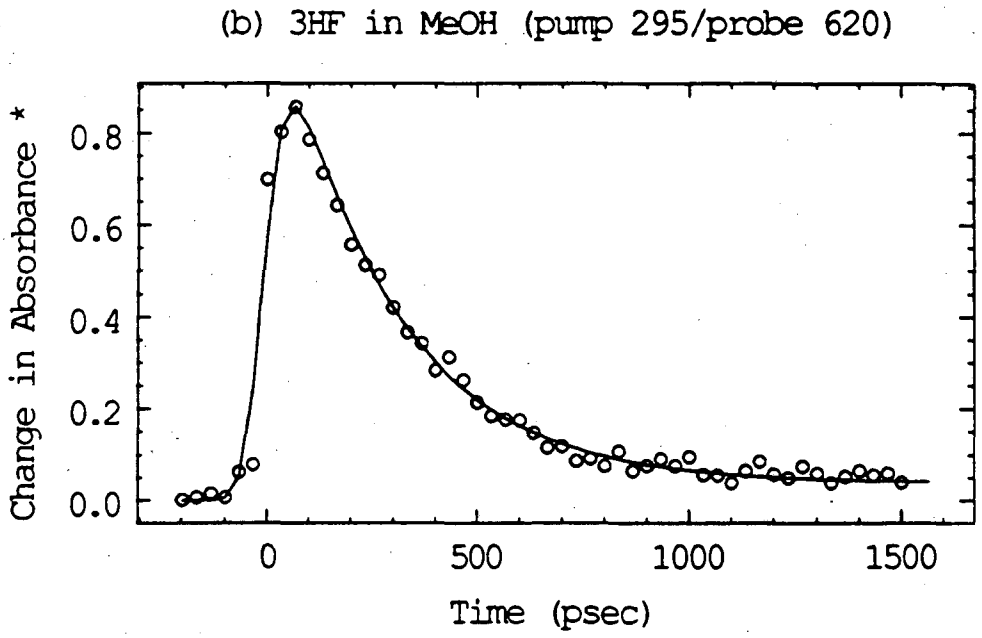

Figure 3.4.3: (a) Long time scan of transient 540 nm stimulated emission of 3HF in MeOH. (b) Long time scan of transient 620 nm absorption of 3HF in MeOH. Circles are data points, lines are fits given by parameters in Table 3.1. The two scans are identical within the noise.

For example, Rulliere and Declemy reported a rise of the 620 nm absorption band on a hundred psec time scale, and also reported the presence of an initial transient absorption at 500-560 nm for 3HF in MCH [19]. This contradicts the results of Dzugan et al., who, in agreement with our results, found the 620 nm absorption rise time faster than their instrumental limit, and detected only stimulated emission present between 500 and 580 nm [18]. Despite their differences, both authors concluded that the 620 nm absorption is from the tautomer excited state. This assignment is further supported by recent theoretical work by Dick in which the positions of the various electronic states of 3HF and the strengths of the transitions between them were computed [32]. The calculation found no transitions of any significant intensity from the excited normal form of 3HF; in addition, good overlap was computed for the $S_1 \rightarrow S_7$ transition, near 620 nm, of the tautomer [32]. Thus, ESPT in 3HF can be studied by monitoring the tautomer formation with transient absorption spectroscopy at 620 nm.

B. Femtosecond Transient Absorption: To elucidate the very fast dynamics of ESPT in 3HF, femtosecond transient absorption measurements were performed. 3HF was excited with the laser second harmonic at 310 nm, and the tautomer formation probed at 620 nm (Figure 3.2.4) with the laser fundamental. Typical scans for 3HF in MCH and MeOH are shown in Figure 3.4.4. The effects of the solvent environment on the ESPT, as well as the effects of varying the relative polarizations of the pump and probe pulses also have been investigated. The polarization experiments are described in Section 3.5.C. All of the data are fit to a dual exponential rise convoluted with a 125 fsec gaussian representing the instrument function, using the procedure described in Chapter 7. The results of all the fits are summarized in Table 3.2.

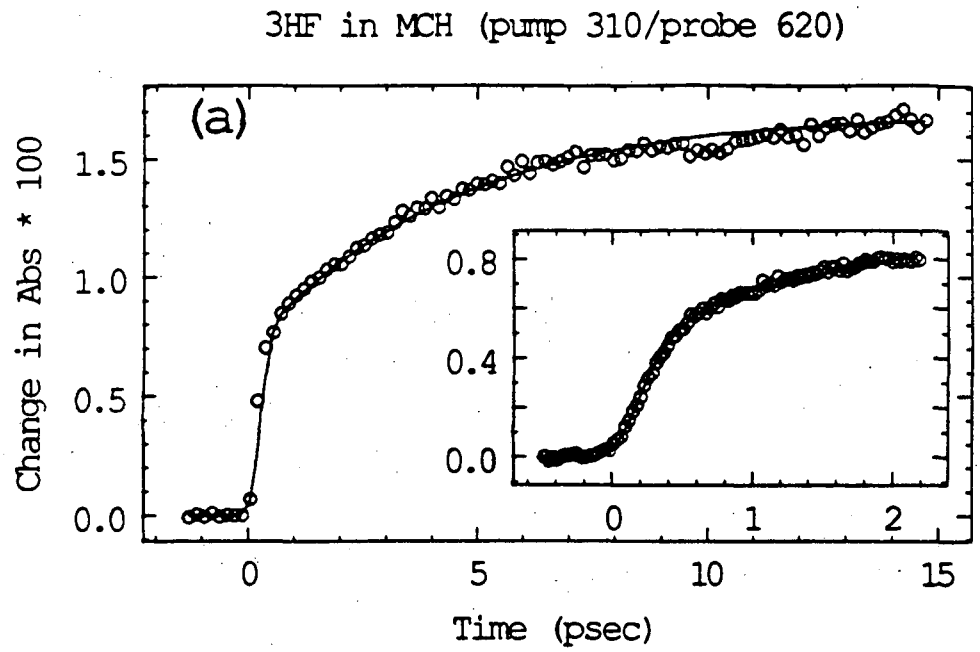

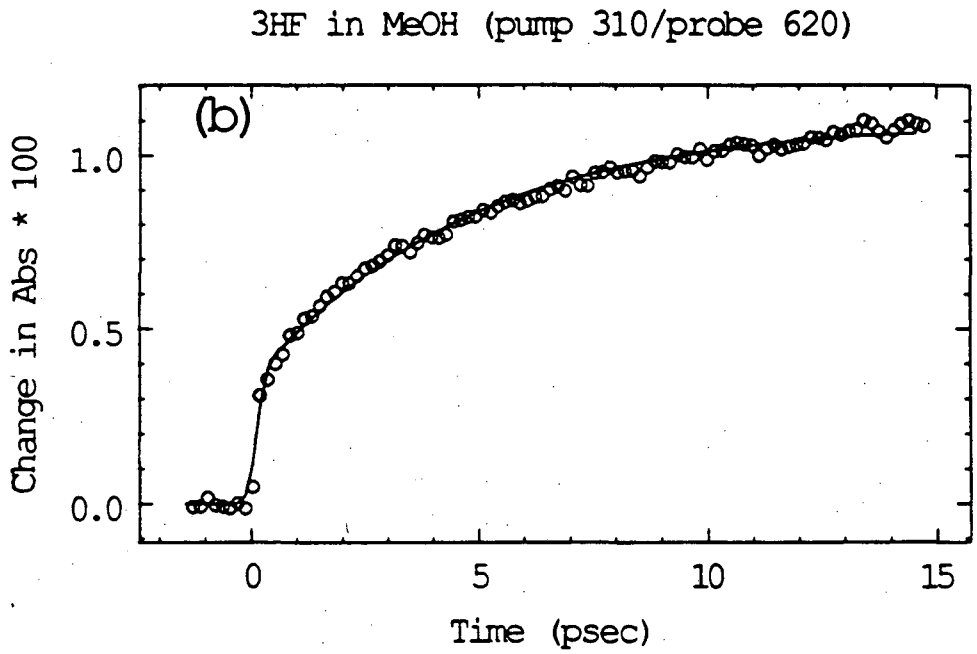

Figure 3.4.4: (a) 620 nm transient absorption of 3HF in MCH. Line is fit given by parameters of Table 3.2, circles are data points. Inset: Shorter time scan -- fit is given by parameters of Table 3.3. (b) 620 nm transient absorption of 3HF in MeOH; fit parameters given in Table 3.2.

Table 3.2: Fit Parameters to Femtosecond 620 nm Absorption Scans[a]

Solvent	Fast Rise Time (fsec)	Slow Rise Time (psec)	Fast/Slow Amp. Ratio
MCH[b]	210±30	9.3±0.5	1.34±0.2
MCH+drop MeOH	160±30	9.7±0.5	0.69±0.2
MCH sat. by MeOH	110[c]	10.2±0.5	0.49±0.15
MeOH	80[c]	10.0±0.3	0.42±0.10
MeOD	85[c]	10.2±0.4	0.47±0.10

[a] Uncertainties based on quality of fit to double exponential rise

[b] MCH has residual hydrogen-bonding impurities; see text

[c] Rise time is less than 125 fsec instrument.function

1. Investigation of Fast Rise Times: The fast transient absorption rises of 3HF in MeOH and MCH were measured with stage steps of 4 μm, or 27 fsec/point (Figure 3.4.4 (a), inset). To determine if the fast rise, and hence, the fast ESPT, is time resolved, these spectra have been rescaled to have the same absorbance at a delay of 1.5 psec, and superimposed on the instrument function (transient absorption of DPB in hexane) in Figure 3.4.5. The fast absorption rise of 3HF in MCH is time resolved, while the fast rise in MeOH is indistinguishable from the instrument function. The fast portion of the MCH rise fits to a 210 ± 30 fsec exponential rise convoluted with the 125 fsec gaussian instrument function; the unresolved fast rise in MeOH fits to the instrument function convoluted with an 80 fsec exponential rise (Table 3.2). The slow rise times, visible in Figure 3.4.5 as a lowering of the 3HF absorptions below that of the instrument function, are essentially the same in both solvents.

2. Effect of Hydrogen-Bonding Impurities in MCH: The presence of stoichiometric amounts of hydrogen bonding impurities can drastically alter the ESPT kinetics of 3HF in non-polar solvents. Following the examples of McMorrow and Kasha [12] and Brucker and Kelley [24], I hoped to better understand the effects of these impurities on the transient absorption spectra by intentionally introducing small amounts of MeOH into the MCH solutions. The results of progressive MeOH addition on the transient absorption of 3HF in MCH are shown in Figure 3.4.6. The upper left portion of the figure shows the ESPT kinetics of 3HF in pure MCH. The lower right trace is for 3HF in pure MeOH. The trace in the upper right corner was taken after one drop (~0.02 mL) of MeOH was injected into the MCH solution through a 20 gauge syringe needle. The sensitivity of the ESPT to the presence of H-bonding

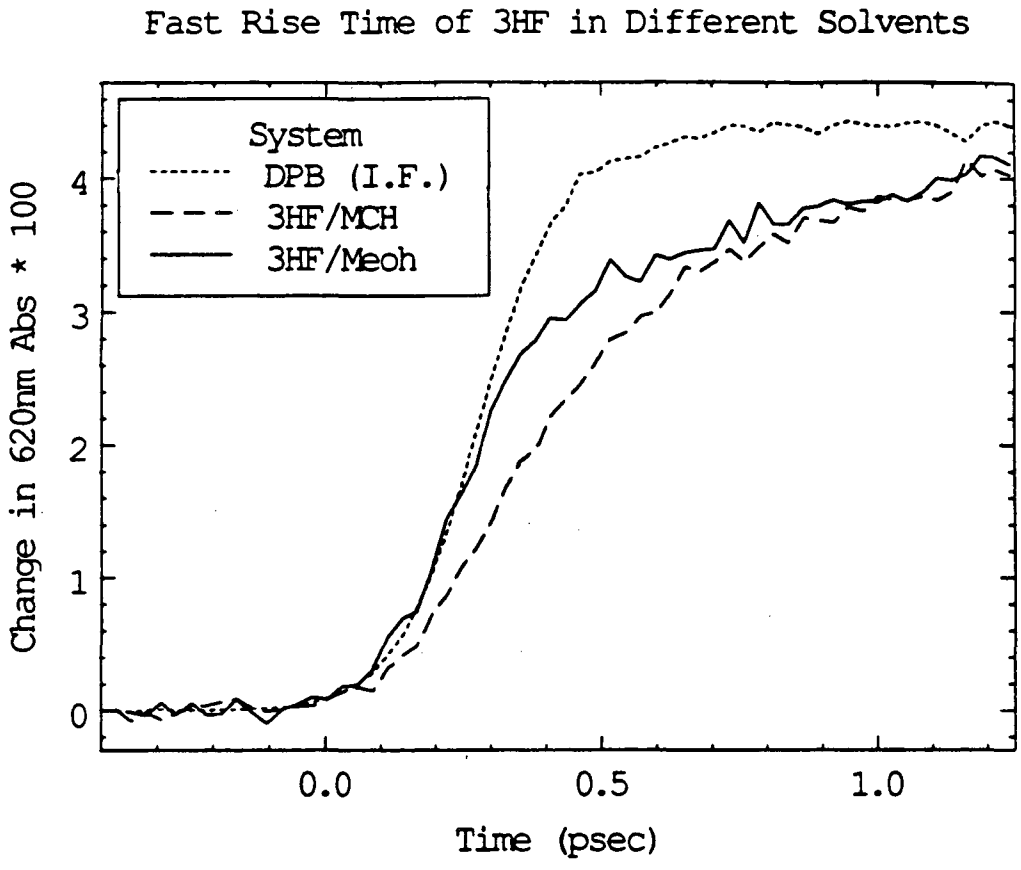

Figure 3.4.5: Fast 620 nm transient absorption rise of 3HF in different solvents. Lines connect the raw data points; dashed is 3HF in MCH, solid is 3HF in MeOH. The dotted line is the instrument response (transient absorption of DPB in hexane). All 3 scans have been scaled to have the same absorbance at a delay of 1.5 psec.

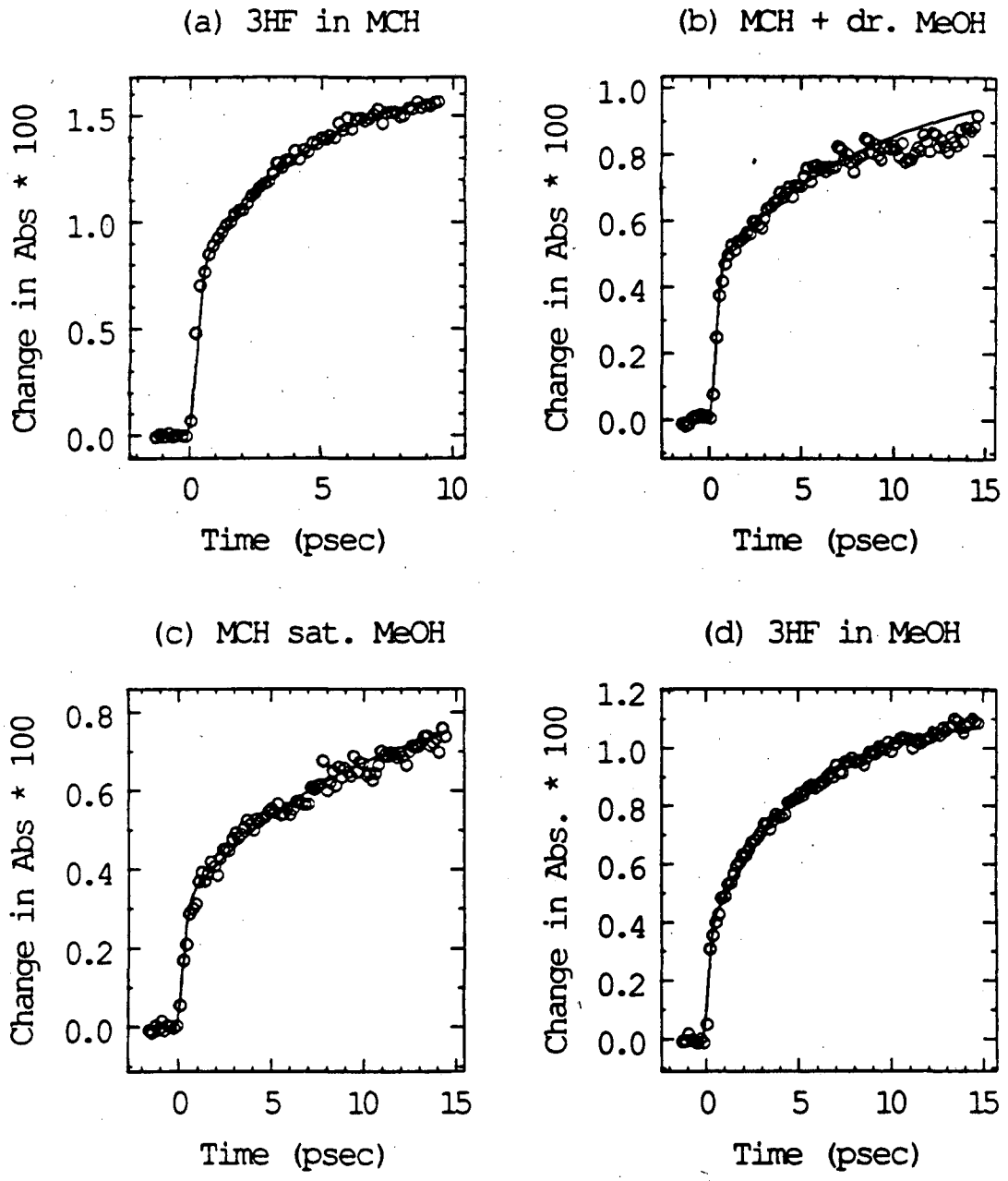

Figure 3.4.6: Effect of MeOH addition on 620 nm absorption dynamics of 3HF. Circles are data points, lines are fits with parameters given in Table 3.2. (a) 3HF in "pure" MCH. (b) Same solution with one drop of MeOH added. (c) Same solution saturated with MeOH. (d) 3HF in pure MeOH.

impurities was readily apparent; the solution fluorescence visibly changed from green to blue upon the addition of this tiny amount of MeOH to the sample. The lower left scan of Fig. 3.4.6 shows the effect of saturating the MCH solution with MeOH.[1] The effects of MeOH addition are clear; as more MeOH is added, the ratio of the fast ESPT component to the slow ESPT component decreases, until the MeOH saturated MCH solution has virtually identical kinetics to the pure MeOH solution. This result is summarized in Figure 3.4.7 and Table 3.2.

Progressive MeOH addition also has a pronounced effect on the fast ESPT process of 3HF in MCH, as shown in Figure 3.4.8 and summarized in Table 3.2. The fast ESPT in MCH is clearly time resolved; addition of one drop of MeOH decreases the rise time significantly; additional MeOH reduces the rise time to that of the pure MeOH solution which is indistinguishable from the instrument function. Since the presence of the slow rise in MCH indicates that there are hydrogen-bonding impurities present [12], the fast rise in MCH will also be affected by these impurities. Because the fast ESPT in hydrogen-bonding environments is faster than in MCH, the true fast ESPT rate in MCH must be slightly slower than the rate measured above.

The measured fraction of slow/fast ESPT in pure MeOH can be used to correct for the effect of hydrogen bonding impurities on the fast rise in MCH. Because the MeOH results have a fast:slow kinetic component ratio of 0.42, and since 43% of the MCH transient absorption is due to the slow kinetic component, ~18% of the total absorption signal is a fast rise due to MeOH-like impurities. This means that roughly 1/3 of the

[1] I refer to an MCH solution as saturated with MeOH when the solution has turned cloudy or has a visible boundary between MCH and MeOH layers.

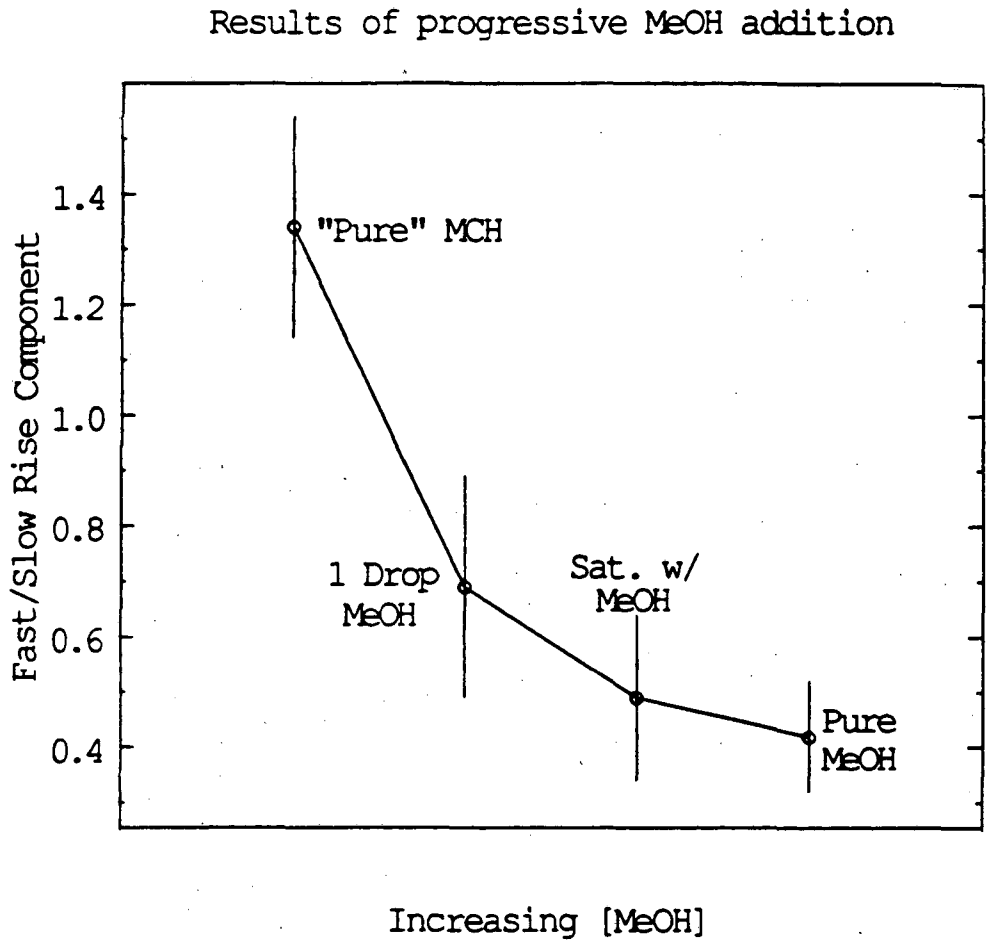

Figure 3.4.7: Effects of progessive MeOH addition on the ratio of fast/slow rise components of the 620 nm transient absorption of 3HF. Error bars are based on the uncertainties from the fits (Table 3.2). MeOH concentration increases arbitrarily across the horizontal axis.

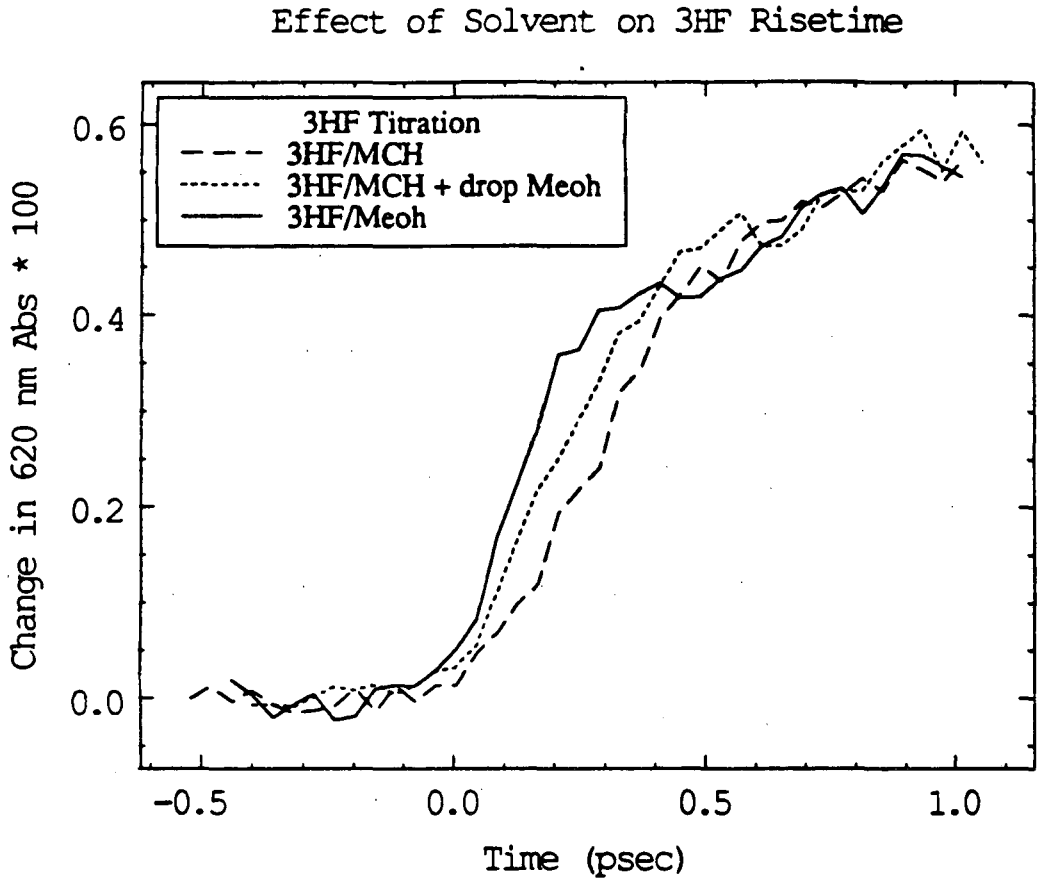

Figure 3.4.8: Effect of progressive MeOH addition on fast 620 nm absorption rise of 3HF. Lines connect the raw data points; dahsed is 3HF in MCH, dotted is 3HF in MCH + one drop MeOH, solid is 3HF in pure MeOH.

57% of the absorption due to the fast rise component is the result of the hydrogen bonding contaminants. By refitting the MCH transient absorption to account for the known ratio and rise times of the H-bonding impurities, the intrinsic rise time for the pure MCH solvent can be obtained. The fit in the inset of Figure 3.4.4 (a) has 3 exponential rises; the fit parameters are summarized in Table 3.3. Two of rises are fixed to have the same time constants and amplitude ratio as the fit to the pure MeOH data (Table 3.2). They are scaled appropriately to fit the slow rise of the MCH transient absorption, and convoluted with the 125 fsec gaussian instrument function. Since these parameters are fixed, the remaining rise of 240 fsec must be due to the inherent proton transfer rate in MCH. An uncertainty of ± 50 fsec is estimated for this figure based on the uncertainties in the fits to the data and error propagation in the deconvolution. Since a portion of the directly measured 210 fsec rise time is pulse-width limited from the impurities, the deconvoluted time of 240 fsec is slower than that directly measured, as expected.

3. Effect of Deuteration: To better understand the mechanism of ESPT, femtosecond transient absorption scans were taken on a sample of 3HF in MeOD. Since the hydroxy proton of 3HF rapidly exchanges with the alcoholic protons, and since MeOD is present in great excess, this sample is essentially a 3DF in MeOD solution. The transient absorption traces, however, showed no changes at all from the corresponding 3HF in MeOH scans. The results were identical to those of Figure 3.4.4 (b), summarized in Table 3.2. This result is somewhat surprising, since it implies that the mass of the proton is not at all important to the ESPT process. This has strong ramifications on the mechanism of the proton transfer, as will be discussed below.

Table 3.3: Fit Parameters Accounting for Impurities in MCH[a]

Rise Time Component	Relative Amplitude
10.0 psec[b]	1.0[c]
80 fsec[b]	0.42[b]
240±50 fsec	0.95±0.15

[a] Fit shown in Figure 3.4.4a (convoluted with 125 fsec gaussian); Data fits equally well to double exponential rise (parameters in Table 3.2); see text

[b] These parameters fixed from fits to pure MeOH data (Table 3.2)

[c] Absolute amplitude for 10 psec component picked by best fit to data

3.5 Discussion

A. Measurement of Intrinsic ESPT -- The Fast Rise in MCH: The 210 fsec fast exponential rise of the excited tautomer absorption in MCH (Figure 3.4.6) is clearly time resolved. As was seen in the early studies of Barbara's group [9,13-15], bi-exponential dynamics for the ESPT of 3HF in MCH are observed. Based on the experiments of McMorrow and Kasha [12], and the results of others who found only single exponential tautomer fluorescence rises in non-polar surroundings [20,22,24], the slow rise in the results can be assigned to the presence of hydrogen bonding impurities in the MCH solvent. The identical rates of the slow component in both MeOH and MCH support this assignment of the slow rise to alcohol-like impurities in MCH. This is confirmed by the results of the progressive MeOH addition experiments (Figures 3.4.7 & 3.4.8, Table 3.2), which show the slow rise amplitude steadily increasing, but the slow rate remaining unchanged as additional hydrogen bonding impurities are introduced. When accounting for the effects of the hydrogen bonding impurities on this fast rise (see above), we determine the ESPT rise time to be 240±50 fsec. This constitutes the first direct measurement of the intrinsic ESPT rate of 3HF.

This ESPT rate can be compared to that measured for other molecules, such as 2-(2'-hydroxyphenyl)benzothiazole (HBT). From the infrared stretching frequencies of their O–H bonds, it is evident that HBT [41] has a stronger intramolecular hydrogen bond than 3HF [42], so ESPT is expected to occur at a higher rate in this molecule than in 3HF. A recent measurement gave 170±20 fsec for the intrinsic ESPT time of HBT [33]. As expected, this time is slightly faster than the measured time of 240±50 fsec

for 3HF. In addition, deuteration of HBT showed no effect on the proton transfer rate [34], also in agreement with the measured results for 3HF.

The ESPT times for both of these molecules are significantly slower than the vibrational period of an O-H stretch. This suggests that optical excitation of 3HF is not directly to the dissociative region of the O-H interatom potential in the excited state, in agreement with the conclusions of others [16,33], and with resonance Raman data which shows no enhancement of any modes with O-H stretching character [48]. Therefore, the reactive pathway for proton transfer involves movement along coordinates other than simple O–H stretching motion. This motion will be along vibrational coordinates which are significantly displaced from their ground state equilibrium positions following absorption of a UV photon by 3HF. The tautomerization can be visualized as the propagation of a wavepacket comprised of all these motions on the multidimensional excited state potential surface, depicted schematically in Figure 3.5.1. The time for the evolution of this wavepacket from the reactant to the product regions of the surface is the time necessary for proton transfer to occur.

In the wavepacket picture proposed by Elsaesser and co-workers to describe ESPT in HBT [33], the measured 170 fsec tautomerization time is interpreted as the period of the vibrational modes displaced upon excitation. The multidimensional nature of the excited state potential surface, however, may complicate this interpretation. The *initial* motion of the wavepacket, determined by the slope of the excited state potential in the Franck-Condon region, will depend strongly on the nature of the vibrations displaced upon electronic excitation but the subsequent evolution of the wavepacket may not.

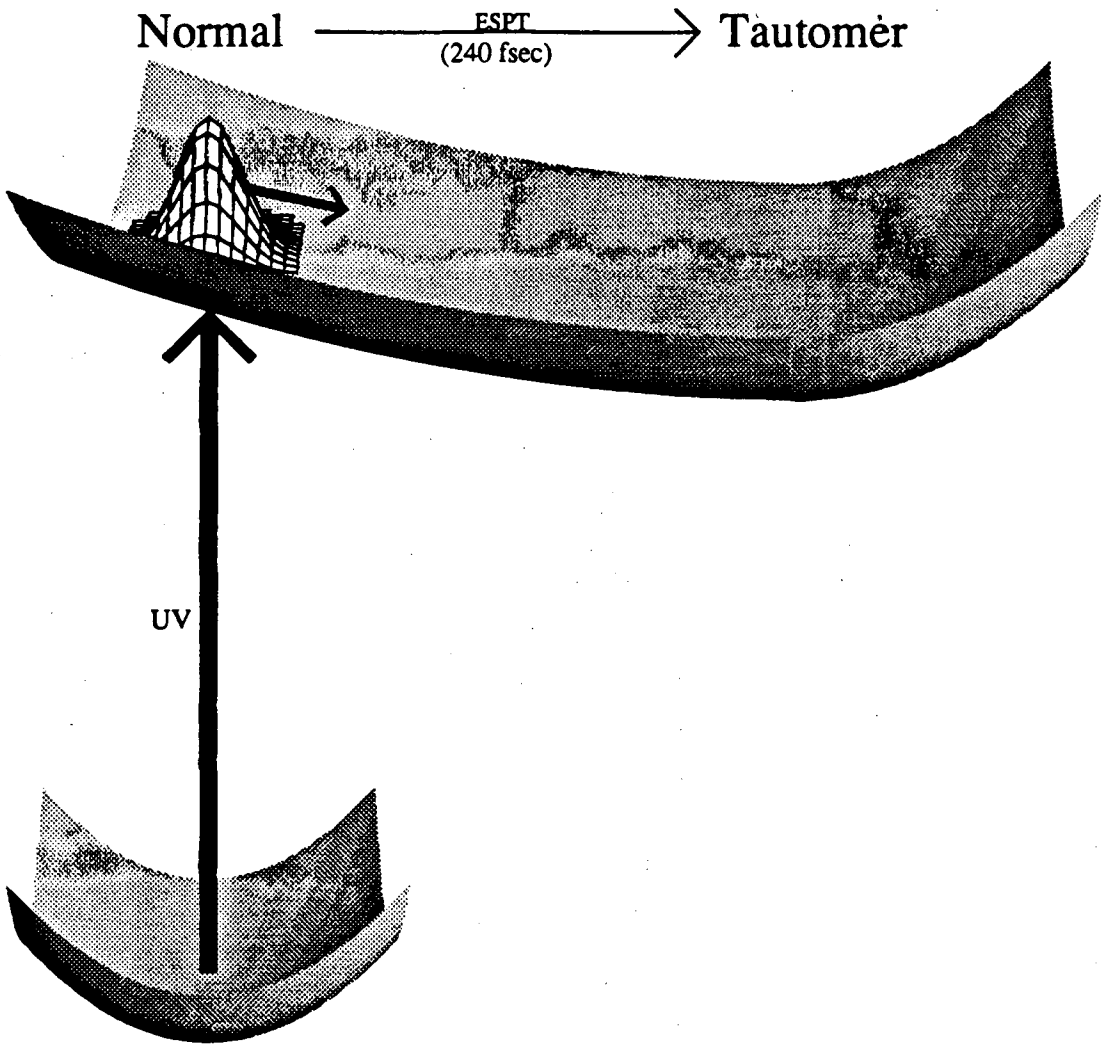

Figure 3.5.1: Schematic illustration of wavepacket motion leading to ESPT. The ground state wavefunction is displaced from equilibrium on the excited surface; subsequent motion along reactive coordinates (energy re-distribution into reactive modes) leads to tautomerization, displacements along other coordinates (e.g. O-H stretch) do not lead directly to product formation.

Therefore, there may not be a simple relationship between the frequency of the modes displaced and the observed time for ESPT. A better picture is that the tautomerization time as controlled by a series of coupled motions which are eventually dissociative in the O-H coordinate, bringing the wavepacket into the product region of the excited state potential surface after 240 fsec. This gives the view of ESPT as essentially controlled by large amplitude low frequency motions. The initial photoabsorption leaves the 3HF molecule vibrationally excited in its electronic excited state. As wavepacket propagation occurs on the excited state, energy eventually flows into a coordinate resembling the O-H stretch, leading to eventual dissociation along this mode and subsequent tautomerization. This process is barrierless; the energy is provided by the excitation photon and tautomerization proceeds without any thermal activation. This picture is supported by the Ar matrix results, which show tautomerization still occurs at 10 K, and the deuteration results, which show that the mass of the proton is unimportant -- the rate limiting step for tautomerization is large amplitude motion, not motion of the proton or thermal activation. This energy redistribution takes 240 fsec.

The 240 fsec ESPT time also allows comment on the possibility that phenyl twisting plays a part in the proton transfer process. Phenyl twisting motion could dynamically modulate the ESPT rate by changing the electronic structure of excited 3HF. Structural studies have suggested that the phenyl twist angle may change the energetics of the ESPT process, but were not conclusive about the dynamic role of phenyl torsion [15]. The lack of viscosity dependence of the slow ESPT rate [14], and the results of high pressure experiments [10,11], however, indicate that phenyl twisting is not strongly coupled to the ESPT. Since large amplitude phenyl torsional motion is

an order of magnitude slower than the observed ESPT rate [43], the measured 240 fsec ESPT time also supports this hypothesis. The proton transfer in 3HF happens too quickly for electronic changes induced by phenyl rotation to be important in the ESPT.

B. Fast ESPT in MeOH -- 3HF Monosolvate: In hydrogen bonding environments, the ESPT of 3HF changes drastically. Two distinct ESPT channels appear, a time unresolved fast component, and a slower component which has been extensively studied [9,13-15]. The slow ESPT process is thermally activated, and has a barrier height of 1.4 kcal/mole in MeOH [14], in accord with the picture of McMorrow and Kasha (Figure 3.2.5). This changes the fluorescence dynamics significantly; molecules which have not yet undergone the slow ESPT can fluoresce in the blue, from the normal configuration of the molecule, or they can tautomerize and fluoresce in the green, leading to a bi-exponential rise of the green fluorescence. Many authors have ascribed this slow ESPT in hydrogen bonding environments (or in the presence of H-bonding impurities in non-polar solvents) to a variety of solvated 3HF species [6-9,12-16,24,25,30,31]. Typical proposed structures for these 3HF-solvent aggregates are pictured in Figure 3.2.6. As described in Section 3.2.E, the $3HF(MeOH)_x$ (x = 1 or 2) complexes have been recently isolated in Ar matrices and characterized [24]. In particular, the 3HF-MeOH monosolvate has been shown to undergo ESPT in less than 10 psec at 15 K [24].

The fast excited tautomer absorption rise we measure for 3HF in MeOH is indistinguishable from our instrument function, indicating that the fast ESPT is taking place in ≤125 fsec. This suggests that an entirely new motion dominates the ESPT reaction coordinate in MeOH, or in other words, that the fast ESPT takes place by a

different mechanism in MeOH than in non-polar solvents. In the picture of ESPT in non-polar environments described earlier, *intra*molecular modes displaced upon excitation lead to tautomerization. In polar solvents, the formation of hydrogen bonded complexes creates new *inter*molecular motions which may play an important role in the tautomerization process. If the new intermolecular modes are also displaced upon excitation, the resulting wavepacket could follow a trajectory on the excited state surface which is altered from that of the unsolvated species, leading to a different measured proton transfer time.

The most likely candidate for this faster, intermolecularly dominated ESPT is the cyclically H-bonded 3HF monosolvate ($3HF(MeOH)_1$) [24] (Fig. 3.2.6 (b)). The fast ESPT mechanism for the monosolvated 3HF could involve dual proton transfer. Excitation of the 3HF changes the acidity and basicity of the carbonyl and hydroxy moieties [2,3]; the now basic carbonyl group can easily accept the closely bound alcohol proton, while the newly acidic hydroxy proton can transfer easily to the deprotonating alcohol. This dual ESPT process is illustrated in Figure 3.5.2. This type of double proton transfer has been postulated for several molecules in hydrogen bonding solvents, including 7-aza-indole [44,45]. Whether this dual transfer process is concerted or sequential cannot be determined from above data.

It is entirely plausible that the dual ESPT in $3HF(MeOH)_1$ is faster than the intrinsic ESPT in the free molecule. The hydrogen bonds in the 3HF solvated complex are likely to be stiffer and therefore, of higher frequency than the intramolecular hydrogen bond of the unsolvated species. This implies that the wavepacket is composed of higher frequency components in the monosolvate than in free 3HF, leading to more

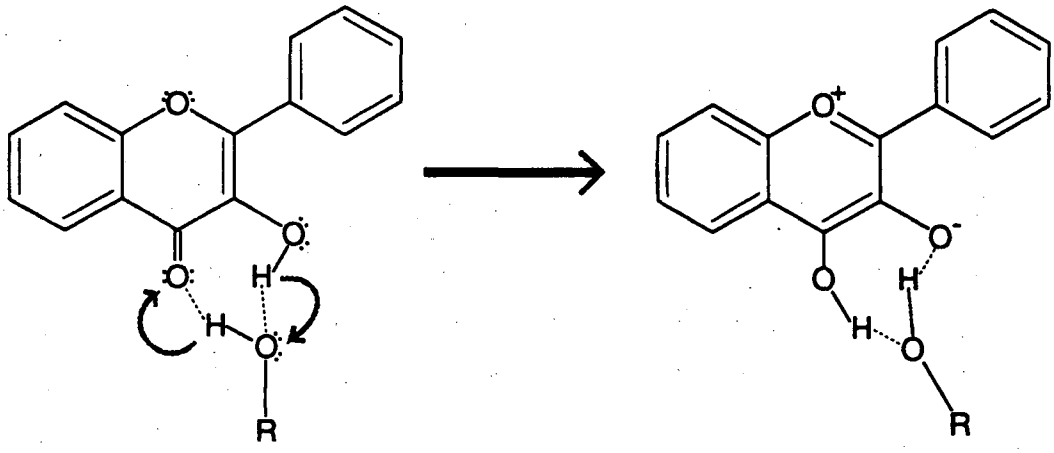

Figure 3.5.2: Possible mechanism for dual proton transfer in the 3HF-MeOH cyclically H-bonded monosolvate. Arrows indicate relative proton motions upon electronic excitation.

rapid tautomerization. In addition, the stronger intermolecular hydrogen bonds in the solvated complex start the protons closer to their final tautomeric positions than the weaker intramolecular hydrogen bond in isolated 3HF, suggesting that the wavepacket would be propagating for less distance on the intermolecular reaction pathway. If the intermolecular hydrogen bond vibration is important to the monosolvate proton transfer reaction coordinate, either or both of these observations can be used to rationalize the more rapid evolution of the wavepacket on the excited state surface of the aggregate than of the isolated molecule.[2] These ideas, and the previously measured 10 psec upper limit for ESPT of the monosolvate at 10 K [24] make the ≤125 fsec time for a dual ESPT mechanism in $3HF(MeOH)_1$ at room temperature reasonable.

The rapid fast ESPT times for the bare 3HF and monosolvated 3HF species have implications for the mechanism of the slower ESPT process. The slow ESPT has been ascribed to the presence of the 3HF disolvate (Figure 3.2.6 (a)). The disolvate itself does not undergo proton transfer [24], so the slow ESPT time is a measure of the time for desolvation of $3HF(ROH)_2$ to become either the monosolvated or the free 3HF species. Several models, including thermally activated desolvation [6], desolvation followed by rate-limiting proton transfer [9,13-15], and Marcus-like solvent polarization fluctuations [16] have been proposed to describe this process. Whatever the mechanism involved, it seems that proton transfer time is virtually

---

[2]Alternatively, this process can be viewed as the original wavepacket comprised of intramolecular vibrations propagating on an electronic surface that has been altered by interaction with the polar solvent. The Stokes shift of the tautomer fluorescence, however, changes less than 200 cm^{-1} between MCH and MeOH[14], implying that the electronic surfaces are not shifted significantly upon polar solvation. Therefore, we prefer the picture of new, intermolecular modes changing the evolution of the wavepacket for 3HF in MeOH.

instantaneous compared to the desolvation time. This is supported by the data of Figure 3.4.2, which shows a transient absorption at 540 nm due to $3HF(MeOH)_2$ decaying smoothly into the stimulated emission of the tautomer. The tautomer emission rises with the disolvate absorption decay time; there is no evidence for any type of bottleneck on the picosecond time scale. This is at odds with the work of Barbara et al., who concluded that there is some intrinsic barrier to ESPT based on deuteration studies. The deuteration studies presented above, however, support the idea of a barrierless, IVR-driven ESPT once the desolvation step occurs. Whether the subsequent proton transfer occurs from the free 3HF, the monosolvate or a mixture of the two species, the ESPT happens rapidly once desolvation of the disolvate is complete.

C. Effect of Polarization: To verify that both the fast and slow rise components of the 620 nm transient absorption are due to the tautomer excited state, and to account for the effects of rotational reorientation of the 3HF during the ESPT, a series of experiments with different relative orientations of the pump and probe pulse polarizations were performed. Figure 3.5.3 shows the 620 nm transient absorption kinetics of 3HF in MCH taken with parallel and perpendicular pump/probe polarizations. Neither the rise times nor the fast/slow rise component ratios change with relative polarization. Experiments performed with relative polarization at the magic angle (54.7°) also showed identical results. This indicates that the absorptions of both kinetic components come from the same electronic state of the molecule (or from different states with parallel transition dipoles), and that the effects of rotational diffusion are not important on this time scale. This independence of the dynamics

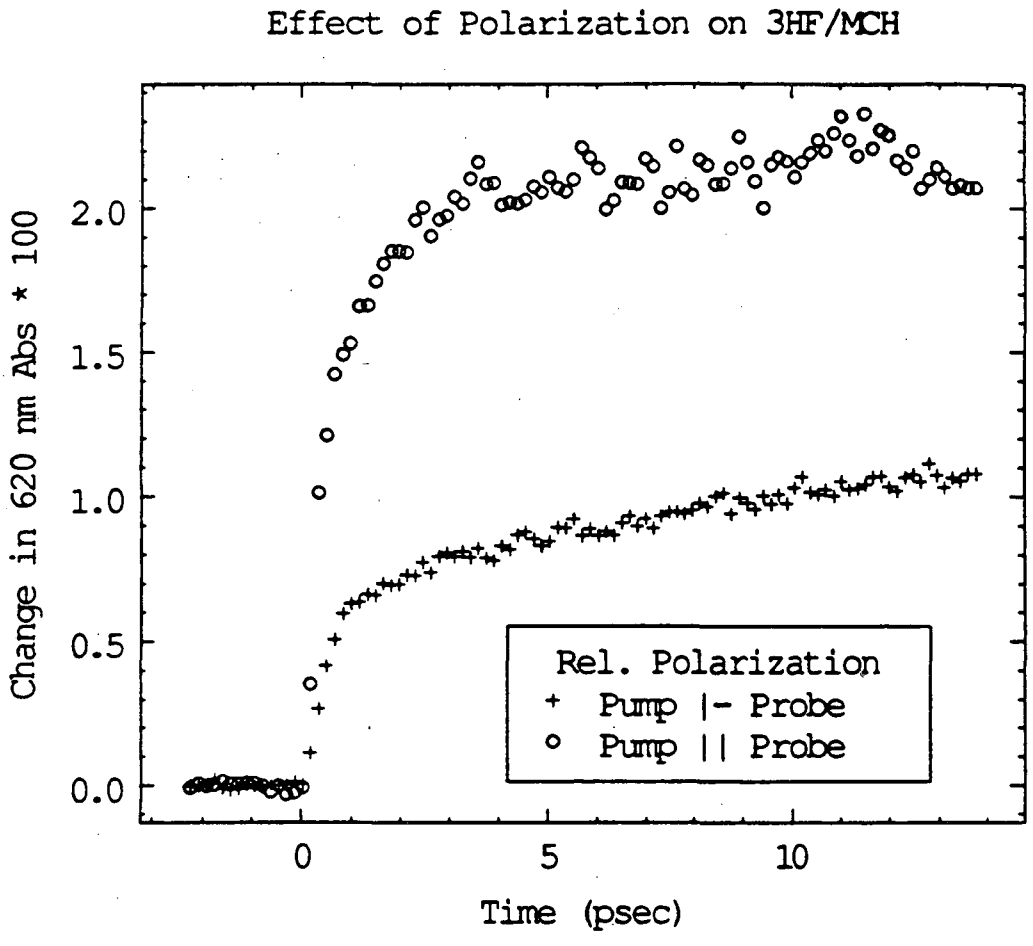

Figure 3.5.3: Effect of relative polarization of pump and probe beams on 620 nm transient absorption of 3HF in MCH. Circles are data for parallel polarizations, crosses are data for perpendicular polarizations. Rise times and fast/slow rise amplitude ratios are the same for both scans.

from relative polarization is in agreement with previous emission studies [9].

The information of Figure 3.5.3 can be used to determine the relative orientations of the transition dipoles of the 3HF ground state and the excited state giving rise to the transient absorption signal. The signal size ratio of 2.3±0.3:1 for parallel:perpendicular orientations indicates that the transition dipole of the tautomer excited state is mostly parallel to that of the initial excitation (the ratio expected for a perfectly parallel transition is 3:1). The anisotropy $A = (I_{\parallel} - I_{\perp})/(I_{\parallel} + 2I_{\perp})$ of this transition is ~0.25, implying an angle of ~20° between the ground state and the transiently absorbing tautomer excited state transition dipoles [46]. Since the molecule has undergone ESPT and now has significant zwitterionic character, we would expect the electronic structure of the excited state to be altered significantly from that of the ground state. This makes the result of nearly parallel transition dipoles somewhat surprising, although not completely unlikely. To the best of my knowledge, no one has reported the orientation of the excited state transition dipole in a molecule that undergoes ESPT. The parallel result, however, is in agreement with recent findings on the tautomer emission dipole orientation of 2-(2'-hydroxyphenyl)benzothiazole (HBT) in non-polar environments [47].

Since the transient absorption kinetics are independent of the relative pump and probe polarizations, the experiments can be performed without the use of the 1/2 wave plate needed change the probe polarization. This allows improved time resolution, as non-compensatable dispersion in the 1/2 wave plate broadens the instrument function from 125 to 140 fsec. To better resolve the fast rise component in MeOH solutions, the experiments above were performed without the 1/2 wave plate.

3.6 Summary

The first investigation of the fast ESPT dynamics of 3HF in alkane and alcohol solvents has been performed. Picosecond stimulated emission spectroscopy indicates that the tautomer is formed in less than 1 psec, and that the 620 nm transient absorption occurs from the tautomer excited state. By studying this absorption with femtosecond time resolution, the fast ESPT of 3HF has been observed in different solvents.

The appearance of a slow ESPT component in MCH indicates the presence of hydrogen-bonding impurities in solution. The ESPT kinetics in hydrogen-bonding environments were studied in MeOH, and the results used to account for the effects of the impurities in the MCH solution. The fast ESPT time in MCH was determined to be 240±50 fsec; the fast ESPT time in MeOH was faster than the 125 fsec instrument response. ESPT times in 3DF/MeOD solutions were identical to those of 3HF/MeOH solutions.

The 240 fsec time scale for the ESPT in MCH is too long for O-H stretching motion and too short for large amplitude phenyl torsion to be of major importance in the proton transfer reaction coordinate. Instead, a model for ESPT based on the evolution of vibrational motions coupled to the electronic excitation is described; the ESPT time corresponds roughly to the propagation time of the wavepacket comprised of the modes displaced. In this way, ESPT can be thought of as an IVR process, not a process involving proton tunneling or direct O-H dissociation. The faster ESPT time in MeOH solution can be explained by consideration of a 3HF-MeOH cyclically H-bonded complex. The ESPT reaction coordinate in this aggregate is comprised of new

modes resulting from hydrogen motion between the 3HF and the solvent molecules. The higher frequency motions constituting the wavepacket and a shorter overall reaction pathway to travel for tautomerization each may contribute to the faster ESPT time in the monosolvate. This suggests that the 3HF monosolvate undergoes ESPT by a dual proton transfer mechanism.

3.7 References

1. P. F. Barbara, P. K. Walsh and L. E. Brus, J. Phys. Chem., 93, 1989, p. 29.
2. E. Vader Donckt, Prog. React. Kinet., 5, 1970, p. 273.
3. J. F. Ireland and P. A. H. Wyatt, Adv. Phys. Org. Chem., 12, 1976 , p. 131.
4. P. K. Sengupta and M. Kasha, Chem. Phys. Lett., 68, 1979, p. 382.
5. Yu. L. Frovlov, Yu. M. Sapozhnikov, S. S. Barer, N. N. Pagodeva and N. A. Tyukavkina, Izv. Akad. Nauk. USSR Ser. Khim., 10, 1974, p. 2364.
6. G. J. Woolfe and P. J. Thistlethwaite, J. Am. Chem. Soc., 103, 1981, p. 6916.
7. M. Itoh, K. Tokumura, Y. Tanimoto, Y. Okada, H. Takeuchi, K. Obi and I. Tanaka, J. Am. Chem. Soc., 104, 1982, p. 4146.
8. M. Itoh and Y. Fujiwara, J. Phys. Chem., 87, 1983, p. 4558.
9. A. J. G. Strandjord, S. H. Courtney, D. M. Friedrich and P. F. Barbara, J. Phys. Chem., 87, 1983, p. 1125.
10. O. A. Salman and H. G. Drickamer, J. Chem. Phys., 75, 1982, p. 572.
11. O. A. Salman and H. G. Drickamer, J. Chem. Phys., 77, 1982, p. 3329.
12. D. McMorrow and M. Kasha, J. Phys. Chem., 88, 1984, p. 2235.
13. A. J. G. Strandjord and P. F. Barbara, Chem. Phys. Lett., 98, 1983, p. 21.

14. A. J. G. Strandjord and P. F. Barbara, J. Phys. Chem., 89, 1985, p. 2355.

15. A. J. G. Strandjord, D. E. Smith and P. F. Barbara, J. Phys. Chem., 89, 1985, p. 2362.

16. G. A. Brucker, T. C. Swinney and D. F. Kelley, J. Phys. Chem., 95, 1991, p. 3190.

17. P. Chou, D. P. McMorrow, T. J. Aartsma and M. Kasha, J. Phys. Chem., 88, 1984, p. 4596.

18. T. P. Dzugan, J. Schmidt and T. J. Aartsma, Chem. Phys. Lett., 127, 1986, p. 336.

19. C. Rulliere and A. Declemy, Chem. Phys. Lett., 137, 1987, p. 64.

20. D. McMorrow, T. P. Dzugan and T. P. Aartsma, Chem. Phys. Lett., 103, 1984, p. 492.

21. M. Itoh, Y. Fujiwara, M. Sumitani, K. Yoshihara, J. Phys. Chem., 90, 1986, p. 5672.

22. B. Dick and N. P. Ernsting, J. Phys. Chem., 91, 1987, p. 4261.

23. N. P. Ernsting and B. Dick, Chem. Phys., 136, 1989, p. 181.

24. G. A. Brucker and D. F. Kelley, J. Phys. Chem., 91, 1987, p. 2856.

25. G. A. Brucker and D. F. Kelley, J. Phys. Chem., 93, 1989, p. 5179.

26. W. E. Brewer, S. L. Studer, M. Standiford and P. Chou, J. Phys. Chem., 93, 1989, p. 6088.

27. W. E. Brewer, S. L. Studer, P. Chou and E. Orton, Chem. Phys. Lett., 158, 1989, p. 345.

28. J. Sepiol and R. Kolos, Chem. Phys. Lett., 167, 1990, p. 445.

29. M. L. Martinez, S. L. Studer and P. Chou, J. Am. Chem. Soc., 112, p. 2427, 1990.

30. D. A. Parthenopoulis and M. Kasha, Chem. Phys. Lett., 173, 1990, p. 303.

31. M. Sarkar and P. K. Sengupta, Chem. Phys. Lett., 179, 1991, p. 68.

32. B. Dick, J. Phys. Chem., 94, 1990, p. 5752.

33. F. Laemer, T. Elsaesser and W. Kaiser, Chem. Phys. Lett., 148, 1988, p. 119.

34. W. Frey, F. Laermer and T.Elsaesser, J. Phys. Chem. 95, 1991, p. 10395.

35. R. L. Hoff, Ph.D. thesis, University of California at Berkeley, 1991.

36. R. L. Fork, B. I. Greene and C. V. Shank, Appl. Phys. Lett., 38, 1981, p. 671.

37. J. A. Valdmanis and R. L. Fork, IEEE JQE, QE-22, 1986, p. 112.

38. W. H. Knox, M. C. Downer, R. L. Fork and C. V. Shank, Opt. Lett., 9, 1984, p. 552.

39. A. L. Harris, M. Berg and C. B. Harris, J. Chem. Phys., 84, 1986, p. 788.

40. M. Berg, A. L. Harris, J. K. Brown and C. B. Harris, Opt. Lett., 9, 1984, p. 50.

41. T. Elsaesser, B. Schmetzer, M. Lipp and R. J. Bauerle, Chem. Phys. Lett., 148, 1988, p. 112.

42. C. J. Pouchet, The Aldrich Library of FT-IR Spectra, Ed. 1., Vol. 2, Aldrich Chemical Co., Milwaukee, 1985, p. 95B.

43. D. Ben-Amotz and C. B. Harris, J. Chem. Phys., 86, 1987, p. 4856.

44. R. S. Moog, S. C. Bovino and J. D. Simon, J. Phys. Chem., 92, 1988, p. 6545.

45. K. C. Ingham and M. A. El-Bayoumi, J. Am. Chem. Soc., 96, 1974, p. 1674.

46. R. C. Cantor and P. R. Schimmel, Biophysical Chemistry Part II: Techniques for the Study of Biological Structure and Function, W. H. Freeman and Co., San

Francisco, 1980, sect. 8-2.

47. B. J. Schwartz, Unpublished Data, 1991.

48. L. A. Peteanu, Unpublished Data, 1991.

Chapter 4: Direct Femtosecond Measurements of Geminate Recombination Times of Small Molecules in Liquids

4.1 Overview

While most chemical reactions take place in solutions, the important role the solvent plays in a chemical reaction is still only poorly understood [1,2]. Through collisions, the surrounding liquid molecules can provide the energy necessary to initiate a particular chemical reaction. Interactions with the solvent can mix the electronic and vibrational states of a reacting species and alter curve crossing, leading to control over product branching ratios. The solvent can also act as a bath, shuttling energy among the various reactive coordinates and providing dissipation for energy that might otherwise cause further reaction to occur. Even well understood gas phase reactions often show surprising behavior in the liquid environment.

Some of these differences between gas and solution phase chemical reactions are illustrated schematically by the generic potential surfaces depicted in Figure 4.1.1. Upon photoexcitation, the gas phase molecule can be trapped in a bound excited state, or undergo curve crossing the dissociative repulsive state. Through collisionally induced predissociation, the liquid environment can change the rate of this crossing, as well as the yield of molecules that actually dissociate. After recombination, the ground state molecules which would remain highly vibrationally excited in the gas phase lose their energy to the solvent. This vibrational cooling process can be the rate-determining step for many chemical reactions, as energy is distributed between the various internal modes of the reacting molecule and the solvent. Since the typical collision rate for a

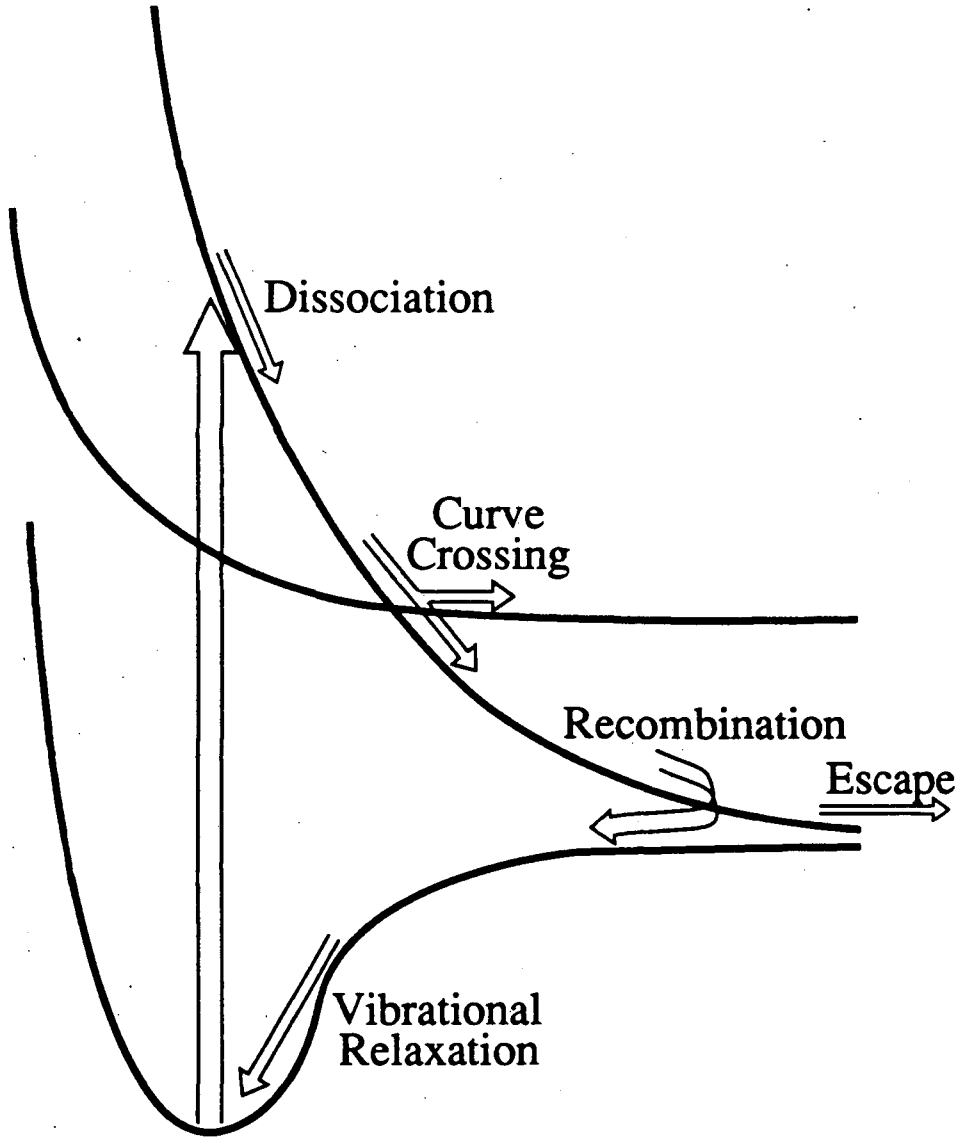

Figure 4.1.1: Generic potential energy surfaces for a photodissociation reaction showing important dynamical processes. After rapid dissociation, the reacting molecule can undergo curve crossing, escape or collide with surrounding solvent molecules to recombine. After recombination, the vibrationally hot ground state molecule cools by exchanging energy with the solvent.

reacting molecule in a normal, room temperature liquid is ~10^{13} s^{-1}, solvent effects which require only a few collisions will happen on the picosecond and subpicosecond time scales. The rates for various solvent effects on chemical reactions are also illustrated in Figure 4.1.1; clearly, femtosecond time resolution is needed to obtain a good microscopic understanding of condensed phase chemical reaction dynamics.

One of the most unique aspects of liquid-phase chemical reactivity is the ability for reacting species to become trapped in a "cage" of solvent molecules. Compared to a gas phase photodissociation reaction, this ability of the solvent to confine the photofragments leads to a reduction in the dissociation yield due to the back reaction of the photoproducts which are trapped in the solvent cage. This process is illustrated in Figure 4.1.2. This caging pushes the dissociating fragments back together on their ground state potential, leading to the recombination pictured in Figure 4.1.1. The recombination of original partners to reform the parent species is known as geminate recombination; recombination with a photofragment from a neighboring photodissociation which has escaped its solvent cage is known as non-geminate recombination. The time scale and details of the mechanism of the geminate recombination process have become a central problem in liquid-phase chemical reaction dynamics [1,2].

Many theories have been proposed to describe this process, most of which rely on some type of stochastic or diffusive motion for the recombination fragments [3-6]. Indeed, in many molecular systems, secondary geminate recombination, the diffusive recombination of original partners which have left the solvent cage, has been well documented [3-7]. This secondary geminate recombinative process, however, takes

Gas Phase: Photodissociation

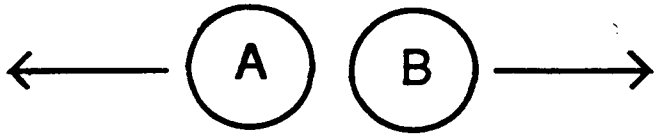

Solution Phase: Photodissociation and Recombination

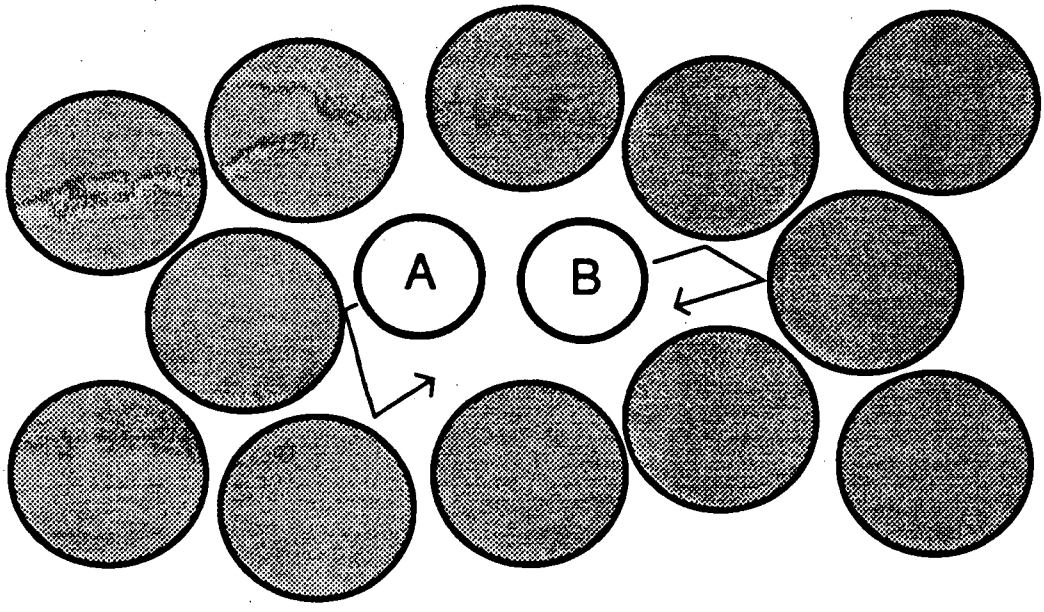

Figure 4.1.2: Schematic illustration of solvent caging showing differences between gas phase and solution phase photodissociation reactions.

place on a time scale of tens of picoseconds or greater [4-8], much longer than solvent caging times which last for less than a few picoseconds. Primary geminate recombination, the recombination of original partners that are still subject to solvent caging, has not been well characterized [1-8]. Previous work has established that the primary recombination takes place in ≤ 1.5 psec [9,10], but the exact time scale and mechanism of this process are not understood.

In this chapter, what may be the first direct observation of this process is described for the photodissociation of methylene iodide (CH_2I_2). In the next section, a brief history of ideas on caging and recombination are given, as well as background information on the specifics of the methylene iodide photodissociation. This is followed by a summary of the experimental apparatus used to measure the recombination dynamics, and summary of the results obtained, and a discussion of the data which includes implications for the mechanism of primary geminate recombination in many chemical systems.

4.2 Background

A. History of Caging: The prototypical system for studying the geminate recombination of radicals has been the photodissociation of I_2 [1,2]. Since the 1934 suggestion of Franck and Rabinowitch [11] that geminate recombination could influence the reaction dynamics of this system, many experimentalists have worked to measure the rate of this process. Early picosecond experiments by Eisenthal et al. examined this process by studying the bleach of the ground state molecular I_2 absorption [12]. After photodissociation, molecular iodine no longer absorbs at 532

nm, leading to a bleach of the sample at this wavelength. By watching this absorption recover after photodissociation, Eisenthal et al. believed they were observing the geminate recombination of I_2. The time scale for this bleach recovery was on the order of 100 psec, in good agreement with diffusive notions of geminate recombination [12].

Molecular dynamics simulations, however, predicted geminate recombination times for molecular iodine which were orders of magnitude faster [13,14] than those observed by Eisenthal's group. Nesbitt and Hynes found in their simulations that the I atoms had little time to diffuse in the cage before recombination; vibrationally hot I_2 molecules were formed very quickly after the photodissociation, but the subsequent cooling of the hot molecules back to thermal equilibrium with the solvent was relatively slow [13]. This lead Nesbitt and Hynes to propose an alternate interpretation of the results of Eisenthal et al.: they assumed that geminate recombination occurred quickly, and that vibrational cooling of the hot, reformed I_2 was responsible for the long bleach recovery observed in the experiments. This is because vibrationally excited I_2 absorbs well to the red of the vibrationally cool I_2, so the ground state absorption would not recover until after all the cooling is complete. (see Figure 4.1.1). Nesbitt and Hynes proposed a test of their re-interpretation; they predicted that vibrational cooling would result in a blue-shift of the transient absorption spectrum of the newly recombined molecular iodine [13].

The spectral blue-shift predicted by Nesbitt and Hynes was confirmed experimentally by the work of Harris et al [15]. Subsequent work by both the Harris group [9] and Hopkins et al. [10] confirmed that geminate recombination of I_2 was essentially complete with 1.5 psec, and that vibrational cooling was responsible for

observed long bleach recovery times. Additional molecular dynamics simulations by Brown et. al. [16,17] of the I_2 photodissociation in liquid Xe further clarified many of the important steps involved in the recombination and subsequent cooling. After photoexcitation in these simulations, the recoiling I atoms usually lost enough energy on their initial collisions with the solvent cage to recombine on a very short time scale. Those atoms that escaped the cage could also undergo recombination with their original or other partners, but on a much longer time scale; the rate becoming essentially controlled by diffusion of the I atom through the Xe. For those atoms that did directly recombine to geminately form molecular iodine, vibrationally hot I_2 appeared just a few hundred femtoseconds after the photofragmentation.

In all the above experiments, however, the photodissociation and subsequent recombination of I_2 is complicated by the fact that iodine undergoes predissociation. The original photoabsorption of iodine is to the bound B state, there is some time delay before curve crossing, whether or not it is collisionally induced takes place and the molecule dissociates. Recent work by Scherer et. al [18] has shown that predissociation lifetime of the B state of I_2 in hexane is around 200 fsec. Once on the dissociative surface, the actual dissociation could then take an additional 100-150 fsec. Thus, the recombination process cannot start until more than 300 fsec after the initial absorption, possibly obscuring important caging dynamics which could occur on faster time scales. To avoid this problem, it is necessary to study a system which is directly dissociative, and which absorbs at wavelengths accessible by present femtosecond technology. One system which meets these requirements is methylene iodide, CH_2I_2.

B. The Photodissociation Dynamics of CH_2I_2: Methylene iodide is an

essentially tetrahedral molecule with two hydrogen and two iodine atoms attached to a central carbon atom. The ground state electronic absorption spectrum, pictured in Figure 4.1.3, consists of several large irregularly shaped bands in the near ultraviolet, all of which have been assigned to $n \rightarrow \sigma^*$ transitions. [19]. Magnetic circular dichroism experiments have shown that these bands actually consist of 5 different electronic transitions [20]. Excitation of all of these bands leads to photodissociation of methylene iodide into $CH_2I + I$ or $CH_2I + I^*$; even though it is energetically allowed, production of $CH_2 + I_2$ is forbidden by symmetry considerations[1] [22].

One of the more interesting aspects of the methylene iodide photodissociation is that the dissociative surfaces for production of ground and spin-orbit excited iodine atoms are mixed, leading to production of both I and I* for single wavelength excitation. This curve crossing has been studied by Leone's group [23,24] and Hunter and Kristjansson [25] who measured wavelength dependant quantum yields for I* production. Since the gas phase I/I* branching ratios are well-known, diiodomethane is a prime candidate for testing the effects of the liquid environment on curve-crossing dynamics.

The methylene iodide photodissociation has also been studied extensively with molecular beam techniques. Photofragment angular distributions have been measured for this photoreaction; when excited with polarized light, the fragments come off in a near cosine distribution [22,26]. This high photofragment anisotropy indicates that excited CH_2I_2 does not have time to rotate significantly before it dissociates,

[1]This is because the wavefunction of the excitation prepared from these transitions has a nodal plane between the two iodine atoms, precluding formation of and I-I bond. Excitation of diiodomethane in the vacuum ultraviolet, however, can lead to production of CH_2 and I_2 [21].

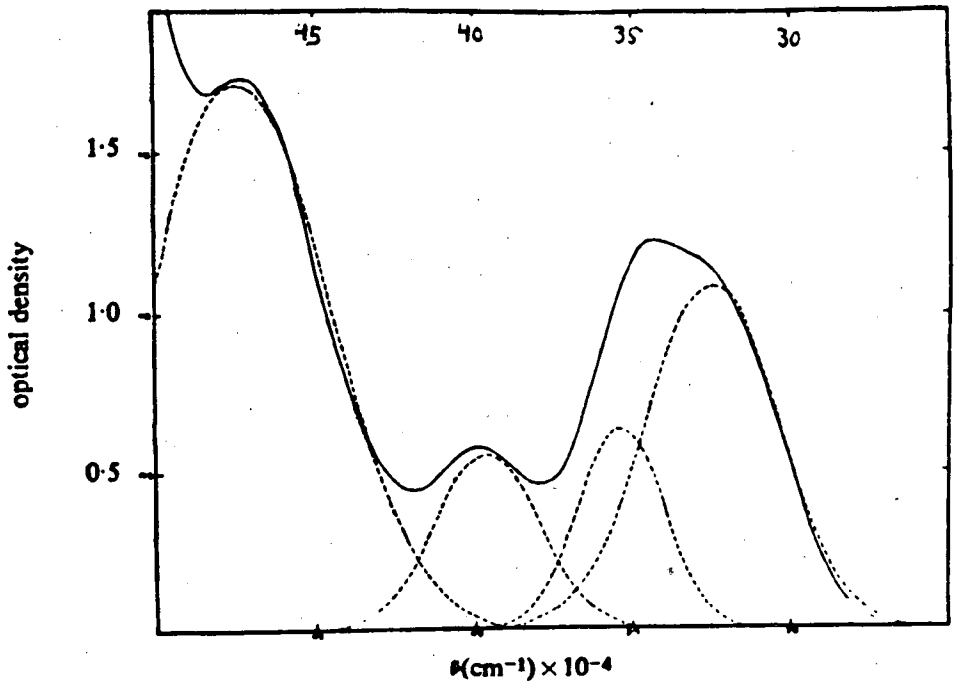

Figure 4.1.3: Electronic absorption spectrum (solid line) of CH_2I_2 in CCl_4. Dashed lines show that four individual Gaussian bands comprise the overall spectrum, after reference 19.

demonstrating that the dissociation is rapid and direct. The kinetic and internal energies of both the CH_2I and the I fragments have also been measured for this photoreaction, leading to a better understanding of the energy partitioning during dissociation [26]. The reaction is slightly unusual in that 80-90% of the available excess energy goes into internal excitation of the CH_2I radical. Thus, the CH_2I fragment produced from this photodissociation is a prime candidate for the study of vibrational cooling in solution.

The flow of excess vibrational energy in the monoiodomethylene radical has also been the subject of several investigations. Zhang and Imre measured the resonance Raman spectrum of CH_2I_2 [27], and found that the early dissociation dynamics proceed along a combination of the I-C-I symmetric and anti-symmetric stretching coordinates. This fits with physical intuition; as the C-I bond elongates during dissociation, the remaining CH_2I will try to reach a more planar configuration, requiring motion along the remaining C-I bond and the CH_2I umbrella coordinate. Zhang. et al. have fit the observed Raman overtones with a wavepacket model incorporating coupling between the two C-I coordinates [28]. In order to correctly fit their spectrum, the calculation required that the dissociation of methylene iodide is complete within 80 fsec, in agreement with the photofragment anisotropy measurements which also implied direct dissociation.

Leone's group has also investigated energy flow within the methylene iodide photodissociation by studying IR emission from the CH_2I radical [29,30]. Although excess vibrational energy was expected to be found in the low frequency C-I stretch and umbrella motions of CH_2I, Leone and coworkers found that after only few

collisions in the gas phase, vibrationally hot CH_2I showed emission from high frequency C-H stretches and bends. This migration of energy from low to high frequency modes implies rapid, facile energy redistribution, a somewhat surprising result given the low number of modes and low degree of anharmonic coupling between them in this radical fragment. This unusual energy behavior and the large separation between the vibrational frequencies in this molecule make it an ideal candidate for studying energy flow in liquid phase chemical reactions with femtosecond Raman or IR spectroscopy.

There has also been limited spectroscopy done on the CH_2I radical itself. Mohan et al. prepared isolated CH_2I in a frozen matrix by ultraviolet irradiation of CH_2I_2 [31]. The radical has a large absorption in the visible, with broad peaks centered near 380 and 590 nm. The 590 nm absorption is of special interest since it coincides nicely with the available femtosecond laser probe wavelength of 620 nm (Chapter 2). Maier et. al., however, have performed virtually the identical experiment as Mohan and coworkers, but have arrived at a slightly different interpretation [32]. The visible peaks reported by Maier et. al. are at 370 and 545 nm, slightly blue-shifted from those of Mohan et. al. By using IR spectroscopy to characterize their trapped intermediate in the matrix as well as UV-visible spectroscopy, Maier and coworkers have assigned the visible absorption to an isomer of methylene iodide: $H_2CI{\bullet\bullet\bullet}I$. Although the I-I bond is weak in the isomer, Maier et al. calculate that it has important effects on the IR spectrum of the molecule; the calculated IR spectrum is in agreement with the experimentally measured IR spectrum. It is not clear whether or not the presence of the weak I-I bond significantly alters the absorption of CH_2I, or if the blue-shift observed by Maier et. al.

is the result of this complexation. In either case, caged CH_2I + I should have a strong absorption in the visible near 620 nm, making it amenable for study with the femtosecond laser system.

4.3 Experimental

A. Femtosecond Laser System: The femtosecond laser system has been previously described in Chapter 2 and in the literature [33]. Briefly, the output of a colliding-pulse-modelocked ring laser amplified by a copper-vapor laser was frequency doubled and used to photodissociate CH_2I_2 at 310 nm, while the 620 nm laser fundamental was used to measure the population dynamics of the CH_2I photofragment. The instrument function, determined by cross-correlation of the UV and visible femtosecond pulses as the transient absorption rise of diphenylbutadiene, was fit to a 120 fsec Gaussian, using the fitting procedures described in Chapter 7. Data collection was performed in a dual-beam geometry, with signal and reference pulses normalized on every laser shot at the 8 kHz repetition rate of the laser. In the transient absorption traces presented below, there were typically 25,000 laser shots averaged at each stage position (time delay).

The observed signals varied linearly with pump intensity and were independent of probe intensity, verifying that multiphoton processes were not important. Care was taken to ensure that no interfering transient absorptions were observed from the neat solvents. The first nsec of the dynamics was independent of the sample concentration; a decay of the signal after 1 nsec due to diffusive non-geminate recombination was observed, however for samples with a > 50 mM concentration.

B. Materials: Samples were 1 - 10 mM of CH_2I_2 in CCl_4, $CHCl_3$ or CH_2Cl_2. Both the sample molecule, obtained from Aldrich, and the spectral grade solvents, obtained from Burdick and Jackson were used as received. The samples were flowed in a jet through a 300 μm nozzle (Spectra-Physics). This prevented the formation of photoproducts on cell walls, and also ensured that a fresh sample volume was being probed every laser shot. UV-visible absorption spectroscopy indicated degradation of the samples after ~1 hour exposure to the femtosecond UV pump pulses (e.g., a visible absorption band appeared, indicating the formation of I_2 photoproduct from diffusive non-geminate recombination). Samples were replaced frequently; no changes in absorption dynamics were observed between fresh solutions and those that had been exposed to the laser for an hour.

4.4 Results

The dynamics of the 620 nm transient absorption for the photodissociation of CH_2I_2 are shown in Figure 4.4.1. The data were taken by exciting the sample with the 310 nm pump pulse, and monitoring the change in absorbance of the sample with the 620 nm probe pulse. The results are fit to a combination of simple exponentials, convoluted with a 120 fsec Gaussian representing the instrument function, using the procedures outlined in Chapter 7. The results fit nicely to an instrument limited rise, with a fast 350 fsec decay superimposed on a slower, 10 psec exponential rise. By extrapolating the slow rise back to t=0, the amplitude ratio of the exponential decay to the initial rise was determined to be 0.38.

The effect of the solvent on the dynamics of the methylene iodide photodissociation

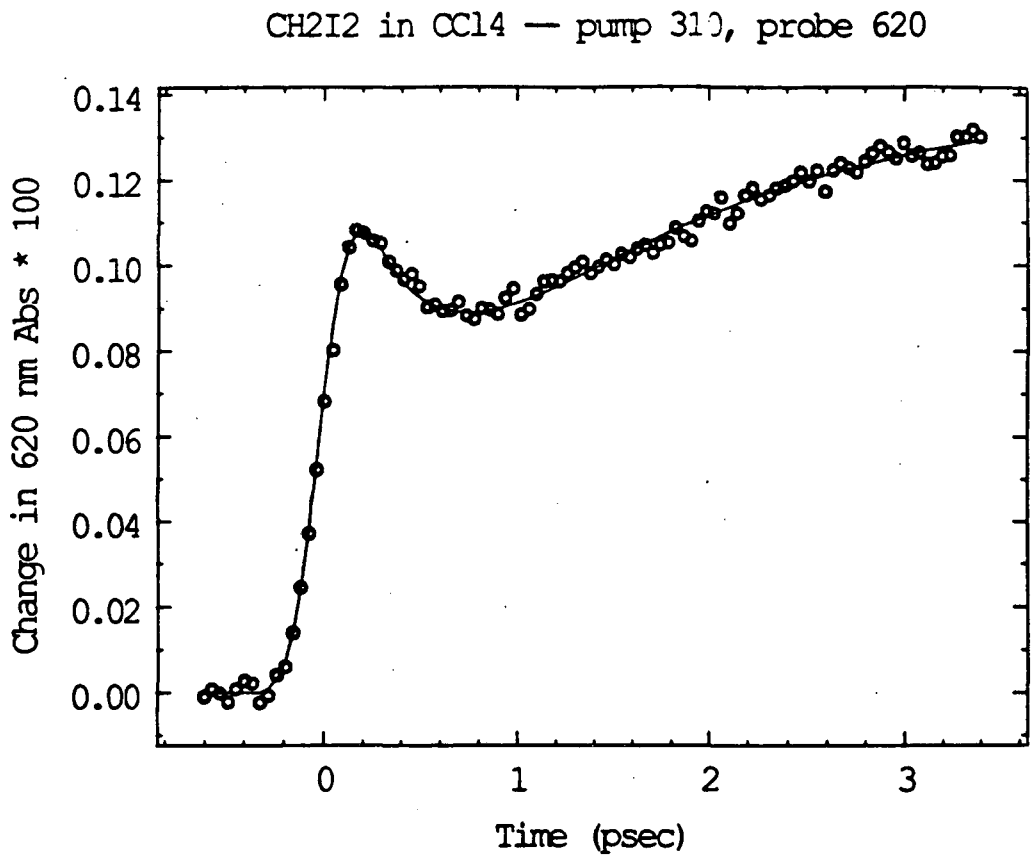

Figure 4.4.1: 620 nm transient absorption of CH_2I_2 in CCl_4. Circles are data points, line is a fit to a combination of simple exponentials. The amplitude ratio between the initial rise and the 350 fsec decay is 0.38.

can be seen in Figure 4.4.2, which shows the 620 nm transient absorption of CH_2I_2 in $CHCl_3$ and CH_2Cl_2. The results fit to the same functional form as the trace of Figure 4.4.1: there is a pulse-width limited rise, followed by a 350 fsec fast exponential decay superimposed on a slower rise. The slow rise times, however, decrease as the solvent is hydrogenated -- the slow rise is faster in methylene chloride than it is in carbon tetrachloride. The amplitude ratio of the fast decay to the initial rise also decreases as the solvent is hydrogenated. This ratio is 0.33 for CH_2I_2 in chloroform, and 0.24 for CH_2I_2 in methylene chloride. The 350 fsec decay time constant is the same within the noise for all three solvents, although the fit to the scan in CH_2Cl_2 is difficult due to the small amplitude of the decay component.

4.5 Discussion

The data of Figure 4.4.1 can be interpreted in the following manner. The rapid absorption rise at 620 nm measures the presence of the CH_2I radical fragment [31,32], indicating that dissociation is essentially complete within the 120 fsec instrument response, in agreement[2] with the gas phase photofragment angular distribution [22,26] and resonance raman data [27,28]. The slow, 10 psec rise time can be assigned to vibrational relaxation; as the vibrationally hot CH_2I fragments cool, their electronic

---

[2]An alternative interpretation, in which the initial absorption rise is due to electronically excited CH_2I2 which dissociates into $CH_2I + I$ in 350 fsec, is not consistent with the resonance Raman and anisotropy data which indicate direct ($\leq$ 100 fsec) dissociation of methylene iodide. This interpretation is also not consistent with the lack of solvent dependence for the observed decay time; it is unlikely that the pre-dissociation lifetime would remain constant in solvents of such widely differing polarity as CCl_4 and CH_2Cl_2.

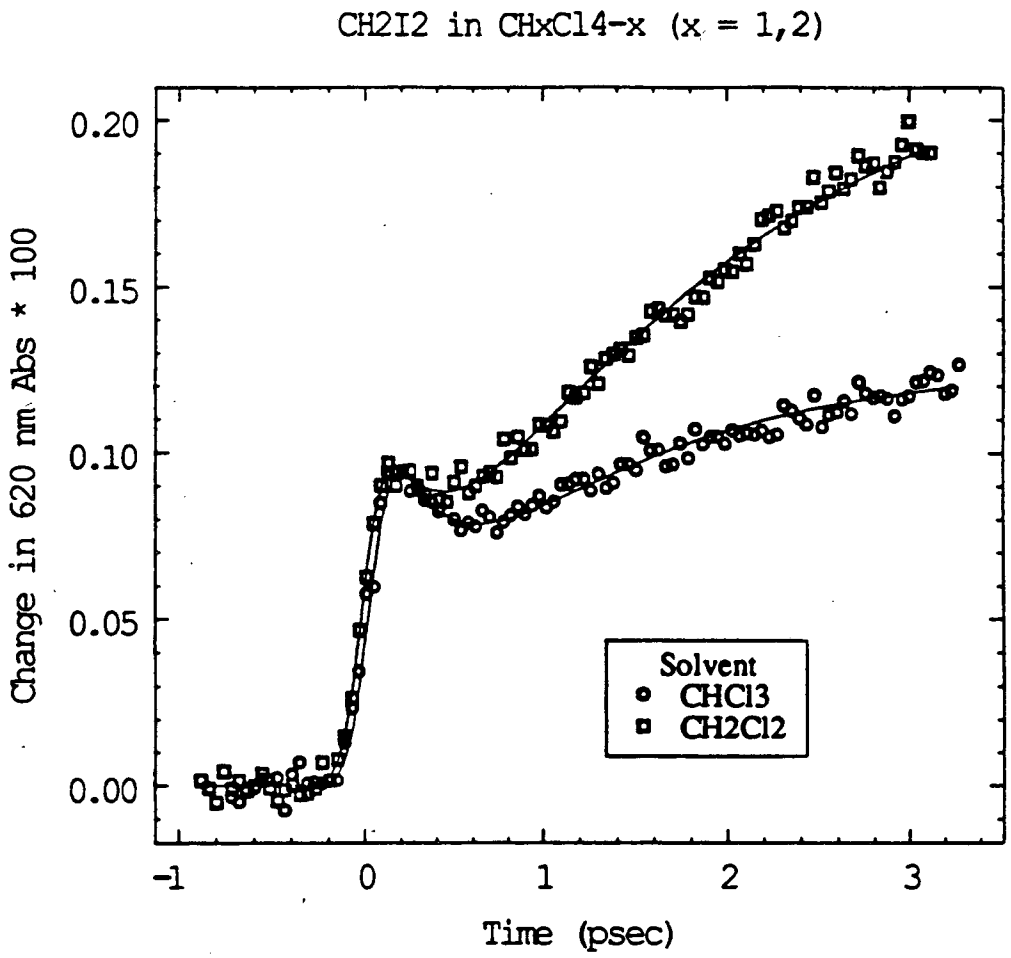

Figure 4.4.2: 620 nm transient absorption of CH_2I_2 in different solvents. Circles are data points in $CHCl_3$, squares are data points in CH_2Cl_2, lines are exponential fits to the data. The the two scans have been scaled to have the same initial rises for better comparison. The amplitude ratio of the 350 fsec decay to the initial rise and is 0.33 for $CHCl_3$ and 0.24 for CH_2Cl_2.

absorption spectra shift better into resonance with the 620 nm probe light.[3] This 10 psec cooling time is typical for small molecules in room temperature molecular liquids [34]. The 350 fsec decay after the initial absorption rise corresponds to a disappearance of the hot CH_2I radicals. Since the gas phase photodissociation quantum yield is unity, the disappearance of CH_2I must be due to geminate recombination of CH_2I and I to reform the parent CH_2I_2 molecule. Comparison to the molecular dynamics simulations of the I_2 photodissociation reaction supports this assignment as observation of the primary geminate recombination. (CH_2I absorption loss due to secondary geminate recombination, the diffusive recombination of fragments which have escaped the solvent cage, can not be easily detected under the vibrational cooling absorption rise).

These results suggest that most of the geminate recombination is controlled non-stochastically. This means that essentially a single collision of the photofragments with the solvent cage could dominate the recombination process, and that the role of subsequent diffusive recombination is secondary. This assumption of a single cage collision allows a crude estimate for the time scale of this primary, non-diffusive geminate recombination. Photodissociation of small molecules has been shown in the

---

[3]As with many small molecules, vibrationally hot CH_2I absorbs to the red of vibrationally cool CH_2I. Since the cool species has its absorption maximum near 620 nm, the Franck-Condon overlap with the 620 nm probe pulse increases as the hot species cools and its absorption blue-shifts.

gas phase [35] to take place in 50-200 fsec.[4] Resonance Raman data indicate that the early dissociative dynamics of small molecules which are similar to methylene iodide are essentially unchanged between the solution and the gas phases [36]. The time scale for a single collision with a solvent molecule in a typical room temperature liquid is about 100-150 fsec. If the photofragments then need an additional 100-150 fsec to collide and recombine on their ground electronic state, this gives an estimate for a total primary geminate recombination time of 250-500 fsec; the dynamical features should be largely independent of the details of the photodissociating molecule and the solvent.

If the primary geminate recombination interpretation holds for the CH_2I_2 dissociation, then it should be possible to vary the amount of recombination by changing the solvent cage, without significantly altering the recombination rate. This idea was tested by studying the dissociation dynamics of CH_2I_2 in $CHCl_3$ and CH_2Cl_2 solutions, as shown in Fig 4.4.2. If the molecules comprising the cage are lighter and more easily brushed aside by the recoiling I atom, then a lower recombination yield would be expected since there should be a higher percentage of I atoms escaping the cage. Those atoms that do recombine, however, should still do so on the same, single cage collision time scale of 350 fsec. The results of Fig. 4.4.2 support the idea of single-collision dominated primary geminate recombination. The amplitude of the 350 fsec decay component is smaller in the lighter solvents, which implies that the recombination yield decreases as the solvent is hydrogenated from CCl_4 to CH_2Cl_2.

---

[4]Assuming direct excitation to a dissociative state, the time scale for photofragmentation will vary depending on the slope of the repulsive potential, the partitioning of the excess energy among the various fragment degrees of freedom as well as the mass of the fragments.

The recombination rate, however, remains at 350 fsec in all the solvents, as expected for the single-collision dominated recombination mechanism. In addition, the vibrational cooling times decrease as the solvent is varied from CCl_4 to CH_2Cl_2, a trend also observed in the vibrational relaxation of I_2 [1].

It would be interesting to compare the relative recombination amplitudes of CH_2I_2 in the various solvents to dissociation quantum yields. Unfortunately, there have been no solution phase quantum yield measurements for CH_2I_2 dissociation reported to the best of my knowledge. Even with known quantum yields, direct comparison with the amplitudes of Figures 4.4.1 and 4.4.2 may be complicated by the fact that the dissociation quantum yields might also include some of the secondary, diffusive geminate recombination. Another test of this primary, non-stochastic geminate recombination idea would be to directly monitor the formation of the newly recombined parent molecule on this same 350 fsec time scale. However, this is experimentally difficult. Ground state bleach experiments are complicated by the fact that the recombined molecules are vibrationally hot, and the bleach will not recover until after the subsequent vibrational cooling. It may be possible to detect the formation of the vibrationally hot recombined parent (which would likely occur in the near UV for CH_2I_2, a difficult wavelength range to study with present femtosecond laser technology), as long as one of the photofragment species does not also absorb in the same wavelength range. Transient IR or Raman on the newly forming bond during the recombinative process may offer the best direct proof (or disproof) of single-collision dominated primary geminate recombination.

In lieu of these technical difficulties, the best way to test this idea is by example.

Since the rate of collision dominated recombination should be very similar for all photodissociation reactions, the same type of results should be obtained for many different molecules. This makes it interesting to compare the dynamics of photodissociating methylene iodide (Figure 4.4.1) with those of photodissociating $Cr(CO)_6$ [37]. (see especially Fig. 2 of reference 37.) The traces are remarkably similar. Joly and Nelson, however, interpret their data for chromium hexacarbonyl as follows: the fast initial absorption rise is due to electronically excited $Cr(CO)_6$; this absorption then decays in ~350 fsec as $[Cr(CO)_6]^*$ dissociates into $Cr(CO)_5$ + CO. The subsequent absorption increases/decreases (depending on probe wavelength) are assigned to solvation and vibrational relaxation of the $Cr(CO)_5$ photofragment; geminate recombination is not considered. This alternative interpretation of predissociation does not seem likely to hold for the CH_2I_2 data of Figure 4.4.1 based on the resonance Raman and gas phase anisotropy data which suggest that the direct dissociation of methylene iodide occurs in much less than 350 fsec.

The data of Joly and Nelson, in fact, could be interpreted in a manner consistent with the observation of geminate recombination of $Cr(CO)_5$ and CO. Many studies [38,39] have indicated that the quantum yield for $Cr(CO)_6$ dissociation in solution is ~0.7;[5] the ~0.3 recombinative yield should have a marked presence on the femtosecond transient absorption spectra, and could explain the observed 350 fsec absorption decay. The striking similarity of transient absorption traces of the $M(CO)_6$ family (M = Cr, Mo, W), however, suggests that curve crossing is either very rapid, or

[5] Note that the quantum yield is solvent dependant, but is ~0.7 in alkane and simple alcohol solvents.

that the dissociation is direct [40]; predissociation times should be different for the different metal atom centers. The dissociation, if direct, should take place quite rapidly as the light CO fragment carries a significant portion of the kinetic energy, and should quickly separate from its $Cr(CO)_5$ partner. This makes the interpretation of the fast decay in the $M(CO)_6$ data as geminate recombination plausible; the dissociation could be rapid, leading to instrument limited rises, and all three species show identical decay times, as would be expected for single-collision primary geminate recombination. IR or Raman experiments, like those suggested above, would help to distinguish between the two possible interpretations of the data.

Other photodissociation studies have also provided data which are consistent with this idea of fast primary geminate recombination. Femtosecond transient absorption studies [41] of $M_2(CO)_{10}$ molecules (M = Mn or Re) in solutions also show a fast 300-500 fsec decay, consistent with the interpretation of primary geminate recombination. Work on photochromic spiropyrans, summarized in Chapter 6, in which the photoexcitation cleaves a ring system leaving the reactive fragments tethered together (similar to the system studied by Scott and Doubleday [6]) shows a ~200 fsec absorption decay which has been interpreted as primary geminate recombination. For this example, tethering by the ring system as well as solvent caging help to confine the reacting fragments, leading to the slightly higher primary geminate recombination rate. In all these systems, the decay of the photoproducts on a 200-500 fsec time scale supports the picture of primary geminate recombination dominated by the initial collisions of the fragments with the surrounding solvent cage.

4.6 Summary

In summary, femtosecond transient absorption spectroscopy has been used to monitor the population of the photofragments produced after the photodissociation of CH_2I_2. All the spectra show transient absorption traces which indicate the disappearance of the CH_2I photofragment on a 350 fsec time scale. This result is consistent with the idea of two distinct components of geminate recombination. The primary, non-stochastic component is dominated by a single collision of the photofragments with the surrounding solvent cage, leading to recombination on the 300-500 fsec time scale. This recombination rate depends primarily on the kinetic energy of the fragments and the density of the surrounding solvent molecules, and hence, is largely independent of the molecular details of the system under investigation. Those fragments that escape the solvent cage can then undergo secondary, or diffusive geminate recombination, but on much longer time scales. The similarity of the CH_2I_2 data to the results obtained on metal carbonyls and other chemical systems suggests that these dual kinetics may be a universal feature of geminate recombination of neutral fragments produced after the photodissociation of small molecules in normal, non-reactive room temperature molecular liquids.

4.7 References

1. A. L. Harris, J. K. Brown and C. B. Harris, Ann. Rev. Phys. Chem., 39, 1988, p. 341 and references therein.
2. J. T. Hynes, Ann. Rev. Phys. Chem., 36, 1985, p. 573.
3. R. M. Noyes, Prog. React. Kinet., 1, 1961, p. 129.

4. J. Schroeder and J. Troe, Ann. Rev. Phys. Chem., 38, 1987, p. 163.

5. H. Hippler, B. Otto, J. Schroeder, V. Schubert and J. Troe, Ber. Bunsenges. Phys. Chem., 89, 1985, p. 240.

6. T. W. Scott and C. Doubleday Jr., Chem. Phys. Lett., 178, 1991, p. 9.

7. M. G. Hyde and G. S. Beddard, Chem. Phys. 151, 1991, p. 239.

8. T. W. Scott and S. N. Liu, J. Phys. Chem., 93, 1989, p. 1393.

9. D. E. Smith and C. B. Harris, J. Chem. Phys., 87, 1987, p. 2709.

10. X. B. Xu, S.-C. Yu, R. Lingle Jr., H. Zhu and J. B. Hopkins, J. Chem. Phys., 95, 1991, p. 2445.

11. J. Franck and E. Rabinowitch, Trans. Farad. Soc., 30, 1934, p. 120.

12. T. J. Chuang, G. L Hoffman and K. B. Eisenthal, Chem. Phys. Lett., 25, 1974, p. 201.

13. D. J. Nesbitt and J. T. Hynes, J. Chem. Phys., 77, 1982, p. 2130.

14. P. Bado, P. H. Berens and K. R. Wilson, Proc. SPIE, 322, 1982, p. 230.

15. A. L. Harris, M. Berg and C. B. Harris, J. Chem. Phys., 84, 1986, p. 788.

16. J. K. Brown, C. B. Harris and J. C. Tully, J. Chem. Phys., 89, 1988, p. 6687.

17. J. K. Brown and C. B. Harris, unpublished results, 1988.

18. N. Scherer and G. R. Flemin, J. Chem. Phys., 96, 1992, p. 5544.

19. M. Ito, P. C. Huang and E. Kosower, Trans. Farad. Soc., 57, 1961, p. 1662.

20. A Gedanken and M. D. Rowe, Chem. Phys., 36, 1979, p. 181.

21. H. Okabe, M. Kawasaki and Y. Tanaka, J. Chem. Phys., 73, 1980, p. 6162.

22. M. Kawalski, S. J. Lee and R. Bersohn, J. Chem. Phys., 63, 1975, p. 809.

23. J. B. Koffend and S. R. Leone, Chem. Phys. Lett., 81, 1981, p. 136.

24. W. H. Pence, S. L. Baughcum and S. R. Leone, J. Phys. Chem., 85, 1981, p. 3844.

25. T. F. Hunter and K. S. Kristjansson, Chem. Phys. Lett., 90, 1982, p. 35.

26. P. M. Kroger, P. C. Demou and S. J. Riley, J. Chem. Phys., 65, 1976, p. 1823.

27. J. Zhang and D. G. Imre, J. Chem. Phys., 89, 1988, p. 309.

28. J. Zhang, E. J. Heller, D. Huber and D. G. Imre, J. Chem. Phys., 89, 1988, p. 3602.

29. S. L. Baughcum and S. R. Leone, SPIE Proc., 158, 1978, p. 29.

30. S. L. Baughcum and S. R. Leone, J. Chem. Phys., 72, 1980, p. 6531.

31. H. Mohan, K. N. Rao and R. M. Iyer, Radiat. Phys. Chem., 23, 1984, p. 505.

32. G. Maier, H. P. Reisenauer, J. Hu, L. J. Schaad and B. A. Hess Jr., J. Am. Chem. Soc., 112, 1990, p. 5117.

33. B. J. Schwartz, L. A. Peteanu and C. B. Harris, J. Phys. Chem., 96, 1992, p.3591.

34. A. Seilmeier and W. Kaiser, in *Ultrashort Laser Pulses and Applications*, edited by W. Kaiser (Springer-Verlag, Berlin, 1988), Chap. 7.

35. see, e.g., M. J. Rosker, M. Dantus and A. H. Zewail, Science, 241, 1988, p. 1200.

36. F. Markel and A. B. Myers, Chem. Phys. Lett., 167, 1990, p. 175.

37. A. G. Joly and K. A. Nelson, J. Phys. Chem., 93, , 1989, p. 2876.

38. S. K. Nayak and T. J. Burkey, Organomet., 10, 1991, p.3747.

39. J. K. Burdett, J. M. Grzybowski, R. N. Perutz, M. Poliakoff, J. J. Turner and R. F. Turner, Inorg. Chem., 17, 1978, p.147.

40. A. G. Joly and K. A. Nelson, Chem. Phys., 152, 1991, p. 69.

41. B. J. Schwartz, J. C. King. J. Z. Zhang and C. B. Harris, unpublished results.

Chapter 5: Ultrafast Studies of 1,4-Diphenyl-1,3-Cyclopentadiene, a Locked s-*cis* Diphenylbutadiene Analog

5.1 Overview

One of the most important differences between gas phase and solution phase chemistry lies in the ability of the solvent to alter the rate of a chemical reaction. In the gas phase, the outcome of a unimolecular reaction can be predicted completely by the initial state of the reactant; transition state and RRKM theories have been successful in describing the rates of gas phase chemical reactions [1]. In solution, however, interactions with the solvent can alter reactant energetics, provide for collisional energy flow into or out of reactive coordinates and sterically hinder large amplitude reactive motion. As a result, transition state theory fails to describe solution reactions, significantly overestimating the reaction rate. By studying the rates of unimolecular reactions (usually, cis-trans isomerization of phenyl-substituted polyenes) in solutions, it may be possible to learn more about the microscopic physics underlying condensed phase chemical reaction rates.

One of the simplest theories describing solution phase reaction rates is Kramers' theory [2]. Kramers assumed that a liquid phase reaction follows the physics of the Langevin equation, which describes the diffusion of a particle over a potential barrier. The Langevin equation is merely Newton's second law with a random fluctuating force kicking energy into the particle, and a dissipative force drawing energy away from the particle (the random force and dissipative force are connected by a fluctuation-dissipation theorem which allows for energy conservation) [3]. By assuming a

piecewise-continuous parabolic potential and making some assumptions about well depths and barrier heights, Kramers was able to obtain an analytic solution to the Langevin equation for one dimensional reactive motion [2]. The Kramers' theory has been discussed recently in a review article [4], and is outlined nicely in the thesis of Rebecca Hoff [5]. The solution Kramers obtained falls into two regimes. In the low viscosity limit, the reaction rate is essentially controlled by the collisions with the solvent which provide the necessary energy to send the particle over the barrier. Increasing the viscosity leads to a higher collision rate, causing a net increase in the reaction rate. In the high viscosity limit, reactive motion is dominated by the dissipative force (viscous drag), slowing the motion of the particle on its way to escape over the barrier. This leads to a decrease in the reaction rate as the viscosity is increased. Thus, there must be a point between these two regimes where the rate reaches a maximum value as it stops increasing with increasing viscosity and starts decreasing. This point is called the Kramers' turnover, and has been recently observed experimentally by fluorescence spectroscopy in the cis-trans isomerization of stilbene in compressed ethane [6] (an earlier claim of the turnover observation by NMR in the ring inversion motion of cyclohexane [7] has been disputed in the literature [8]).

There have been many experimental tests of Kramers' theory by the study of cis-trans isomerization in systems such as stilbene [6], diphenylbutadiene (DPB) [9,10], 1-1'-binapthyl [11,12] and DODCI [13] as well as others [5]. Kramers' theory does not explain the rate data available for all these different systems. For example, even though 1-1'-binapthyl can move only along a single torsional coordinate and its isomerization rate in alkane solvents fits quite well to Kramers' theory [11], its isomerization rate in

alcohol solvents deviates significantly from Kramers' expression [12]. This makes it important to examine both the assumptions that go into the Kramers' theory and the validity of using systems like those listed above as test cases for Kramers' proposal.

There are several reasons why Kramers' theory could fail to explain the isomerization rate data for some or all of these systems. First, Kramers' theory is for motion along a one-dimensional reaction coordinate; the result does not hold if motion along two coupled dimensions is important to product formation. Recent work has determined that the isomerization coordinate of stilbene is not one-dimensional [14], although results suggest that the structurally similar DPB does undergo a one-dimensional reaction [9]. And, as mentioned above, 1-1'-binapthyl clearly follows a one dimensional reaction path but the theory fails in alcohol solutions. Second, Kramers' result depends on the frequency and height of the barrier to reaction. In most cases, the reaction coordinate for isomerization is not known, so the barrier height and frequency are fit as adjustable parameters. Many fits, however, produce physically unrealistic values for simple isomerative motion. Third, most tests of Kramers' theory assume that the friction along the reaction coordinate is proportional to the macroscopic solution viscosity, i.e. that hydrodynamics holds microscopically for an isomerization reaction. This assumption can be replaced by the assumption that the microscopic friction is proportional to the rotational diffusion time of the molecule (the rotational diffusion time should be linear with the viscosity by the Stokes-Einstein-Debye equation according to hydrodynamics [3], but the experimental deviation from linearity can be quite significant). This type of procedure, known as Kramers-Hubbard analysis, avoids some of the assumptions of hydrodynamics and can significantly

improve the fit to isomerization rate data [9,12], but does not work in all cases. Finally, Kramers's theory assumes that the Langevin equation correctly describes the physics behind solution phase isomerization dynamics. The Langevin equation inherently assumes that the random forces acting on the particle are delta-correlated; that is, the force acting at one time on the particle has no memory of what the forces were at previous times. This assumption can be avoided by re-solving the Kramers' problem with the Generalized Langevin Equation (GLE) (which includes solvent memory effects) [15], or by invoking models involving clustering of the solvent around the reacting species [10].

With all these various assumptions surrounding the test of Kramers' theory, it is surprising that there are few attempts to correlate isomerization behavior with spectroscopic information. One of the most widely studied isomerizations is that of DPB [5,9,10,16], yet it is not even clear what symmetry the first electronic excited state of DPB has or which electronic state is correlated with the isomerization. In the literature, both phenyl twisting [16] and carbon backbone torsion [9] have been assigned to the large amplitude motion underlying the observed dynamics. Rebecca Hoff and I spent a great deal of time trying to clarify this situation by studying substituted butadienes such as DPB, 1,1',4,4'-tetraphenylbutadiene (TPB) and 1,1',4,4'-tetraphenyl-2-methylbutadiene (TPMB) with ultrafast transient absorption spectroscopy [5]. While some progress was made in sorting through the various literature claims [5], much of the data interpretation was hindered by the lack of spectroscopic knowledge available for these systems. In this chapter, some additional work on phenyl-substituted butadienes is described.

Since the completion of Rebecca's thesis [5], there have been several new spectroscopic studies reported on DPB and some rigid DPB analogs [17,18]. In collaboration with the Kliger group at U. C. Santa Cruz, studies of DPB and 1,4-diphenyl-1,3-cyclopentadiene (DPCP) were undertaken, the results of which have definite implications on the spectroscopy and excited state dynamics of phenyl-substituted butadiene systems. In the following section, a brief recap of the history of spectroscopic studies on DPB from Rebecca's thesis [5] is given, followed by a summary of the newer studies [17,18] and their implications for the state-ordering in DPB. The subsequent section summarizes the experimental apparatus used for the new ultrafast studies on DPCP. This is followed by a presentation of the experimental results, and a discussion of the results in terms the history in Rebecca's thesis and the newer studies by the Kliger group.

5.2 Background

A. Electronic Structure of DPB: The isomerization reactions of the diphenylpolyenes [19,20] mimic those of important biological systems, such as the cis-trans isomerization of retinal, the primary event in the vision process [21] or photochemical transformations in the skin which are mediated by the polyene steroid hormone vitamin D [22]. Conjugated polyenes are also finding applications as organic conductors and possible non-linear optical materials [23]. Given that in addition, they are also readily spectroscopically accessible, the diphenylpolyenes have been the subject of intense study [5,17-20]. Structurally, the all-*trans* unsubstituted diphenylpolyenes have nearly C_{2h} symmetry. Thus, their electronic states are characterized in terms of

the A_g or B_u representations of the C_{2h} symmetry group, even through the actual symmetry of the polyene usually deviates from C_{2h}. The electronic ground state of all the diphenylpolyenes have been assigned to the totally symmetric A_g representation; the symmetry of the first singlet electronic excited state (S_1) has been found to be dependant on the polyene chain length. Diphenylhexatriene and longer chain polyenes have a lowest excited singlet state with A_g symmetry, while the S_1 state of stilbene (diphenylethylene) has B_u symmetry. For diphenylbutadiene (DPB), however, there has been considerable controversy over the ordering of the electronic excited states, especially for DPB in solutions.

The conflicting evidence for the state ordering in DPB has been well summarized in several places [5,17,18]. In the gas phase, the best available evidence points to the S_1 state being the $2A_g$ state, with the $1B_u$ state lying ~1200 cm^{-1} higher in energy [24]. In condensed environments, however, interactions with the surrounding medium can significantly affect the energies of the excited states and may, in fact, invert the ordering of the two levels. Studies done on DPB in an ethanol-isopentane-ether (EPA) glass found that the $1B_u$ state was only 130 cm^{-1} higher in energy than the $2A_g$ [25], while emission studies in room temperature liquids assign $1B_u$ symmetry to the S_1 state [26]. Since the more ionic $1B_u$ state is expected to be more strongly stabilized by the solvent polarizibility than the $2A_g$ state [19] and the two states lie so close together in EPA glass, it is not surprising that the two states are probably well-mixed in condensed environments, and that the state ordering in solution has been controversial.

One of the more unusual contributions to the question of state ordering in DPB has been the work of Rulliere et al. [16]. As summarized in the thesis of Rebecca Hoff [5],

these authors assumed that the level inversion between the gas and solution phases is a dynamic process controlled by interactions with the solvent. Their hypothesis is based on the observed dynamics of the transient absorption spectrum ($S_N \leftarrow S_1$) of DPB in solutions. Rulliere and coworkers observed a shoulder in the transient absorption spectrum, and found that the rise kinetics of the main spectral peak and the shoulder were different (80 vs. 100 psec), indicating a change in the level ordering as a function of time after excitation. In their interpretation [16], the initial one-photon excitation is to the higher lying $1B_u$ state; large amplitude motion (which they assign to phenyl twisting based on theoretical calculations [27]) which is assisted by the solvent, causes the levels to invert, and the $2A_g$ state is thermally populated from the now lower lying $1B_u$. Data taken by Rebecca and myself [5], however, does not support theses conclusions. Transient absorption scans taken at both the $S_N \leftarrow S_1$ absorption maximum and the shoulder were identical and show only instrument limited ($\leq$ 120 fsec) rise times [5]. This result is in agreement with other studies [10]; no evidence for a slower, solvent or wavelength dependant rise time was observed. The S_1 lifetimes measured by Rulliere and coworkers ($\geq$ 700 psec) are also in conflict with literature results [5]. In addition, the possibility of large amplitude phenyl twisting motion significantly affecting the excited state absorption spectrum or lifetime clashes with notions of the DPB isomerization being essentially one dimensional along the carbon backbone torsional coordinate [5,10,11]. Although it is possible that solvent-assisted level inversion does occur in this system and is simply not well coupled to the transient electronic absorption spectrum, the evidence for such a mechanism in DPB is extremely weak [5].

Clearly, an alternate explanation for the absorption, emission and transient absorption spectra of DPB is needed to provide a better understanding of the electronic structure and excited state properties of this diphenylpolyene. By comparing the properties of the flexible DPB molecule to more rigid analogs [17,18,28], it should be possible to gain a great deal of information about state ordering and excited state dynamics of DPB.

B. Comparison of the Electronic Properties of DPB and DPCP: Since the completion of Rebecca's thesis [5], there have been significant advances in the understanding of the electronic properties of DPB. Studies of DPB in solvents of differing polarizibility have lead to a better understanding of the S_1 transient absorption spectrum [17], and the role of free rotation around the butadiene single bond on the electronic structure of DPB has become better understood by comparisons with rigid DPB analogs [17,18,28]. The structures of some of these analogs are shown in Figure 5.2.1.

1. Electronic Structure of DPCP: The structure of 1,4-diphenyl-1,3-cyclopentadiene (DPCP), depicted in Figure 5.2.1 (c), is essentially that of DPB locked into a cis configuration around the butadiene single bond (compare to Figure 5.2.1 (b), the structure of s-*cis* DPB). To better understand the effects of the s-*cis* conformation on the electronic spectra of diphenylpolyenes, Ci et al. studied the excitation spectrum of DPCP in solvents of varying polarizibility as well as in a supersonic expansion [18]. The absorption spectrum of DPCP mirrors that of DPB, but its maximum is red-shifted by ~1200 cm-1 with respect to that of DPB, in good analogy with other polyenes which have known spectra for the s-*cis* and s-*trans* conformations [29]. Ci et

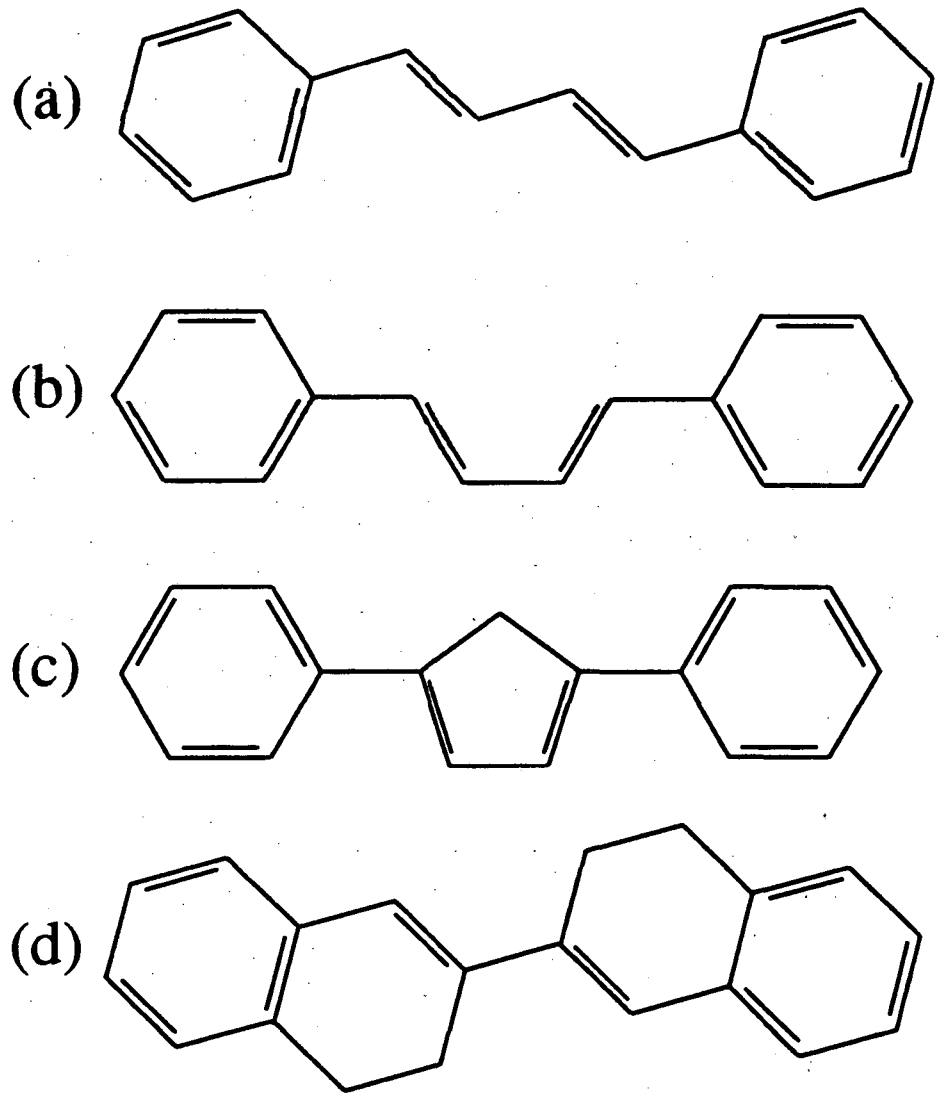

Figure 5.2.1: Structure of all-*trans* 1,4-diphenyl-1,3-butadiene (DPB) and some rigid analogs. (a) s-*trans* DPB. (b) s-*cis* DPB. (c) DPCP (a rigid s-*cis* DPB analog). (d) HHN (a rigid s-*trans* DPB analog). Note that all-*trans* DPB (structures (a) and (b)) can freely rotate around the central butadiene single bond, as indicated by the 's- ' prefix.

al. also noted that the fluorescence excitation spectrum of DPCP overlaps the emission spectrum, a result in contrast to that of longer diphenylpolyenes, leading to the possibility that the S_1 state has $1B_u$ symmetry. Since solvent polarizibility affects B_u states and A_g states quite differently [19], the shift in the fluorescence excitation maximum has a different slope with index of refraction depending on the symmetry of the excited state. Experimental results show an extremely large shift with changing index, indicating that the lowest excited state of DPCP in solutions is the 1Bu [18]. By extrapolating the position of the excitation maximum to zero polarizibility and comparing with the spectrum taken in the supersonic expansion, Ci et al. were able to assign the gas phase absorption of DPCP. The results indicate that the lowest excited singlet state of isolated DPCP is the $2A_g$, with the origin of the $1B_u$ state lying ~1100 cm^{-1} higher in energy [18]. Thus, the state ordering of DPCP shifts upon solvation; Ci et al. estimate that the $1B_u$ and $2A_g$ states should be degenerate in a solvent with an index of refraction of 1.25 [18].

The electronic properties of DPCP can be compared to those of DPB [18]. The origin for the $1A_g \rightarrow 2A_g$ transition in isolated DPCP is nearly 1400 cm^{-1} in energy lower than that of isolated DPB. Since the addition of alkyl groups to a polyene chain only results in a very small red-shift (~150 cm^{-1} for methyl-hexatriene [30]), most of this 1400 cm^{-1} shift must be due to locking the backbone of the molecule in the s-*cis* configuration [18]. Molecular mechanics calculations indicate that DPCP is rigorously planar in both the cyclopentadiene ring and the phenyl torsional angles, while the s-*cis* form of DPB has two stable minima with either a large twist in the diene, or small twists in both the diene and phenyl twist coordinates [18]. Since the red-shift of the

absorption maximum between DPB and DPCP was similar to that for other molecules, and the transient absorption spectrum of DPB was similar to that of HHN (a nearly planar locked s-*trans* DPB analog, shown in Figure 5.2.1 (d) [28]), it seems unlikely that small deviations from planarity have a significant effect on the level ordering in the diphenylpolyenes. Thus, DPCP does make a good spectroscopic analog for s-*cis* DPB.

2. *Evidence for s-*cis *Rotamers in the Electronic Structure of DPB:* As summarized in the previous section, the solvent-assisted level inversion model proposed by Rulliere et al. to explain the state ordering of DPB is not well supported by their data. To further test this model, Wallace-Williams and coworkers studied the excited state absorption spectrum of DPB in solvents of varying polarizibility [17]. As with DPCP, states with A_g character should show a much smaller shift with solvent polarizibility than the more ionic states with B_u symmetry. This leads to a definite prediction from the model of Rulliere et al.: as the solvent polarizibility is increased, the separation between the $2A_g$ and $1B_u$ states should increase, leading to an increased splitting in the excited state absorption spectrum. In addition, this separation should cause there to be less thermal population of the $2A_g$ state after the level inversion. Thus, the absorption assigned to the $1B_u$ level should significantly gain in intensity at the expense of that assigned to the $2A_g$ as the polarizibility is increased. The experiments of Wallace-Williams et al., however, show just the opposite trends: the peak assigned to the $2A_g$ state appears to increase in intensity as the polarizibility is increased, and the observed peaks do not shift relative to one another as the polarizibility is changed [17]. Thus, it appears that both the data and the model

presented in the work of Rulliere et al. [16] are inconsistent with established results.

To explain the observed shifts of the $S_N \leftarrow S_1$ absorption spectrum, Wallace-Williams et al. invoke the presence of different rotamers of DPB (Figure 5.2.1 (a) and (b)). The barrier to interconversion of s-*cis* and s-*trans* forms of diphenylpolyenes has been estimated to be 2-3 kcal/mol, with the s-*trans* configuration lying lower in energy [31]. This implies that 1-2% of DPB molecules at room temperature are in the energetically unfavored s-*cis* form. The experiments on DPCP described above indicate that s-*cis* DPB should have its ground state absorption significantly red-shifted from the s-*trans* conformation. Thus, excitation at 355 nm near the red wing of the DPB ground state absorption most likely produces an enhanced population of excited s-*cis* rotamers since the s-*cis* conformer has a much larger cross-section at this redder wavelength than does the s-*trans* species [17]. Changes in the polarizibility of the solvent shifts the absorption spectrum of DPB; since the 355 nm excitation is right on the red edge, shifting the polarizibility significantly changes the excitation cross-section for the s-*trans* conformer. Thus, the ratio of s-*cis* to s-*trans* conformers excited at 355 nm is a strong function of solvent polarizibility, explaining the trends observed by Wallace-Williams et al. [17]. This model is further supported by similar studies probing the transient absorption of DPCP as a function of polarizibility [17]. The $S_N \leftarrow S_1$ absorption of DPCP is significantly red-shifted from that of DPB, implying that the red shoulder in the DPB transient absorption spectrum is due to the s-*cis* rotamer. The S_1 absorption spectrum of DPCP also showed little change with solvent polarizibility, as would be expected from this model since only one rotamer contributes to the observed signal [17].

All of the data taken together indicate that the model (and some of the data) of Rulliere and coworkers [16] is incorrect. This still leaves some open questions as to the state ordering in DPB, the role of rotamers in the isomerization of DPB as well as the general use of diphenylpolyenes as tests of Kramers' and other solution phase reaction rate theories. The subsequent sections describe picosecond and femtosecond transient absorption experiments on DPCP and related compounds, and discuss some of the implications for the isomerization reaction in these systems.

5.3 Experimental

A. Femtosecond Laser System: The femtosecond laser system has been previously described in Chapter 2 and in the literature [32]. Briefly, the output of a colliding-pulse-modelocked ring laser amplified by a copper-vapor laser was frequency doubled and used to photoexcite DPCP and the related systems at 310 nm, while the 620 nm laser fundamental was used to measure the resulting $S_N \leftarrow S_1$ absorption dynamics. The instrument function, determined by cross-correlation of the UV and visible femtosecond pulses as the transient absorption rise of DPB, was fit to a 120 fsec Gaussian, using the fitting procedures described in Chapter 7. Data collection was performed in a dual-beam geometry, with signal and reference pulses normalized on every laser shot at the 8 kHz repetition rate of the laser. In the transient absorption traces presented below, there were typically 25,000 laser shots averaged at each stage position (time delay).

B. Picosecond Laser System: Experiments were also performed with a picosecond laser system which has also been described in the literature [33,34].

Briefly, the picosecond laser pulses were generated by a dye laser (Coherent, CR-599) synchronously-pumped by an Ar^+ laser (Spectra-Physics, Model 2030) and amplified at 10 Hz in a three-stage dye amplifier pumped by a Q-switched Nd-YAG laser (Molectron 34-10) [34]. The final output (1 mJ/pulse, 590 nm and 1 ps FWHM) was frequency-doubled in a KDP crystal to produce about 100 μJ of 295 nm UV light. This UV pulse was time-delayed with respect to the residual 590 nm light with a translation stage and then used to excite the molecules. The residual 590 nm light was focused into a water cell to generate a white light continuum. The transient absorption was probed at the desired wavelength selected from the white light continuum through band pass filters (10 nm FWHM). The experiments were performed by splitting the probe beam into signal and reference beams which were detected by two silicon photodiodes (EG&G Electro-Optics, DT-110). The UV was focused collinearly with the signal beam into the sample with a 10 cm focal length lens. Signals from the solvent molecular ions due to multiphoton ionization were observed with high UV intensity; thus, the UV power was attenuated to a point (around 3 μJ) to avoid multiphoton effects on either the sample molecules or the solvent [5].

C. Materials: Samples were 0.1 - 1.0 mM of DPCP or TPCP in straight chain alkane solutions (hexane - hexadecane). DPCP, prepared by the procedure of Drake and Adams [35] and recystallized from ethanol, was obtained from Wallace-Williams in the Kliger group, and used as received. TPCP (99%), purchased from Aldrich, and the spectral grade solvents, obtained from Burdick and Jackson were used as received. A sample of HHN was provided by W. Atom Yee of the Kliger group at U. C. Santa Cruz. The samples were flowed in a jet through a 300 μm nozzle (Spectra-Physics)

(femtosecond experiments) or circulated in a 1 mm flow cell by a peristaltic pump. This ensured that a fresh sample volume was being probed every laser shot. UV-visible absorption spectroscopy indicated no significant degradation of the sample during the course of the experiments.

5.4 Results

A. DPCP Transient Absorption: The transient absorption dynamics of DPCP in n-hexane solution pumped with 295 nm light and probed at several wavelengths throughout the S_1 absorption band are shown in Figures 5.4.1 and 5.4.2. These wavelengths correspond to the features observed in the DPCP transient absorption [17]: the sharp peak at 720 nm, the broad shoulder centered near 650 nm and the red edge of a second shoulder in the absorption around 600 nm. The data, fit using the procedures outlined in Chapter 7, shows an instrument limited rise ($\leq$ 1 psec) followed by a slower rise of ~ 15 psec with a much smaller amplitude at all 3 wavelengths, as shown in Figure 5.4.1 (the amplitude ratio of ~5:1 for the initial to slower rise makes an accurate determination of the slow rise time difficult). The absorption at all 3 wavelengths then undergo a single exponential decay with a lifetime of 1.9 ± 0.1 nsec, as can be seen in Figure 5.4.2. Femtosecond transient absorption scans taken at 620 nm after 310 nm excitation showed identical results: an instrument limited absorption rise of $\leq$ 120 fsec, followed by a slower 15 psec rise of smaller amplitude and a decay of ~2 nsec. The observed absorption dynamics also showed no dependence on the presence of oxygen in the solution or the power of the pump laser in the regime used for these experiments.

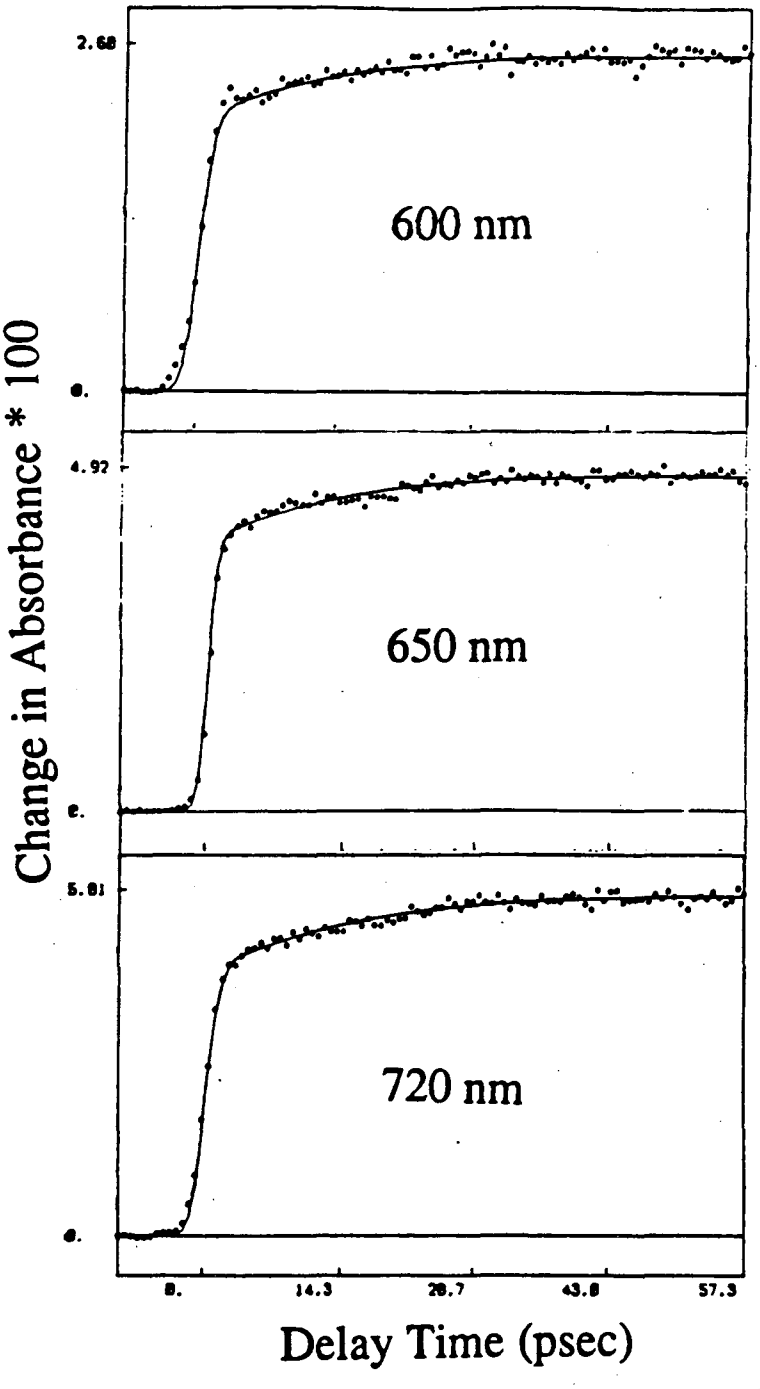

Figure 5.4.1: Transient absorption of DPCP in hexane on the time scale up to 60 psec. Dots are data points, lines are fits to the data using the techniques describedin Chapter 7. All 3 wavelengths show an instrument limited initial rise followed by a slower 15 psec increase; the three traces are identical within the signal to noise.

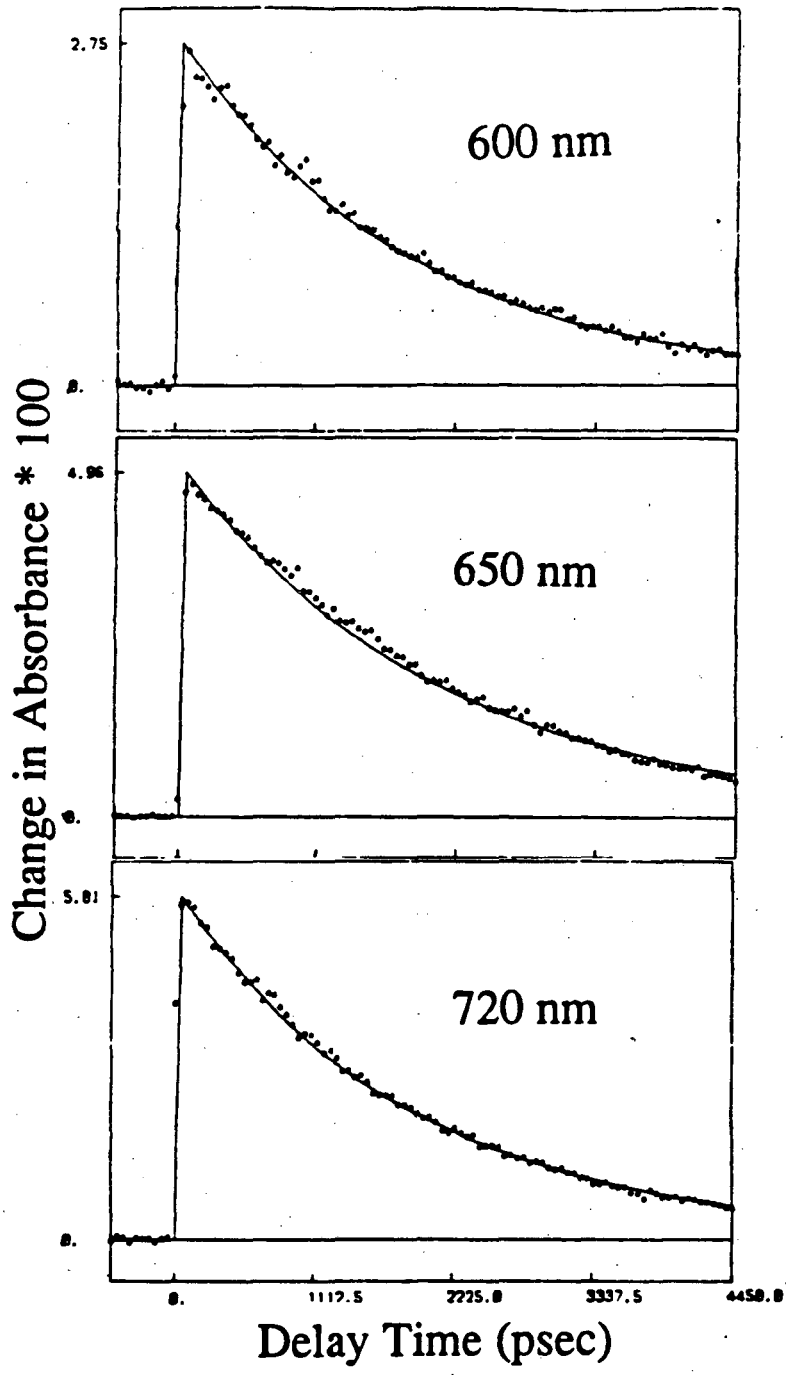

Figure 5.4.2: Same as Figure 5.4.1 except for the time scale up to 4.5 nsec. All 3 wavelengths show identical 1.9 nsec decays. Similar scans in hexadecane solutions also showed no significant differences

The observed signal sizes are in reasonable agreement with the transient absorption spectrum taken by Wallace-Williams et al. [17] after 355 nm excitation: the 650 nm absorption is twice as intense as that at 600 nm, and the 720 nm signal is 20-30% larger than that at 650 nm. This fact, combined with the identical dynamics observed between the 295 nm pumped picosecond and 310 nm excited femtosecond scans supports the conclusion that the same S_1 excited state is being prepared by excitation anywhere within the first DPCP absorption band (270 - 400 nm).

To measure the effects of solvent polarizibility and viscosity on the transient absorption dynamics of DPCP, experiments were performed on decane and hexadecane solutions of DPCP. The results for all three probe wavelengths were identical to those measured in the hexane solutions within the signal to noise and the corresponding error in the fit. This is in agreement with the static transient absorption results, which showed no significant spectral changes between the solvents of differing polarizibility. The lack of viscosity dependence in the dynamics also indicates that there is no significant large amplitude motion associated with the excited electronic state of DPCP.

B. Transient Absorption of TPCP and HHN: In keeping with the work done in Rebecca's thesis [5] where the dynamics of tetraphenylbutadiene (TPB) were examined for comparison to the dynamics of DPB, we have measured the transient absorption dynamics for 1,2,3,4-tetraphenyl-1,3-cyclopentadiene (TPCP). TPCP has the identical structure to DPCP (Figure 5.2.1 (c)), but with an extra phenyl group at each of the other cyclopentadiene vertices containing a double bond (the bottom cyclopentadiene corners as depicted in the figure). The static (nsec) transient absorption

spectrum of TPCP in hexane, taken by Stacie Wallace-Williams using the same methods as reference 17, is shown in Figure 5.4.3 [36]. The spectrum shows a single broad featureless peak centered near 690 nm. The low signal to noise ratio of this scan indicates that the S_1 lifetime for this species is much shorter than the 2 nsec instrument response time. Figure 5.4.4 (a) presents the transient absorption dynamics of TPCP in hexane taken with the picosecond laser system pumping at 295 nm and probing at 690 nm, the peak of the S_1 absorption. The results show an instrument limited absorption rise of ≤ 1 psec, followed by a single exponential decay with a lifetime of 90 psec. The short lifetime is in agreement with an estimate based on the signal size of the static transient absorption spectrum [36]. Transient absorption data taken at 550 nm and 740 nm showed identical dynamics within the signal to noise. Femtosecond transient absorption experiments exciting TPCP with 310 nm light and probing at 620 nm also displayed identical dynamics, with the initial absorption rise instrument limited at ≤ 120 fsec.

To test the effects of solvent polarizibility and viscosity on the dynamics of TPCP, experiments were also performed in hexadecane solutions. Figure 5.4.4 (b) shows the 690 nm transient absorption of TPCP in hexadecane. The results show an instrument limited rise on the picosecond system, followed by a single exponential absorption decay of 280 psec. It is interesting to note that the ten-fold viscosity change between hexane and hexadecane produced an excited state lifetime change of a factor of 3. This same type of behavior has been observed for DPB and other flexible diphenylpolyenes, and is usually assigned to large amplitude isomerative motion, an assignment which does not seem tenable for TPCP due to its sterically locked carbon

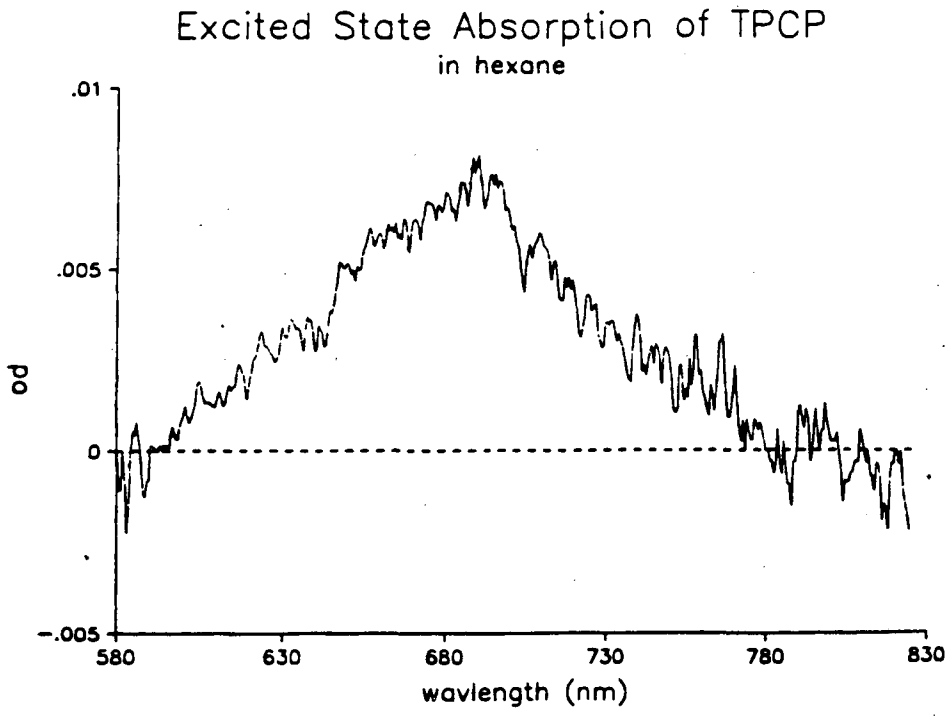

Figure 5.4.3: Nanosecond transient absorption spectrum of TPCP in hexane, provided by S. Wallace-Williams. The low signal-to-noise indicates a short excited state lifetime for TPCP.

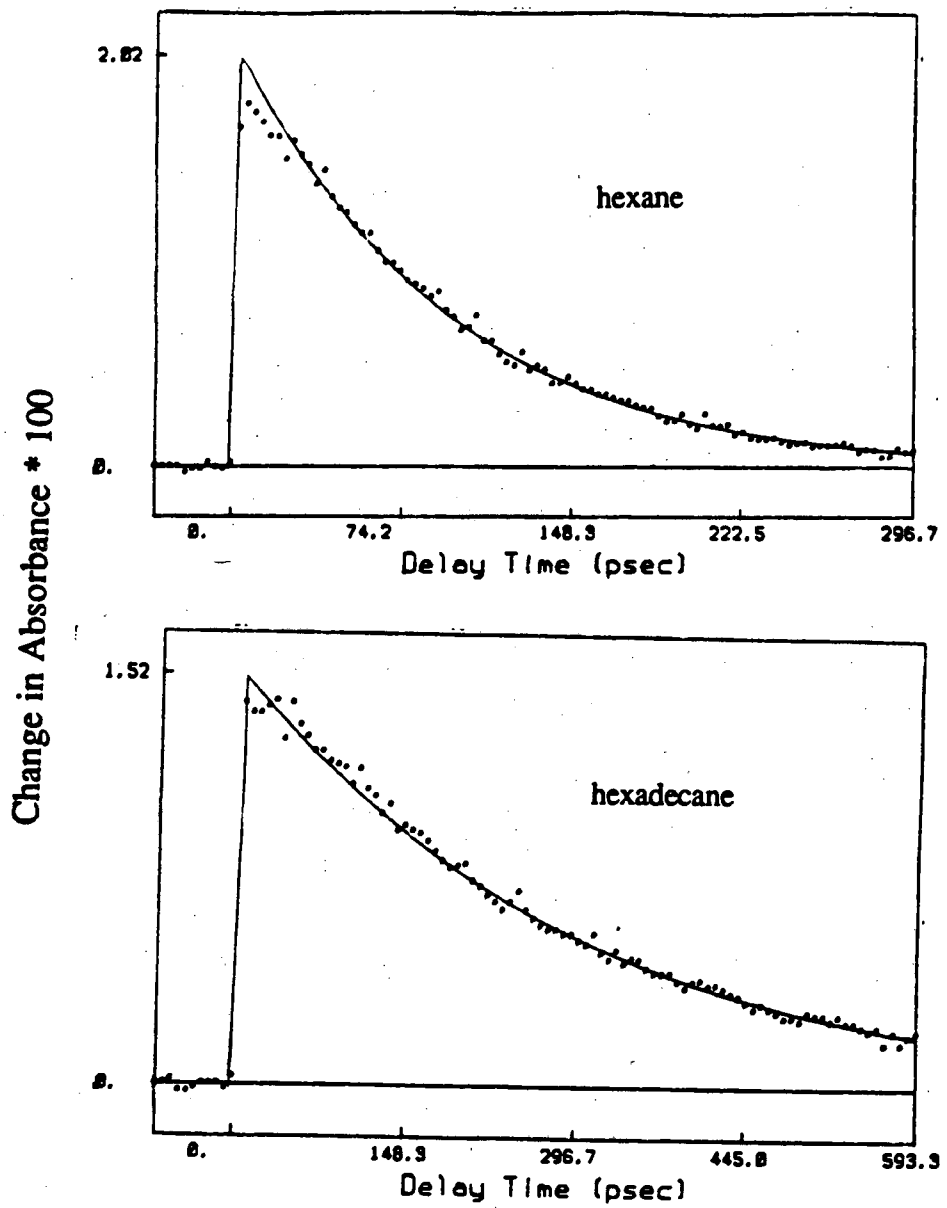

Figure 5.4.4: Transient absorption of TPCP at 690 nm in hexane (top) and hexadecane (bottom). Note that the time scales for the two scans are different: the hexane absorption decays in 90 psec, whereas the hexadecane signal takes 280 psec to decay. Shorter time scans show no faster dynamics, only an instrument limited rise.

backbone.

Transient absorption experiments were also performed on hexane solutions of HHN, a sterically hindered s-*trans* DPB analog shown in Figure 5.2.1 (d). The electronic structure and nsec transient absorption spectrum of HHN have been considered previously in the literature [28]. The signal size and quantum yield of HHN have been used to estimate an S_1 lifetime of ≤ 100 psec. Transient absorption results taken with the picosecond laser system probing at 690 nm show an instrument limited rise, followed by a small ~ 5 psec decay and a longer ~220 psec exponential decay. The amplitude ratio between the 5 and 220 psec components is roughly 6:1. Absorption dynamics probed at 620 nm were identical within the fit errors to those at 690 nm. The 220 psec lifetime is not in good agreement with the previous ≤ 100 psec estimate. Chromatographic results run on the HHN sample found evidence for an impurity with an absorption band starting to the blue of 330 nm; thus, the previous studies on HHN exciting at 355 nm [28] were unaffected by the presence of this impurity, whereas the present results obtained on the picosecond laser system may not accurately reflect the dynamics of pure HHN.

5.5 Discussion

A. Electronic Structure and State Ordering of Diphenylpolyenes: The transient absorption dynamics of DPCP show definite support for the rotamer model of the DPB transient absorption spectrum [17]. The same phenyl twisting motion proposed to invert the ordering of the excited electronic states of DPB [16] is also available to DPCP; according to this model, locking the butadiene backbone in the s-*cis*

configuration should have little effect on the transient absorption dynamics. The results of the previous section are clearly at odds with this prediction. The identical dynamics at all 3 probe wavelengths suggests that the entire transient absorption band reflects the evolution of a single excited state. There is no evidence for thermal population of one state at the expense of another, nor any wavelength dependent shifts suggesting and significant state-dependent dynamics. Thus, the peaks and shoulders in the DPCP transient absorption spectrum [17] are better assigned to a C=C stretching progression from a single electronic manifold, not to absorption from differing A_g and B_u states.

The lack of dynamics on early time scales also eliminates the possibility of large amplitude motion, such as phenyl twisting, playing an important role in the excited state electronic structure of DPCP. As discussed in Chapter 3, large amplitude phenyl twisting motion usually occurs on the time scale of 1-3 psec in low viscosity solutions. The small 15 psec rise observed in the DPCP absorption dynamics is an order of magnitude too long to reflect large amplitude phenyl torsion. This conclusion is also supported by the hexadecane results: the dynamics of the nearly barrierless phenyl twist should scale more or less linearly with viscosity. The results show no dynamical changes for an order of magnitude viscosity increase; hence, large amplitude motion is not important to the excited state structure of DPCP. The 15 psec rise is probably best assigned to vibrational relaxation in the S_1 state, in agreement with the cooling rate of other conjugated hydrocarbons in molecular solvents (see Chapter 4). Vibrational cooling is usually accompanied by a blue-shift in the electronic absorption (see Chapter 4). The lack of this signature in the DPCP spectrum can be explained by the extremely small amplitude of the 15 psec rise; it would be extremely difficult to tell a 12 psec and

an 18 psec rise from those observed given the small amplitude of this component and the experimental signal to noise ratio. Thus, a small blue-shift during cooling would be masked by the small amplitude of the signal. The small amplitude of the cooling signature would be expected for DPCP; extensive studies on similar molecules, including stilbene and DPB have failed to observe vibrational cooling in transient absorption. This implies that all these systems have very little displacement between their S_1 and S_N electronic states, resulting in little change in the S_1 electronic absorption spectrum with vibrational excitation.

The lack of change in dynamics with solvent polarizibility is also consistent with the rotamer model of the excited state absorption. In DPB, solvent assisted level inversion [16] would imply a difference in the repopulation dynamics in solvents of differing polarizibility due to the shifting of the $1B_u$ state with respect to the $2A_g$. While this was not observed for DPB [5], the model would also predict the same phenomenon for DPCP. The observation of no changes with polarizibility is consistent with the rotamer picture [17], where the existence of only the s-*cis* rotamer should cause little changes in the transient spectrum with changing polarizibility.

Results on TPCP and HHN also support these general conclusions. The lack of wavelength dependence in the transient absorption traces shows that no dynamical level ordering effects are important. Neither of these species shows dynamics consistent with phenyl twisting motion; the 5 psec decay in the HHN trace (which may be due to impurities) cannot be due to phenyl torsion since the phenyl rings are locked in the butadiene plane in this molecule (Figure 5.2.1 (d)).

All the studies point to the conclusion that solvent assisted level inversion [16] is not

important to the excited state dynamics of diphenylpolyenes, and that the existence of different conformers around the butadiene single bond must be considered to explain the observed dynamics and dependence on solvent polarizibility.

B. Isomerization of Diphenylpolyenes as Tests of Chemical Rate Theories: The results presented above in combination with work presented in the thesis of Rebecca Hoff [5] show that the use of diphenylpolyenes as tests of Kramers' theory is not very straightforward. In particular, DPB has been extensively used as a model of a one-dimensional unimolecular reactions [5,9,10]. By studying its excited state lifetime as a function of solvent friction (viscosity) and assuming that the change in lifetime reflects the rate of an underlying non-radiative process (isomerization), DPB has been used to support several different chemical rate theories. Lee et al. [9] defend the choice of DPB as a model system because the rate can be described by a one-dimensional Kramers-Hubbard fit. By synthesizing various stiff DPB's in which the phenyl groups were not free to rotate, they concluded that phenyl torsion did not play an important role in the excited state dynamics of DPB [5,9]. No one in the literature, however, has considered the effect of rotamers or worried about the excited state ordering in the isomerization of these systems. A brief comparison of all the DPB analogs studied here and in Rebecca's thesis [5] show that the isomerative motion in these systems is not well understood.

1. DPB: In this case, the excited state lifetime varies nicely with solvent viscosity, in accordance with a one dimensional isomerization which can be described by the Kramers-Hubbard model. Recent work on stilbene [14], however, shows that phenyl twisting motion is important to the excited state dynamics, and that the stilbene

isomerization is not truly one-dimensional.

2. *TPB:* Tetraphenylbutadiene, the same molecule as DPB with 2 additional phenyl groups, shows no change in excited state lifetime as a function of viscosity [5]. The S_1 state of TPB lives for ~2.0 nsec, essentially, the radiative lifetime of DPB. Somehow, the presence of the two extra phenyl groups must shut off the large amplitude isomerization, and not open any other channels for non-radiative decay. This is surprising in comparison to the stiff DPB's of Lee et al., where the radiative lifetime decreased significantly as molecular constraints were increased [9].

3. *TPMB:* Tetraphenylmethylbutadiene, the same molecule as TPB with an extra methyl group at the butadiene 2 position, shows extremely complex excited state dynamics [5]. The observed dynamics could not be explained in terms of isomerization along any combination of simple coordinates, and still remain somewhat of a mystery [5]. It is not clear why the presence of the methyl group should make such a huge change in the dynamics compared to the relatively simple kinetics observed in DPB and TPB.

4. *DPCP:* This s-*cis* DPB rotamer analog shows no evidence for viscosity dependent isomerization, and has the ~2.0 nsec radiative lifetime of DPB. This is in good agreement with the ideas of Lee et al., showing that phenyl twisting is not important and that DPB cannot isomerize when its butadiene backbone is constrained.

5. *TPCP:* This s-*cis* TPB analog shows behavior almost identical to that of DPB; a simple viscosity dependent S_1 lifetime. This is difficult to rationalize in comparison to DPCP, where all non-radiative channels were shut off by constraining the butadiene moiety. It also shows the reverse trend of adding additional phenyl groups to DPB:

creation of TPB from DPB resulted in additional hinderance which turned off the isomerization channel; creation of TPCP from DPCP created a non-radiative channel with isomerization-like behavior where none existed before.

6. HHN: Although dynamical results on this molecule are inconclusive due to the presence of impurities, the extremely short lifetime adds further doubt to the exact role of non-radiative processes changing the excited state lifetime of DPB. It is unclear why HHN and the other locked-phenyl stiff DPB compounds have significantly shorter S_1 lifetimes (by more than an order of magnitude) than do DPB, TPB and DPCP. Clearly, some types of constraints on DPB motion provide new non-radiative channels for decay (possible internal conversion or intersystem crossing), but others leave the molecule to decay with its natural radiative lifetime. Without a better understanding of these mechanisms, it seems unwise to assign the observed motions in DPB as simple one-dimensional isomerization.

The above observations indicate the lack of a consistent picture of the excited state dynamics of all these DPB analogs. Prudence dictates that all these observations, the structure of the electronic excited state, the existence of additional non-radiative channels and the presence of different rotamers be considered before using DPB and related species as tests of solution phase chemical rate theories.

5.6 References

1. see, e.g., B. J. Berne, M. Borkovic and J. E. Straub, J. Phys. Chem., 92, 1988, p. 3711 and references therein.
2. H. A. Kramers, Physica, 7, 1940, p. 284.

3. D. A. McQuarrie, Statistical Mechanics, Harper and Row, New York, 1976, Chapters 20-22.
4. P. Hanggi, P. Talkner and M. Borkovec, Rev. Mod. Phys., 62, 1990, p. 251.
5. R. L. Hoff, Ph.D. Dissertation, University of California, Berkeley, 1991.
6. M. Lee, G. R. Holtom and R. M. Hochstrasser, Chem. Phys. Lett., 118, 1985, p. 359.
7. D. L. Hasha, T. Eguchi and J. Jonas, J. Am. Chem. Soc., 104, 1982, p. 2290.
8. B. D. Ross and N. S. True, J. Am. Chem. Soc., 105, 1983, p. 4871.
9. M. Lee, J. N. Haseltine, A. B. Smith III and R. M. Hochstrasser, J. Am. Chem. Soc., 111, 1989, p. 5044 and references therein.
10. Ch. Gerke, J. Schroder, D. Schwarzer, J. Troe and F. Voss, J. Chem. Phys., 92, 1990, p. 4805 and references therein.
11. D. P. Millar and K. B. Eisenthal, J. Chem. Phys., 83, 1985, p. 5076.
12. R. M. Bowman, K. B. Eisenthal and D. P. Millar, J. Chem. Phys., 89, 1988, p. 762.
13. S. P. Velsko, D. H. Waldeck and G. R. Fleming, J. Chem. Phys., 78, 1983, p. 249.
14. N. S. Park and D. H. Waldeck, J. Phys. Chem., 94, 1990, p. 662.
15. R. F. Grote and J. T. Hynes, J. Chem. Phys., 73, 1980, p. 2715.
16. C. Rulliere, A. Declemy and Ph. Kottis, Laser Chem., 5, 1985, p. 185.
17. S. E. Wallace-Williams, S. Moller, K. M. Hanson, R. A. Goldbeck, D. S. Kliger and W. A. Yee, Photochem. and Photobio., in press, 1992.
18. X. Ci, B. E. Kohler and T. A. Shaler, J. Phys. Chem., in press, 1992.

19. B. S. Hudson, B. E. Kohler and K. Schulten, Excited States, Vol. 6, E. C. Lim, Ed., Academic Press, New York, 1982.

20. J. Salteil and J. L. Charlton, Rearrangments in Ground and Excited States, Vol. 3, P. Mayo, Ed., Academic Press, New York, 1980.

21. see, e.g. R. R. Birge, Biochim. Biophys. Acta, 1016, 1990, p. 293.

22. see, e.g. W. G. Dauben, B. Disanayaka, D. J. J. Funhoff, B. E. Kohler, D. E. Schilke and B. Zhou., J. Am. Chem. Soc., 113, 1991, p. 8367.

23. see, e.g. B. E. Kohler, Conjugated Polymers: The Novel Science of and Technology of Conducting and Nonlinear Optically Active Materials, J. L. Bredas and R. J. Silbey, eds., Kluwer Press, Dodrecht, 1991.

24. see J. S. Horowitz, B. E. Kohler and T. A. Spiglanin, J. Chem. Phys., 83, 1985, p. 2186 and references therein.

25. J. A. Bennett and R. R. Birge, J. Chem. Phys., 73, 1980, p. 4234.

26. S. P. Velsko and G. R. Fleming, J. Chem. Phys., 76, 1982, p. 3553.

27. C. Rulliere, A. Declemy, Ph. Kottis and L. Ducasse, Chem. Phys. Lett., 117, 1985, p. 583.

28. W. A. Yee, J. S. Horowitz, R. A. Goldbeck, C. M. Einterz and D. S. Kliger, J. Chem. Phys.., 87, 1983, p. 380.

29. M. E. Squillacote, R. S. Sheridan, O. L. Chapman and F. A. L. Anet, J. Am. Chem. Soc., 101, 1979, p. 3657.

30. W. J. Burma, B. E. Kohler and K. Song, J. Chem. Phys., 94, 1991, p. 4691.

31. J. R. Ackerman and B. E. Kohler, J. Chem. Phys., 80, 1984, p. 45.

32. B. J. Schwartz, L. A. Peteanu and C. B. Harris, J. Phys. Chem., 96, 1992, p. 3591.

33. A. L. Harris, M. Berg and C. B. Harris, J. Chem. Phys., 84, 1986, p. 788.

34. M. Berg, A. L. Harris, J. K. Brown and C. B. Harris, Opt. Lett., 9, 1984, p. 50.

35. N. L. Drake and J. R. Adams, J. Am. Chem. Soc., 61, 1939, p. 1326.

36. S. Wallace-Williams, private communication, 1992.

Chapter 6: Ultrafast Studies of Photochromic Spiropyrans in Solutions

6.1 Overview

Photochromic molecules have the unusual property that they change color when irradiated of light of one wavelength, and change back to their original color when irradiated with light of another wavelength [1]. Photochromism was not presented in a scientific publication until the 1870's [2], nearly concurrent with reports of the strange phenomenon of a painted gate post which appeared black in daylight but white at night [3]. Scientific studies on photochromic substances were quite limited before 1930 [4-8], but World War II spawned a resurgence of interest in the phenomenon [9-12]. The history and what is known of the mechanism of photochromism have been well documented in several review articles [13-15], and several books have also been written on the subject [1,16,17]. Despite all this research, the microscopic details of the mechanism of photochromism remain poorly understood.

The lack of molecular understanding of photochromism has ramifications for industry. Photochromic molecules have been used in such wide ranging applications as sunglasses (which are dark in direct sunlight but not indoors), high density optical storage, optical switching, image processing and displays [1,9,16,18]. Most of these applications use the photochromic compound in a condensed media, such as a thin film, liquid or glass. A detailed understanding of the mechanism of photochromism, combined with knowledge of how this mechanism is affected by the surrounding condensed phase environment could lead to a renaissance in the applications of these materials. Mechanistic knowledge could allow the design of new molecules which are

tailored to suit a particular application. Understanding of the environmental effects could be used to enhance or shut off particular side reactions, leading to better use of existing photochromic devices. Clearly, experiments probing the basic chemistry of these compounds could payoff in changes to everyday life.

Only in the last few years have ultrafast laser techniques been directed toward unveiling the mechanism of photochromism in these compounds. Picosecond and femtosecond transient absorption [19], transient resonance Raman [20,21] and time resolved fluorescence [22] have recently been applied to photochromic spiropyrans and spirooxazines in films and solutions. The basic mechanistic details are slowly becoming understood in terms of the simple ideas of the preceding chapters: geminate recombination, isomerization and vibrational cooling all play roles in determining the photochromic behavior of these molecules.

In this chapter, picosecond and femtosecond transient absorption spectroscopy are used to study the photochromic molecule 1',3',3'-trimethyl-6-hydroxyspiro[2H-1-benzopyran-2-2'-indoline] (HBPS). In the next section, a brief history of work on this molecule and related photochromic spiropyrans is presented. This is followed by a summary of the apparatus used for the experiments, a presentation of the results obtained and a discussion of the data which includes comparison of the observed photodynamics to other systems and the implications of these dynamics on the photochromic properties of this molecule.

6.2 Background

A. Photochromic Spiropyrans and Sprioxazines: One of the most important

classes of photochromic materials are spiropyran and spirooxazine compounds. These compounds have been studied extensively, [18-30] with the nitro derivatives of spirobenzopyran receiving the most attention [23-26]. Several models have been proposed to explain the properties and photochromic reaction mechanisms of these molecules based on both frequency domain [9-17,31,32] and time domain [18-29] spectroscopic studies. Time-resolved experiments have been carried out using techniques such as laser flash photolysis [23-27] and time-resolved resonance Raman scattering [20,21,28]. These studies found that the reaction dynamics for spiropyrans with a nitro group are significantly different from those without a nitro group. A triplet state was found to play an important role in the photochemical reaction process of spiropyrans containing a nitro group, as indicated by the sensitivity of the dynamics to presence of O_2 [19-22]. For molecules containing no nitro group, the photoreaction was dominated by singlet states. These studies have improved the understanding of the reaction mechanisms of photochromic spiropyrans.

Previous studies have also found that the photochromic reaction of spiropyran and spirooxazine molecules features the dissociation of a C-O bond, producing a distribution of isomers [18-30]. However, the rate and mechanism of the initial reaction steps for these molecules are yet to be determined. Furthermore, there is still no consistent model to explain all the experimental observations due to the extremely fast C-O dissociation rate and to the complications caused by the presence of more than one merocyanine isomer produced in the reaction process [18].

The advent of femtosecond lasers has made it possible to directly study extremely fast rate processes. The experiments carried out by Ernsting and Arthen-

Engeland were the first directed toward the study of the ultrafast photochromic reaction dynamics [18,29]. They studied indoline-spiropyrans in n-pentane and found that the first merocyanine isomer is formed in its ground electronic state in 0.9 - 1.4 ps. Ernsting and Arthen-Engeland further reported that the internally hot (~900 K) primary merocyanine product may isomerize on the picosecond time scale, resulting in a distribution of isomers. Very recently, Tamai and Masuhara reported an investigation of the photochromic reaction of a spirooxazine with 200 fs time resolution [19]. The rate constants for the C-O bond cleavage and relaxation from a "transition state" to a metastable merocyanine were estimated to be approximately $(700\ fs)^{-1}$ and $(470\ fs)^{-1}$, respectively. Tamai and Masuhara suggested that thermal relaxation could play an important role in the merocyanine dynamics. Both of the above studies indicate that the C-O bond dissociation is indirect, that is, it takes several vibrational periods to cleave the C-O bond. This is in contradiction with other observations which suggest that the C-O dissociation is direct [18,33]. Thus, the rate for C-O dissociation and the time scale for product isomerization need further investigation.

B. HBPS: 1',3',3'-trimethyl-6-hydroxyspiro[2H-1-benzopyran-2,2'-indoline] (HBPS), shown in Figure 6.2.1 A, is a very interesting molecule. In solid films, this compound has the unique property of being photochromic between two different colored states produced by photoexcitation of the colorless parent molecule [30]. This is different from most of the other photochromic spiropyrans, in which photochromism occurs between the parent molecule and one of its merocyanine photoproducts. Thus far, no study has been conducted on HBPS in solutions. In this chapter, the first experimental investigation of the photochromic reaction dynamics of

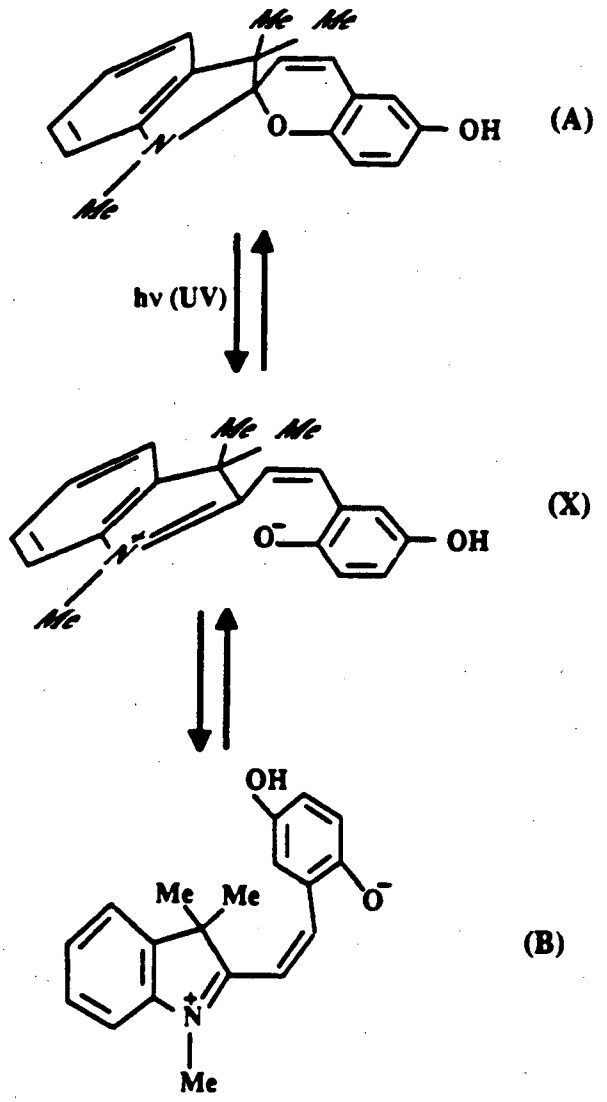

Figure 6.2.1: Structure and proposed reaction process of HBPS. A is the parent HBPS molecule in its ground electronic state; X denotes the nascent photoproduct; B represents one of several possible merocyanine isomers.

HBPS in solutions is reported, with a focus on the dynamics from 100 fs to a few nanoseconds. The C-O dissociation rate and the formation rate of the first merocyanine isomer were measured directly. The subsequent energy relaxation dynamics of the nascent photoproduct and the redistribution of the isomers were monitored up to 4 ns. The effects of temperature, solvent polarity and viscosity on the dynamics were also investigated. A simple model is proposed to explain the observed data. The next section presents the experimental results obtained. This is followed by a discussion of the data, and a brief recap of the experimental apparatus used to obtain the results.

6.3 Results

A. Ground State Absorption Spectrum: The electronic absorption spectrum of HBPS in n-propanol at room temperature is shown in Figure 6.3.1. In the near UV region there are two strong broad bands peaked around 300 nm and 345 nm, respectively, which are very similar to that observed in the spectrum for solid HBPS in a thin film [30]. The n-propanol solution of HBPS exhibits a slightly red color, as is evident from an extremely weak band around 550 nm in the absorption spectrum. This red color is probably caused by presence of a small amount of residual merocyanines in the sample. The current investigation is focused on the intense 300 nm band; the very weak visible absorption is not expected to interfere with the experiment. The solid film study demonstrated that the transient absorption spectrum of the photoproduct from UV photolysis has two bands peaked around 400 nm (blue) and 600 nm (red), respectively [30]. In the present study, the dynamics of the photoproducts in solution are monitored by varying the probe wavelength across these two bands.

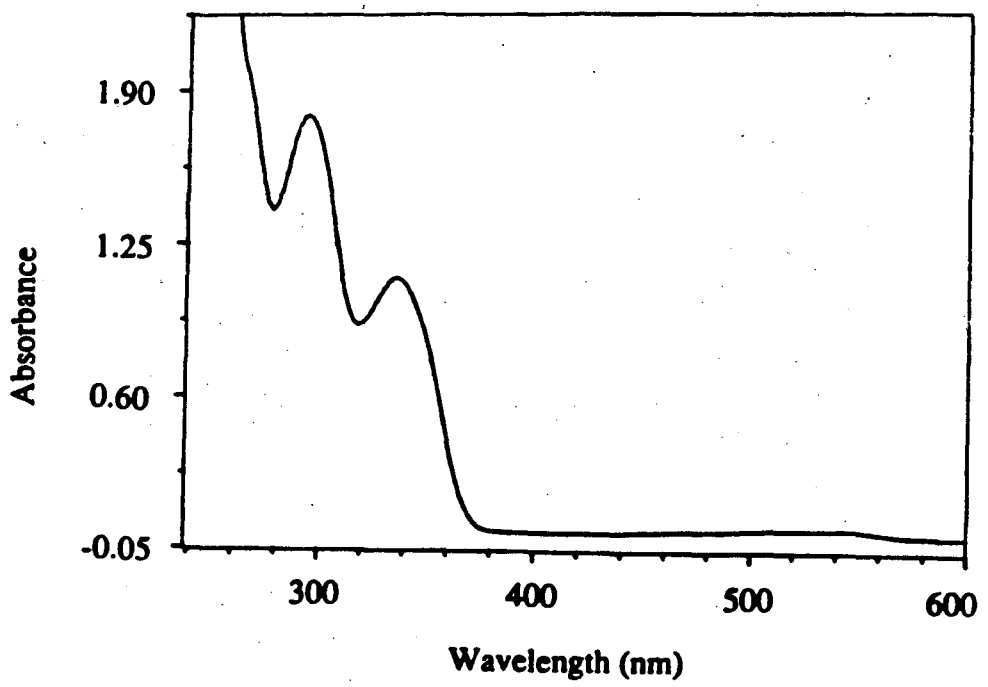

Figure 6.3.1: Electronic absorption spectrum of 0.1 mM HBPS in n-propanol at room temperature.

B. Femtosecond Transient Absorption: Figure 6.3.2 shows the transient spectrum of HBPS in n-propanol when excited at 310 nm and probed at 620 nm with 100 fs laser pulses. The spectrum features a pulse-width limited rise with a fast decay, followed by a "slow" rise. The data are fit with a single exponential decay with a time constant of 180 fs and a single exponential rise of ≤ 2 ps plus an offset, convoluted with a Gaussian of 100 fs to represent the laser pulse. The pulse-width limited rise (<100 fs) indicates that the newly formed species is generated in < 100 fs. The subsequent fast decay shows a disappearance of the species on the time scale of 180 fs. Apparently, the "slow" ≤ 2 ps rise is an indication of population growth of this species or increase in absorbance due to another species (e.g. an isomer) absorbing at 620 nm.

C. Picosecond Transient Absorption: The dynamics on longer time scales were followed by using a picosecond laser system with 295 nm pump pulses and a variety of probe wavelengths. The same electronic state is reached with the 295 nm light and the 310 nm light, thus the subsequent reaction dynamics are expected to be the same or at least very similar.

1. Red Transient Absorption Band: Figure 6.3.3 shows the transient spectrum from 1 ps to 26 ps for several different probe wavelengths (500 nm to 650 nm), covering the red transient absorption band [30]. Figures 6.3.4 and 6.3.5 show scans for the same probe wavelengths on much longer time scales (up to about 1 ns). Scans with various time scales are necessary for appropriate data fitting, as discussed in Chapter 7, as well as for better visualization of the dynamics. For each probe wavelength, the transient decay spectra typically feature a pulse-width limited rise (< 1 ps), then a rise or decay (depending on the probe wavelength) with a time constant of a

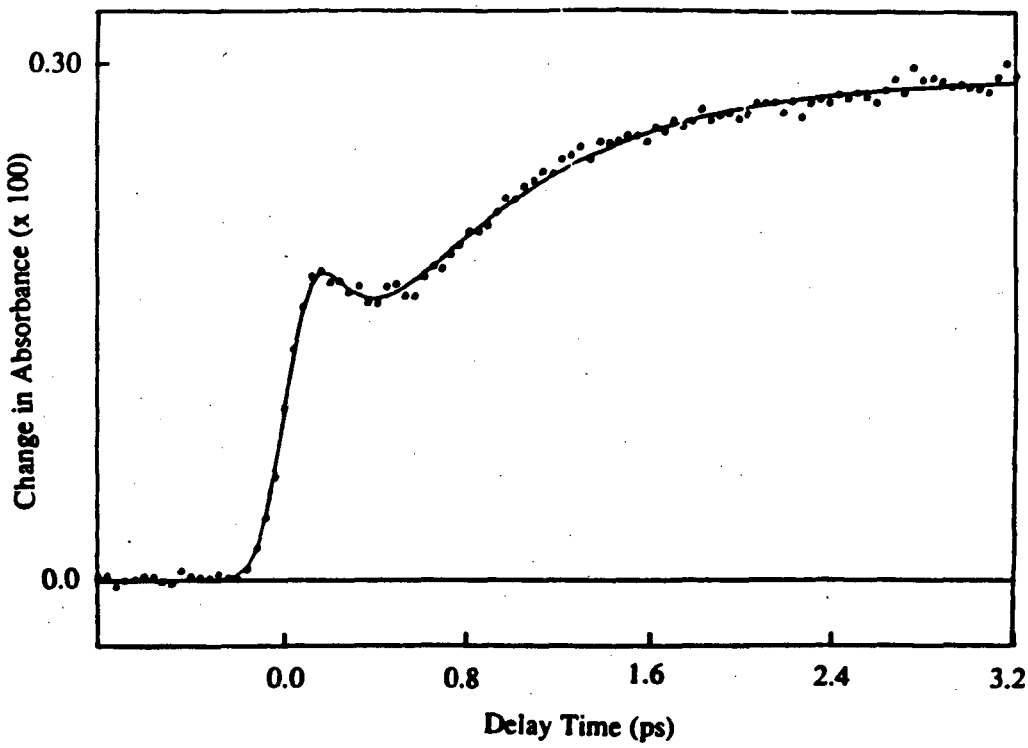

Figure 6.3.2: Femtosecond transient absorption of 2.0 mM HBPS in n-propanol excited with 310 nm light and probed at 620 nm. Circles are experimental data, line is a fit to a 180 fsec exponential decay and a > 700 fsec exponential rise plus an offset.

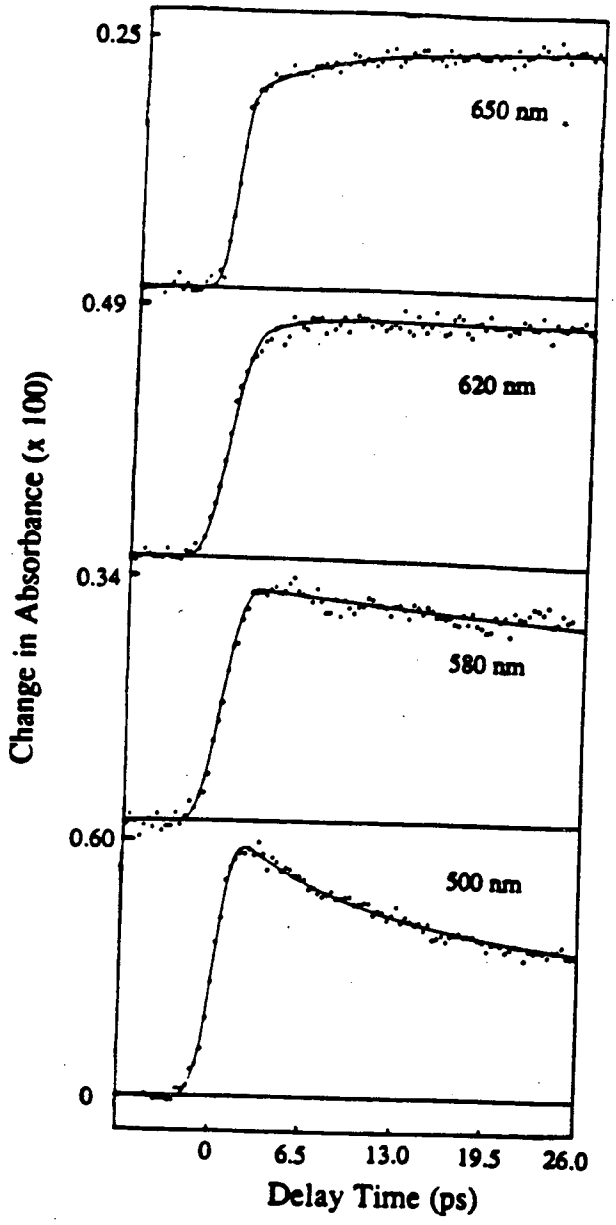

Figure 6.3.3: Transient absorption from 1 to 25 psec of 2.0 mM HBPS in n-propanol excited with 295 nm light and probed at a variety of wavelengths. Circles are experimental data, lines are fits given in Table 6.1.

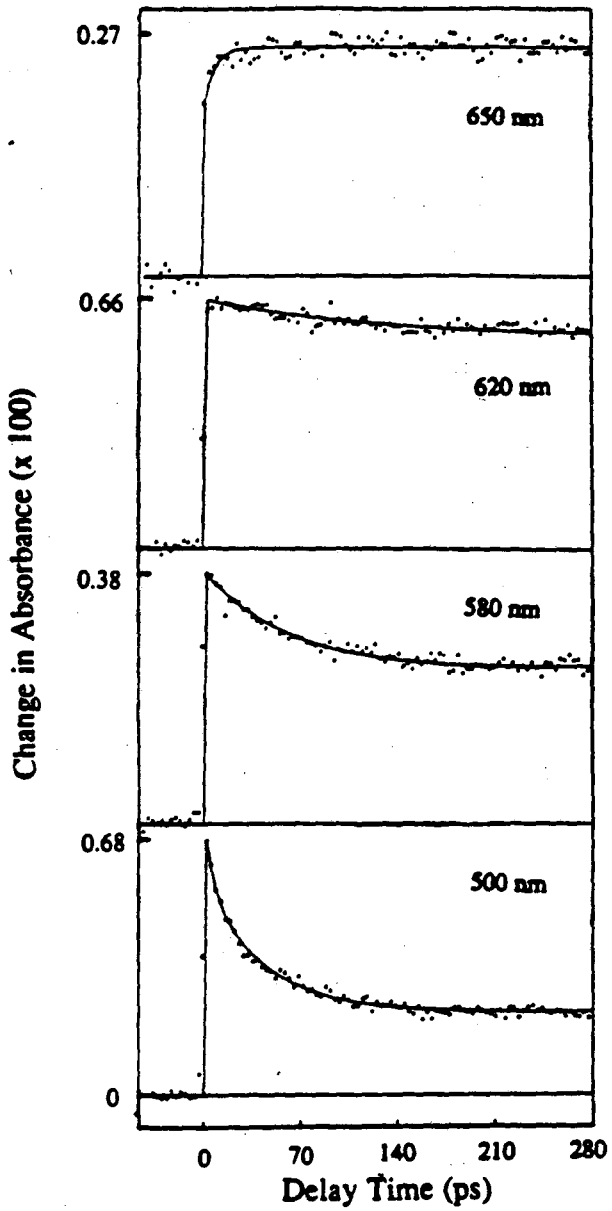

Figure 6.3.4: Same as Figure 6.3.3, but on the 1 to 280 psec time scale.

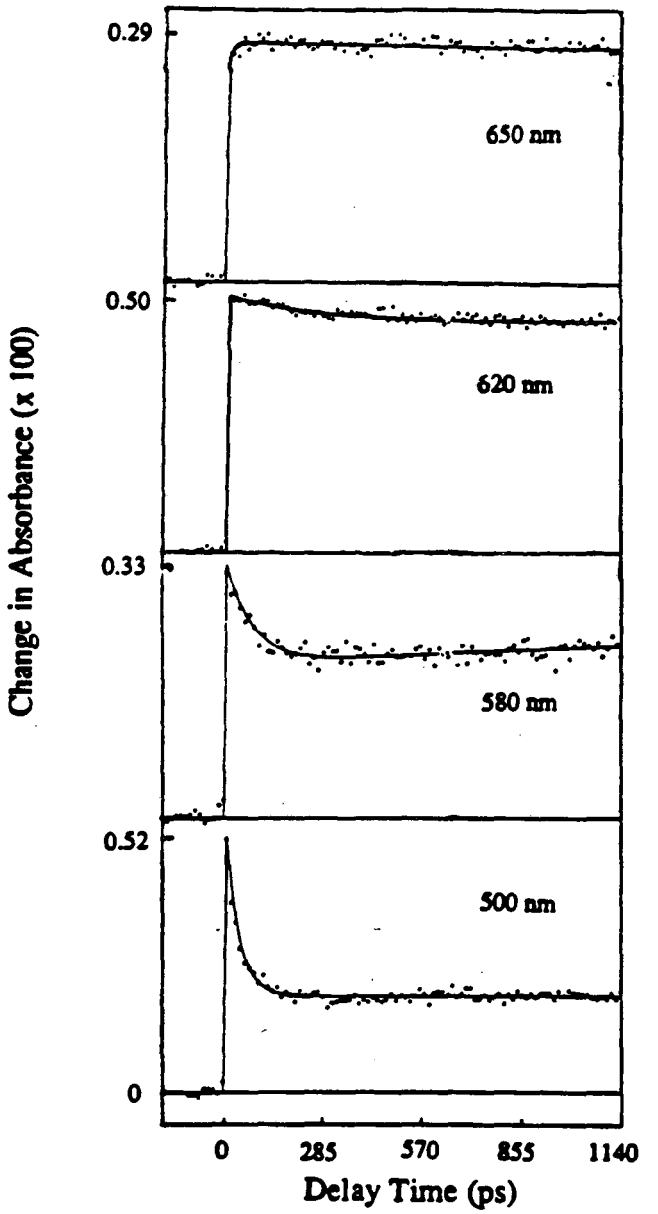

Figure 6.3.5: Same as Figure 6.3.3, but on the 1 to 1.14 nsec time scale.

few picoseconds, followed by a slower decay on a 45 - 180 ps time scale. The spectrum does not change on nanosecond time scales as confirmed from additional scans out to 4 ns.

To obtain a more quantitative understanding of the dynamics, the experimental data are fit with a simple analytical function. The fit (solid curve) to the data (dots) for each probe wavelength is performed using either a double exponential decay with an offset (500 nm and 580 nm) or a single exponential rise plus a single exponential decay with an offset (620 nm and 650 nm), convoluted with a Gaussian of about 1 ps. Several features observed in these transient spectra are worth discussion. At 620 nm, the pulse-width limited rise is consistent with the femtosecond data discussed above, where a 100 fs pulse-width limited rise was observed. Then, the fast rise ($\leq$ 2 ps) (Figure 6.3.3) corresponds to the "slow" rise observed in the femtosecond data (Figure 6.3.2). The long time decay feature has a time constant of around 180 ps (Figures 6.3.4 and 6.3.5). A closer examination of Figures 6.3.4 and 6.3.5 reveals a sensitive dependence of the dynamics on the probe wavelength. For instance, the 180 ps decay component observed at 620 nm becomes much faster at 580 nm (64 ps) and 500 nm (45 ps) but disappears at 650 nm. Thus, the general trend is that the decay becomes faster at shorter wavelengths, suggesting a red shift of the transient absorption spectrum of the photoproduct. Furthermore, the fast $\leq$ 2 ps rise observed at 620 nm becomes slower at 650 nm (6 ps). At bluer wavelengths, such as 580 nm, this fast component disappears; and at even bluer wavelengths, such as 500 nm, instead showing a fast rise, the spectrum displays a fast 6 ps decay. The parameters used in fitting the data are summarized in Table 6.1.

Table I. Fitting Parameters for Different Probe Wavelengths and Solvents [a]

Solvent	Wavelength (nm)	Time Constant (ps)	Pre-exponential Factor [b]
n-propanol	450	8±2	0.40
		106±5	0.20
		offset	0.43
	500	6±2	0.15
		45±5	0.31
		offset	0.22
	580	64±5	0.14
		offset	0.24
	620	2±1	-0.05
		180±5	0.11
		offset	0.55
	650	6±2	-0.05
		offset	0.25
methanol	580	36±5	0.14
		offset	0.31
n-hexanol	580	101±5	0.18
		offset	0.41
cyclohexane	580	40±5	0.15
		offset	0.32

a. The fits to the data are performed using either a double exponential decay with an offset or a single exponential rise plus a single exponential decay with an offset, convoluted with a Gaussian of about 1 ps.

b. Positive to indicate a decay and negative to indicate a rise.

Table 6.1: Fit Parameters for Different Probe Wavelengths and Solvents

2. *Blue Transient Absorption Band:* In addition to the red transient absorption band from 500 - 700 nm, the blue transient absorption band peaked around 400 nm was also examined. When probed at 450 nm, the transient spectra for different time scans (Figure 6.3.6) show qualitatively similar features to those observed for the 600 nm band (Figures 6.3.3-5). This suggests that the same species is responsible for both the 400 nm and 600 nm bands and that these bands correspond to two different electronic transitions of this species. This interpretation is consistent with the solid film study [30] and studies on similar spiropyrans and sprioxazines [18-29]. Quantitatively, the decay time constants are different from those of the 600 nm band. For example, the fast and slow decays are 8 ps and 106 ps respectively, suggesting that the spectrum shift rate is different for the 400 nm band compared to the 600 nm band.

D. Solvent Effects: Preliminary experiments were also carried out to examine the dependence of the dynamical features on parameters such as the solution temperature, solvent viscosity and solvent polarity. The effect of temperature on the dynamics was studied by performing the experiments in n-propanol at 0°C and -78°C. Lowering the temperature is expected to slow down processes such as diffusion-controlled C-O bond reformation or isomerization of the merocyanines. The data obtained in this temperature range failed to reveal any significant change in the dynamics compared to that observed at room temperature. It should be interesting to conduct the experiment at even lower temperatures. However, this is limited by the experimental apparatus available.

Investigation of the solvent dependence shows that the observed dynamical features, especially the slow decay component, are sensitive to the viscosity of the

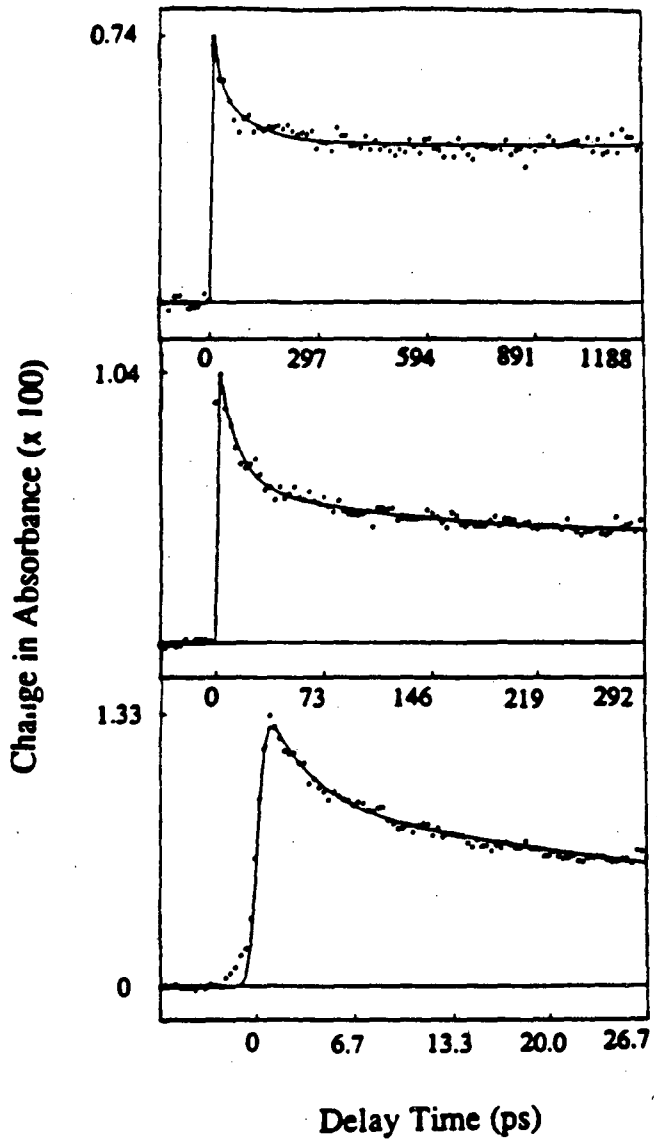

Figure 6.3.6: Transient absorption on a variety of time scales of 2.0 mM HBPS in n-propanol excited with 295 nm light and probed with 450 nm light. Circles are data points, lines are fits given in Table 6.1.

solvent. Measurement of the transient spectra in several alcohols with very different viscosities at the same probe wavelength (580 nm) shows a drastic change in the decay rate, as shown in Figure 6.3.7. The time constants are: 36 ps for methanol (viscosity is 0.6 cp), 64 ps for n-propanol (2.2 cp) and 101 ps for n-hexanol (5.4 cp). This demonstrates a clear correlation between the decay time and the viscosity of the solvent: slower decays for larger viscosities. The decay time is roughly proportional to the viscosity, consistent with diffusive models. This slow decay component was also measured in a non-polar solvent, cyclohexane, and it was found that the decay time at 580 nm (40 ps) is essentially the same as that in a polar solvent methanol (36 ps). The viscosities of cyclohexane and methanol are very similar, 0.66 cP and 0.60 cP, respectively. Thus, this result indicates that the slow decay dynamics are not particularly sensitive to solvent polarity/polarizability. A more detailed discussion of the experimental results and possible interpretations of the data are given next.

6.4 Discussion

A. Molecular Structure and Electronic Absorption Spectrum: The HBPS molecule consists of a 2H-pyran moiety and a second moiety that are orthogonal to each other and are held together by a common spiro carbon atom (Figure 6.2.1 A). The interaction between the π-electron systems of these two parts is not significant as the moieties are not co-planar and there is no conjugation between them; thus, the absorption spectrum of the molecule resembles the sum of the spectra for the two parts [37]. The molecule therefore does not absorb in the visible region and appears colorless. As mentioned above, excitation of a solid HBPS film with UV light

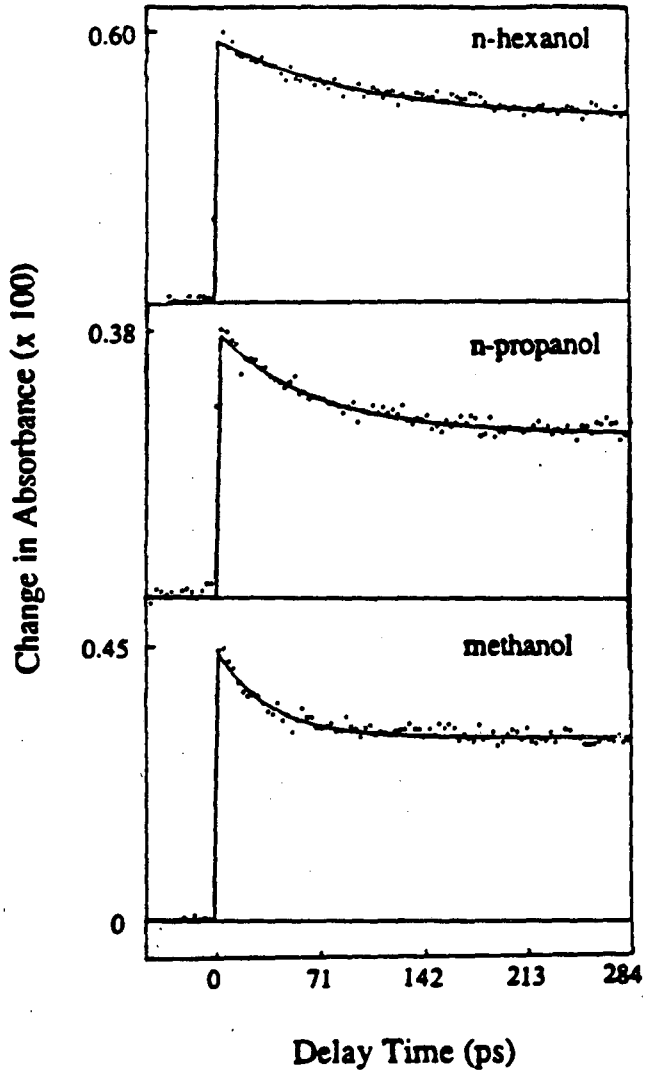

Figure 6.3.7: Transient absorption of 2.0 mM HBPS in a variety of straight-chain alcohols excited with 295 nm light and probed with 580 nm light. Circles are data points, lines are fits given in Table 6.1.

produces a species with two absorption bands in the visible peaked around 400 nm and 600 nm [30]. This is probably absorption of a planar merocyanine product with a conjugated π-electron system between the two parts of the molecule (Figure 6.2.1 B). Based on the studies performed on several similar spiropyran and spirooxazine molecules in solids as well as in solutions [18-29], the first step of the photoreaction is expected to proceed through the breaking of the C-O bond, resulting in the generation of a metastable species, labeled X in Figure 6.2.1. This nascent product is not stable since the two halves of the molecule are still orthogonal to each other. The molecule will subsequently rearrange (isomerize) to form a merocyanine species, labeled B, with the two parts of the molecule in the same plane. The π-electrons will conjugate, providing extra stability and causing the molecule to absorb in the visible. Several isomers are possible, and only one of them, B, is shown as an illustration. The following discussion is centered around the dynamics of the metastable species X and the isomers B.

B. Dynamics on the Femtosecond Time Scale: Direct Dissociation and Bond Reformation: The pulse-width limited rise observed in the femtosecond data (Figure 6.3.2) shows that the species produced from 310 nm excitation of HBPS is generated in less than 100 fs. The initial rise is due to absorption of either the excited parent molecule, A*, or the newly formed species X. If the absorption is due to A*, an explanation for the subsequent 180 fs decay could be A* leaving the Franck-Condon region in the excited state, i.e. dissociation. If this was true, the 180 fs time constant would indicate indirect dissociation of the C-O bond. On the other hand, if the initial absorption is due to the nascent metastable X species, the fast rise would indicate that

the dissociation of C-O occurs in less than 100 fs (essentially direct) and the 180 fs decay could be attributed to C-O bond reformation, i.e. the X to A back reaction. This process is equivalent to geminate recombination, where the initial pair of photofragments recombine following dissociation due to the "caging effect" of the solvent, discussed at length in Chapter 4. Without further information, it is difficult to decide which interpretation, indirect dissociation or direct dissociation/geminate recombination, better applies to the data.

Additional information about the dissociation comes from studies on similar spiropyrans and from comparison to other molecules. The direct dissociation model is consistent with a study carried out on spirooxazines and spironaphthopyrans by Aramaki and Atkinson [20,28]. Using transient absorption and transient resonance Raman techniques, their data also lead to the suggestion that C-O dissociation is direct. Direct dissociation is further supported by the fact that the quantum yield for the photochromic reaction of indolinspiropyrans does not depend on temperature in the range of 0-100°C [38] and the fact that the reaction still proceeds at 4 K in a polymer matrix [39], both of which point toward a photochemical reaction without an activation barrier [18,33]. It is also interesting to notice that the dynamical features observed for HBPS for the first few hundreds of femtoseconds are very similar to those seen for several molecules, including metal carbonyls in similar solvents [40]. Either explanation, indirect dissociation and geminate recombination, could be applied to interpret the similar fast rise and decay features observed in these systems, as discussed in Chapter 4. The data presented in Chapter 4 on the directly dissociative molecule CH_2I_2 also shows similar dynamical features, strongly supporting the direct

dissociation/geminate recombination model. In the particular case of HBPS, the C-O reformation is equivalent to the geminate recombination process in CH_2I_2 and metal carbonyls, but with a slightly faster rate due to the fact that the HBPS molecule never falls apart completely. As illustrated in Figure 6.4.1, the dissociation proceeds mainly along the purely repulsive, diabatic curve (dashed line) to produce X in its ground electronic state. Reformation of the broken C-O bond in X is responsible for the 180 fs fast decay.

C. Dynamics on the Picosecond Time Scale -- Vibrational Relaxation and Isomerization: The ≤ 2 ps rise observed at 620 nm and the 6 ps decay at 500 nm can be attributed to vibrational energy relaxation of the newly formed photoproduct, X, based on a comparison with other, similar molecules which show vibrational relaxation on these same time scales [41,42]. The dominant feature on the picosecond time scale is the 45 ps - 180 ps decay, which is faster at shorter wavelengths and slower at longer wavelengths (Figures 6.3.3-6). This faster decay at shorter probe wavelengths (red-shifting spectrum) is in contrast to the typically observed blue shift for vibrational relaxation in many molecules in similar solvents [36, Chapter 4]. Even though the reversed trend does not completely rule out the possibility of vibrational relaxation (depending on the Franck-Condon factors), it is very likely that a different mechanism is in operation is this case. An alternative explanation is that this red shift is due to isomerization. The existence of several merocyanine isomers has been suggested from previous experiments [18]. Figure 6.4.1 illustrates schematically this idea of a red-shifting spectrum when X isomerizes to form B, which absorbs at longer wavelengths. This interpretation is supported by a study of the viscosity dependence of the decay

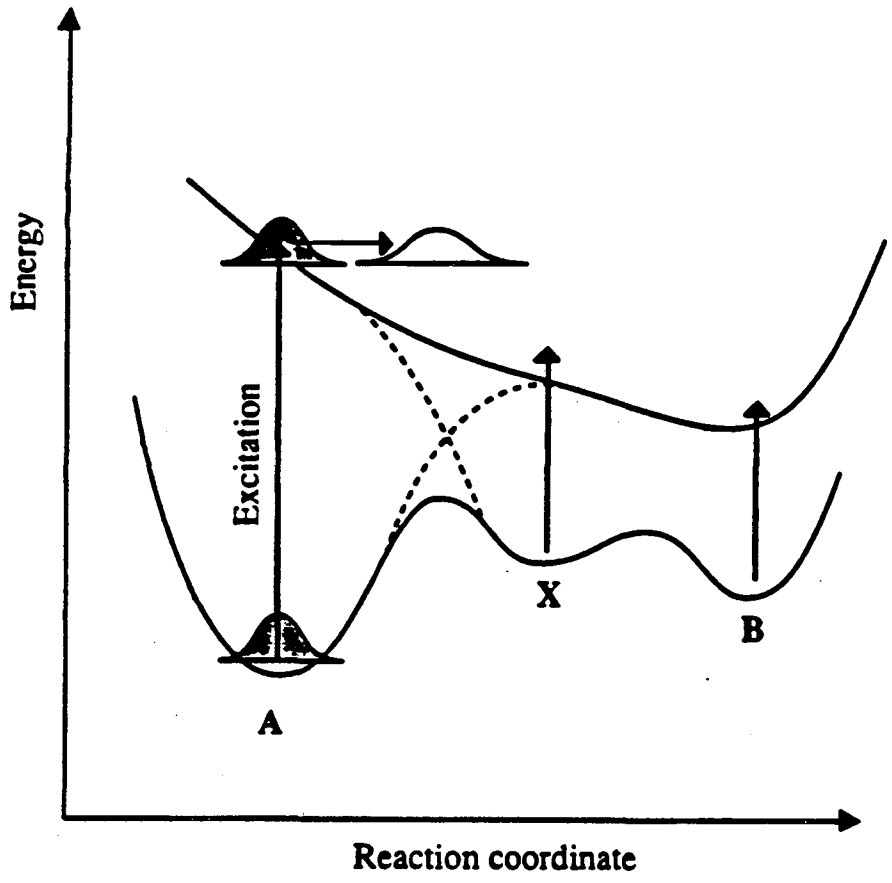

Figure 6.4.1: Schematic illustration of the photochemical reaction process of HBPS. The solid curves represent the adiabatic surfaces while the dashed lines indicate the diabatic surfaces. The reaction proceeds mainly along the diabatic surfaces; i. e., direct dissociation of the C-O bond. A, X, and B refer to the structures pictured in Figure 6.2.1. These curves reflect that the isomers B are more stable than X, and have absorption spectra that are red-shifted with respect to that of X. Both X and B are less stable than A in it ground electronic state.

time constant, as will be discussed in more detail below.

The dynamics were monitored out to 4 ns, and the transient spectra do not show appreciable changes after a few hundred picoseconds. This shows that the merocyanine photoproducts live for many nanoseconds in room temperature solution after their formation. They could correspond to the colored states observed in solid HBPS films [30]. Direct confirmation of this would require performing the experiment out to a much longer time scale and, ideally, in low temperature solutions.

D. Effect of Solvent Viscosity and Polarity: The dependence of the slow decay component on the viscosity of the solvents was very clear from the data obtained in alcohols: slower decays for larger viscosities (Figure 6.3.7). This strongly supports the interpretation of isomerization. It is especially interesting to notice that the decay time constant appears to be linearly proportional to viscosity, which follows the Smoluchowski equation for diffusive isomerization [43]. An alternative explanation for this slow decay is solvation of the charged-separated photoproduct (dielectric relaxation) in the polar solvent [44]. This was tested by examining the dynamics in polar versus non-polar solvents. At the same excitation (295 nm) and probe (580 nm) wavelengths, the decay is essentially the same in the non-polar solvent cyclohexane (40 ps) as that in the polar solvent methanol (36 ps), two solvents with similar viscosities. This test strongly supports the explanation of isomerization over dielectric solvation since dielectric relaxation is expected to be sensitive to solvent polarity. Another possible explanation for the slow decay is secondary geminate recombination of the tethered C-O bond, similar to that observed by Scott and Doubleday in their study of azo compounds in liquid alkanes [45]. This explanation is not likely to hold for the

case of HBPS; the transient spectra show a red shift, whereas secondary recombination would lead to a uniform decrease of the transient absorption band. In addition, the decay time scales are much shorter than those observed for tethered secondary recombination [45]. Thus, the slow (45 - 180 ps) decay can be reasonably assigned to isomerization.

E. Model for Photochromic Reaction: Based on the study and the discussion given above, a simple mechanistic model is proposed for the photoreaction of HBPS in room temperature solutions (see Figure 6.4.1). Excitation of the parent HBPS in its ground electronic state (A) near 300 nm promotes the molecule to one of its singlet excited states (A*). The molecule dissociates directly along the C-O bond in less than 100 fs, producing a metastable species (X). After its formation, this metastable species can revert to the parent molecule A in about 180 fs by undergoing geminate recombination on the ground state potential energy surface, or it can vibrationally relax in a few picoseconds. This vibrational cooling is then followed by isomerization to form a more stable merocyanine product, B on the time scale of ≥ 100 ps. The merocyanine species B absorbs at longer wavelengths compared to X, and more than one B isomer may be present in the solution. The various isomers are stable on the time scale of many nanoseconds. The two different photochromic states (II and III) discussed in reference 30 most likely correspond to the different merocyanine isomers.

6.5 Experimental

A. Picosecond and Femtosecond Laser Set-ups: The experiments were performed with either a femtosecond or a picosecond laser system. Both laser systems

have been described before, in Chapter 2 as well as in the literature [34,35]. Briefly, the picosecond laser pulses were generated by a dye laser (Coherent, CR-599) synchronously-pumped by an Ar^+ laser (Spectra-Physics, Model 2030) and amplified at 10 Hz in a three-stage dye amplifier pumped by a Q-switched Nd-YAG laser (Molectron 34-10) [34]. The final output (1 mJ/pulse, 590 nm and 1 ps FWHM) was frequency-doubled in a KDP crystal to produce about 100 μJ of 295 nm UV light. This UV pulse was time-delayed with respect to the residual 590 nm light with a translation stage and then used to excite the molecules. The residual 590 nm light was focused into a water cell to generate a white light continuum. The photoproducts generated by photolysis of the parent molecules were probed at the desired wavelength selected from the white light continuum through band pass filters (10 nm FWHM). The experiments were performed by splitting the probe beam into signal and reference beams which were detected by two silicon photodiodes (EG&G Electro-Optics, DT-110). The UV was focused collinearly with the signal beam into the sample with a 10 cm focal length lens. Signals from the solvent molecular ions due to multiphoton ionization were observed with high UV intensity; thus, the UV power was attenuated to a point (around 3 μJ) so that no signal was observable from the corresponding pure solvent [36].

For the femtosecond laser system [35], a cavity-dumped CPM laser was amplified by a copper vapor laser-pumped, 6-pass bow-tie amplifier to produce 620 nm, 100 fs pulses (3 μJ/pulse) at 8 kHz. This output was doubled in a 300 μm KDP crystal to produce 0.5 μJ, 310 nm pulses. The UV light was used to excite the sample and the residual fundamental light was spatially filtered and used to probe the resulting dynamics. The delay stage, data acquisition and analysis are similar to the picosecond

system described above. The pump and probe beams were focused through the sample (a 100 μm flow jet) with a 10 cm focal length lens at a 10° angle, giving an estimated spot size of 50 μm. As with the above experiment, care was taken to assure that the signal was linear with pump power, and that there was no signal from the blank solvent.

B. Materials: A 2 mM sample solution was prepared by dissolving HBPS (Eastman Kodak) in n-propanol (Fisher Chemical, spectrograde). To avoid photoproduct build-up, either a 1 mm quartz flow cell or a 100 μm flow jet was used. A flow jet for the sample was necessary for the femtosecond experiments to ensure that the photoproducts with long lifetimes generated from one laser pulse will not interfere with the dynamics in the next laser pulse. A peristaltic pump (Cole-Parmer) was used to flow the sample through the 1 mm flow cell for the picosecond laser experiments.

6.6 Conclusions

In summary, the photochromic reaction dynamics of 1',3',3'-trimethyl-6-hydroxyspiro[2H-1-benzopyran-2,2'-indoline] in solutions have been studied with picosecond and femtosecond transient electronic absorption spectroscopy. The initial C-O bond dissociation is found to occur in less than 100 fs following UV excitation. A small fraction of the dissociated molecules reform the C-O bond on the time scale of 200 fs. The nascent photoproduct is found to vibrationally relax in a few picoseconds and to isomerize on the time scale of ≥ 100 ps. Further experiments need to be conducted to achieve a more complete understanding of the reaction mechanism,

especially the dependence of the dynamics on solvent molecular structure and temperature. With further study, it may be possible to vary the structure of the molecule, or the solvent parameters such as polarity, temperature or dielectric constant to gain better control over photochromism in this system, and eventually, to allow for better photochromic applications.

6.7 References

1. G. H. Brown, ed. Photochromism, Wiley, New York, 1971.
2. E. ter Meer, Ann. Chem., 181, 1876, p. 1.
3. T. L. Phipson, Chem. News., 43, 1881, p. 283.
4. W. Z. Marckwald,. Phys. Chem. (Leipzig), 30, 1899, p. 140.
5. W. Wislicenus, Ann. Chem., 277, 1893, p. 366.
6. H. Biltz and A. Wienands, Ann. Chem., 308, 1899, p. 1.
7. L. Harris, J. Kaminsky and R. G. Simard, J. Am. Chem. Soc., 57, 1935, p. 1151.
8. C. V. Gheorghiu and V. Matei, Bull. Soc. Chim., 6, 1939, p. 1324.
9. E. Fischer and Y. Hirshberg, J. Chem. Soc. 1952, p. 4522.
10. Y. Hirshberg and E. Fischer, J. Chem. Soc. 1953, p. 629; ibid, 1954, p. 297; ibid, 1954, p. 3129.
11. R. Heiligman-Rim, Y. Hirshberg, and E. Fischer, J. Chem. Soc. 1961, p. 156; ibid, 1962, p. 2465; ibid, 1962, p. 2470.
12. Y. Hirshberg, J. Am. Chem. Soc., 78, 1956, p. 2304.
13. G. H. Brown and W. G. Shaw, Rev. Pure Appl. Chem., 11, 1961, p. 2.
14. J. H. Day, Chem. Rev., 63, 1963, p. 65.

15. R. Exelby and R. Grinter, Chem. Rev., 65, 1965, p. 247.

16. A. V. El'tsov, ed., Organic Photochromes, Consultants Bureau, New York, 1990.

17. H. Dürr and H. Bouas-Laurent, eds., Photochromism: Molecules and Systems, Studies in Organic Chemistry, 40, Elsevier, Amsterdam, 1990.

18. N. P. Ernsting, B. Dick and Th. Arthen-Engeland, J. Phys. Chem., 95, 1991, p. 5502 and references therein.

19. N. Tamai and H. Masuhara, Chem. Phys. Lett., 191, 1992, p. 189.

20. S. Aramaki and G. H. Atkinson, J. Am. Chem. Soc., 114, 1992, p. 438.

21. S. Hashimoto, A. Shimojima, Y. Yuzawa, H. Hiura, J. Abe and H. Takahashi, J. Mol. Struct., 242, 1991, p. 1.

22. T. Minami, N. Tamai, T. Yamazaki and Y. Yamazaki, J. Phys. Chem., 95, 1991, p. 3588.

23. S. A. Krysanov and M. V. Alfimov, Laser Chem., 4, 1984, p. 129.

24. S. A. Krysanov and M. V. Alfimov, Chem. Phys. Lett., 91. 1982, p. 77.

25. Y. Kallsky, T. E. Orlowski and D. J. Williams, J. Phys. Chem., 87, 1983, p. 5333.

26. C. Lenoble and R. S. Becker, J. Phys. Chem., 90, 1986, p. 62.

27. C. Lenoble and R. S. Becker, J. Photochem., 34, 1986, p. 83.

28. S. Aramaki and G. H. Atkinson, Chem. Phys. Lett., 170, 1990, p. 181.

29. N. P. Ernsting, B. Dick and Th. Arthen-Engeland, Pure Appl. Chem., 62, 1990, p. 1483.

30. T. Yoshida, A. Morinaka and N. Funakoshi, J. Chem. Soc., Chem. Commun. 1988, p. 437.

31. S. Kurita, A. Kashiwagi, Y. Kurita, H. Miyasaka and N. Mataga, Chem. Phys.

Lett., 171, 1990, p. 553.

32. G. H. Heller, Chem. Ind., 18, 1978, p. 193.

33. B. Bagchi and G. R. Fleming, J. Phys. Chem., 94, 1990, p. 9.

34. A. L. Harris, M. Berg, and C. B. Harris, J. Chem. Phys., 84, 1986, p. 788.

35. B. J. Schwartz, L. A. Peteanu and C. B. Harris, J. Phys. Chem., 96, 1992, p. 3591.

36. J. Z. Zhang and C. B. Harris, J. Chem. Phys., 95, 1991, p. 4024.

37. N. W. Tyer Jr. and R. S. Becker, J. Am. Chem. Soc., 92, 1970, p. 1289.

38. A. S. Dvornikov, Ya. N. Malkin and V. A. Kuz'min, Izv. Akad. Nauk. SSSR, Ser. Khim., 7, 1982, p. 1520.

39. K. Horie, K. Hirao, N. Kenmochi and I. Mita, Makromol. Chem., Rapid Commun., 9, 1988, p. 267.

40. A. G. Joly and K. A. Nelson, Chem. Phys., 152, 1991, p. 69.

41. D. W. Oxtoby, Ann. Rev. Phys. Chem., 32, 1981, p. 77.

42. J. Chesnoy and G. M. Gale, Ann. Phys. Fr., 9, 1984, p. 893.

43. J. A. McLennan, Introduction to Non-equilibrium Statistical Mechanics, Prentice-Hall Inc., London, p.48.

44. E. W. Castner Jr., B. Bagchi, M. Maroncelli, S. P. Webb, A. J. Ruggiero and G. R. Fleming, Ber. Bunsenges. Phys. Chem., 92, 1988, p. 363.

45. T. W. Scott and C. Doubleday Jr., Chem. Phys. Lett., 178, 1991, p. 9.

Chapter 7: Fitting the Data

7.1 Overview

For any experimental apparatus, no matter how sophisticated, the data obtained does little good unless it can be analyzed in a meaningful way to test the predictions of a model or provide physical insight into the microscopic phenomena under investigation. The rises and decays observed in ultrafast transient absorption experiments offer new insights only if they can be assigned to a particular process or fundamental motion. One of the basic assumptions used in interpreting most ultrafast data is that process observed follows first order kinetics. This means that the probability of the process occurring is proportion to the population of reacting species:

$$dN/dt = - k N \tag{1}$$

where N represents the species population, and k is a proportionality constant. The negative sign indicates that most processes involve the disappearance of the species N with time. Equation (1) is easily solved by dividing both sides by N, multiplying both sides by dt, integrating and exponentiating to give:

$$N(t) = C_1 \exp[- k t] \tag{2}$$

where C_1 is a constant of integration, and the proportionality constant k is often called the rate constant for the process, since it determines how rapidly (or slowly) the exponential in Equation (2) takes to die out. It is common to see Equation (2) written as $N(t) = C_1 \exp[- t / \tau_1]$, where $\tau_1 = 1 / k$ is the time constant for the process, that is, the time it takes for the process to proceed 1 / e of the way to completion.

Equation (1) is a good physical model for many of the processes studied by

ultrafast laser techniques. For example, the probability of a vibrationally hot species cooling by giving energy to the solvent should be proportional to the number of hot molecules remaining, leading to an exponential change in absorption with time. Equations (1) and (2) can also describe many diverse reaction features, such as the fluorescence lifetime, the rate of isomerization, etc.

Given that the solution to Equation (1) is Equation (2), it is possible to solve more complicated kinetic models involving multiple or coupled kinetic processes. For example, if the decay of one absorbing species results in the formation of a newly absorbing species which then goes on to decay, the process can be modelled as:

$$dN_1/dt = - k_1 N_1$$

$$dN_2/dt = k_1 N_1 - k_2 N_2 \tag{3}$$

where N_1 and N_2 are the populations of the two different species. Matrix techniques can be used to solve this series of coupled equations, giving solutions:

$$N_1(t) = C_1 \exp[- t/ \tau_1]$$

$$N_2(t) = C_1' \exp[- t/ \tau_2] - C_2' \exp[- t/ \tau_1] \tag{4}$$

where the constants C_1' and C_2' are related to the τ_i's and each other by the initial conditions. As Equations (2) and (4) demonstrate, ultrafast phenomena which are described by first-order or coupled first-order processes will need to be fit by combinations of decaying and rising exponentials.

In addition to simple first order processes, ultrafast transient spectra may also show complex, non-exponential behavior. Relaxation in glasses and polymers often follows the empirical stretched exponential function (also known as the Williams-Watt function or the Kolrausch exponential):

$$N_1(t) = C_1 \exp[-(t/\tau_1)^\beta] \tag{5}$$

where $0 \leq \beta \leq 1$. Many physical models have been proposed to explain dynamics which follow this empirical function, or the function can be thought of simply as a continuous distribution of first order kinetic processes:

$$\exp[-(t/\tau_1)^\beta] = \int f(x) \exp[-t/x]\, dx \tag{6}$$

where τ_1 and β depend on the choice of the weighting function f(x) in the above expression. One example of stretched exponential behavior in ultrafast phenomenon lies in the cooling of vibrationally hot I_2 in liquid Xe (see references, Chapter 4). The cooling from v = 20 to v = 19 has a slightly different first order rate constant than the cooling from v = 19 to v = 18, etc., all the way down to v = 0. This nearly continuous distribution of first order rate constants leads to net stretched exponential behavior decay for the total excess vibrational energy as a function of time.

Another example of non-exponential behavior comes from the solutions to the diffusion equation. Depending on the potential surface, the rate of disappearance of a species due to diffusion follows:

$$N_1(t) = C_1\, t^{-\alpha} \tag{7}$$

where $0 \leq \alpha \leq 1$, and $\alpha = 1/2$ corresponds to diffusion on a completely flat potential surface.

In order to determine whether or not a particular ultrafast process follows first order kinetics, stretched exponential or diffusional behavior, the data must be fit to Equation (4), (5) or (7), or linear combinations of these equations. The fitting procedure must be able to determine which function(s) best fit the data, and should provide values of the

C_i's, τ_i's, β or α to which physical rate constants, absorption amplitudes, etc. can be assigned. In this chapter, the software used to fit the data presented in the previous chapters is described. The next section presents a brief history of the development of the code. This is followed by a description of how to use the code to fit data taken on the picosecond or femtosecond laser systems. Modifying the code to allow for fitting to new functions is described in the next section, and the chapter closes with a section describing the accuracy of the fits, and a general procedure for assuring consistent fits on different time scales. The actual code used for fitting the software is presented in Appendices II - VI.

7.2 History

Although computer algorithms for curve fitting have been around for a long time, fitting ultrafast transient absorption data to various functions can be a slightly tricky business. Exponential and other strongly varying functions can be difficult to fit with grid search and other standard fitting procedures; it is easy for the algorithm to get stuck in a local minimum in parameter space, leading to a fit that looks bad to the eye, but gives the minimum possible error for that particular algorithm. This makes it desirable to fit the data manually as well as with a fitting procedure; the parameters from the manual fit can be used to seed the computer algorithm, leading to an improved chance of finding the global minimum in parameter space, not just some local minimum.

The Silicon Graphics (SGI) Iris I Workstation has the capability of performing graphics functions extremely quickly. This makes it possible to do real-time interactive

curve fitting -- it is possible to adjust the parameters of a given fitting function by hand with the dial and button box on the computer, and have the fitted curve on the screen respond essentially instantaneously to the new parameter input. Mark Paige and Keenan Brown wrote a FORTRAN program, cfitmp, to allow the user to fit ultrafast data manually by merely tweaking the dials on the D & B box. This manual fit could then be used as a seed for a grid search minimization algorithm to attempt to find the global best fit to the data. The executable, and all the code necessary to implement this program can be found in the user/people/cfit directory on the SGI in the Harris group. The code has been described in Mark Paige's thesis, and will not be discussed in further detail here.

The cfitmp program has one main disadvantage -- it fits ultrafast data only to simple combinations of exponentials. This is a serious drawback when one of the exponential time scales is approaching the instrumental resolution; both the amplitude and the time scale of this component can be fit incorrectly. Consider the example of bi-exponential dynamics consisting of a 3 psec and a 100 psec decay with a 1:1 amplitude ratio. When this function is convoluted with a 1.2 psec Gaussian representing the instrument function of the picosecond laser system, a straight bi-exponential fit does not do a good job of reproducing the parameters. The bi-exponential fit cannot describe the curvature in the data near $t = 0$, and gives a 5 psec and a 100 psec decay with a ~ 1:2 amplitude ratio. Thus, the effect of the convolution is to make fast decays appear to have a smaller amplitude and a slower decay time than the actual dynamics they reflect. The only provision in the software for treating this phenomenon is to exclude the few psec worth of data points from the minimization algorithm, a procedure which basically

ignores the fast 3 psec decay in the example above.

In the preceding chapters, many of the absorption decay and rise times were on the order of 250-350 fsec, just a few times longer than the instrumental resolution of ~ 120 fsec. Both the relative amplitudes, as well as the decay times were important to the interpretation of the data, whether it was determining the effects of hydrogen bonding impurities on ESPT or the relative caging of the different chlorinated methane solvents. This makes is especially important to fit this data to a functional form which includes convolution with the instrument function. The need to fit convoluted functions to data is the inspiration for the program convfit.

The convfit program allows the user to fit data to combinations of simple exponentials, stretched exponentials or power law decays by using the SGI D & B box to adjust the fit parameters. This required a substantial modification of the original cfitmp program. First, the ability to perform Gaussian convolutions and adjust the Gaussian half-width as a parameter of the fit had to be added to the program. Unfortunately, the minimization routine used by cfitmp requires the computation of the derivative of the fitting function with respect to each adjustable parameter. The convolution requires that these derivatives be computed by numerical integration -- there is no analytic expression for the derivative of a convolution. Thus, the program convfit does not use the minimization routine that cfitmp uses (the part of the cfitmp code that calls the minimization routine, however, has been left intact, in case ambitious future users wish to write code to enable minimization of convoluted functions). Second, a variety of non-exponential functions, such as the stretched exponential and power law decays had to be added to the program. This required changing the

assignments and ranges of some of the adjustable parameter in the program. Finally, the lack of minimization and the difficulty of making good eyeball fits to the data mandates the plotting of the residuals (the differences between the data points and the fit). The convfit program computes the residuals and plots them in real time as the adjustable parameters are tweaked.

The code to compile and run convfit is presented in Appendices II-VI. The code has been documented with comment statements to make it easy to understand and modify. Many statements in the code are specific to use as cfitmp; these "dinosaurs" have not been removed, but have been marked as not being relevant to convfit. Large sections of the code are specific to convfit (especially the entire program cvfitfunc.f), these areas and the functions they serve have also been duly noted. The remainder of the code remains as in the original cfitmp program; it works equally well with either cfitmp or convfit.

The next section describes how to use the present version of convfit to fit data taken on the picosecond or femtosecond laser systems. This is followed by a prescription for modifying the code to include new convoluted functions, and a discussion of techniques for assuring best fits and minimizing errors.

7.3 Using Convfit

A. Preparing Data for Convfit: The convfit program is reasonably simple to use. For data taken with the data collection program 'new' (written by Dan Russell and described in his thesis) on either the picosecond or femtosecond laser system, little modification needs to be done to fit the data with convfit. The output of the data

collection program consists of individual scans, stored as binary numbers. The programs 'add' and 'tran' or 'tran2', also described in Dan Russell's thesis, are used to average the binary individual scans together, and then to translate them into ascii format. Tran2 is used to translate data taken on the picosecond laser system when the stage is double passed (an alternative version, tran4, exists for the 4 pass configuration), and tran is the translation program for data collected on the femtosecond laser system. The final ascii output from one of the translation programs is in the format:

filename (name of the average file)
y or n (indicating whether or not the signal is a bleach)
numpoints (number of data points)
tzero (number of the last data point on the baseline before the rise)
date (date the scan was taken)
shots per step (usually the number of averaged shots per point)
timestep (in picoseconds, correctly adjusted for number of passes)
comment (usually blank or containing a sentence ending with a ~)
data
:
:

The data are still in the format of signal/reference (or reference/signal for femtosecond data), and must be converted to change in absorbance before being properly fit. The program logs.f, presented in Appendix I, reads in an ascii data file, converts the data into change in absorbance, and outputs the converted data to another ascii file with the original format. Logs.f can be found in the directory /usr/users/ben/data/dataprogs/ on the microvax iodine in the Harris group. Data files are easily transferred from the experimental computer to iodine via ethernet with the program FTP. Logs.f can be easily compiled with the command 'f77 logs.f -o logs', and the executable run with the command 'logs <input file >output file', where output file will contain the data in

change in absorbance format. Because the translation stage on the femtosecond laser system runs in the reverse direction from that on the picosecond laser system, the order of the data must be reversed before subtracting the baseline and computing the change in absorbance. A modified version of logs.f, called reverse.f, can also be found in same directory. Its executable, rev, works in the identical fashion to logs, but also reverses the order of the data points. The comments in the program listing of logs.f in Appendix I indicate the changes that need to be made when converting data from either the picosecond or femtosecond laser systems. Note that the output file of logs or rev may need to be edited to adjust the value of tzero, for fitting, and to remove the '~' character that may appear in the comment line.

B. Executing Convfit: Once the data have been converted, the file is ready to be read into the convfit program on the SGI. The convfit executable can be found in the directory /user/people/ben/fitstuff on krypton.cchem.berkeley.edu. Simply type 'convfit' from the UNIX prompt, and the program will request the name of the data file to be fit. The name of the data file, including the correct path from the directory in which convfit was executed, must be supplied at this point. If convfit can not find the data file specified, or if the specified data file does not correspond to the format given above, the program will end, and a FORTRAN read error statement will be issued. Common sources for this error include: incorrect specification of the path to the data file from the convfit executable directory; presence of the ~ in the comment statement (which must be removed); and variable type mismatch, such as using floating point numbers for the number of shots per step or the location of tzero instead of integers.

When the file has been successfully read, the program will post a menu giving a

choice of the presently available functions. The version listed in Appendices II and III (current as of 10/92) offers a choice of bi-exponential decay, biexponential rise followed by a single exponential decay, two different coupled rise and decay sequences, the Kolrausch exponential and the diffusional power law decay. All the available functions can be convoluted with a Gaussian of arbitrary width, and are compatible with real-time plotting of the residuals. The user then chooses the desired function by typing its number (1 through 6), and pressing return. The program will then present the fit and residual screen, and the user can commence manual fitting of the data.

The fit and residual screen is organized in the following fashion. The top of the screen shows the function chosen, lists the present values of all the parameters and the current least squares error of the fit in green. The upper right section of the screen shows the layout of the dial and button box, indicating which knobs correspond to which adjustable parameters. The large window in the center of the screen shows the data points in red (with the chosen tzero point in blue), and the window axes are marked with the delay time in picoseconds (x-axis) and the change in absorbance * 100 (y-axis). The green line in this window is the fitting function given by the present values of the fit parameters depicted in green above the window. This line usually starts off flat, through 0, since all the parameters are initially set to zero. The rectangle at the bottom of the screen show the residuals for the present fit. The solid green line marks where the difference between the fit and the data point is zero; the red dots indicate the difference between the data point and the present fit. The vertical scale in the residual box is 1.6 X that of the fitting window, magnifying small differences to allow finer parameter adjustments to better minimize the residuals. If the residuals are

too large (or too small) to fit in the residual box, they are simply plotted at the edge of the box. The parameters printed in yellow at the lower right of the screen are for use with the minimizer in cfitmp; they should remain zero at all times in convfit.

C. Fitting with Convfit: In order to use the convolution abilities of convfit to their maximum potential, it is important to choose the correct value of tzero for the data being fit. Unfortunately, the value of tzero used for the logs program is usually not the best choice for the convfit program. The tzero parameter is used by logs to compute the baseline by averaging all the points before tzero; thus, tzero should be chosen as the last point on the baseline. For data with an instrument-limited rise, the correct value of tzero for fitting with convfit should be the data point which is closest to being half way up the rise. This can be 3 or 4 points higher than the tzero chosen for the logs program, depending on the step size. For data with a slower than instrument limited rise, the tzero should be chosen to be a few points above the baseline, so that a reasonable convolution parameter (0.1-0.14 psec for femto data, 0.9-1.4 psec for pico data) nicely fits the curvature in the data below the chosen tzero point. When in doubt, trial and error works well as a method for optimizing this choice. Usually, there will be two choices of tzero which will result in equally good fits with parameters which are essentially identical, and all other choices for tzero lead to significantly inferior fits.

To change the value of tzero, the convfit program must be exited, and the tzero value (the fourth line) in the data file edited with the user's preferred editor. The convfit program is then re-executed as described above, with the modified file used as input.

Once a satisfactory tzero point has been chosen, data can be fit simply by tweaking the dials on the D & B box. Each dial corresponds to one of the function parameters,

as outlined by the figure at the upper right of the screen. Turning the dials clockwise increases parameter values; counterclockwise decreases them. The parameters should be adjusted until the green curve in the fitting window goes smoothly through the data points, the residuals are evenly distributed around the zero line with no visible slope, and the least squares error has reached a minimum. For functions with instantaneous (pulse-width limited) rises, the error from data points on the rise will be weighted more in the value of err than the error from the rest of the points due to the rapid change in absorbance between data points in this region. Occasionally, a smaller value of err can be obtained for a poorer overall fit by minimizing the much larger rise error at the expense of the rest of the data. Thus, care should be taken not to place too much emphasis on the residuals near tzero for data with sharp initial rises. Additional advice on how to tweak the parameters will be given in section 5, below.

Once the desired fit is achieved, the fit window can be printed on the HI plotted by pressing the 'hard copy' button on the D & B box (Note: button labels are below the button they label). The button should be held down until a 'beep' is heard from the SGI console. The HI plotter should have pens and paper already in position when this button is pressed. Pen 1 will print the frame and parameters of the plot; pen 2 will plot the data points and pen 3 will trace out the fitted curve. To exit the convfit program, press the exit button on the D & B box (the button at the lower right of the box) until the 'beep' is heard, or use <control>-c. The other buttons on the D & B box are labelled for the cfitmp program, and should not be used when executing convfit.

D. Troubleshooting: Like most complex pieces of software, the convfit program occasionally hangs up for no apparent reason. Most of the crashes, however, do have a

specific cause and can be easily remedied.

The most common error encountered in executing convfit is the 'file opening error', described in section B above. This error can be remedied as described, by correcting the path to the file or correcting any variable type mismatches. Occasionally, an 'end of file reached' error is encountered, when a data point is accidentally deleted during editing or the numpoints parameter at the beginning of the file is larger than the actual number of data points. This error is fixed by correcting the numpoints value in line 3 of the file, or by adding dummy data points to the beginning or end of the data string until the number of data points and the value of numpoints are in agreement.

The other common problem with the program involves difficulty with the hard copy function. The HI plotter must be on and freshly reset, and linked via serial line to iodine for plotting to be enabled. The executable convplot must be present in the directory /usr/users/karen/drplot on iodine, and the command file cfitplotben must be present in the same directory as the convfit executable. The comments at the beginning of the convplot.f program (Appendix VI) and the next section which describes compiling the program give more details on making sure that all the sections of code necessary for plotting are present.

One difficulty with diagnosing errors is that if the program stops, the screen does not always clear to show the usual text window and reveal what the error message is. To recover the usual text window, use the 'gclear' command and press return (this has to be done without seeing what is being typed if the program is stuck in convfit graphics mode). After the gclear command is executed, the text window should be present, with the last error message printed directly above the gclear command.

The final problem that is easily solved involves initialization of the D & B box. Occasionally a user may find that the program executes correctly, but that the dials and buttons do not seem to be functioning. If the D & B hasn't blown its fuse (a reasonably common occurrence) and is still plugged in, the likely problem is lack of initialization. Upon executing convfit, the LED display at the bottom of the D & B box should read ". . IRIS . .". If instead, the display gives the numerical value of the dial presently being tweaked, the D & B box needs to be re-initialized. This requires that the SGI computer be rebooted, usually requiring the aid of the system manager. After re-booting, the program should work normally.

In the unusual event that the program locks up and various combinations of <control>-c and gclear do not make any headway, the best way to exit convfit is to do so from a remote login. From iodine, execute the command "rlogin krypton.cchem -l username", and type username's password at the prompt. From the UNIX prompt, execute the command "ps -acgux". This should display the list of current working processes on the SGI, one of which should be convfit. Note the process identification number (PID#) for convfit, and execute "kill -9 PID#", followed by "gclear". This should restore the SGI console. See the system manager for more help with this procedure. If all else fails, rebooting the SGI will always take care of any problem.

7.4 Modifying Convfit

As can be seen from Appendices II-VI, the convfit program is large, but with a little guidance, is easily modified. The program comes in two parts: the convfit program itself, which runs on the SGI and performs the actual fitting; and the convplot program,

which runs on the microvax iodine and send the data and fit from convfit to the HI plotter for a hard copy. These are separate programs, and are compiled separately, even though convplot is called from convfit as a system command.

A. Compilation of Convfit: The program convfit consists of several FORTRAN files, library routines and system commands which must be linked together at the time of compilation for everything to work smoothly. On the SGI, the following files (or their object files) must all be present in the same directory (usually the /user/people/ben/fitstuff directory) to compile convfit:

1. Convfit.f: This is the main part of the program, presented with detailed comments in Appendix II. All the screen graphics calls are done from this part of the code, as is the call to initiate the HI plotter from the convplot program on iodine. Many things must be changed in this portion of the code when adding new functions; these changes will be described below.

2. Cvfitfunc.f: This file, presented in Appendix III, contains the subroutine fitfunc, called from convfit.f and convfitest.f, which computes the fitted curve (green curve in the fit window) and the residuals from the current parameter values, converts them to the appropriate graphics coordinates, and passes them back to the main program for plotting on the screen. This file contains all the mathematical computation of the fits and convolutions; each function is computed separately, and new functions can be added by mimicking the structure of the functions already present.

3. Convfitest.f: This file contains the code that computes the errors in the fitting parameters from the best minimizer fit. The best fit parameters are increasingly perturbed until the least squares error changes by a preset fraction; the value of the

perturbation that causes the appropriate change in the fitting error is the uncertainty for that parameter. This section of code does not function with Convfit, but contains several calls to the fitfunc subroutine, so it must be modified if the parameters passed by fitfunc are changed. Usually, this file is left as an object file during recompilation.

4. *Monte.o and Recip.o:* These two files are the object files for the monte carlo algorithm used by the minimizer, and the numerical recipes library used in some of the function calls from convfit and monte. These files are primarily for use with the minimizer, and do not need to be changed when modifying convfit. They are left as object files for compilation.

5. *Cben.c and Cfitplotben:* The file cben.c, summarized in Appendix IV B, contains the definitions of the system commands called from convfit. The most important of these is the command chiplot(), which executes the system file /usr/people/cfit/cfitplotben, summarized in Appendix IV A. Note that cben.c must be present in the same directory as the convfit program (usually /usr/people/ben/fitstuff), but that cfitplotben must be in the directory specified by the path indicated in the cben.c file. This file only needs to be recompiled if new system calls are added to the code, so it is usually left as an object file.

6. *Makefile:* The makefile for convfit, shown in Appendix V, gives linking and library inclusion instructions to the FORTRAN compiler for recompiling the convfit program. When all the files listed above and the makefile are in the same directory (except for cfitplotben), convfit can be compiled by executing the UNIX command "make convfit". The last line of this file contains the listing of all the programs necessary for compilation and linking to take place. Note that Appendix V shows all

the files listed as object files except for convfit.f and cvfitfunc.f. This is the usual case when recompiling, since these are the only two files that need to be routinely changed for modifying or adding new functions.

7. *Cfitben.dat:* This is a temporary file which contains the fit parameters, data points and computed points for the fitted curve. This file is passed to the convplot program on iodine when the 'hard copy' button is pressed, allowing convplot to reproduce the fit window display on the SGI as a plot on the HI plotter. If this file does not exist in the path specified by cfitplotben, a file opening error will result, and no hard copy will be generated.

B. Compilation of Convplot: The convplot program, listed in Appendix VI, is designed to take the data and fit parameters from the convfit program on the SGI, and plot them on the Houston Instruments (HI) plotter. Since the HI plotter is connected to the microvax iodine by a serial line, the convplot program must be run from iodine, requiring convfit to call convplot on a different computer. This is done when the command chiplot() (defined in cben.c, Appendix IV) is executed in the hiplot() subroutine in convfit.f. Chiplot() has been defined as a system command which executes the file cfitplotben. The file cfitplotben (Appendix IV) executes a remote copy (rcp) of the cfitben.dat file (containing the data points, fitted curve points and curve fitting parameters for plotting) from the SGI to a temporary location on iodine. Cfitplotben then establishes a remote shell (rsh) on iodine, executes the convplot program in the /usr/users/karen/drplot directory, and then removes the temporary copy of cfitben.dat.

The convplot program contains many calls to subroutines specific to the HI plotter.

These subroutines have been defined in the programs pltsb.f and hiplot.f written by Keenan Brown. A slightly modified version of these routines to allow the plotter to better mimic the SGI fit window display is present as benhiplot.f, also present in the /usr/users/karen/drplot directory. To compile convplot, simply execute the UNIX command 'f77 convplot.f benhiplot.o -o convplot'. Since the fortran file benhiplot.f takes several minutes to recompile and never needs modification, it is much more convenient to recompile convplot with the object file benhiplot.o.

C. Adding New Functions to Convfit: To add new functions to convfit, the actual code must be modified. All the necessary modifications are done to the files convfit.f and cvfitfunc.f. Convplot.f must be modified as well to make the function labels on the plot match the new function.

1. Modifying Fitfunc: The easiest way to add or modify a function is to start with the file cvfitfunc.f, where the actual fits are computed in the subroutine fitfunc. All the function information is contained in neat sub-blocks; func = 3 (menu function 1) is found in lines 300-399; func = 4 (menu function 2) is found from lines 400-499, etc. When modifying or adding a new function, the easiest thing to do is to mimic one of the sub-blocks already present.

To add a function, determine the parameters needed for the functional form desired (param(0) is C_1, param(1) is C_2, param(2) is b_1, etc.) Add a statement to check that any of the parameters used in exponentials (usually the b and a parameters) do not lead to numbers closer to zero than exp[-12] or larger than exp[12], as the SGI does not handle underflow and overflow errors gracefully. A simple if statement of the form 'if(abs(tstep/param(i)).gt.12) then expression', where expression is the appropriate

action to avoid error, will suffice.

Exponentiation is a slow computational process; computing the exponential of a parameter at each time step would make convfit run too slowly for smooth real time parameter tweaking. The fact that the product of exponentials is the exponential of the sum, however, can be used to so that each exponential is computed only once per parameter. For each parameter value, the exponential for one timestep (exp(-tstep/param(i))) is computed, and assigned to a constant (icexp, i = a1, b1, etc.). The running value of the exponential (i.e., the value of the exponential at each time step) at the first time step (ic) is simply this constant. Since subsequent time steps come at the same time intervals as the first step does from tzero, the exponential can be computed by multiplying its present value by its first value (ic = ic * icexp). In this manner, all the exponentials for a given fit can be propagated one step at a time, using only multiplications and no exponentiation.

By setting up a do loop starting 1 point after tzero to the number of points, the value of the unconvoluted fit at each point can be computed. The fitted values should be stored in the array sharp(i) (named for the fact that the unconvoluted fit often has sharp, spiky features), which has already been pre-loaded with 0's, so that sharp(i) = 0 for i ≤ tzero. The values of the exponentials can be propagated using the trick described above, and the next point of the fit computed. Note that the exponentials are not propagated until after the fitted value has been computed; if they are propagated first, they have effectively already decayed for one timestep at tzero, causing the amplitude of the exponential to depend on the choice of time constant.

Once the unconvoluted fit has been stored in sharp(i), the convolution can be

performed. This is done by calling the subroutine convolution(sharp, gauss), where gauss has already been computed as 15 point normalized Gaussian array with a σ given by parameter a_1. (If a parameter other than a_1 is desired for the Gaussian σ, the appropriate change must be made immediately above line 200. For example, the bi-exponential rise (func = 4) uses a_1 as a time parameter; b_2 is used as the convolution parameter in this case). The convolution subroutine returns the array conv(i), which is the brute force convolution of sharp(i) and gauss(i); conv(i) has numpoints elements, and contains the values for the convoluted fit at each time step.

With the values of the convoluted fit, the residuals and least squares error can be calculated. The residuals should be stored in the array residuals(i), and computed from residuals(i) = data(i) - conv(i), the difference between the data and the fit at each time step. The least squares error is the sum of the squares of the residuals, and should be stored in the variable err.

If the parameters have not changed since the last time step, there is no need to replot the fit and residual windows. The flag plot is zero if this is the case; a test to see if plot is zero can be done, and control returned to the main program if no updating is necessary.

If updating the fit window is necessary, the graphics coordinates for the fit values must be computed, and stored in the array ploty(i). The parameter yscale, passed to the fitfunc subroutine from the main program, is the ratio of the number of y graphics points in the fit window to the maximum data amplitude. Bline contains the y graphics coordinate for the data value of 0 in the fit window. Thus, the graphics coordinates can be computed from the fit amplitude values with the statement ploty(i) = yscale*conv(i)

+ bline. Once the fit graphics coordinates are stored in ploty(i), control can be returned to the main program.

2. *Modifying Convfit.f:* The best way to update the main program (convfit.f) to match the modifications made in the fitfunc subroutine is to search for the variable func in convfit.f, and modify all the statements which depend on the value of func associated with the new or modified function.

The first modification that is necessary is in the menu subroutine. The menu must be updated to reflect the new function (remember, menu function number = func - 2) in the appropriate write statements. At the end of the menu subroutine is a test of func to indicate how many parameters are associated with each function choice. Since polling the extra parameters does not significantly slow the program execution, the default value of nfit = 9 (the number of fit parameters) can be used for any function.

The next modification is in the initgraph subroutine. If the new function requires any special ranges of the parameters (such as extra fine control for small parameters or limiting a parameter value between 0 and 1), the changes must be done at this point. Use an if statement to test to see if the new func value has been chosen, and modify the appropriate dialc statement for the desired parameter. Note that the dial ranges, using the setval command, may also need to be modified as well.

The labels subroutine prints out the choice of function at the top of the fit window. This subroutine must be updated to print out the new function for the appropriate choice of func, by modifying the appropriate write statement.

The subroutine params needs be modified only if there are special restrictions on one of the parameters (such as restricting the Kolrausch exponent to be between zero

and one). Insert a test statement so that when the new func is chosen, the appropriate parameter is tested and restricted.

The swap subroutine must be modified to reflect the changes made in the initgraph subroutine. (This routine is used to poll the D & B box during the swap of graphics buffers). This is done with the appropriate if statements.

As with the fitfunc subroutine, all the modifications listed above can mimic the statements present for the other functions in a particular subroutine.

3. Modifying Convplot.f: The only thing to modify in this program when a new function is created is the label that prints out at the top of the plot. As with convfit.f, this is most easily accomplished by searching for the occurrence of the parameter funcnum (convplot's version of func), and modifying where necessary. The section which prints the label in convplot begins at line 240; line 250 contains the labels for func = 4, line 260 for func = 5, etc. Note that the labels are split into two parts, fun1a and fun1b, which correspond to different plot addresses on the HI plotter. It is important that fun1a hold exactly 38 characters (a task easily accomplished by alignment with the fun1a's for other funcnums); fun1b can be of essentially arbitrary length (if it is too long, the label will run off the end of the plot).

7.5 Maximizing Use of Convfit

A. Choosing the Correct Function: One of the greatest difficulties in interpreting ultrafast data is assigning the observed transients to underlying physical processes. To fit the data and determine the rates of these microscopic processes, a kinetic model (similar to those presented in Section 1 above) must be developed, the solution of

which provides a functional form for fitting the data. Choosing the kinetic model before fitting the data is important; oftentimes, data will fit equally well to several different functional forms. For example, a Kolrausch decay with $\beta = 1/2$ (highly non-exponential) and a few percent random noise added fits very nicely (on some time scales) to a biexponential decay. A bi-exponential decay where the two time constants are similar can be easily fit by a single exponential or single exponential plus offset if the data is a little noisy. Thus, physical insight should be used to choose a general kinetic model and provide a fitting function for a given set of data.

The best check that a function really describes the data is to fit the data on two (or more) very different time scales. If the parameters for the fit on one time scale differ greatly from those for the fit to the same function on a different time scale, the chosen function probably does not the represent the correct underlying physics. This emphasizes the importance of taking multiple scans at different time scales; the data can be best fit when the amplitudes of the different signal components have not changed between the different scans. The functional form of the fit can also be tested by comparing scans taken at nearby wavelengths. A model which fits the data at one wavelength should fit the data at an adjacent wavelength with only slight changes in parameter amplitudes and time constants. If a function fits one wavelength well and a nearby wavelength poorly, a different kinetic model is probably necessary.

B. Fitting the Data: Once the model function has been chosen, the best way to fit the data is to start with the longest time scale and work towards shorter times. The most important thing to look for on the longest time scale is whether or not the signal has recovered. If the signal has not returned to the baseline, the difference should be fit

with an offset on the longest possible time scale, and this value of the offset amplitude should be used for all the shorter time scale fits. This is important because small changes in the value of the offset amplitude can lead to large changes in decay time parameters. For example, a single exponential decay with a 30% offset can look like a decay with almost twice the time constant on a 20% offset when fit on a very short time scale. Note that keeping the same offset amplitude between scans is only effective for data taken consecutively -- scans taken on different days or after the overlap has been changed will have different absolute signal magnitudes, and hence, different offset and component amplitudes. Scaling the magnitudes of scans taken on different days is tricky; unless small time steps are used, it is possible to miss the maximum value of the signal, making amplitude comparisons between scans difficult.

Once the offset, if any, has been determined from the long time scan, the next longest feature of the data should be fit. For exponentials, a good rule of thumb is that only fits where 1 - 2.5 decay time constants are present should be trusted. For example, a 100 psec exponential fits best on a time scale from ~100 - 250 psec. Fitting this decay on a 30 psec or 500 psec time scale will result in errors due to the lack of dynamic range or the small number of data points on the decay. So, on a scan with the appropriate time scale of best fit for the longest decay component, the offset amplitude should be dialed in, and just the long component (amplitude and time constant) fit as well as possible. When this is accomplished, a shorter scan can be fit, this time pre-dialing the values for the offset and the long decay (which may also look like an offset depending on how much the time scale changed between scans). The next-shortest decay feature should be fit on its appropriate time scale, and the process repeated until

the entire function has been fit. The fits can be checked for consistency by refitting the longer time scans with the parameters determined by the shorter time scans. The fits should be reasonably consistent between all the scans, taking into account the change in accuracy with time scale (for example, there is no significant difference in fit quality between a 3 and a 15 psec decay on a 500 psec time scale). If the fits are highly inconsistent between the different time scales, a different functional form (and hence, a different kinetic model) is probably required. To ensure that fits are consistent between different time scales, it is important to obtain the parameters only from the time scale of best fit.

When comparing amplitudes between fits on different time scales, it is important to remember that decays appear to have a smaller amplitude on longer time scales then they do on their best fit time scale. This is because the effective convolution parameter changes with the time scale, meaning that the highest amplitude of a given decay is essentially missed between the sampled data points on the longer time scale. Thus, small changes in amplitude (especially of faster decay components) between scans of different time scales does not necessarily indicate an inconsistency.

Finally, in cases where a physical picture of the microscopic dynamics is not available, the fits to the data can be used to suggest or guide the choice of a kinetic model. In these instances, it is best to employ Occam's Razor when choosing the fitting function. The simplest function, a single exponential, is a one parameter fit (the exponential amplitude is given by the signal size, and isn't a statistically independent adjustable parameter). A bi-exponential, however, contains three parameters -- the two time constants and the amplitude ratio between the two components. This actually has

a higher order than the Kolrausch function or a single exponential plus offset, which are only two parameter fits. The function with the least number of variable parameters which still fits the data at all the wavelengths and time scales is the function of choice.

Choosing the best fitting function with the fewest number of variable parameters is the best way to suggest a model with the simplest possible underlying physics. For example, it is easy to fit a single exponential plus offset with a series of different bi-exponentials; the two different fits, however, correspond to different kinetic models and will lead to a different interpretation of the underlying microscopic dynamics. Checks between the different time scales should show the inconsistent behavior for the bi-exponential fits, but when in doubt, use the simplest possible explanation to describe the physics behind the data -- choose the fit with the smallest number of variable parameters.

Appendix I: Program Logs.f

```
C This program is designed to take an ascii datastring and not reverse
C the order of the points. This is especially useful for data files
C taken on the pico system when the stage runs forwards. It also
C computes the signal in change-in-absorbance instead of norm. This
C requires that the file have a correct t=0 point (i.e. the last point
C before the rise or the 1st pt of the rise). Files should look like this:
C
C filename
C y or n (whether or not it's a bleach)
C numpoints (total number of points in the scan)
C tzero (that is, how many points before the rise starts)
C date
C shots per point
C timestep (in fsec or psec)
C blank line (where comment would go if there was one)
C data
C :
C :
C
C
C This program can be easily modified to reverse the order of the data
C points for data taken on the femto laser, where the stage runs backwards.
C
C Note that for either pico or femto data, the tzero point of the output file will
C have to be moved to the center of the rise if convplot is used to fit the data,
C tzero can be left alone if cfit is used.

      implicit real(a-h,o-z)
      real timestep, shperpt, tzero, base
      real data(1500)
      character*40 fname
      character*8 bleach
      character*40 date

C Read in initial file info

      read(5,100) fname
100   format(a20)

      read(5,110) bleach
110   format(a5)

      read(5,*) numpoints
      read(5,*) tzero
```

```
      read(5,120) date
120   format(a20)
      read(5,*) shperpt
      read(5,*) timestep

C Read data in original order

      do 10 j = 1,numpoints
         read(5,*) data(j)
10    continue

C Compute baseline average before t=0

      base = 0
      do 5 j = 1, int(tzero) - 1
         base = base + data(j)
5     continue
      base = base/(int(tzero) - 1)

C Divide out baseline from all data to get pure % transmission and convert
C to change in absorbance*100 (note: alog10(x) is base 10 log for real #'s)
C % Trans is computed as 1/data since we take ref/signal and we actually
C want trans to go down for transient absorption. After the log is taken
C the number is flipped back so that trans abs still goes up when plotted.
C For femto data, we use signal/ref, so this has to be modified for use on
C data from the femto laser.

      do 15 j = 1,numpoints
         data(j) = 100./(base/data(j))
         data(j) = 100.*( 2. - alog10(data(j)) )
15    continue

C Write out file info again

      write(6,100) fname
      write(6,110) bleach
      write(6,*) numpoints
      write(6,*) int(tzero)
      write(6,120) date
      write(6,*) int(shperpt)
      write(6,*) timestep

C Write absorbance data out in original order for pico data
C For femto data, write out data(numpoints - k) to get data in reverse order

      do 20 k = 1,numpoints
```

```
      write(6,*) data(k)
20    continue

      end
```

Appendix II: Program Convfit.f

```
      program convfit
$ INCLUDE /usr/include/fortfpe.h
C     by mark paige--modified for convolutions by ben schwartz 10/90
C     compile with recip.f, convfitfunc.f, cben.o, monte.f and convfitest.f
C     (Note: do not compile with unmodified MP fortran files; it will
C      cause convolutions to crash)
C     remodified to plot residuals in real time by ben schwartz 4/91
C     Final comments modified 10/92

C The original version of this program, called cfit.f, was
C designed to work with the minimizer, but could not do
C convolutions or plot residuals. Much of this code is
C identical to that written by Mark, but the modifications
C are interspersed enough to make it difficult to just put
C them in separate subroutines.

#include "fgl.h"
#include "fdevice.h"
#include "fget.h"

C Dimension all the variables and set up the common blocks of variables used
C in many of the subroutines. Many of the variables are from the original
C Mark Paige/Keenan Brown/Dan Russell version of the program, which uses the
C minimizer to help find fits without convolutions. The minimizer, excluded
C points, and finding errors in parameters do not work with the convolutions,
C due to the lack of available analytic derivatives.
C The common block call is useful since it creates a look up table of the
C variables being passed, saving lots of time (especially important with
C convolutions because the convolution must be recomputed every time a
C parameter is changed). All the block variables must be passed each time
C the common/block call is used.

C Finally, many of the graphics and D & B box commands used in this program are
C instructions particular for use on the SGI model Iris I computer, and are not standard
C FORTRAN (the -Zg compiler option (see makefile listing) includes the SGI
C graphics library in the compilation). See the SGI graphics manual for details.

      dimension initsw(0:31)
      dimension dialc(0:7),gparam(0:8),sparam(11,0:8),yparam(0:8)
      real bline,data(500),datax(500),datay(500),dialc,resid(500)
      real err,errmin,errsd(9),fitave(9),gparam
      real greeny(500),sdata(500),sdatay(500),sparam,tstep,xscale,xnum,xtick
      real yellowy(500),yerr,ymin,ynum,yparam,yscale,ytick
      integer bounds(2),curson,cursx,excludel,excluder,fitlist(9),func,gcurve
```

```
      integer i,loop,nfit,nlevels,nparam,npts,nsaved,rpoints,set,shots
      integer smooth,tzero,ycurve
      character bleach
      character*12 date
      character*20 name
      character*80 comment
      logical initsw

      common/block1/npts,tstep,tzero,shots
      common/block2/name,bleach,date,comment
      common/block3/data,datax,datay,gcurve,gparam,rpoints,ycurve,yparam
      common/butn1/excludel,excluder.curson,cursx,bounds,smooth,func,nsaved
      common/butn2/errmin,sparam,dialc,yerr,bline,yellowy,yscale,xscale
      common/minim1/fitlist,nfit,nparam
      common/fitst1/fitave,errsd

C This is the main loop of the program -- almost everything is called in
C various subroutines

      loop = -1
C Set the error checking so the core doesn't dump if something crashes
      call setfpe(NOCOREDUMP,ALL)
C Read in the data
      call getdata
   1  (bline,data,datax,datay,xscale,xnum,xtick,yscale,ynum,ytick,ymin,sdata,
   1  sdatay)
C Print the menu of functions on the screen
      call menu(func)
C Print the graphics boxes, initialize stuff
      call initgraph(dialc,errmin,excludel,excluder,func,gcurve,rpoints,set,
   1  tstep,ycurve,nsaved,yscale,initsw,curson,smooth,gparam)
10    call tpoff
      call box(xnum,xtick,ytick,ynum,bline)
      call knobs
      call labels(func)
C SGI double buffer allows for smoother looking real-time graphics
      call swapbu
      loop=loop+1
      if (loop.eq.0) go to 10

C This clears the screen where the data and curves go on each pass of the loop
50    call color(BLACK)
      call rectf(100.,300.,699.,600.)

C Clear out residual rectangle and redraw 0 line
      call rectf(100.,100.,699.,200.)
```

```
      call color(GREEN)
      call move2i(100,150)
      call draw2i(699,150)

      call tick(xtick,ytick)
      if (curson.eq.1) go to 75
C Get the input of the D & B box, compute all the parameters
      call dials(dialc,gparam)
      call params(gparam,1,err,func)
      call params(yparam,2,yerr,func)
C Actually compute the fitting function and get the x,y value of the fit
      call fitfunc
     1 (bline,data,err,excludel,excluder,func,gparam,1,greeny,yscale,xscale,
     1 resid)
C  Plot the fitted (green) or stored (yellow) curve
75    if (gcurve.eq.1) call curve(datax,greeny,1)
      if (ycurve.eq.1) call curve(datax,yellowy,2)
C  Plot the data and the residuals on the screen
      if (rpoints.eq.1)
     1 call plotdat(excludel,excluder,npts,tzero,datax,datay,1)
      call plotresids(resid,datax,yscale)
C Dinosaur check in case smoothing is being used
      if (smooth.gt.0)
     1 call plotdat(excludel,excluder,npts,tzero,datax,sdatay,2)
      if (curson.eq.-1) go to 100
      call cursor(bounds,curson,cursx,datax,datay,npts,tzero)
      if (curson.lt.0) call button(set,initsw,sdata,sdatay,ymin,greeny)
      go to 150
C Get input from the buttons of the D & B box
100   call button(set,initsw,sdata,sdatay,ymin,greeny)
150   call swapbu
      go to 50

      end

c ***********************************
C This subroutine imputs the data from a standard output (see listing logs.f)
C and uses the filename, date, tzero, etc. as well as massaging the data
C for ease of plotting

      subroutine getdata

     1 (bline,data,datax,datay,xscale,xnum,xtick,yscale,ynum,ytick,min,sdata,
     1 sdatay)
      integer i,npts,shots,tzero
      real bline,data(500),datax(500),datay(500),max,min
```

```
      real sdata(500),sdatay(500),tstep
      real xnum,xscale,xtick,yscale
      real ynum,ytick
      character bleach
      character*12 date
      character*20 name
      character*70 fname
      character*80 comment

      common/block1/npts,tstep,tzero,shots
      common/block2/name,bleach,date,comment
C Specify the input file to be fitted; note that there is no good error checking
C if the file can't be easily found -- a potential point for improvement
      write(0,*)'Enter filename: '
      read(0,1)fname
1     format(a70)
      open(unit=4,file=fname,status='old')

      name='                    '
      date='            '
      comment='                                        '

C Read in header info in the standard tran output format

      read(4,10)name
      read(4,11)bleach
      read(4,*)npts
      read(4,*)tzero
      read(4,12)date
      read(4,*)shots
      read(4,*)tstep
      read(4,13)comment

10    format(a20)
11    format(a1)
12    format(a12)
13    format(a80)

C Read in data; keep track of highest and lowest data point

      min=1.0e20
      max=1.0e-20
      do 50 i=1,npts
      read(4,*)data(i)
      sdata(i)=data(i)
      if (data(i).lt.min) min=data(i)
```

```
50      if (data(i).gt.max) max=data(i)

        close(unit=4)

C Scale data for use in graphics box (box is 300 by 600 graphics units; graph
C will be place in the center 256 x 490 rectangle of this box)

        yscale=255./(max-min)
        xscale=490./((npts-tzero)*tstep)

C the baseline for the y coordinate is at 312
C tzero point is put on 200 in the x coordinate
        do 75 i=1,npts

        datay(i)=(data(i)-min)*yscale + 312.

        sdatay(i)=datay(i)
75      datax(i)=(i-tzero)*tstep*xscale + 200.

C  Problems with baseline -- since tzero is often half-way up rise for
C  functions with convolutions, don't want base-line to include these points.
C  So, if there are more than 15 pts. before tzero, use the ave of the first
C  5 as the baseline, otherwise, force the baseline to be 0 (this assumes that
C  the logs program was given the last point before the rise as tzero.  If
C  the baseline still looks funny, then change tzero and run the file through
C  the logs program again.

        bline = 312. - min*yscale

C  This next little loop was for the original program w/o convolutions, where
C  the position of the baseline was all the points before tzero (i.e. tzero is at
C  end of baseline points before initial rise, not halfway up the rise)
C     if(tzero.gt.15)then
C        do 100 i=1,tzero-10
C           bline=bline + datay(i)
C100       continue
C        bline=bline/(tzero-10.)
C     endif

        xnum=(npts-tzero)*tstep
        xtick=xnum*xscale + 200.

C Check to see if data is a bleach -- if so, reverse axis for ease of plotting
        ynum=max
        if ((bleach.eq.'y').or.(bleach.eq.'Y')) ynum=min
        ytick=ynum*yscale + 312.
```

```
      if (ynum.lt.0.) ytick=312.
      return
      end

c ***********************************
C This subroutine prints the menu out on the screen after the file is read in.

      subroutine menu(func)

      integer fitlist(9),func,nfit
      common/minim1/fitlist,nfit,nparam

17    call cclear

      write(0,*)'Welcome to the new, improved, real-time interactive fitting'
      write(0,*)'     station with convolutions *and* residuals.'
      write(0,*)'Pull up the dial and button box and get comfortable. Today"s
 1 menu is:'
      write(0,*)' '
      write(0,*)'1:  c1*exp[-t/b1] + c2*exp[-t/b2] + a2'
      write(0,*)'   convoluted with gaussian of width a1'
      write(0,*)' '
      write(0,*)'   Bi-exponential Decay with convolution and offset'
      write(0,*)' '
      write(0,*)' '
      write(0,*)'2:  {c1*(1-exp(-t/a1)) + c2*(1-exp(-t/a2)}*[exp(-t/b1) + c3]
 1 + c4'
      write(0,*)'          convoluted with gaussian of width b2'
      write(0,*)'
      write(0,*)'   Bi-exponential rise, Exponential Decay w/ convolution &
 1 offset'
      write(0,*)' '
      write(0,*)' '
      write(0,*)'3:  c1*exp(-t/a2) + c2[1 - exp(-T/b1)]*exp(-T/b2) + c4'
      write(0,*)'   convoluted with gaussian of width a1 with T = t - c3'
      write(0,*)' '
      write(0,*)'   Exponential decay w/ delayed rise '
      write(0,*)'   followed by second decay with offset and convolution'
      write(0,*)' '
      write(0,*)' '
      write(0,*)'4:  c1*exp(-t/b1) + c2[1-exp(-T/b1)]*exp(-T/b2) + [1-exp(-T/
 1b2)]*c4'
      write(0,*)'   convoluted with gaussian of width a1 with T = t - c3'
      write(0,*)' '
      write(0,*)'   The TPMB model function -- with stimulated emission abili
 1ty'
```

```
      write(0,*)' '
      write(0,*)' '
      write(0,*)'5:  c1*exp[-(t/b1)^a2] + c2  convoluted with gaussian of widt
   1h a1'
      write(0,*)' '
      write(0,*)'   Kolrausch (stretched exponential) with convolution and
   1 offset'
      write(0,*)' '
      write(0,*)'6:  c1*t^-b1 + c2*t^-b2 + c3 convoluted with gaussian of wid
   1th a1'
      write(0,*)' '
       write(0,*)' DO NOT USE THE MINIMIZER, SMOOTHING, OR
EXCLUDED POINTS'
       write(0,*)' WITH FUNCTIONS CONTAINING CONVOLUTIONS, OR
THIS PROGRAM'
       write(0,*)' WILL CRASH MOST HORRENDOUSLY.  SEE BEN FOR
DETAILS
      write(0,*)' Enter function number: '

      read(0,*)func

C Note that the variable func is 2 higher than the corresponding number in
C the menu.  This is a dinosaur from the minimizer, where func = 1,2 are
C used for minimization testing.  So, the biexponential (menu choice 1) has
C func = 3, etc.  I left these dinosaurs in place in case anyone was ambitious
C enough to want to write a minimizer for the non-analytic functions.....

      func=func + 2

      do 50 i=1,9
50    fitlist(i)=i

      if (func.eq.3) nfit=6
      if (func.eq.4) nfit=9
      if (func.eq.5) nfit=9
      if (func.eq.6) nfit=9
      if (func.eq.7) nfit=6
      if (func.eq.8) nfit=9
      if (func.gt.8) go to 17
      nparam=nfit

      return
      end

c ***********************************************
C This subroutine sets up all the parameter ranges for the dials for each
```

C function.

```
      subroutine initgraph(dialc,errmin,excludel,excluder,func,gcurve,
    1 rpoints,set,tstep,ycurve,nsaved,yscale,initsw,curson,smooth,gparam)

#include "fgl.h"
#include "fdevice.h"

      dimension initsw(0:31)
      dimension dialc(0:7),gparam(0:8)
      integer curson,excludel,excluder,func,gcurve,nsaved
      integer rpoints,set,smooth,ycurve
      real dialc,errmin,tstep,yscale
      logical dummy,initsw

C Note that a lot of these variables are dinosaurs from the minimizer routine
      excludel=-1
      excluder=-1
      gcurve=1
      rpoints=1
      ycurve=-1
      errmin=1.e20
      nsaved=0
      set=1
      curson=-1
      smooth=-1
      gparam(8)=tstep/10.

C the dialc command allocates the range of the dials on the dial box. Dial
C 0 is the lower left, 1 the lower right, etc. The setting is important,
C otherwise the dials are way too touchy or it takes forever to turn them
C to get the parameter you need. Also note that amplitude coefficients
C (e.g. dials 0 and 1) are set according to the y scale; the time parameters
C (e.g. dials 2 and 3) are set according to the time step.

      dialc(0)=255./yscale/1000.
      dialc(1)=dialc(0)
      dialc(2)=tstep/10.
      dialc(3)=dialc(2)

C  For menu functions 3 and 4, want to be able to make b2 param really big

      if((func.eq.5).or.(func.eq.6)) dialc(3) = 5.*dialc(3)

C  a1 should be less sensitive as a convolution parameter (except function
C  2, where b2 is the convolution parameter and a1 is a rise time)
```

```
      dialc(4) = 0.2*dialc(2)

      if(func.eq.4) then
         dialc(4) = dialc(2)
         dialc(3) = 0.2*dialc(3)
      endif

      dialc(5)=dialc(2)

      if(func.eq.3) dialc(5) = dialc(0)

C  For Kolrausch, the power should be finely adjustable between 0 and 1
C  and the time constant is also correspondingly more sensitive
      if(func.eq.7) then
         dialc(5) = dialc(2)*0.01
         dialc(2) = dialc(2)*0.2
      endif

C  For the diffusion eqn fit, the powers should be finely adjustable between
C  0 and 1

      if(func.eq.8) then
         dialc(2) = dialc(2)*0.01
         dialc(3) = dialc(3)*0.1
      endif

      dialc(6)=dialc(0)

      if ((func.eq.6).or.(func.eq.5)) dialc(6)=dialc(2)
      dialc(7)=dialc(0)

      call prefpo(0,1023,0,767)
      call winope("fit",3)
      call textpo(100,750,0,200)
      call double
      call gconfi

c     dials 0-7, 0=c1,1=c2,2=b1,3=b2,4=a1,5=a2,6=c3,7=c4
C These routines determine how many steps the dials have; i.e. dial 0 will
C have 32001 settings, and will range from -dialc(0) to dialc(0), etc.

      call setval(DIAL0,0,-15000,15000)
      call setval(DIAL1,0,-15000,15000)
      call setval(DIAL2,1,1,30000)
      call setval(DIAL3,1,1,30000)
```

```
      call setval(DIAL4,1,1,30000)
      call setval(DIAL5,1,1,30000)
      if(func.eq.3) call setval(DIAL5,0,-15000,15000)
      call setval(DIAL6,0,-15000,15000)
      if ((func.eq.6).or.(func.eq.5)) call setval(DIAL6;0,0,30000)
      call setval(DIAL7,0,-15000,15000)

C     for bi-exp rise, want to be able to make one of the rises instantaneous

      if (func.eq.4) then
         call setval(DIAL4,0,0,30000)
         call setval(DIAL5,0,0,30000)
      endif

      do 50 i=0,31
      initsw(i) = .FALSE.
50    if (getbut(111+i)) initsw(i) = .TRUE.
c     if (getbut(SW0)) initsw(0) = .TRUE.

      call frontb(dummy)
      call color(BLACK)
      call clear
      dummy = .FALSE.
      call frontb(dummy)
      return
      end

c     ************************************************
      subroutine knobs
c     draws knobs on screen

#include "fgl.h"
#include "fdevice.h"

      character*4 label

      call color(WHITE)
      call circfi(950,700,15)
      call circfi(1000,700,15)
      call circfi(950,650,15)
      call circfi(1000,650,15)
      call circfi(950,600,15)
      call circfi(1000,600,15)
      call circfi(950,550,15)
      call circfi(1000,550,15)
      call color(BLUE)
```

```
      call cmov2i(940,695)
      write(label,10)'c3'
10    format(a2)
      call charst(label,2)
      call cmov2i(990,695)
      write(label,10)'c4'
      call charst(label,2)
      call cmov2i(940,645)
      write(label,10)'a1'
      call charst(label,2)
      call cmov2i(990,645)
      write(label,10)'a2'
      call charst(label,2)
      call cmov2i(940,595)
      write(label,10)'b1'
      call charst(label,2)
      call cmov2i(990,595)
      write(label,10)'b2'
      call charst(label,2)
      call cmov2i(940,545)
      write(label,10)'c1'
      call charst(label,2)
      call cmov2i(990,545)
      write(label,10)'c2'
      call charst(label,2)
      return
      end

c     ************************************************
      subroutine labels(func)
c     print labels on screen

#include "fgl.h"
#include "fdevice.h"

      character*105 label
      integer func

      call color(GREEN)

      call cmov2i(100,730)
      if (func.eq.4) go to 15
      if (func.eq.5) go to 25
      if (func.eq.6) go to 35
      if (func.eq.7) go to 45
      if (func.eq.8) go to 55
```

```
      write(label,10)
  1   'c1*exp[-t/b1] + c2*exp(-t/b2) + a2 conv w/ gaussian width a1'
10    format(61a)
      call charst(label,61)
      go to 135

15   write(label,20)'{c1*(1-exp(-t/a1) + c2*(1-exp(-t/a2)}*[exp(-t/b1) + c3]
  1   + c4   conv w/ gaussian width b2'
20    format(81a)
      call charst(label,81)
      go to 135

25    write(label,30)'c1*exp(-t/a2) + c2*[1 - exp(-T/b1)]*exp(-T/b2) + c4;
  1 T = t-c3, conv w/ gaussian a1'
30    format(86a)
      call charst(label,86)
      go to 135

35    write(label,40)'c1*exp(-t/b1) + c2*[1 - exp(-T/b1)]*exp(-T/b2) + [1 -
  1 exp(-T/b2)]*c4   T = t - c3, conv w/ gaussian a1'
40    format(104a)
      call charst(label,104)
      go to 135

45    write(label,46)'c1*exp[-(t/b1)^a2] + c2 conv with gaussian of width a1'
46    format(58a)
      call charst(label,58)
      go to 135

55    write(label,56)'c1*t^-b1 + c2*t^-b2 + c3 conv with gaussian of width a1'
56    format(59a)
      call charst(label,59)
      go to 135

135   call cmov2i(100,700)
      write(label,140)'c1 = '
140   format(5a)
      call charst(label,5)
      call cmov2i(100,670)
      write(label,140)'a1 = '
      call charst(label,5)
      call cmov2i(100,640)
      write(label,140)'b1 = '
      call charst(label,5)
      call cmov2i(300,700)
```

```
      write(label,140)'c2 = '
      call charst(label,5)
      call cmov2i(300,670)
      write(label,140)'a2 = '
      call charst(label,5)
      call cmov2i(300,640)
      write(label,140)'b2 = '
      call charst(label,5)
      call cmov2i(500,700)
      write(label,140)'c3 = '
      call charst(label,5)
      call cmov2i(500,670)
      write(label,140)'c4 = '
      call charst(label,5)
      call cmov2i(500,640)
      write(label,140)'a3 = '
      call charst(label,5)
      call cmov2i(700,700)
      write(label,140)'error = '
      call charst(label,8)

C Stuff below here still prints on the screen, but gets no parameters
C since the minimizer is not used

      call color(YELLOW)
      call cmov2i(800,400)
      write(label,50)'Minimizer Parameters:'
50    format(22a)
      call charst(label,21)
      call cmov2i(800,375)
      write(label,140)'c1 = '
      call charst(label,5)
      call cmov2i(800,350)
      write(label,140)'a1 = '
      call charst(label,5)
      call cmov2i(800,325)
      write(label,140)'b1 = '
      call charst(label,5)
      call cmov2i(800,300)
      write(label,140)'c2 = '
      call charst(label,5)
      call cmov2i(800,275)
      write(label,140)'a2 = '
      call charst(label,5)
      call cmov2i(800,250)
      write(label,140)'b2 = '
```

```
      call charst(label,5)
      call cmov2i(800,225)
      write(label,140)'c3 = '
      call charst(label,5)
      call cmov2i(800,200)
      write(label,140)'c4 = '
      call charst(label,5)
      call cmov2i(800,175)
      write(label,140)'a3 = '
      call charst(label,5)
      call cmov2i(800,150)
      write(label,60)'error = '
60    format(8a)
      call charst(label,8)

      return
      end

c     ********************************
      subroutine box(xnum,xtick,ytick,ynum,bline)
c Draws box and data for the plot and the residuals.

#include "fgl.h"
#include "fdevice.h"

      character*15 xlabel
      integer i
      real bline,xnum,xtick,ynum,ytick

C Do the main plot window first

1     call color(BLACK)
      call clear
      call color(WHITE)
      call rect(99.,299.,700.,601.)
c     tick marks
      call cmov2(197.,610.)
      write(xlabel,3)'0'
3     format(a1)
      call charst(xlabel,1)
      call cmov2(60.,bline)
      call charst(xlabel,1)

      call cmov2(xtick-35.,610.)
      write(xlabel,5)xnum
5     format(f8.1)
```

```
      call charst(xlabel,8)

      call cmov2(10.,ytick)
      write(xlabel,10)ynum
10    format(g10.4)
      call charst(xlabel,10)

C Stuff below here draws box for residuals

      call rect(99.,99.,700.,201.)
      call cmov2(99.,210.)
      write(xlabel,4)'Residuals'
      call charst(xlabel,9)
4     format(a9)

C Put '0' line in center of residual box

      call cmov2(60.,150.)
      write(xlabel,3)'0'
      call charst(xlabel,1)
      call color(GREEN)
      call move2i(100,150)
      call draw2i(699,150)

      return
      end

c     ************************************************************
      subroutine tick(xtick,ytick)
c     draw x tick marks

#include "fgl.h"
#include "fdevice.h"

      real xtick,ytick

      call color(WHITE)
      call move2(200.,601.)
      call draw2(200.,580.)
      call move2(xtick,601.)
      call draw2(xtick,580.)

      call move2(99.,ytick)
      call draw2(120.,ytick)
      return
      end
```

```
c       ************************************************
        subroutine cursor(bounds,curson,cursx,datax,datay,npts,tzero)
C This subroutine keeps the cursor under control; it does not need to be modified
C  when changing or adding functions

#include "fgl.h"
#include "fdevice.h"

        integer bounds(2),curson,cursx,i,j,npts,tzero
        logical vals(5)
        real datax(500),datay(500)

        if (curson.gt.0) go to 9
        curson=-curson
        cursx=tzero+1
        bounds(1)=-1
        bounds(2)=-1
        go to 50

9       do 10 i=1,5
10      vals(i)=.FALSE.

75      vals(1)=getbut(ONEKEY)
        vals(2)=getbut(TWOKEY)
        vals(3)=getbut(NINEKE)
        vals(4)=getbut(ZEROKE)
        vals(5)=getbut(RETKEY)

        do 76 j=1,5
76      if (vals(j)) go to 100
        go to 75
100     vals(1)=getbut(ONEKEY)
        vals(2)=getbut(TWOKEY)
        vals(3)=getbut(NINEKE)
        vals(4)=getbut(ZEROKE)
        vals(5)=getbut(RETKEY)
        do 101 k=1,5
101     if (vals(k)) go to 100

        if (j.ne.5) go to 125
        if (bounds(1).ne.-1) go to 150
        if (bounds(1).eq.-1) bounds(1)=cursx

125     if (j.eq.1) cursx=cursx-1
        if (j.eq.2) cursx=cursx-10
```

```
      if (j.eq.3) cursx=cursx+10
      if (j.eq.4) cursx=cursx+1

      if (cursx.gt.npts) cursx=npts
      if (cursx.le.tzero) cursx=tzero+1

50    call color(WHITE)
      call move2(datax(cursx),301.)
      call draw2(datax(cursx),599.)
      call color(BLUE)
      call circf(datax(cursx),datay(cursx),1.)

      if (bounds(1).eq.-1) return
      call color(BLUE)
      call move2(datax(bounds(1)),301.)
      call draw2(datax(bounds(1)),599.)
      call color(WHITE)
      call circf(datax(bounds(1)),datay(bounds(1)),1.0)

      return

150   bounds(2)=cursx
      curson=-curson
      if (bounds(2).gt.bounds(1)) return
      bounds(2)=bounds(1)
      bounds(1)=cursx
      return
      end

c     ********************************************
      subroutine keyon
C This subroutine is used for manual input of the a3 parameter (and
C minimizer stuff) after pressing the appropriate button on the D & B box.

#include "fgl.h"
#include "fdevice.h"

      character*3 junk

      call tpon
      call cclear
      write(0,*)' Enter yes to start keyboard input '
5     read(0,10)junk
10    format(a3)
      if (junk.ne.'yes') go to 5
      return
```

```
      end

c     ************************************************
      subroutine fitpar
C This is a dinosaur subroutine which is used when the minimizer is invoked.

      integer fitlist(9),i,j,nfit,nparam
      character ans(9)
      common/minim1/fitlist,nfit,nparam

      write(0,*)' Fit to specified parameters '
      write(0,*)' Enter y or n to fit specified parameter '

      write(0,*)' c1: '
      read(0,10)ans(1)
10    format(a1)
      write(0,*)' a1: '
      read(0,10)ans(5)
      write(0,*)' b1: '
      read(0,10)ans(3)
      write(0,*)' c2: '
      read(0,10)ans(2)
      write(0,*)' a2: '
      read(0,10)ans(6)
      write(0,*)' b2: '
      read(0,10)ans(4)
      write(0,*)' c3: '
      read(0,10)ans(7)
      write(0,*)' c4: '
      read(0,10)ans(8)
      write(0,*)' a3: '
      read(0,10)ans(9)

      j=1
      nfit=0
      do 50 i=1,9
      if (ans(i).ne.'y') go to 50
      nfit=nfit+1
      fitlist(j)=i
      j=j+1
50    continue

      do 75 i=1,9
      if (ans(i).eq.'y') go to 75
      fitlist(j)=i
      j=j+1
```

```
75      continue

        return
        end

c       ************************************************
        subroutine button(set,initsw,sdata,sdatay,ymin,greeny)

C This subroutine set ups the functions of the buttons on the D & B box.
C Most of the buttons are for minimizer or excluded point use...
C This subroutine does not have to be modified when changing functions.

#include "fgl.h"
#include "fdevice.h"

        dimension initsw(0:31)
        dimension dialc(0:7),gparam(0:8),in(0:8),sparam(11,0:8),yparam(0:8)
        real bline,best,data(500),greeny(500)
        real datax(500),datay(500),dialc,err,errmin,errsd(9),fitave(9)
        real gparam,in,mdata(500),sdata(500),sdatay(500),sig(500),sparam
        real yellowy(500),time(500),tstep,xscale,yscale,yerr,yparam,ymin
        integer curson,cursx,bounds(2),excluder,excludel,func,gcurve
        integer npts,nsaved,rpoints,set,shots,smooth,tzero,ycurve
        integer sfactor
        logical initsw
        character ans
        character*3 junk

        common/block1/npts,tstep,tzero,shots
        common/block3/data,datax,datay,gcurve,gparam,rpoints,ycurve,yparam
        common/butn1/excludel,excluder,curson,cursx,bounds,smooth,func,nsaved
        common/butn2/errmin,sparam,dialc,yerr,bline,yellowy,yscale,xscale
        common/fitst1/fitave,errsd

        if (curson.eq.-13) go to 135
        if (curson.eq.-14) go to 141
        if (smooth.eq.2) go to 148

        if (initsw(0).eqv.getbut(SW0)) go to 10
        call ringbe
        call swap(func,dialc,gparam,yparam)
        call minim(data,excludel,excluder,func,npts,tstep,tzero,yparam)
        ycurve=1
        call fitfunc
  1     (bline,data,yerr,excludel,excluder,func,yparam,1,yellowy,yscale,xscale)
        call params(yparam,2,yerr,func)
```

```
      if (yerr.gt.errmin) go to 5
      call savep(yparam,sparam,11)
      errmin=yerr
5     call csleep
      call ringbe

10    if (initsw(1).eqv.getbut(SW1)) go to 20
c     remove interactive (green) curve
      call ringbe
      gcurve=-gcurve
      call csleep

20    if (initsw(2).eqv.getbut(SW2)) go to 30
c     remove minimizer (yellow) curve
      call ringbe
      ycurve=-ycurve
      call csleep

30    if (initsw(3).eqv.getbut(SW3)) go to 40
c     remove data points (red)
      call ringbe
      rpoints=-rpoints
      call csleep

40    if (initsw(4).eqv.getbut(SW4)) go to 50
c     put minimizer (yellow) params into interactive (green) params
      call ringbe
      call swap(func,dialc,yparam,gparam)
      call csleep

50    if (initsw(5).eqv.getbut(SW5)) go to 60
c     save interactive (green) params
      call ringbe
      nsaved = nsaved + 1
      if (nsaved.eq.11) nsaved=1
      call savep(gparam,sparam,nsaved)

60    if (initsw(6).eqv.getbut(SW6)) go to 70
c     put stored params into interactive (green) curve
      call ringbe
      do 61 i=0,8
61    in(i)=sparam(set,i)
      call swap(func,dialc,in,gparam)
      set=set + 1
      if ((set.gt.nsaved).or.(set.gt.10)) set=1
```

```
70      if (initsw(7).eqv.getbut(SW7)) go to 80
c       put best fit params into interactive (green) curve
        call ringbe
        do 75 i=0,8
75      in(i)=sparam(11,i)
        call swap(func,dialc,in,gparam)

80      if (initsw(8).eqv.getbut(SW8)) go to 90
c       send interactive (green) params to plotter via iodine
        call ringbe
        call hiplot(data,func,gparam,greeny,yscale,bline)

90      if (initsw(9).eqv.getbut(SW9)) go to 130
        call ringbe
        call monte(func,data,gparam,excludel,excluder,initsw(9))
        call swap(func,dialc,gparam,gparam)

130     if (initsw(13).eqv.getbut(SW13)) go to 140
        call ringbe
        curson=-13
        call cursor(bounds,curson,cursx,datax,datay,npts,tzero)
        return
135     curson=-1
        excludel=bounds(1)
        excluder=bounds(2)

140     if (initsw(14).eqv.getbut(SW14)) go to 150
        curson=-14
        call cursor(bounds,curson,cursx,datax,datay,npts,tzero)
        return
141     curson=-1
        call keyon
144     write(0,*)' Enter smoothing factor: '
        read(0,*)sfactor
        write(0,*)'sfactor = ',sfactor
        do 146 i=bounds(1),bounds(2)
146     mdata(i-bounds(1)+1)=data(i)
        call smooft(mdata,bounds(2)-bounds(1)+1,1.0*sfactor)
        do 147 i=bounds(1),bounds(2)
        sdata(i)=mdata(i-bounds(1)+1)
147     sdatay(i)=(sdata(i)-ymin)*yscale + 312.
        smooth=2
        return
148     call swapbu
        write(0,*)' Is the smoothing acceptable? '
        read(0,149)ans
```

```
149     format(a1)
        if (ans.eq.'n') go to 144
        call cclear
        call tpoff
        smooth=1

150     if (initsw(15).eqv.getbut(SW15)) go to 160
        call ringbe
        smooth=-smooth
        call csleep

160     if (initsw(16).eqv.getbut(SW16)) go to 170
        call ringbe
        call swap(func,dialc,gparam,yparam)
        call minim(sdata,excludel,excluder,func,npts,tstep,tzero,yparam)
        ycurve=1
        call fitfunc
   1    (bline,data,yerr,excludel,excluder,func,yparam,1,yellowy,yscale,xscale)
        call params(yparam,2,yerr,func)
        if (yerr.gt.errmin) go to 5
        call savep(yparam,sparam,11)
        errmin=yerr
165     call csleep
        call ringbe

170     if (initsw(17).eqv.getbut(SW17)) go to 180
        call keyon
        call fitpar
        call tpoff

180     if (initsw(18).eqv.getbut(SW18)) go to 190
        call ringbe
        call fitest(func,data,gparam,excludel,excluder,initsw(18))
        call swap(func,dialc,gparam,gparam)
        call ringbe

190     if (initsw(19).eqv.getbut(SW19)) go to 200
        call ringbe
        call swap(func,dialc,fitave,gparam)

200     if (initsw(20).eqv.getbut(SW20)) go to 310
        call ringbe
        call paramin(gparam)

310     if (initsw(31).eqv.getbut(SW31)) return
        call setdbl(0)
```

```
      call tpon
      call textin
      call cexit
      stop

      end

c     ************************************************
      subroutine dials(dialc,gparam)
C This subroutine gets the current values for all the dials

#include "fgl.h"
#include "fdevice.h"

      dimension dialc(0:7),gparam(0:8)
      real dialc,gparam

      gparam(0)=getval(DIAL0)*dialc(0)
      gparam(1)=getval(DIAL1)*dialc(1)
      gparam(2)=getval(DIAL2)*dialc(2)
      gparam(3)=getval(DIAL3)*dialc(3)
      gparam(4)=getval(DIAL4)*dialc(4)
      gparam(5)=getval(DIAL5)*dialc(5)
      gparam(6)=getval(DIAL6)*dialc(6)
      gparam(7)=getval(DIAL7)*dialc(7)

      return
      end

c     ************************************************
      subroutine params(param,colour,err,func)
C This subroutine prints parameters on screen

#include "fgl.h"
#include "fdevice.h"

      dimension param(0:8)
      integer colour,func
      real err,param
      character*80 label

C the colour label is used to plot both minimizer and dial parameters...
      if (colour.ne.1) go to 5
      call color(BLACK)
C erase all the previously printed parameters
      call rectf(160.,625.,290.,715.)
```

```
      call rectf(360.,625.,490.,715.)
      call rectf(560.,625.,690.,715.)
      call rectf(760.,625.,890.,715.)
      call color(GREEN)
      go to 8

5     call color(BLACK)
      call rectf(900.,140.,1000.,385.)
      call color(YELLOW)

8     if (colour.eq.1) call cmov2i(160,700)
      if (colour.eq.2) call cmov2i(900,375)
      write(label,9)param(0)
9     format(f8.3)
10    format(f8.2)
      call charst(label,8)
      if (colour.eq.1) call cmov2i(160,670)
      if (colour.eq.2) call cmov2i(900,350)
      write(label,10)param(4)
      call charst(label,8)
      if (colour.eq.1) call cmov2i(160,640)
      if (colour.eq.2) call cmov2i(900,325)
      write(label,10)param(2)
      call charst(label,8)
      if (colour.eq.1) call cmov2i(360,700)
      if (colour.eq.2) call cmov2i(900,300)
      write(label,9)param(1)
      call charst(label,8)
      if (colour.eq.1) call cmov2i(360,670)
      if (colour.eq.2) call cmov2i(900,275)
C This keeps the fractional exponents in the Kolrausch and diffusion fit
C from becoming larger than 1. These statements must be changed if changing
C functions 5 or 6 on the menu.
      if((func.eq.7).and.(param(5).gt.1.)) param(5) = 1.
      if((func.eq.8).and.(param(2).gt.1.)) param(2) = 1.
C     if((func.eq.8).and.(param(3).gt.1.)) param(3) = 1.
      write(label,10)param(5)
      call charst(label,8)
      if (colour.eq.1) call cmov2i(360,640)
      if (colour.eq.2) call cmov2i(900,250)
      write(label,10)param(3)
      call charst(label,8)
      if (colour.eq.1) call cmov2i(560,700)
      if (colour.eq.2) call cmov2i(900,225)
      write(label,9)param(6)
      call charst(label,8)
```

```
      if (colour.eq.1) call cmov2i(560,670)
      if (colour.eq.2) call cmov2i(900,200)
      write(label,9)param(7)
      call charst(label,8)
      if (colour.eq.1) call cmov2i(560,640)
      if (colour.eq.2) call cmov2i(900,175)
      write(label,10)param(8)
      call charst(label,8)
      if (colour.eq.1) call cmov2i(760,700)
      if (colour.eq.2) call cmov2i(900,150)
      write(label,50)err
50    format(e10.3)
      call charst(label,10)
      return
      end

c     ************************************************
      subroutine plotdat(excludel,excluder,npts,tzero,x,y,colour)
C This is where the data points are actually plotted on the screen

#include "fgl.h"
#include "fdevice.h"

      integer colour,excludel,excluder,i,npts,tzero
      real x(500),y(500)

      if (excludel.eq.-1) go to 20
c     excluded points
      call color(WHITE)
      do 10 i=excludel,excluder
10    if (x(i).gt.99) call circf(x(i),y(i),1.0)

c     data points
20    call color(RED)
C   Colour is used here for the point at tzero
      if (colour.eq.2) call color(BLUE)

      do 30 i=1,tzero-1
30    if (x(i).gt.99) call circf(x(i),y(i),1.0)

C This stuff is dinosaur for excluded points
      if (excludel.ne.-1) go to 50
      do 40 i=tzero+1,npts
40    call circf(x(i),y(i),1.0)
      go to 60
```

```
50      do 55 i=tzero+1,excludel-1,1
55      call circf(x(i),y(i),1.0)

        do 56 i=excluder+1,npts
56      call circf(x(i),y(i),1.0)

C tzero should be plotted in blue
60      call color(BLUE)
        call circf(x(tzero),y(tzero),1.0)

        return
        end

c       ****************************************
        subroutine curve(x,y,colour)

C This subroutine plots the curve (either green or yellow) on the graph
C Note that both the graphical x and y values of the curve must be passed
C when this is called (see convfitfunc.f)

#include "fgl.h"
#include "fdevice.h"

        integer i,npts,shots,tzero,colour
        real x(500),y(500),tstep
        common/block1/npts,tstep,tzero,shots

        if (colour.eq.1) call color(GREEN)
C       if (colour.eq.2) call color(YELLOW)
        call move2(x(1),y(1))

C       x=200.
        do 10 i=1,npts
        if (y(i).gt.600) y(i)=600.
        if (y(i).lt.300) y(i)=300.
        call draw2(x(i),y(i))
        call move2(x(i),y(i))
C10     x=x+1.
10      continue

        return
        end

C*****************************************************
        subroutine plotresids(y,x,scale)
```

```
C This subroutine plots the residuals, updating each time the green curve
C is updated

#include "fgl.h"
#include "fdevice.h"

      integer i,npts,shots,tzero
      real y(500),x(500),tstep,resid(500),scale
      common/block1/npts,tstep,tzero,shots

C compute graphics co-ord for residual points from actual resids. The 0
C resid line is at graphics y = 150, the box height is 100 pixels, the scale
C is 1.6X the scale of the datapoint box. The loop checks to see if
C resids are so big that they would fall outside the box, and if so,
C puts points on the appropriate edge of the box.

      scale = scale
      call color(RED)

      do 10 i = 1,tzero - 1
         resid(i) = y(i)*scale*1.6 + 150.
         if(resid(i).gt.199.)then
            resid(i) = 199.
         else if(resid(i).lt.101)then
            resid(i) = 101.
         endif
         call circf(x(i),resid(i),1.0)
10    continue

C Do the residual for tzero separately

      call color(BLUE)

      resid(tzero) = y(tzero)*scale*1.6 + 150.
      if(resid(tzero).gt.199.)then
         resid(tzero) = 199.
      else if(resid(tzero).lt.101.)then
         resid(tzero) = 101.
      endif
      call circf(x(tzero),resid(tzero),1.0)

      call color(RED)

      do 20 i = tzero + 1,npts
         resid(i) = y(i)*scale*1.6 + 150.
         if(resid(i).gt.199.)then
```

```
            resid(i) = 199.
          else if(resid(i).lt.101.)then
            resid(i) = 101.
          endif
          call circf(x(i),resid(i),1.0)
20      continue

        return

        end

C ***********************************************************
        subroutine swap(func,dialc,in,out)

#include "fgl.h"
#include "fdevice.h"

        dimension dialc(0:7),in(0:8),out(0:8)
        real dialc,in,out
        integer func,i

        do 10 i=0,8
10      out(i)=in(i)

        call setval(DIAL0,int(out(0)/dialc(0)),-15000,15000)
        call setval(DIAL1,int(out(1)/dialc(1)),-15000,15000)
        call setval(DIAL2,int(out(2)/dialc(2)),1,30000)
        call setval(DIAL3,int(out(3)/dialc(3)),1,30000)
        call setval(DIAL4,int(out(4)/dialc(4)),1,30000)
        call setval(DIAL5,int(out(5)/dialc(5)),1,30000)
        if(func.eq.3)call setval(DIAL5,int(out(5)/dialc(5)),-15000,15000)
        call setval(DIAL6,int(out(6)/dialc(6)),-15000,15000)
        if ((func.eq.3).or.(func.eq.5)) call setval(DIAL6,int(out(6)/
    1   dialc(6)),0,30000)
        call setval(DIAL7,int(out(7)/dialc(7)),-15000,15000)

        if (func.eq.4) then
           call setval(DIAL4,int(out(4)/dialc(4)),0,30000)
           call setval(DIAL5,int(out(5)/dialc(5)),0,30000)
        endif

        return
        end

c       ***********************************************
C This is the dreaded minimizer subroutine, which is ignored for now, but calls
```

```
C other subroutines in the monte.f, etc.  This is why this program must be compiled
C with other programs than convfitfunc.f (see Makefile)

      subroutine minim(data,excludel,excluder,func,npts,tstep,tzero,param)

      dimension param(0:8)
      dimension alpha(9,9),covar(9,9)
      integer func,excludel,excluder,lista2(9),ma,npts,tzero,i,j,mfit
      real data(500),mdata(500),sig(500),t,time(500),tstep,param
      real alamda,chisq

      common/minim1/lista2,mfit,ma
      j=0
      t=0.
      do 25 i=tzero+1,npts
      t=t+tstep
      if ((i.ge.excludel).and.(i.le.excluder)) go to 25
      j=j+1
      time(j)=t
      mdata(j)=data(i)
25    continue

      sig(1)=0.0
      sig(2)=0.0
      do 100 i=1,tzero
      sig(1)=sig(1)+data(i)
100   sig(2)=sig(2)+data(i)*data(i)
      sig(1)=sqrt((tzero*sig(2)-sig(1)*sig(1))/(tzero*(tzero-1)))

      do 125 i=2,j,1
125   sig(i)=sig(1)

      alamda=-1.
      do 150 i=1,20
150   call mrqmin(time,mdata,sig,j,param,ma,lista2,mfit,
     1 covar,alpha,ma,chisq,alamda,func)

      call mrqmin(time,mdata,sig,j,param,ma,lista2,mfit,
     1 covar,alpha,ma,chisq,0.,func)

      do 200 i=2,5
      if (param(i).lt.tstep/10.) param(i)=tstep/10.
200   if (param(i).gt.3000.*tstep) param(i)=3000.*tstep

      if ((param(6).lt.0.).and.((func.eq.3).or.(func.eq.5))) param(6) = 0.
      return
```

```
      end

c     ******************************************

      subroutine savep(in,sparam,set)

      dimension in(0:8),sparam(11,0:8)
      real in,sparam
      integer i,set

      do 10 i=0,8
10    sparam(set,i)=in(i)

      return
      end

c     ************************************************
C This subroutine calls the convplot executable on iodine in the
C ~karen/drplot directory.  It also passes the data for the parameters,
C data points and fitted curve points to convplot for plotting

      subroutine hiplot(data,func,gparam,greeny,yscale,bline)

#include "fgl.h"
#include "fdevice.h"

      dimension gparam(0:8)

      integer excludel,excluder,func,i,npts
      integer shots,tzero
      character bleach
      character*12 date
      character*20 name
      character*80 comment
      real bound(9),data(500),errsd(9),fitave(9),gparam,tstep,greeny(500)
      real yscale

      common/block1/npts,tstep,tzero,shots
      common/block2/name,bleach,date,comment
      common/fitst1/fitave,errsd

      excludel = 0.
      excluder = 0.

C  Write out all the file head info (and excluded point info dinousaurs)
      open(unit=4,file='/usr/people/ben/fitstuff/cfitben.dat',status='old')
```

```
      write(4,*)func
      write(4,*)name
      write(4,*)bleach
      write(4,*)npts
      write(4,*)tzero
      write(4,*)excludel
      write(4,*)excluder
      write(4,*)date
      write(4,*)shots
      write(4,*)tstep

C Write out all the fit parameters in order a1, a2, b1, b2, etc.
      write(4,*)gparam(4)
      write(4,*)gparam(5)
      write(4,*)gparam(2)
      write(4,*)gparam(3)
      write(4,*)gparam(0)
      write(4,*)gparam(1)
      write(4,*)gparam(6)
      write(4,*)gparam(7)
      write(4,*)gparam(8)

C dinosaur for writing the errors in fits from the minimizer
      write(4,*)errsd(5)
      write(4,*)errsd(6)
      write(4,*)errsd(3)
      write(4,*)errsd(4)
      write(4,*)errsd(1)
      write(4,*)errsd(2)
      write(4,*)errsd(7)
      write(4,*)errsd(8)
      write(4,*)errsd(9)

C find the smallest data point
      min = 0.
      do 19 i = 1,npts
         if(data(i).lt.min) min = data(i)
19    continue

      do 20 i=1,npts
20    write(4,*) data(i)+min

C Actually write out the computed fit coordinates for plotting to the plotter
C since there is no analytic expression to compute them on site.

C Back convert the passed graphics points into actual coordinate points
```

```
      do 21 i = 1,npts
         write(4,*) (greeny(i) - bline)/yscale
21    continue

      close(unit=4)

      call chiplot

      return
      end

c     ******************************************
      subroutine paramin(param)
C  Get parameter a3 when necessary

      dimension param(0:8)
      real param

      call keyon

      write(0,*)' Enter a3: '
      read(0,*)param(8)

      call tpoff

      return
      end

      subroutine fpecleanup(error)

      write(0,*)'FP error'
      end
```

Appendix III: Program Cvfitfunc.f

```
C This is the code cvfitfunc.f, which contains the subroutine fitfunc called by
C convfit.f for curve fitting with convolutions and residuals.

      subroutine fitfunc
C
C Note: This section of code has been completely rewritten by BJS to
C include convolutions in the fitting program. It will not work with
C Mark's regular fitmp.f program. The graphics calls and data allocation
C have been completely redone--please compile with convfit.f for correct
C graphics. BJS 10/90

     1  (bline,data,err,excludel,excluder,func,param,plot,ploty,yscale,xscale,
     1 residuals)

        dimension param(0:8), sharp(500), conv(500), gauss(16)
        dimension bc(9), ac(9)
        integer excludel,excluder,func,i,npts,plot,shots,tzero
        real a1c,a1exp,a2c,a2exp,a3c,a3exp,b1,b1c,b1exp,b2c,b2exp,bline
        real c3exp,c3c,data(500),dt,err,errc,gaussarea,sharp,gauss,conv
        real param,ploty(500),talter,tgauss,t2,tstep,yscale,xscale
        real residuals(500)

        common/block1/npts,tstep,tzero,shots
        common conv

C Compute 15 pt gaussian for convolution with fitted function and
C store in array gauss. Note that 2.50663 is sqrt(2*Pi). If sigma
C is too wide or too narrow for 15 pts, the gaussian will not be
C normalized. Thus, the area is computed (rectangular integration)
C and the truncated gaussian is normalized as best as possible. For
C fits with a 1/2 width of 8 or 9 points, this leads to an integration
C error of a few %, which in turn, will cause an error in the ratio
C of short to long component amplitudes. This could be corrected by
C using more points in the Gaussian, but it would also slow down the
C program, and would require padding the data with extra points before
C tzero for the convolution.

        gaussarea = 0.

C figure out how many time steps wide the sigma of the gaussian is
C (this depends on func -- usually it is param(4)--a1, but sometimes
C it is param(3)--b2 when a1 is used as a fit parameter.

        sigma = param(4)/tstep
```

```
      if(func.eq.4) sigma = param(3)/tstep
      if(sigma.lt.1.) sigma = 1.

      do 200 l = 1,15
         gauss(l) = exp(-(l-8)*(l-8)/(2.*sigma*sigma))/(2.50663*sigma)
         if((gauss(l).gt.1.e09).or.(gauss(l).lt.1.e-09)) gauss(l) = 0.
         if(sigma.eq.1) gauss(l) = 0.
         gaussarea = gaussarea + gauss(l)
200   continue

C If gaussian has sigma less than one point, then turn gaussian into
C a 1 pt delta function (i.e. convolute with rectangle of width and
C heigth one, so there is no effective convolution)

      if(sigma.eq.1) then
         gauss(8) = 1.
         gaussarea = 1.
      endif

C Normalize gaussian area

      do 210 l = 1,15
         gauss(l) = gauss(l)/gaussarea
210   continue


C  sharp is the array of the fitted, unconvoluted function at each tstep
C  (mnemonic here is that the data has a sharp point when not convoluted)
C  conv is the convoluted fit at each tstep; err is the least squares error
C  between the convoluted fit and the data

C  zero out the arrays to be used
      err = 0.

      do 250 i = 0,tzero
         sharp(i) = 0.
         conv(i) = 0.
250   continue


C Depending on func, branch to the appropriate computation of sharp
C If func = 3 (menu choice #1 -- biexponential decay), fall through to default

      if (func.eq.4) go to 400
      if (func.eq.5) go to 500
```

```
      if (func.eq.6) go to 600
      if (func.eq.7) go to 700
      if (func.eq.8) go to 800

C Compute points from fit and store in array sharp for func = 3
C Note:  Calculating exponentials for each timestep is torturously slow,
C so take advantage of the fact that product of exp's is exp of sum and
C multiply by exp(-tstep/decay) on each pass--only compute the exp once.
C (Note: Krypton has a severe underflow problem: results of calculations
C smaller than e^-12 give garbage, hence the extra checks on exp magnitudes)

      if( (tstep/param(2)).gt.12) then
         b1cexp = 0.
         b1c = 0.
      else
         b1cexp = exp(-tstep/param(2))
         b1c = 1.
      endif

      if( (tstep/param(3)).gt.12) then
         b2cexp = 0.
         b2c = 0.
      else
         b2cexp = exp(-tstep/param(3))
         b2c = 1.
      endif

      do 305 i = tzero + 1, npts
         sharp(i) = param(0)*b1c + param(1)*b2c + param(5)
         b1c = b1c*b1cexp
         b2c = b2c*b2cexp
305   continue

C Now do convolution with gaussian and store in array conv

      call convolution(sharp,gauss)

C Compute the residuals (difference between the data and the convoluted fit,
C and keep track of the least squares error)

      do 310 i=1,npts
         residuals(i)=data(i) - conv(i)
         err=err + residuals(i)*residuals(i)
310   continue

      if (plot.eq.0) return
```

```
c       calculate graphics coordinates for every coord on x axis(200-699)

        do 350 i=1,npts
           ploty(i)=yscale*conv(i) + bline
350     continue

        return

C Stuff below this point is for func = 4
C Again, check for underflow error in exponential

400     if( (tstep/param(2)).gt.12) then
          b1cexp = 0.
          b1c = 0.
        else
          b1cexp = exp(-tstep/param(2))
          b1c = 1.
        endif

C Check to see if rise is instantaneous; if so, avoid divide by 0 error

        a1cexp = 0.
        a1c = 0.

        if( (param(4).ne.0).and.((tstep/param(4)).lt.12) ) then
           a1cexp = exp(-tstep/param(4))
           a1c = a1cexp
        endif

        a2cexp = 0.
        a2c = 0.

        if( (param(5).ne.0).and.((tstep/param(5)).lt.12) ) then
           a2cexp = exp(-tstep/param(5))
           a2c = a2cexp
        endif


403     do 405 i = tzero + 1, npts
          sharp(i) = (param(0)*(1. - a1c) + param(1)*(1. - a2c))*(b1c
     1            + param(6)) + param(7)
          b1c=b1c*b1cexp
          b2c=b2c*b2cexp
          a1c=a1c*a1cexp
          a2c=a2c*a2cexp
```

```
405   continue

      call convolution(sharp,gauss)

      do 410 i = 1, npts
         residuals(i) = data(i) - conv(i)
         err = err + residuals(i)*residuals(i)
410   continue

      if(plot.eq.0) return

      do 450 i=1, npts
         ploty(i) = yscale*conv(i) + bline
450   continue

      return

C Stuff below this point is for func = 5
C Note that c3 is a time offset parameter for this choice of func
C t2 is the correct delay time for the onset of the rise, which
C is computed with the propagators risec and riseexp.

500   t2 = -param(6)

      if( (tstep/param(2)).gt.12) then
         b1exp = 0.
         b1c = 0.
      else
         b1exp = exp(-tstep/param(2))
         b1c = 1.
      endif

      if( (tstep/param(5)).gt.12) then
         a2exp = 0.
         a2c = 0.
      else
         a2exp = exp(-tstep/param(5))
         a2c = 1.
      endif

      if( (tstep/param(3)).gt.12) then
         b2exp = 0.
         b2c = 0.
      else
         b2exp = exp(-tstep/param(3))
         b2c = 1.
```

```
      endif

      riseexp = b1exp
      risec = 1.
      a2c = 1.

      do 510 i = tzero + 1, npts
         t2 = t2 + tstep
         if(t2.le.0.)go to 505
         risec = risec*riseexp
         b2c = b2c*b2exp
505      sharp(i) = param(0)*a2c + param(1)*(1. - risec)*b2c + param(7)
         b1c = b1c*b1exp
         a2c = a2c*a2exp
510   continue

C Now do the convolution and compute the error

      call convolution(sharp,gauss)

      do 520 i = 1, npts
         residuals(i) = data(i) - conv(i)
         err = err + residuals(i)*residuals(i)
520   continue

      if(plot.eq.0) return

      do 530 i = 1, npts
         ploty(i) = yscale*conv(i) +  bline
530   continue

      return

C Stuff below this point is for func = 6.  This is the same as func = 5
C except the offset now has a rise time equal to the slower exp decay.

600   t2 = -param(6)

      b1exp = exp(-tstep/param(2))
      b1c = 1.

      b2exp = exp(-tstep/param(3))
      b2c = 1.

      riseexp = b1exp
      risec = 1.
```

```
      slowrise = b2exp
      slowc = 1.

      do 610 i = tzero + 1, npts
         t2 = t2 + tstep
         if(t2.le.0)go to 605
         risec = risec*riseexp
         slowc = slowc*slowrise
         b2c = b2c*b2exp
605      sharp(i) = param(0)*b1c + param(1)*(1. - risec)*b2c
  1            + (1. - slowc)*param(7)
         b1c = b1c*b1exp
610   continue

      call convolution(sharp,gauss)

      do 620 i = 1,npts
         residuals(i) = data(i) - conv(i)
         err = err + residuals(i)*residuals(i)
620   continue

      if(plot.eq.0) return

      do 630 i = 1, npts
         ploty(i) = yscale*conv(i) + bline
630   continue

      return

C Stuff below this point is for func = 7 -- the stretched exponential or
C Kolrausch function. Note that the exponential propagation trick can no
C longer be used with the fractional power inside the exponent.

700   if(param(5).gt.1) param(5) = 1.

      do 710 i = tzero + 1,npts
         expon = ((i - (tzero + 1))*tstep/param(2))**param(5)
         if(expon.gt.12) expon = 12.
         if(param(5).lt.0.01) expon = 1.
         sharp(i) = param(0)*exp(-expon) + param(1)
710   continue

      call convolution(sharp,gauss)

      do 720 i = 1,npts
```

```
          residuals(i) = data(i) - conv(i)
          err = err + residuals(i)*residuals(i)
720     continue

        if(plot.eq.0) return

        do 750 i = 1,npts
          ploty(i) = yscale*conv(i) + bline
750     continue

        return

C Stuff below this point is for the diffusion fit: t^-n.  As with the Kolrausch
C fit, the exponential propagation trick can not be used.  Note that params 2
C and 3 are always less than one, otherwise the function blows up.

800     if(param(2).gt.1) param(2) = 1.
C       if(param(3).gt.1) param(3) = 1.

        do 810 i = tzero + 1,npts
          time = (i - (tzero))*tstep
          sharp(i) = param(0)*time**(-param(2)) + param(1)*time**(-param(3))
   1      + param(6)
810     continue

        call convolution(sharp,gauss)

        do 820 i = 1,npts
          residuals(i) = data(i) - conv(i)
          err = err + residuals(i)*residuals(i)
820     continue

        if(plot.eq.0) return

        do 850 i = 1,npts
          ploty(i) = yscale*conv(i) + bline
850     continue

        return

        end

C       ***************************************************
        subroutine convolution(sharp,gauss)
```

```
C     computes convolution of the fitted function passed in array sharp
C     with the convoluting function passed in array gauss. Convolution
C     is simple brute force. Conv is set equal to sharp in regions where
C     the tail of the convolution doesn't overlap the function.
C
C     Attempts to do the convolution with fft turned out to be slower
C     than brute force and less accurate for this many points. fft may
C     be advantageous, however, if the number of convoluted points is
C     increased (either by longer data sets or a more accurate gaussian)

      dimension sharp(500),gauss(16),conv(500)
      integer npts,tzero,shots
      real tstep,sharp,gauss,conv

      common conv
      common/block1/npts,tstep,tzero,shots

      do 2000 k = 8, npts - 8
         conv(k) = 0.
         do 2010 m = 1,15
            conv(k) = conv(k) + sharp(k-8+m)*gauss(m)
2010     continue
2000  continue

      do 2020 k = npts-7, npts
         conv(k) = sharp(k)
2020  continue

      return

      end
```

Appendix IV: Handling Routines for the HI Plotter Called from Convfit.f

A. CFITPLOT.BEN: This file, cfitplot.ben, executed by the command chiplot called in the hiplot subroutine of convfit.f. The command chiplot is defined in the file cben.c, shown below. It executes this file, which remote copies the file cfitben.dat (which contains all the info necessary for convplot to plot the data and fit on the hi plotter) into a temporary file on iodine, establishes a remote shell on iodine and executes the convplot program on Karen's drplot subdirectory on iodine, and then removes the temp file.

```
rcp /usr/people/ben/fitstuff/cfitben.dat iodine:/tmp/cfit.dat
rsh iodine /usr/users/karen/drplot/convplot
rsh iodine rm /tmp/cfit.dat
```

B. CBEN.C: This file, cben.c, defines the system commands called from the program convfit. For example, the fortran command cclear is defined as the system command "clear". The made up command chiplot, called from the hiplot subroutine in convfit.f is defined in the file cfitplotben, listed above.

```
        fortran cclear()
{
        system("clear");
}

        fortran cfitest()
{
        system("/usr/people/cfit/cfitest&");
}

        fortran chiplot()
{
        system("/usr/people/cfit/cfitplotben&");
}

        fortran csleep()
{
        sleep(1);
}

        fortran cexit()
{
        exit(0);
}
```

Appendix V: Makefile and Compilation of Convfit

This is what directs the fortran compiler to compile and link all the different files that make up the curve fitting program. To recompile the convfit program, put the makefile and all the files listed under convfit together in the same directory, and type 'make convfit' from the UNIX prompt. Note that most of the files listed below are object files; they are dinosaurs from the cfit program, and are not changed at all when creating new functions. Only convfit.f and cvfitfunc.f need to be recompiled; the object files are used for linking. (Note: if the definition of the subroutine fitfunc in cvfitfunc.f is changed to pass new or different parameters, corresponding changes must also be made in the file convfitest.f)

```
INCLUDES = -I/usr/include/gl2 -I/usr/people/gifts/mextools/include
CFLAGS  = -Zg -Zf -O
LIBS = /usr/lib/libimage.a \
        /usr/people/gifts/mextools/portlib/libport.a

ALL =  fontn

default: install

all: $(ALL)

clean:
        rm -f $(ALL) *.o

install: all
        -chown root loadav
        -chgrp sys loadav
        -chmod 4755 loadav

.c:
        cc $(CFLAGS) -o $@ $<

cfit:
        cc -Zf -Zg cfitmp13.c minim.o auxl.o up.o util.o -lm

convfit:
        f77 -Zg -Zf -O convfit.f convfitest.o monte.o cben.o cvfitfunc.f recip.o -lm
```

Appendix VI: Program Convplot.f

```
C Program convplot.f

c ***********************************************
c       plots data and fit
c ***********************************************
C by Mark Paige--modified by Ben Schwartz 10/90 to plot convolutions
C from the convfit program on kyrpton
C Compile this program with benhiplot.f (modified version of Keenan's
C hiplot.f or pltsb.f); there should be an object file (benhiplot.o or hiplot.o)
C present in the directory with this program.

C Here's how it works: the convfit program on krypton calls subroutine
C chiplot() in the hiplot subroutine. The object file cben.o tells the
C compiler that the fortran subroutine chiplot is really a system command
C that executes the program cfitplotben in /usr/people/cfit on krypton.
C This program, cfitplotben, calls for a remote shell on iodine, copies
C the temporary file cfitben.dat (in /usr/people/ben/fitstuff on krypton)
C to /tmp/cfit.dat on iodine, and then executes the program convplot on
C iodine in ~karen/drplot. This program, convplot, must be compiled with
C the modified version of keenan's hiplot.f (called benhiplot.f) to
C access the hi plotter and plot convolutions correctly. The program
C cfitplotben on krypton then removes the copy of cfit.dat from
C /tmp on iodine, and then closes the remote connection, returning
C control back to the convfit program on krypton. cfitben.dat is kept in
C ~ben/fitstuff on krypton for later inspection (note: status = 'old' --
C it will be overwritten each time convfit is executed.)

      program convplot

C Set up to read in all the stuff that was written into the cfitben.dat file in the
C hiplot subroutine in convfit.f

      integer bound1,bound2,funcnum,npts,shots,tzero
      character*1 bleach(3),date(13),filename(20)
      character*15 info1,info2
      character*70 fun1a,fun1b
      real a1,a2,a3,b1,b2,c1,c2,c3,c4,error,err(9)
      real baseline,data(500),sign,tstep,x0,xmax,xmin,y0,ymax,ymin
      real resultsx(1000),resultsy(1000)

      open(UNIT=4,FILE='/tmp/cfit.dat',STATUS='OLD')

      read(4,20)funcnum
20    format(i5)
```

```
      call getline(4,filename)
      call getline(4,bleach)
C     i=1
C22   if ((bleach(i).eq.'n').or.(bleach(i).eq.'N').or.(bleach(i).eq.'y').or.
C    1 (bleach(i).eq.'Y')) go to 23
C     i=i+1
C     if (i.lt.4) go to 22
C23   if (i.eq.4) i=3
      sign=1.0
      if ((bleach(i).eq.'y').or.(bleach(i).eq.'Y')) sign = -1.
      read(4,20)npts
      read(4,20)tzero
      read(4,20)bound1
      read(4,20)bound2
c     avoid c to fortran array indexing confusion
c     bound1=bound1+1
c     bound2=bound2+1
      call getline(4,date)
      read(4,20)shots
      read(4,30)tstep
30    format(f15.4)
C    call getline(4,comment)
      read(4,30)a1
      read(4,30)a2
      read(4,30)b1
      read(4,30)b2
      read(4,30)c1
      read(4,30)c2
      read(4,30)c3
      read(4,30)c4
      read(4,30)a3

      do 40 i=1,9
40    read(4,30)err(i)

      do 50 i=1,npts
50    read(4,30)data(i)

C Read in the computed fit values (green curve) for use in plotting

    do 52 i = 1,npts
      read(4,30) resultsy(i)
52   continue

      close(UNIT=4)
```

```
      baseline = 0.
C     do 60 i=1,tzero
C60     baseline = baseline + sign*data(i)
C     baseline = baseline/tzero

C If data is a bleach signal (bleach flag = y or Y, then multiply everything by -1 so
C data still plots the same way

      do 61 i=1,npts
61    data(i) = sign*(data(i) - baseline)

C Compute x and y values for plotting the fit curve
      do 65 i = 1,npts
         resultsy(i) = sign*resultsy(i)
         resultsx(i) = (i - tzero)*tstep
65    continue

C Recompute the least squares error
172   error = 0.
      do 173 i = 1,npts
         error = error + (data(i) - resultsy(i))**2.
173   continue

C Keep track of minimum and maximum x and y values for both the data and the
C fitted curve for use in picking the plotting axes, etc.
190   xmin = -1.*tstep*(tzero-1)
      xmax = tstep*(npts-tzero)

      ymax = data(1)
      ymin = data(1)

      do 185 i=1,npts
      if (data(i).gt.ymax) ymax = data(i)
185   if (data(i).lt.ymin) ymin = data(i)

      do 186 i=1,npts
      if (resultsy(i).gt.ymax) ymax = resultsy(i)
186   if (resultsy(i).lt.ymin) ymin = resultsy(i)

C want y range of plotting box to be 10% bigger at each end the data and fitted curve
      ymax=ymax*1.1
      ymin = ymin - (ymax-ymin)*0.1

C Subroutines called below are defined in the package hiplot.f or pltsb.f, and are
C specific for use on the hi plotter.
c     start opens file for plot, move pen1 to home, puts plotter
```

```
c       in absolute positioning mode
c       save(1) saves file after plot
c       rbound(xmin,xmax,ymin,ymax) - scales data and draw box
c       rtickxy(xstart,xinterval,ystart,yinterval) - tick marks beginning
c                       at xstart and ystart
c       rvector(x1,y1,x2,y2) - draws vector between two points

        zero = 0.0
         x0=xmin
         y0=ymin
        call select(1)
        call start(1)
C       call window(0.,4.5,11.,5.5)
        call save(0)
        call rbound(x0,xmax,y0,ymax)
        call rtickxy(zero,xmax/4.,zero,ymax/1.1)
        call rvector(x0,0.,xmax,0.)

        if (bound1.gt.0) go to 230
        call pen(2)
        do 225 i=1,npts
225     call rplot((i-tzero)*tstep,data(i),3)
c125    call rcircle((i-tzero)*tstep,data(i),4)
        go to 240

230     do 231 i=1,bound1-1
c231    call rcircle((i-tzero)*tstep,data(i),4)
231     call rplot((i-tzero)*tstep,data(i),3)

        do 232 i=bound2+1,npts
c232    call rcircle((i-tzero)*tstep,data(i),4)
232     call rplot((i-tzero)*tstep,data(i),3)

C Depending on the chosen function, write the appropriate functional form
240     if (funcnum.eq.4) go to 250
        if (funcnum.eq.5) go to 260
        if (funcnum.eq.6) go to 270
        if (funcnum.eq.7) go to 280

        fun1a = 'Fit to c1*exp(-t/b1) + c2*exp(-t/b2) &'
        fun1b = '+ a2 conv w/ gaussian of width a1 &'
        go to 300

250     fun1a = 'Fit to [c1*(1 - exp(-t/a1)) + c2*(1 -&'
        fun1b = ' exp(-t/a2))]*[exp(-t/b1) + c3] + c4 conv gaussian b2&'
        go to 300
```

```
260     fun1a = 'Fit to c1*exp(-t/b1) + c2*(1 - exp(-T&'
        fun1b = '/b1))*exp(-T/b2) + c4 conv w/ gaussian of width a1&'
        go to 300

270     fun1a = 'Fit to c1*exp(-t/b1) + c2*(1 - exp(-T&'
        fun1b = '/b1))*exp(-T/b2) + (1 - exp(-T/b2))*c4 conv gauss a1&'
        go to 300

280     fun1a = 'Fit to c1*exp[(-t/b1)**a2] + c2 conv &'
        fun1b = 'w/ gaussian of width a1&'
        go to 300

300     call pen(1)
        call label(200,1435,fun1a)
        call label(860,1435,fun1b)

C Don't want to plot the ± signs for the minimizer errors, so these are commented out
        info1 = 'a1 = &'
        call label(200,1395,info1)
        call number(275,1395,a1,0)
Cinfo2 = ' +/- &'
Ccall label(475,1395,info2)
Ccall number(525,1395,err(1),0)

        info1 = 'b1 = &'
        call label(200,1355,info1)
        call number(275,1355,b1,0)
Ccall label(475,1355,info2)
Ccall number(525,1355,err(3),0)

        info1 = 'c1 = &'
        call label(200,1315,info1)
        call number(275,1315,c1,2)
Ccall label(475,1315,info2)
Ccall number(525,1315,err(5),2)

        info1 = 'a2 = &'
        call label(800,1395,info1)
        call number(875,1395,a2,0)
Ccall label(1075,1395,info2)
Ccall number(1125,1395,err(2),0)

        info1 = 'b2 = &'
        call label(800,1355,info1)
        call number(875,1355,b2,0)
```

```
Ccall label(1075,1355,info2)
Ccall number(1125,1355,err(4),0)

      info1 = 'c2 = &'
      call label(800,1315,info1)
      call number(875,1315,c2,2)
Ccall label(1075,1315,info2)
Ccall number(1125,1315,err(6),2)

      i=2
C     if ((funcnum.eq.5).or.(funcnum.eq.6).or.(funcnum.eq.7).or.
C  1  (funcnum.eq.8)) i=0
      info1 = 'c3 = &'
      call label(1400,1395,info1)
      call number(1475,1395,c3,i)
Ccall label(1675,1395,info2)
Ccall number(1725,1395,err(7),i)

      info1 = 'c4 = &'
      call label(1400,1355,info1)
      call number(1475,1355,c4,2)
Ccall label(1675,1355,info2)
Ccall number(1725,1355,err(8),2)

      info1 = 'a3 = &'
      call label(1400,1315,info1)
      call number(1475,1315,a3,0)
Ccall label(1675,1315,info2)
Ccall number(1725,1315,err(9),0)

500   info1 = 'error = &'
      call label(1810,1200,info1)
      call number(1810,1160,error,1)

      call label(1810,1000,filename)
C     call label(1810,900,date)
      call inumber(1810,800,shots,1)
      info1 = 'shots&'
      call label(1855,770,info1)
      info1 = 'T0 = &'
      call label(1810,670,info1)
      call inumber(1855,670,tzero,1)
C     call label(200,10,comment)

      call labelx('Delay Time (psec)&')
      if (sign.eq.-1.) call labely ('Change in Absorbance (x-100) &')
```

```
      if (sign.ne.-1.) call labely('Change in Absorbance (x100) &')

      call pen(3)
C     resultsy(1)=0.

      call rvplt(resultsx,resultsy,int(npts))

      if (bound1.le.0) go to 700
      call pen(3)
      do 600 i=bound1,bound2
c600  call rcircle((i-tzero)*tstep,data(i),4)
600   call rplot((i-tzero)*tstep,data(i),3)

700   call finish
      stop

      end


      subroutine getline(unitnum,larray)

c     gets line from specified unit

      character*1 larray(81),letter
      integer unitnum

c     reads in characters until carriage return seen
      i=0
10    call fgetc(unitnum,letter)
      i=i+1
      if (ichar(letter).eq.10) go to 20
      larray(i)=letter
      go to 10

20    larray(i)='&'
      return
      end
```

LAWRENCE BERKELEY LABORATORY
UNIVERSITY OF CALIFORNIA
TECHNICAL INFORMATION DEPARTMENT
BERKELEY, CALIFORNIA 94720